Effects of Heating and Load History on the Behavior of Lead-Rubber Bearings
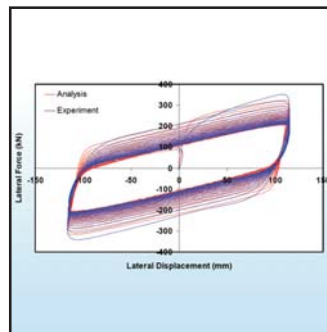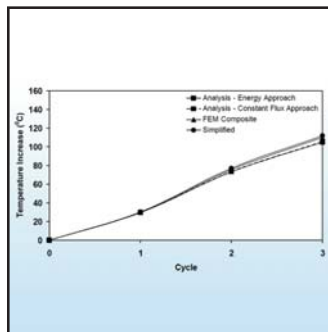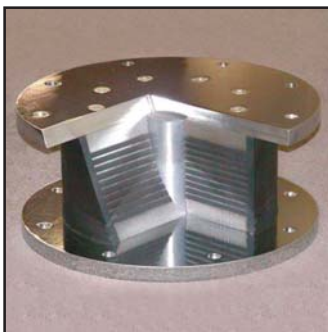
by

Ioannis V. Kalpakidis and Michael C. Constantinou

NOTICE

This report was prepared by the University at Buffalo, State University of New York as a result of research sponsored by MCEER through a contract from the Federal Highway Administration. Neither MCEER, associates of MCEER, its sponsors, the University at Buffalo, State University of New York, nor any person acting on their behalf:

a. makes any warranty, express or implied, with respect to the use of any information, apparatus, method, or process disclosed in this report or that such use may not infringe upon privately owned rights; or

b. assumes any liabilities of whatsoever kind with respect to the use of, or the damage resulting from the use of, any information, apparatus, method, or process disclosed in this report.

Any opinions, findings, and conclusions or recommendations expressed in this publication are those of the author(s) and do not necessarily reflect the views of MCEER or the Federal Highway Administration.

Effects of Heating and Load History on the Behavior of Lead-Rubber Bearings

by

Ioannis V. Kalpakidis[1] and Michael C. Constantinou[2]

1 Post-doctoral Research Associate, Department of Civil, Structural and Environmental Engineering, University at Buffalo, State University of New York
2 Professor, Department of Civil, Structural and Environmental Engineering, University at Buffalo, State University of New York

MCEER
University at Buffalo, State University of New York
Red Jacket Quadrangle, Buffalo, NY 14261
Phone: (716) 645-3391; Fax (716) 645-3399
E-mail: *mceer@buffalo.edu*; WWW Site: *http://mceer.buffalo.edu*

Preface

The Multidisciplinary Center for Earthquake Engineering Research (MCEER) is a national center of excellence in advanced technology applications that is dedicated to the reduction of earthquake losses nationwide. Headquartered at the University at Buffalo, State University of New York, the Center was originally established by the National Science Foundation in 1986, as the National Center for Earthquake Engineering Research (NCEER).

Comprising a consortium of researchers from numerous disciplines and institutions throughout the United States, the Center's mission is to reduce earthquake losses through research and the application of advanced technologies that improve engineering, pre-earthquake planning and post-earthquake recovery strategies. Toward this end, the Center coordinates a nationwide program of multidisciplinary team research, education and outreach activities.

MCEER's research is conducted under the sponsorship of two major federal agencies, the National Science Foundation (NSF) and the Federal Highway Administration (FHWA), and the State of New York. Significant support is also derived from the Federal Emergency Management Agency (FEMA), other state governments, academic institutions, foreign governments and private industry.

The Center's Highway Project develops improved seismic design, evaluation, and retrofit methodologies and strategies for new and existing bridges and other highway structures, and for assessing the seismic performance of highway systems. The FHWA has sponsored three major contracts with MCEER under the Highway Project, two of which were initiated in 1992 and the third in 1998.

Of the two 1992 studies, one performed a series of tasks intended to improve seismic design practices for new highway bridges, tunnels, and retaining structures (MCEER Project 112). The other study focused on methodologies and approaches for assessing and improving the seismic performance of existing "typical" highway bridges and other highway system components including tunnels, retaining structures, slopes, culverts, and pavements (MCEER Project 106). These studies were conducted to:

- assess the seismic vulnerability of highway systems, structures, and components;
- develop concepts for retrofitting vulnerable highway structures and components;
- develop improved design and analysis methodologies for bridges, tunnels, and retaining structures, which include consideration of soil-structure interaction mechanisms and their influence on structural response; and
- develop, update, and recommend improved seismic design and performance criteria for new highway systems and structures.

The 1998 study, "Seismic Vulnerability of the Highway System" (FHWA Contract DTFH61-98-C-00094; known as MCEER Project 094), was initiated with the objective of performing studies to improve the seismic performance of bridge types not covered under Projects 106 or 112, and to provide extensions to system performance assessments for highway systems. Specific subjects covered under Project 094 include:

- development of formal loss estimation technologies and methodologies for highway systems;
- analysis, design, detailing, and retrofitting technologies for special bridges, including those with flexible superstructures (e.g., trusses), those supported by steel tower substructures, and cable-supported bridges (e.g., suspension and cable-stayed bridges);
- seismic response modification device technologies (e.g., hysteretic dampers, isolation bearings); and
- soil behavior, foundation behavior, and ground motion studies for large bridges.

In addition, Project 094 includes a series of special studies, addressing topics that range from non-destructive assessment of retrofitted bridge components to supporting studies intended to assist in educating the bridge engineering profession on the implementation of new seismic design and retrofitting strategies.

This report presents a comprehensive investigation of the effects of lead core heating and cumulative travel on the behavior of lead-rubber bearings. A literature review and an experimental study of the effects of temperature on the mechanical properties of lead are presented. A theory for predicting the temperature rise of the lead core in lead-rubber bearings subjected to lateral motion is developed based on principles of mechanics. The theory reduces the complex three-dimensional thermo-mechanical problem into a numerically solvable initial value problem on the history of temperature of the core and the strength of the bearing. The accuracy of the theory is verified through comparison to experimental results and results of finite element analysis of several bearings. The theory is then used to establish principles of similarity and scaling that can be used in reduced scale testing of lead-rubber bearings. Furthermore, a model of the behavior of lead-rubber bearings that can be incorporated in dynamic response history analysis programs is described and validated through experiments. Studies on the dynamic response of seismically isolated structures using the proposed model demonstrate the importance of accounting for the effects of lead core heating in calculating the peak seismic response of seismically isolated structures.

ABSTRACT

The lead-rubber bearing has been extensively used as a seismic isolation device in both seismic retrofit and new construction of buildings and bridges. Its behavior is markedly affected by heating of its lead core during cyclic motion. The phenomenon is characterized by reduction of the characteristic strength of the bearing with increasing number of cycles and has been observed in numerous experimental studies; however, it has not been analytically described so that predictions of behavior can be made for analysis and design. Moreover, a previous study demonstrated that large cumulative travel resulting from service loadings has effects on the characteristic strength of the bearing but the conditions that affect these changes are not well understood.

This work presents a comprehensive investigation of the effects of lead core heating and cumulative travel on the behavior of lead-rubber bearings. First, a literature review and an experimental study of temperature effects on the mechanical properties of lead are presented. Then, a theory for the prediction of the lead core temperature when the bearing undergoes cyclic motion is developed on the basis of principles of mechanics. The theory accomplishes a reduction of the complex three-dimensional thermo-mechanical problem to an initial value problem on the history of temperature of the core and strength of the bearing that can be numerically solved. An explicit approximate solution is also presented. The accuracy of the theoretical solution is verified by comparing its results to those of experiments and complex finite element analyses of several bearings. The theoretical solution is used to establish principles of similarity and scaling that can be used in the reduced scale testing of lead-rubber bearings. Moreover, a model of behavior

of lead-rubber bearings for incorporation in dynamic response history analysis programs is described. The model is capable of describing the lateral force-displacement relation of lead-rubber bearings including the lead core heating effects. Experiments conducted in cyclic and random motions are used to demonstrate the validity of the model. The model is used to conduct analyses of a representative seismically isolated structure and to demonstrate the significance of accounting for lead core heating in the prediction of the peak response.

Finally, the effect of cumulative travel on the characteristic strength of lead-rubber bearings is investigated through the evaluation of existing experimental results and the conduction of a new series of tests. The results show that, depending on its amplitude, the cumulative motion may indeed affect the strength of the bearings and this should be considered in analysis and design.

ACKNOWLEDGEMENTS

TABLE OF CONTENTS

TABLE OF CONTENTS (CONT'D)

LIST OF FIGURES

LIST OF FIGURES (CONT'D)

LIST OF TABLES

LIST OF TABLES (CONT'D)

SECTION 1

INTRODUCTION

Numerous studies have demonstrated the benefits of seismic isolation for the mitigation or elimination of damage in structural systems and nonstructural components during strong earthquake shaking. Among the various types of seismic isolation bearings, lead-rubber isolators have been extensively used both in seismic retrofit and new construction of buildings and bridges either exclusively or along with other devices (damping devices or other types of seismic isolators).

The lead-rubber bearing was invented in 1975 by W. H. Robinson in New Zealand (Skinner et al., 1993). It consists of a steel reinforced elastomeric bearing with a core of lead. Figure 1-1 shows the internal construction of a lead-rubber bearing. Note that the top and bottom (flange) plates of the bearing are connected to the end plates of the rubber bearing through countersunk bolts. This type of construction allows for confinement of the lead core. The core is typically cut longer than the height of the rubber bearing and is compressed upon bolting of the flange plates to the end plates. The lead core expands laterally and wedges into the rubber layers between the shim plates. Under such (confined) conditions, the lead core provides excellent energy dissipation capacity (with a magnitude dependent on the diameter of the lead plug). A detailed contemporary description of the behavior of lead-rubber bearings may be found in Constantinou et al. (2007b).
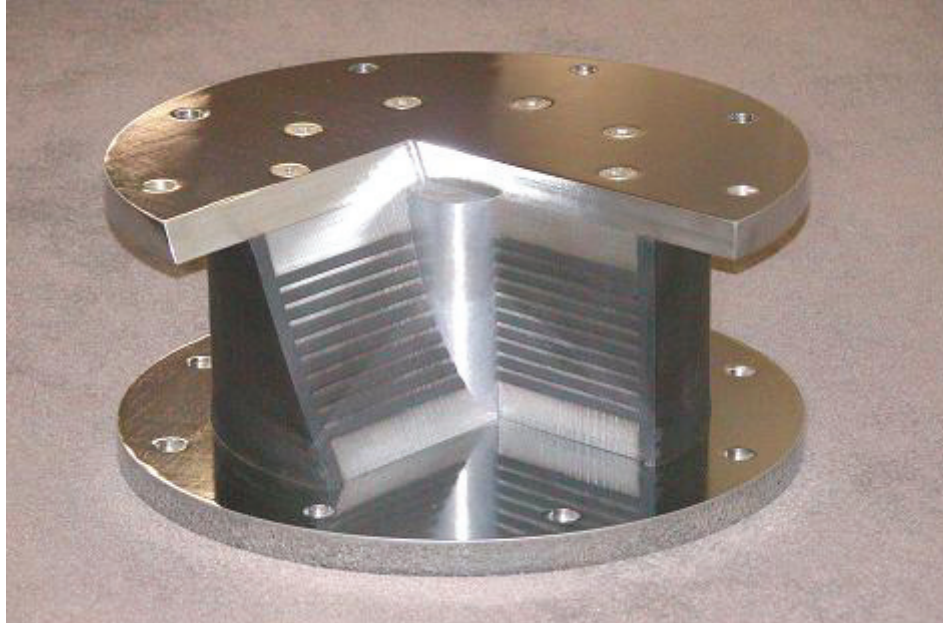
FIGURE 1-1 Internal Construction of a Lead-Rubber Bearing (Courtesy of DIS)

Lead-rubber bearings have also been constructed using multiple lead cores. There are a few applications of multiple core lead-rubber bearings in Japan and one in California, all in bridges. Figure 1-2 shows a schematic of a multiple core lead-rubber bearing used for bridge applications in Japan. The figure also shows lateral restrainers that were employed in Japan for the seismic isolation of bridges, where bridges were isolated only in the longitudinal direction. Such practice is not used in the United States (Constantinou et al., 2007b).
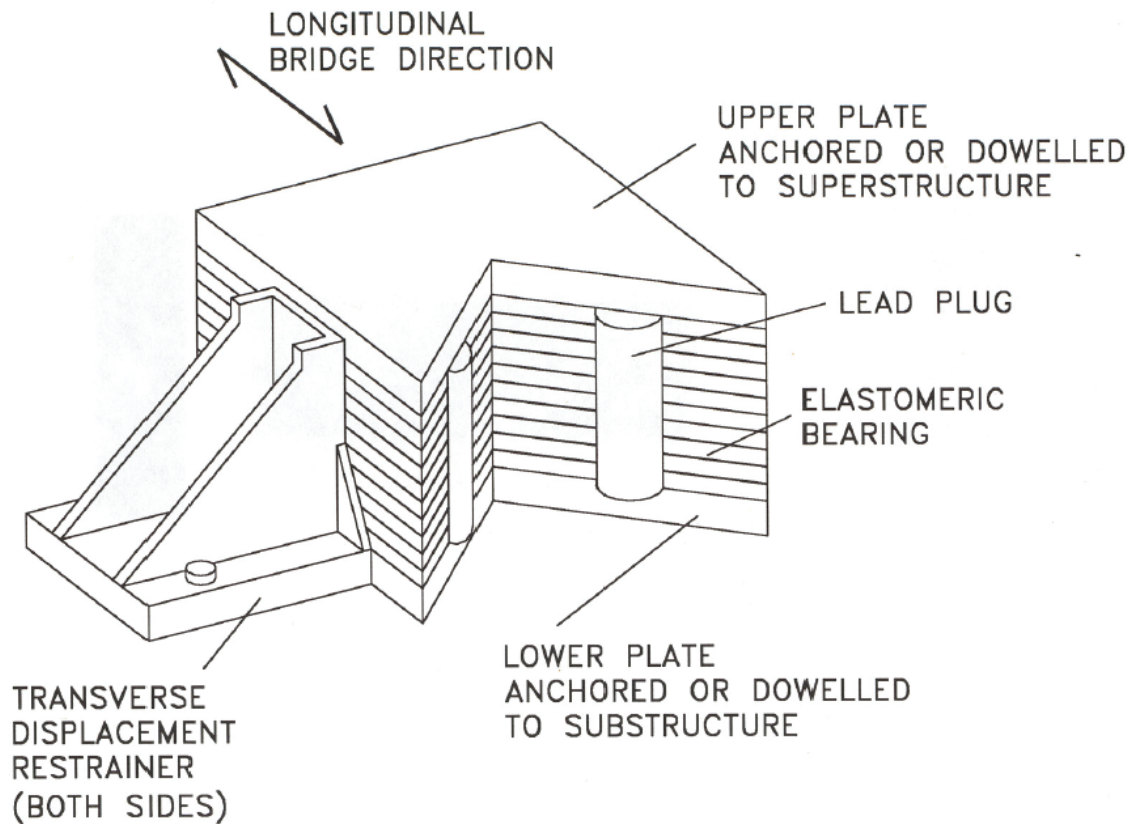
FIGURE 1-2 Multiple-Core Lead-Rubber Bearing Used in Japan (Constantinou et al., 2007b)

Lead-rubber isolation bearings are assumed to have the idealized behavior shown in Figure 1-3. The critical parameters are the characteristic strength Q_d and the post-elastic stiffness K_d. These two parameters are related to the geometric and material properties of the bearing as follows:

$$Q_d = A_L \sigma_{YL} \tag{1-1}$$

$$K_d = f_L \frac{GA_r}{T_r} \tag{1-2}$$

3

where f_L is a parameter that accounts for the effect of the lead core on the post-elastic stiffness (expected to be close to unity), G is the effective shear modulus of rubber, σ_{YL} is the effective yield strength of lead, T_r is the total rubber thickness, A_r is the bonded rubber area, and A_L is the area of the lead core. Equation (1-1) neglects the contribution of rubber towards the characteristic strength of the bearing. This contribution is small under normal conditions and is typically indirectly accounted for in the value of effective yield stress of lead. However, this contribution becomes important in low temperature conditions and needs to be separated from that of the lead in order to more accurately predict the behavior of lead-rubber bearings. This approach is followed in this work.
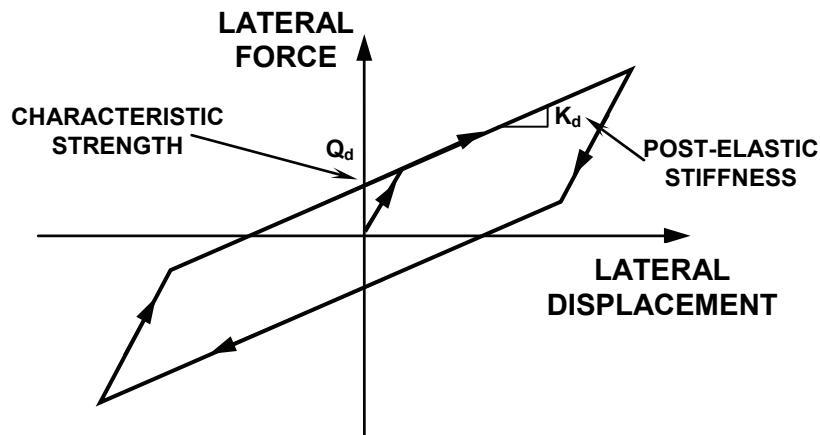
FIGURE 1-3 Idealized Force-Displacement Loop of a Lead-Rubber Bearing

The characteristic strength of lead-rubber bearings is responsible for the capability of the bearings to dissipate energy. This strength is dependent, apart from the aforementioned confinement of the lead core, on the rate of strain of shear deformation of the lead core and the history of loading in terms of (a) the cumulative slow movement of large travel

due to traffic and thermal loadings, and (b) the number, amplitude and frequency of high speed seismic motion cycles due to heating effects.

Test data presented in Constantinou et al. (2007b) on lead-rubber bearings show substantial increases in the characteristic strength at low speeds following cumulative travel of 1.6 km at small amplitude of slow cyclic motion. However, the origin of the phenomenon could not be identified, leading to speculation that the effect is not only dependent on the cumulative travel but also on the amplitude of imposed deformation and on heating effects due to the inevitable accelerated fashion of conducting such tests (motion representing several years of in-service conditions was imposed over a period of about one month).

The effect of lead heating on the characteristic strength of lead-rubber bearings is best illustrated with the example bearing of Figure 1-4 for which the measured energy dissipated per cycle (directly related to the characteristic strength) in high speed, large amplitude motion is shown in Figure 1-5. In this example, the energy dissipated per cycle drops to about 60% of the starting value within five cycles. More data presented in Constantinou et al. (2007b) show a complex dependency of the strength on the conditions of motion but which can be directly related to the temperature of the lead core and the dependency of the mechanical properties of lead on temperature. Although this phenomenon has been known for many years (e.g., see Tyler and Robinson, 1984), there has been no attempt to analytically describe it.
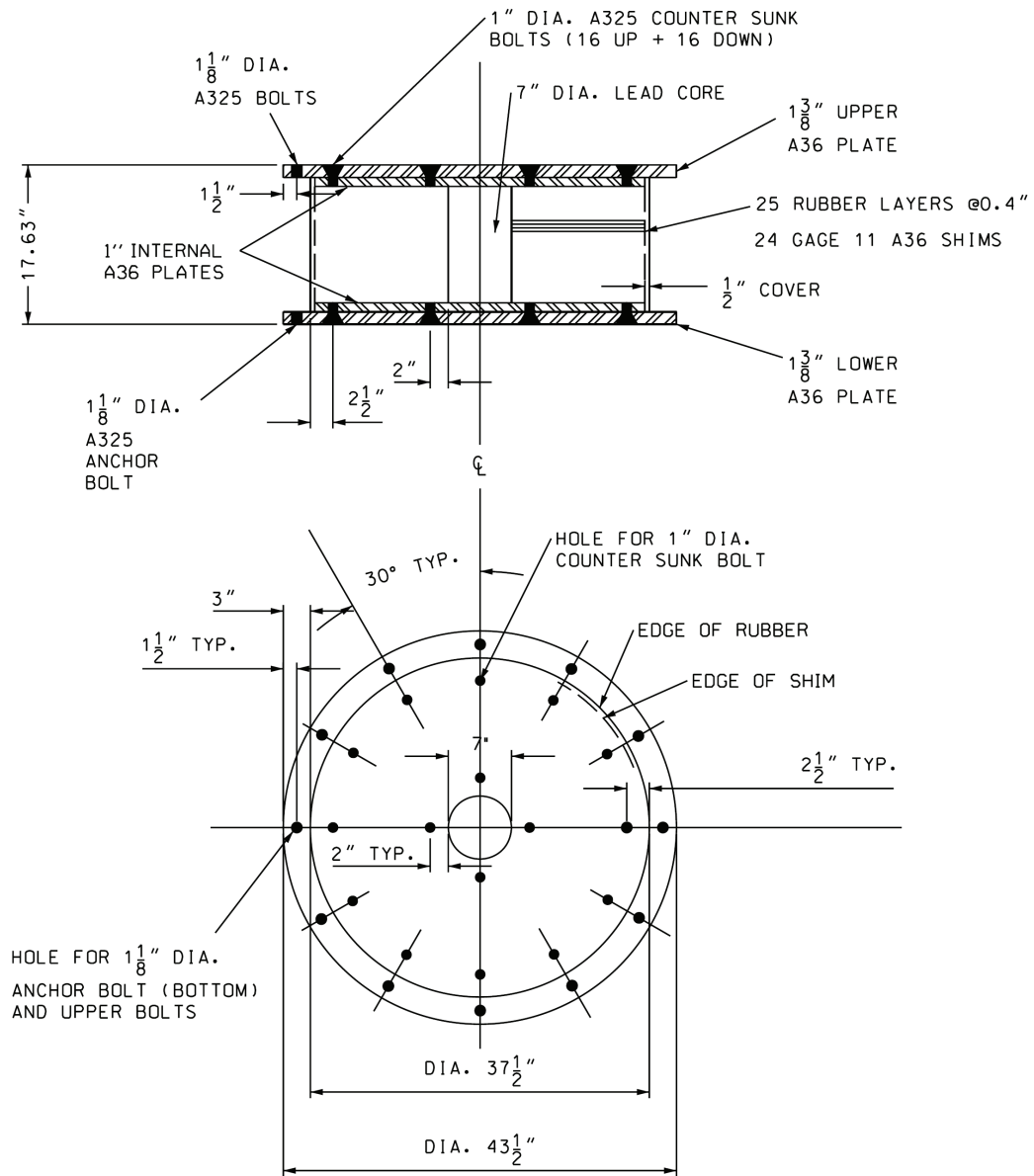
FIGURE 1-4 Tested Large Scale Lead-Rubber Bearing (1 inch=25.4 mm) (Constantinou et al., 2007b)
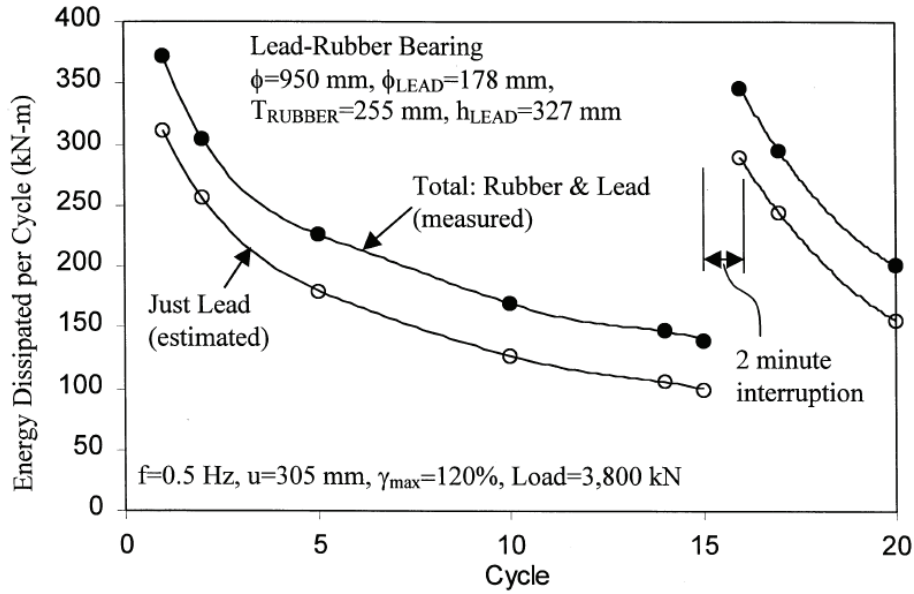
FIGURE 1-5 Energy Dissipation per Cycle in the Lead-Rubber Bearing of Figure 1-4 (Constantinou et al., 2007b)

Analytical prediction of the characteristic strength of lead-rubber bearings is important in many respects because it permits (a) development of models for dynamic analysis which account for this important phenomenon; (b) determination of bounds on the characteristic strength values for use in simplified analysis; (c) development of scaling principles in the testing of lead-rubber bearings, either at smaller scale or at different loading histories in consistency with the capability of available testing machines; (d) evaluation and use of available test data for different geometries of bearings and test conditions (i.e., allows the development of principles of "similarity").

This report seeks to develop a scientific understanding of the effects of heating and load history on the mechanical behavior of lead-rubber bearings. It focuses on the following issues: (i) investigation of the material properties and behavior of lead, and the effect of heating on the mechanical properties of lead through a literature review and testing of

7

lead specimens at various temperatures and speeds, (ii) theoretical prediction of the lead core temperature and of the strength of a lead-rubber bearing undergoing cyclic motion, (iii) verification of the aforementioned predictions by comparing them with experimental results and finite element analysis results, (iv) development of scaling principles for the testing of lead-rubber bearings, (v) development of a simple model for dynamic analysis of lead-rubber bearings that accounts for strength reduction due to lead core heating and that is used for investigating its effects on the seismic response of isolated structures, and (vi) further study of the effects of cumulative travel on the characteristic strength of lead-rubber bearings and investigation of the effects of amplitude of cyclic motion.

The document consists of nine sections. Section 1 provides a brief review of the lead-rubber isolation device. Information on how it was invented is given and its internal construction is briefly described. Reference is made to previous representative research studies involving this type of isolation hardware, its properties and behavior are briefly described and an introduction to the phenomena of lead core heating and cumulative travel effect is provided.

Section 2 includes a literature review on the behavior and properties of lead, a description of testing of lead specimens and an attempt to establish a link between strength and temperature of lead based on testing and literature data. Rate effects are discussed.

Section 3 describes a mathematical model for the prediction of lead core heating of lead-rubber bearings under cyclic motion of large amplitude.

8

Section 4 provides a series of experimental results on lead-rubber bearings of various geometries and at various initial temperatures and subjected to periodic motion of several amplitudes and frequencies for verification of the results of Section 3. Results of finite element heat transfer analyses for the same cases are presented for comparison.

Section 5 proposes an updated hysteretic model for lead-rubber bearings to account for the effects of lead core heating. The model is verified by comparing analytical and experimental results for harmonic and random motion tests.

Section 6 describes an analytical investigation of the effects of lead core heating on the seismic response of structures isolated with lead-rubber bearings. The model presented in Section 5 is utilized for this purpose.

Section 7 presents the current state of understanding of the effects of cumulative travel on the properties of lead-rubber bearings through the presentation of tests conducted in the past. This is followed by presentation of the results of a new series of tests conducted to further investigate these effects.

Section 8 summarizes the document and presents conclusions.

Section 9 provides a list of references.

SECTION 2

THE MECHANICAL BEHAVIOR OF LEAD

2.1 Introduction

Lead (Pb) is in the Fourth Group of the Periodic Table and has an atomic number of 82. It is a member of the cubic crystal system and its crystal structure is face-centered cubic (FCC) of the A1 type (Hofmann, 1970). This means that it is expected to remain ductile even at very low temperatures; it does not experience the "ductile-to-brittle transition" like, for instance, metals/alloys with BCC (body-centered cubic) or HCP (hexagonal close-packed) crystal structures (Callister, 1999) which become brittle at low temperatures. The melting point of lead is 327^0C for purity larger than 99.94% (corroding lead) and 326^0C for purity larger than 99.90% (chemical lead) (American Society for Metals, 1979). The coefficient of linear expansion is $29.1x10^{-6}/^0C$ for temperatures between 20^0C and 100^0C. The elastic modulus at room temperature may be assumed around 17 GPa. The shear modulus is between 5.4 and 7.6 GPa and may be assumed to be about 6 GPa. Poisson's ratio is 0.44 (Hofmann, 1970). Note that the elastic properties cannot be exactly known even for pure lead because of the difficulty in defining elastic behavior for a material like lead. Also, the mechanical properties are affected by impurities, even at very small concentrations. The chemical composition of the impurities is important as well. For example, a lead-antimony alloy of 99.1% purity may have almost twice the tensile strength of a lead-tin alloy of 99% purity (for more details, see the tensile strength diagrams on p. 198 of Hofmann, 1970).

Although lead is an extensively used material, there are only few sources of data about its mechanical behavior. Most of the material is either old or incomplete. This section attempts to provide a review of those characteristics that are related to the mechanical behavior of lead, and, consequently, of lead-rubber bearings. The review is based on data collected from the literature and is supplemented by experimental data obtained in lead specimen testing conducted at the University at Buffalo.

It should be noted that lead in lead-rubber bearings is of high purity, with values exceeding 99.9%. In cases where the purity is lower (e.g., 99%), the chemical composition of the impurities may have important effects on the strength, as noted earlier.

2.2 Plastic Deformation

In a perfect crystal, the plastic deformation can take place by a slip process in which simultaneous translation of one plane of atoms over another occurs. No dislocations are involved in this case. This occurs at a stress level that is referred to as the ideal strength above which the deformation is no longer elastic and becomes catastrophic. However, it is rare that a perfect crystal with no defects is found in nature; deformation, therefore, occurs through the movement of dislocations or vacancies before the ideal strength level is reached (Guruswamy, 2000).

The mechanisms by which plastic flow of a metal takes place involve processes occurring on the atomic scale. At all temperatures above absolute zero, thermally activated movement of atoms and dislocations is present. The extent of thermal activation increases

12

with the homologous temperature T/T_M, where T is the temperature of interest and T_M is the melting point (both in ^{0}K). The low melting point of lead and its alloys makes the contribution of thermal activation to plastic flow very significant, even at room temperature, which corresponds to a homologous temperature of around 0.5. Evaluation of mechanical property data on lead and lead alloys requires an appreciation of the different mechanisms of plastic flow that are operative at room temperature and at elevated temperatures, to which lead alloys will be subjected (Guruswamy, 2000).

At low temperatures, plastic deformation mechanisms include dislocation glide and twinning. At higher temperatures, materials show time-dependent plastic deformation or creep under an applied stress. At very high temperatures (homologous temperature above 0.6) and stress levels, power-law creep may be accompanied by repeated recrystallization (Guruswamy, 2000).

The mechanisms of plastic deformation of lead may superimpose in complicated ways. The contribution of each mechanism can be described by a rate equation which relates strain rate to the stress, the temperature, the structure of the material at that instant and material properties. The stress and temperature range of dominance of each of the mechanisms of plasticity and the rates of flow they produce can be summarized using deformation mechanism maps. Such maps allow the determination of the operative deformation mechanism and the creep strain rate as a function of normalized stress σ/μ and normalized temperature T/T_M (where μ is the shear modulus and T_M is the melting temperature). In general, metals having similar atomic bonding and crystal structure have

similar mechanical properties expressed in normalized form, and are said to belong to a specific isomechanical group (Guruswamy, 2000).

Deformation mechanism maps for pure lead with a grain size of 10 μ m can be found on p. 105 of Guruswamy (2000). Three principal fields are shown: low-temperature plasticity, power-law creep (which sets in at about $0.3T_M$), and diffusional flow (which appears at high temperature and low stress) regions. Above $0.7T_M$ (i.e. above about 150^0C), dynamic recrystallization (which makes creep rates hard to predict) is observed in lead (Guruswamy, 2000).

In FCC metals (which include lead), the yield strength is generally determined by the density of discrete obstacles or defects they contain. When pure, it is the density and arrangement of dislocations that determines the flow stress, which, therefore, depends on the state of work hardening of the metal. Annealing lowers the yield strength (Guruswamy, 2000).

The internal structure of a metal is changed when plastic deformation takes place. This is evident through changes in the properties of the metal. For example, plastically deformed metals become stronger; the stress-strain curve continues to rise after the yield strength is exceeded. The percentage of cold work (amount of plastic strain introduced during processing) is conveniently referred to as an index of plastic deformation and is defined as the percent decrease in cross-sectional area from deformation (Van Vlack, 1980).

Plastic deformation corresponds to the motion of large numbers of dislocations (Callister, 1999). However, dislocations interfere with the movements of other dislocations.

Dislocation entanglements increase the strength of the material; strain hardening as well as ductility reduction result from plastic deformation (Van Vlack, 1980).

Plastically deformed crystals have more energy than unstrained crystals because they are loaded with imperfections and dislocations. The atoms will move to form a more perfect, unstrained array if given a chance. Such a chance arises when the crystals are exposed to high temperatures. This process is known as annealing. High temperatures cause greater thermal vibrations of the lattice which permit a reordering of the atoms into less distorted grains. This process of growing new crystals from previously deformed ones is called recrystallization. It requires atom movements and rearrangements which occur more readily at high temperatures (Van Vlack, 1980).

For lead, room temperature corresponds to a high homologous temperature of around 0.5. Therefore, marked changes in microstructure happen even at room temperature and even more easily at higher temperatures expected to develop in high speed, large amplitude motion in lead-rubber bearings. Such changes could involve recovery, recrystallization and grain growth, and age hardening followed by age softening (Guruswamy, 2000). Thus, before further discussion of the mechanical properties of lead is made, it would be useful to briefly discuss the processes of recovery, recrystallization and grain growth in polycrystalline metals – as well as how they are influenced by solute elements, temperature and prior strain – and then investigate how these processes affect the behavior of lead in specific.

2.3 Recovery, Recrystallization and Grain Growth

When a polycrystalline metal deforms, its grains elongate and the number of defects (such as dislocations and vacancies) in each grain increases significantly. The effects of plastic strain, however, may be "cancelled" after some time; if the temperature is high enough, the metal returns to a state free from the effects of plastic strain through the interrelated processes of recovery, recrystallization and grain growth (Skinner et al., 1993).

During recovery, the stored energy of the deformed grains is reduced by the dislocations moving to form lower energy configurations such as subgrain boundaries, and by the annihilation of vacancies at internal and external surfaces. Recrystallization occurs when small, new, undeformed grains nucleate among the deformed grains and then grow at their expense. Further grain growth occurs as some of the new grains grow at the expense of others. The driving force for recrystallization is the stored energy of deformation of the extruded grains, while the decrease in the surface energy of the many recrystallized grains causes grain growth to occur (Skinner et al., 1993).

The temperature at which recrystallization just reaches completion in one hour is called recrystallization temperature. It is typically between 1/3 and 1/2 of the absolute melting temperature of a metal or alloy and depends on several factors, such as the amount of prior cold work and the purity of the alloy. As the percentage of cold work increases, the recrystallization temperature drops and reaches a limiting value at high deformations. Normally it is this minimum recrystallization temperature that is specified in the literature. Alloying raises the recrystallization temperature. There is some critical value

of cold work below which recrystallization cannot be triggered; it is between 2 and 20% cold work. A -4^0C recrystallization temperature is reported for lead (Callister, 1999). According to the American Society for Metals (1979), lead of 99.999% purity has a recrystallization temperature below 0^0C.

It should be noted that the rate of recrystallization is very temperature-sensitive (Skinner et al., 1993). In other words, the time from its beginning to its completion for a specific metal and for a specific level of cold work may vary significantly with relatively much less significant temperature variations. Van Vlack (1980) refers to the case of 75% cold-worked commercially pure aluminum alloy which recrystallized within one minute at 350^0C, 60 minutes at 300^0C and 40 days at 230^0C. Additionally, the recrystallization temperature for a specific metal drops as the amount of cold work increases (Van Vlack, 1980). In general, one can say that higher amounts of cold work and higher temperatures facilitate (that is, result in "easier" and "faster") recrystallization.

It should, therefore, be stressed that the triggering and completion of recrystallization as well as the time between them, the temperature and the percentage of cold work are interrelated. Any recrystallization data should report the amount of cold work, the annealing temperature and the amount of time the metal was exposed to that temperature.

Hofmann (1970) presents results from tests conducted with lead which was not of the degree of purity that lead is typically available today and used in lead-rubber bearings. In these tests the appearance of recrystallization was determined from measurements of the softening of lead. According to the results, even at a work deformation as low as 5%, room temperature (20^0C) is high enough to trigger recrystallization (see p. 190 of

Hofmann, 1970). Hofmann (1970) also reports that the beginning of recrystallization shifts to lower temperatures and less amounts of work on increasing the degree of purity of the lead.

After the completion of recrystallization, the strain-free grains will continue to grow if the metal specimen is left at the elevated temperature. This is called grain growth and does not need to be preceded by recovery and recrystallization. It may occur in all polycrystalline materials, metals and ceramics alike (Callister, 1999). It is important to note that the size of the grains is directly related to the strength of the material; the larger the grains, the smaller the strength – see p. 199 of Hofmann (1970) for an ultimate tensile strength vs. grain size plot for lead. Apart from the size of the grains, other factors affecting the strength of a metal include its composition, its crystal structure and the strength of the intercrystalline grain boundaries (Nadai, 1950).

The size of the grains following annealing depends on the annealing temperature (the higher the temperature the larger the grains) as well as on insoluble impurities (which inhibit grain growth). Additionally, the degree of cold work before annealing has a significant effect on the subsequent grain size. In the case of high amounts of cold work, the grain size is small even after completion of grain growth while for low amounts of cold work the grain growth caused can be quite significant. For lead this critical degree of cold working is about 1% elongation (Rollason, 1973).

2.4 Mechanical Properties

In general, it may be said that the mechanical properties (e.g., ultimate strength) of lead mainly depend on the following factors: speed of deformation (rate effects), crystal structure (grain size, dislocation density etc.), degree of plastic deformation (percentage of cold work – strain hardening effects), temperature, and others. It should be noted that each of the above effects is not independent of the rest. In fact, two or more of the above effects may be present at the same time, either producing the same effect (i.e. one "supporting" the other) or opposite effects (i.e., one "canceling" the other). It would be useful, therefore, to briefly present the effect of each of the above factors and the possible interactions among them.

The following information is based on limited and mostly old data on lead that exist in the literature. The conclusions drawn are, therefore, open to completion and further discussion on the basis of a complete and extensive experimental study of lead.

Because of creep, a permanent plastic deformation occurs in lead and lead alloys at stress levels well below the yield point at room temperature. Thus, measured yield points of lead and lead alloys depend on the duration of the test and the strain rate. The tensile strength of lead drops with a decreasing strain rate, and with longer duration tests, it approaches the creep strength/creep limit (Guruswamy, 2000).

A graph showing the variation of the ultimate tensile strength of lead with the speed of testing can be found on p. 198 of Hofmann (1970) who also reports (p. 190) that "the occurrence of recrystallization can also be discerned, in part, in the tensile test diagrams"

of p. 198. It is evident in those diagrams that there is a testing speed above which the strength of the lead ceases to depend on the strain rate. For refined lead that strain rate is approximately 0.017 sec^{-1} (refined pure lead has a minimum purity of 99.97% according to ASTM International, Annual Book of ASTM Standards (2005), Vol. 02.04, Designation B29-03, p. 8). No temperature of testing is reported but it would be reasonable to assume that the tests took place at room temperature. In other words, the strain rate beyond which the rate effects disappear is assumed to be 0.017 sec^{-1} at room temperature (20^{0}C).

The reason why in slow tests the strength is lower should be, at least in part, the occurrence of recrystallization during testing. As already mentioned, recrystallization of lead is easily triggered even at room temperature. Recrystallization cancels, at least to some degree, strain hardening and thus in slow tests, where there is enough time for its effects to commence, lead appears to be less strong than in the case of fast tests. The strain rate value beyond which the rate effects disappear should be temperature dependent and should increase as the temperature increases because higher temperatures result in faster recrystallization. It is reminded that increasing the temperature favors and accelerates recrystallization, thus a higher speed of testing would be necessary at high temperatures in order to overcome the softening caused by recrystallization (so that there is not enough time for the material to start recrystallizing).

Data showing the effect of temperature on the ultimate tensile strength (UTS) of lead is given on pp. 198-199 of Hofmann (1970). The trend is clear: higher temperature corresponds to lower tensile strength for lead. Table 2-1 reproduces the data from p. 199

of Hofmann (1970). Another set of strength-temperature data for chemical lead (99.9% purity) is presented in Table 2-2 (data reproduced from p. 502 of American Society for Metals, 1979).

TABLE 2-1 Ultimate Tensile Strength of Lead as Function of Temperature (Data Obtained from Hofmann, 1970) (Unknown Lead Purity; Unknown Strain Rate)

Temperature (^{0}C)	20	82	150	195	265
Tensile Strength (MPa)	13.2	7.8	4.9	3.9	2.0

TABLE 2-2 Ultimate Tensile Strength of Lead as Function of Temperature (Data Obtained from American Society for Metals, 1979) (99.9% Lead Purity; Unknown Strain Rate)

Temperature (^{0}C)	38	66	93	121	149	177
Tensile Strength (MPa)	15.5	13.1	10.3	9.3	7.2	4.8

It would be useful to review and attempt to evaluate together data on the temperature effects and data on the rate effects upon the tensile strength of lead. The graphs in Figure 2-1 attempt to give an idea of how a combined strength vs. temperature vs. strain rate graph should look like according to the separate (and sort of limited) data provided by Hofmann (1970).
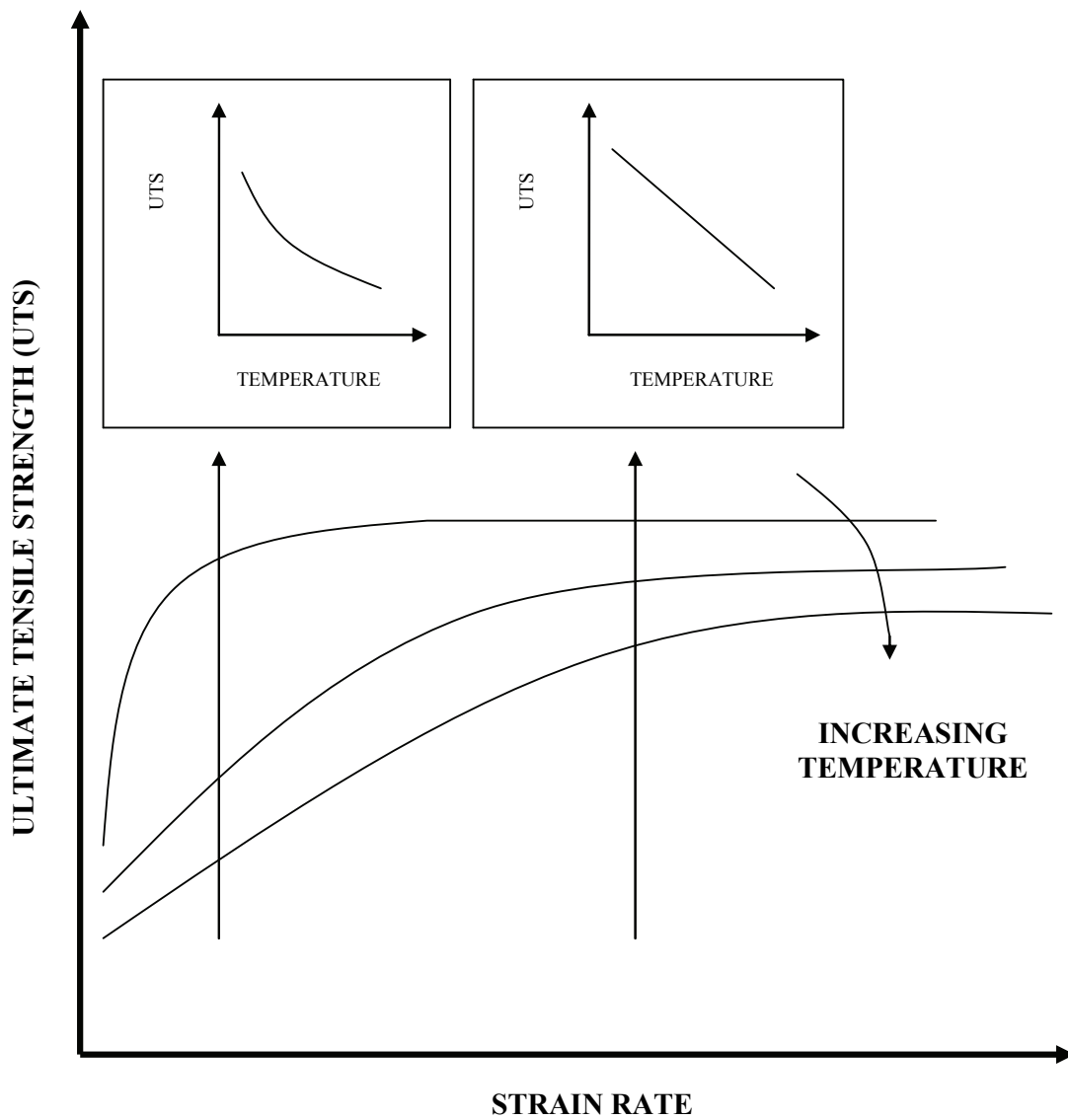
FIGURE 2-1 Trends of the Effects of Strain Rate and Temperature on the Tensile Strength of Lead

2.5 Testing of Lead Specimens

The main purpose of the tests was to investigate the effect of temperature on the ultimate tensile strength (UTS) of lead. The testing aimed at establishing a relationship between the UTS of lead and temperature and checking any effects of strain rate on the behavior of lead complementary to the information provided in the preceding sections. The ultimate tensile strength is studied because it is clearly defined, whereas other properties such as the yield strength cannot be defined uniquely for lead. It is presumed herein that the ultimate strength bears a relation with the "effective yield stress" used for lead-rubber bearings.

The results of these tests are to be evaluated along with the information and data already presented and should lead to the adoption of a UTS vs. temperature relationship. This relationship may then be used in analyses attempting to predict the temperature of the lead core and, consequently, the characteristic strength of a lead-rubber bearing subjected to cyclic motion.

In order to determine a relationship between the strength of lead and temperature, a series of tension tests were conducted at two different speeds and at various values of temperature using standard specimens of lead of 99.99% purity of the dimensions shown in Figure 2-2 (where $A=100$ mm, $B=20$ mm, $C=20$ mm, $D=12.7$ mm, $L=140$ mm). Also see ASTM International, Annual Book of ASTM Standards (2005), Vol. 03.01, Designation E8-04, p. 68, Specimen 3.
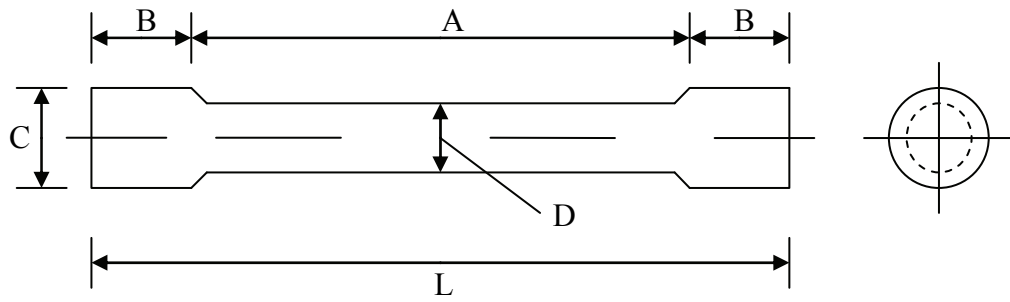
FIGURE 2-2 Lead Specimen Geometry (ASTM International, 2005)

An MTS axial-torsion machine was used for the tests. Three thermocouples (model No. TT-T-24 from Omega Engineering) were placed on the specimen as shown in Figure 2-3 to measure its temperature. They were labeled 1 to 3 from top to bottom of the specimen. Note that the specimen is shown with sleeves at both ends used for securing it in the grips of the test machine. These sleeves held the specimen by pressure instead of a threaded connection that would have caused failure of the specimen in the grips rather than the specimen body.
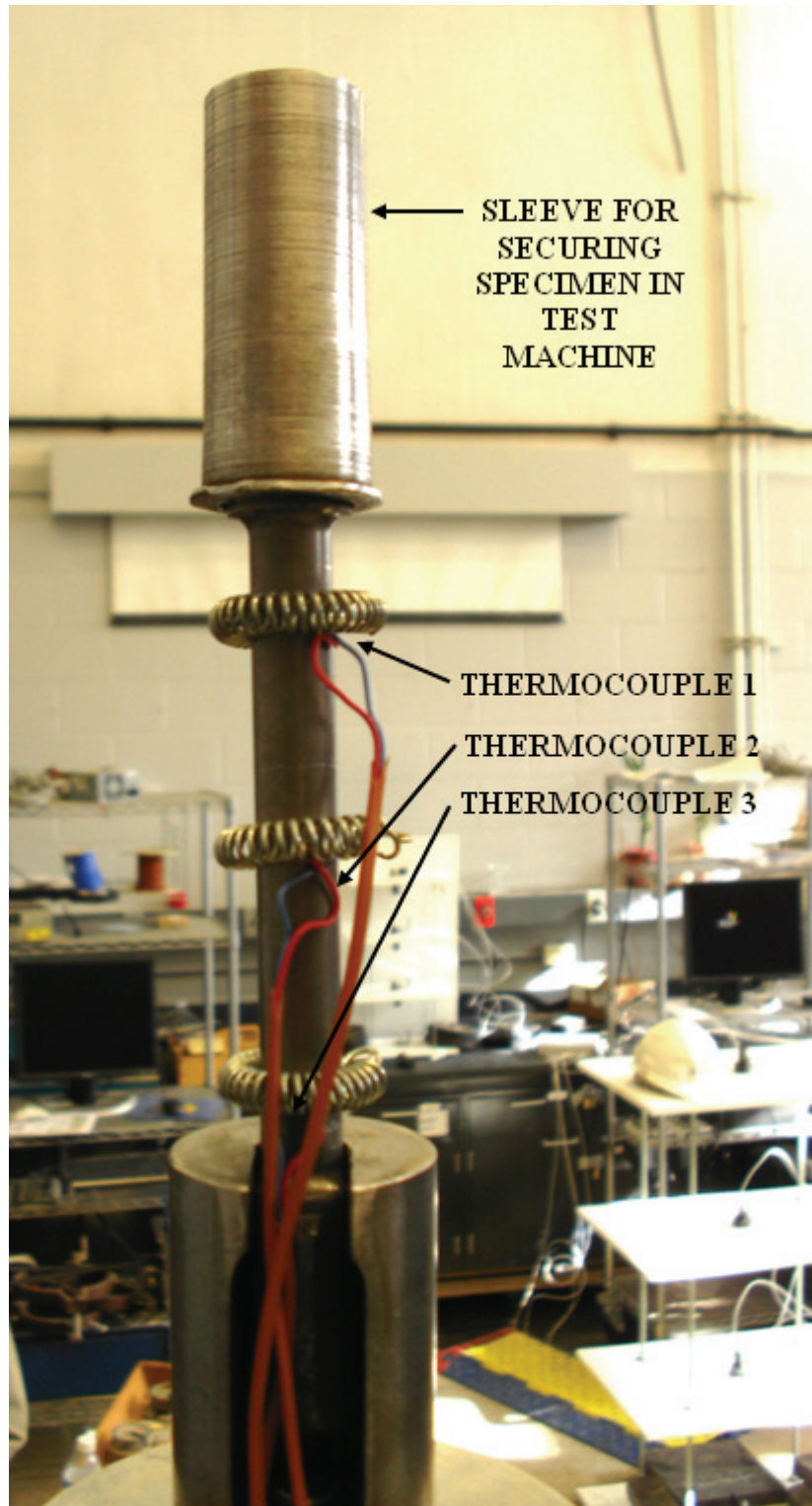
FIGURE 2-3 Lead Specimen with Thermocouples

The maximum testing speed that the machine could achieve is approximately 50 mm/s. Two testing speeds were selected: a low one (0.75 mm/s – corresponding to a tensile strain rate of 0.0075 sec^{-1}) and a high one (25 mm/s – corresponding to a tensile strain rate of 0.25 sec^{-1}).

Heating of the specimens was achieved by placing them inside the insulated heating element shown in Figure 2-4. The element consisted of a metal cage surrounded by a heating tape and insulating material. For the cases of low temperature testing (two cases – see Table 2-3) the same element was used with the specimen placed inside a tube with holes and dry ice placed between the tube and the metal cage creating a refrigerator (see Figure 2-4). The testing process may be briefly described as follows.

Tension testing began once the temperature was stabilized and relatively homogeneous among the three thermocouples. Results from testing a total of 8 lead specimens are presented in Figures 2-5 and 2-6 (stress-strain plots) and Table 2-3 (strength data). Stress was defined as the applied force divided by the original specimen area and strain was defined as the total change of length of the specimen (measured as motion of the machine head) divided by the length of the reduced section of the specimen (100 mm). Note that the strain rate of 0.25/sec was achieved by imposing motion of constant speed to the specimen on one side equal to 25 mm/sec (25 mm/sec divided by length of 100 mm=0.25/sec). This strain rate is average over the length of the specimen. Similarly, a speed of 0.75 mm/sec was imposed for an average rate of strain of 0.0075/sec. Figure 2-7 shows all strength data that have been presented in this section (Hofmann, 1970; American Society for Metals, 1979; authors' experiments) combined into one graph.

The test data demonstrate that the ultimate strength increases with increases in strain rate. As discussed earlier, this is due to the fact that during a tensile test the deformed specimen begins to recrystallize before failure, especially at low testing speeds and high temperatures. In such cases, the effect of strain hardening should be counteracted by the ongoing recrystallization, thus resulting in lower tensile strength values.

The results presented here are discussed in further detail as well as in connection with the phenomenon of lead core heating in Section 3. At this point only the resemblance of the graphs in Figure 2-7 to those of Figure 2-1 is being mentioned; this resemblance may be considered a confirmation of the assumption that the rate dependence of the strength of lead arises, at least in part, from the occurrence of recrystallization and the dependence of its effects on the duration of testing.

In summary, the following aspects of behavior of lead are important:

(a) The ultimate tensile strength of lead decreases in approximately linear fashion with increasing temperature at high strain rates and decreases in a nonlinear fashion at low strain rates.

(b) The existence of impurities increases the ultimate tensile strength of lead.

(c) The ultimate tensile strength of lead drops as the size of its grains increases.

(d) Plastic strain causes the ultimate tensile strength of lead to increase (strain hardening).

(e) Increasing the strain rate causes the strength of lead to increase but this effect disappears beyond a likely temperature-dependent limit value of strain rate. At temperature of about 20^0C this limit is 0.017/sec.

(f) Recrystallization of lead may be triggered even at low temperatures because of the low melting point of lead. Recrystallization is favored by higher temperatures and higher plastic strains and inhibited by impurities.

(g) Recrystallization makes lead more ductile but less strong by canceling the effects of plastic deformation on the microstructure of the material.
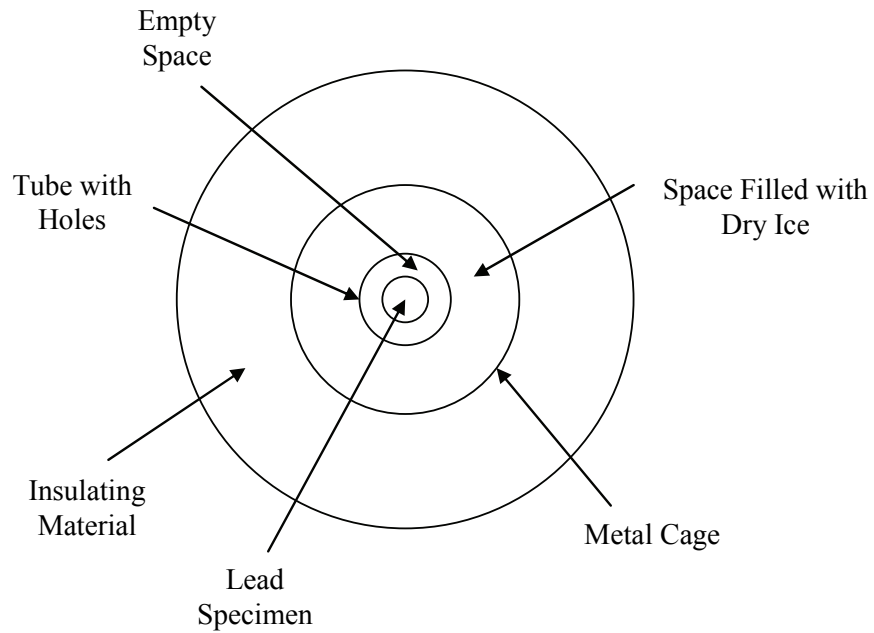
FIGURE 2-4 Heating Element Used for Controlling the Temperature of Lead Specimens for High Temperature Tests (Top) and Schematic of Testing Configuration (Top View) for Low Temperature Tests (Bottom)

TABLE 2-3 Values of Ultimate Tensile Strength of Lead

Specimen No.	Temperature (^{0}C)	Strain Rate (sec^{-1})	Ultimate Tensile Strength (MPa)
1	56	0.25	19.0
2	20	0.25	21.8
3	138	0.25	13.3
4	-30	0.25	27.2
5	-30	0.0075	24.1
6	20	0.0075	18.1
7	101	0.0075	9.9
8	99	0.25	15.3
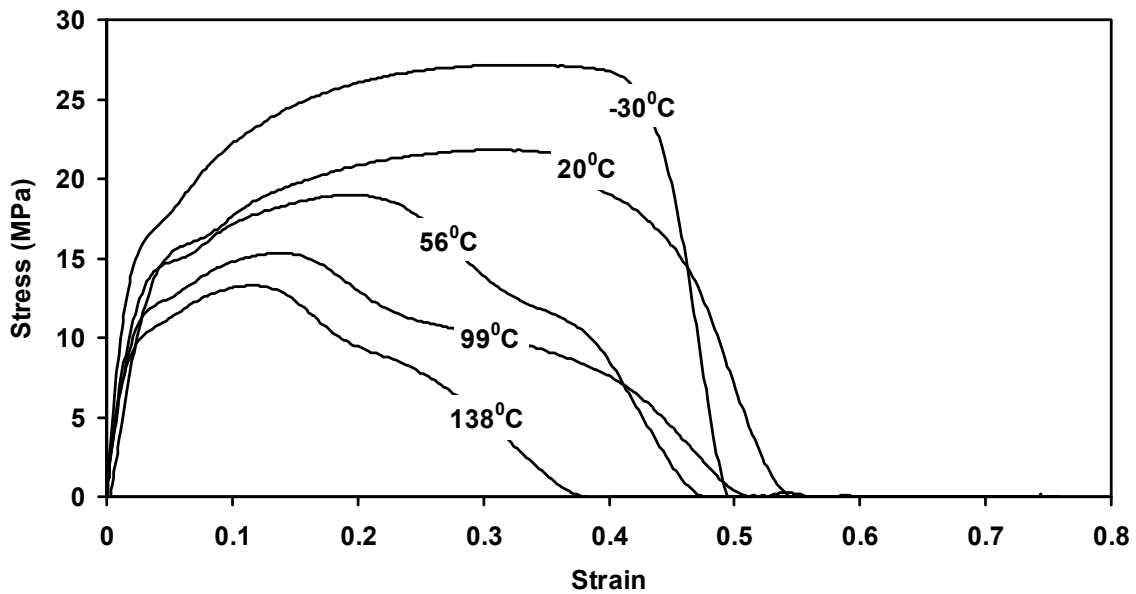
FIGURE 2-5 Stress-Strain Relation of Lead at 0.25/sec Strain Rate (Fast Tests)
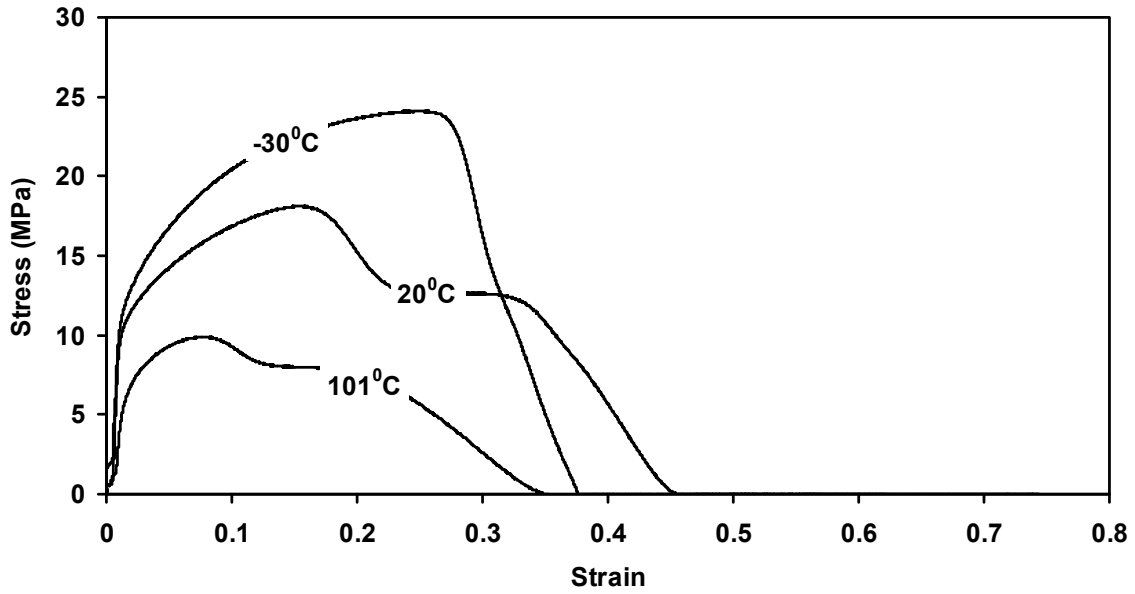
FIGURE 2-6 Stress-Strain Relation of Lead at 0.0075/sec Strain Rate (Slow Tests)
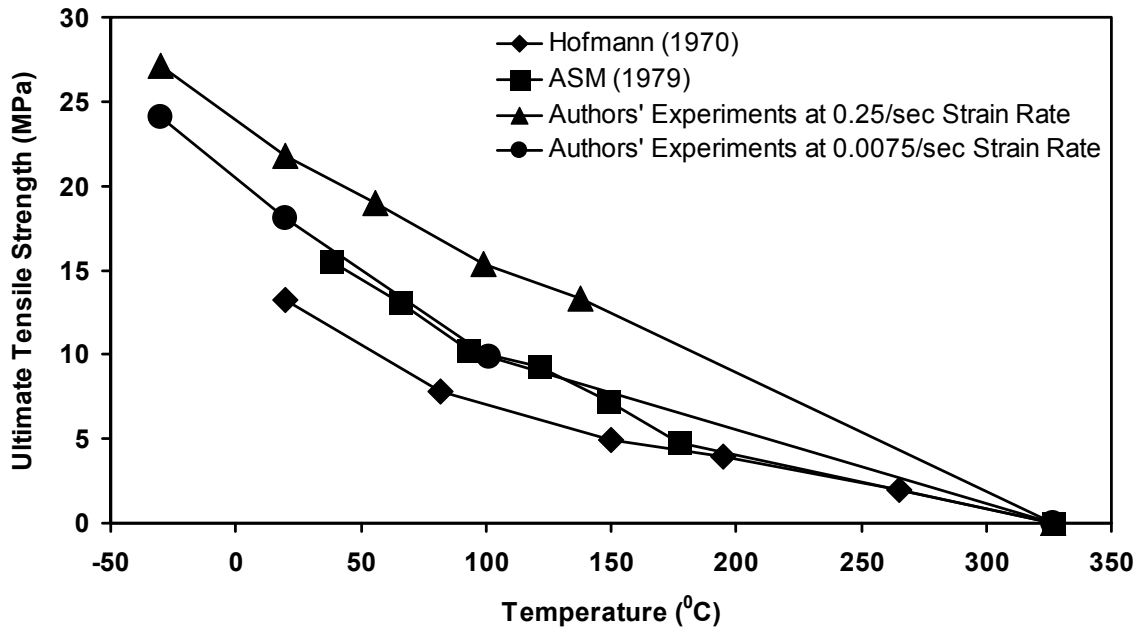
FIGURE 2-7 Ultimate Tensile Strength of Lead as Function of Temperature and Strain Rate

SECTION 3

HEATING OF LEAD-RUBBER BEARINGS – THEORY

3.1 Introduction

When a lead-rubber bearing is subjected to lateral cyclic motion, heat is generated, primarily in the lead core, from where it flows vertically and radially into the steel end and shim plates, respectively. Heat is also generated in the rubber but this is typically small and can be ignored (Constantinou et al., 2007b).

It is well established that the energy dissipated per cycle and the characteristic strength of lead-rubber bearings reduce with an increasing number of cycles. The reduction is substantial in the first few cycles of motion. For example, Figure 1-5 presents the energy dissipated per cycle of the large size lead-rubber bearing of Figure 1-4. The testing was conducted under dynamic conditions with a peak velocity of nearly 1 m/sec. Figure 1-5 shows both the measured dissipated energy and the estimated contribution to the dissipated energy by the lead core. For this calculation, it was assumed that the rubber contribution to the equivalent viscous damping ratio or effective damping of the bearing is 0.04.

It is clear from this figure that there is a substantial reduction in energy dissipation per cycle in the initial cycles after which the energy dissipated per cycle tends to stabilize. A brief interruption of the testing and a restart, results in an almost complete recovery of the original energy dissipation per cycle. These observations clearly demonstrate that the reduction in the energy dissipation per cycle is the result of heating of the lead core. The

core will reach a near constant temperature after a number of cycles when the rate of heat generation is equal to the rate of heat lost by conduction through the steel plates. The near complete recovery after the 2-minute interruption in the testing clearly demonstrates the significance of heat conduction.

The thermal properties of lead, rubber and steel are given in Table 3-1, which presents data obtained from several sources (American Society for Metals, 1991; American Society for Metals, 1992; Lide, 1993; Hofmann, 1970 and Guruswamy, 2000). Note that thermal properties of lead are practically unaffected by temperature up to the melting point. Another important observation is that rubber has a much lower thermal conductivity and thermal diffusivity than either lead or steel. Accordingly, it may be assumed that heat conducts entirely through the steel shim plates and the steel end plates of the bearing.

TABLE 3-1 Properties of Lead, Steel and Rubber

Temperature (^{0}C)	-25	25	75	125	225	327[1]
Thermal Conductivity[2], k (W/(m ^{0}C))						
Lead[3]	36.0	35.3	34.7	34.0	32.8	31.4
Rubber	-	0.16	-	-	-	-
Carbon Steel[4]	-	54.0	53.0	51.0	47.0	44.0
Thermal Diffusivity[2], α (m^2/s)						
Lead[3]	-	2.42×10^{-5}	2.34×10^{-5}	2.29×10^{-5}	2.14×10^{-5}	2.00×10^{-5}
Rubber	-	7.24×10^{-8}	-	-	-	-
Carbon Steel[4]	-	1.48×10^{-5}	-	-	-	-
Specific Heat[2], c (J/(kg ^{0}C))						
Lead[3]	127	129	131	132	137	142
Rubber	-	1700	-	-	-	-
Carbon Steel[4]	-	450	-	-	-	-
Density[2], ρ (kg/m^3)						
Lead[3]	-	11360	11300	11240	11170	11000
Rubber	-	1300	-	-	-	-
Carbon Steel[4]	-	7900	-	-	-	-

1. Temperature just prior to melting of lead

2. $k = \alpha \rho c$

3. 99.99% pure lead

4. Less than 0.5% carbon

3.2 Dependence of the Effective Yield Stress on Temperature

The reduction in the energy dissipation per cycle is the result of the reduction in the effective yield stress of lead with increasing temperature. The effective yield stress of lead has been defined in Section 1.

The yield stress of lead cannot be accurately measured due to the tendency of the material to creep; also see Section 2 for a brief description of the complexity of lead plastic behavior. However, the ultimate strength (which should be somehow related to the effective yield stress) can be measured and representative data have been shown in Figure 2-7.

The lead core absorbs energy by resisting motion, so the heat produced within the lead core is in fact the work of the resisting force in the core. This force is the product of the effective yield stress and the cross-sectional area of the lead core. The experimental results presented in Figure 1-5 show a gradually decreasing energy dissipated per cycle (EDC), thus implying that the effective yield stress σ_{YL} drops as the temperature of the lead plug increases. There are no direct data for such a relationship between σ_{YL} and temperature. A reasonable assumption would be to consider that the ratio of the effective yield stress of lead σ_{YL} to the ultimate stress of lead σ_{ult} is constant at all temperatures.

That is, assuming that σ_{ult} is a function $f(T_{Lt})$, then

$$\frac{\sigma_{YL}}{\sigma_{YL0}} = \frac{f(T_{Lt})}{f(T_{L0})} \tag{3-1}$$

where σ_{YL} is the effective yield stress at temperature of lead T_{Lt} and σ_{YL0} is the initial effective yield stress, defined as the effective yield stress at the initial (or starting) temperature T_{L0}. The ratio σ_{YL}/σ_{YL0} in (3-1) will be referred to as the normalized effective yield stress. In order to establish a relation between σ_{YL} and temperature, one should determine a relationship between σ_{ult} and temperature and have an estimate of the initial effective yield stress σ_{YL0}.

There are four sets of experimental data on the ultimate tensile strength in Figure 2-7. On the basis of these data, the relationship between σ_{ult} and the temperature of lead, T_{Lt}, could be either exponential or linear as described by (3-2) and (3-3), respectively:

$$\sigma_{ult} = E_1 \cdot \exp(- E_2 \cdot T_{Lt}) \qquad (3\text{-}2)$$

$$\sigma_{ult} = L_2 - L_1 \cdot T_{Lt} \qquad (3\text{-}3)$$

The parameters in (3-2) and (3-3) were determined by best fitting the available data on σ_{ult} and temperature. Table 3-2 summarizes information on the best fitting curves for the four sets of data and Figures 3-1 to 3-4 compare prediction by (3-2) and (3-3) to the test data. There are two advantages that favor the use of an exponential relationship between σ_{YL} and temperature against the use of a linear or bilinear one. The important parameter in predicting the characteristic strength of lead-rubber bearings is the normalized effective yield stress presented in (3-1). When using the exponential and linear expressions for the ultimate stress, equation (3-1) becomes, respectively:

$$\frac{\sigma_{YL}}{\sigma_{YL0}} = \exp(-E_2 \cdot T_L) \qquad\qquad (3\text{-}4)$$

$$\frac{\sigma_{YL}}{\sigma_{YL0}} = \frac{L_2 - L_1 \cdot T_{Lt}}{L_2 - L_1 \cdot T_{L0}} \qquad\qquad (3\text{-}5)$$

The advantage in using the exponential expression is seen in the facts that (a) only the increase in temperature of the lead T_L appears and (b) only one parameter (E_2) is needed to describe the ratio of strengths. However, the exponential relation is valid in a range of temperatures (based on Figure 3-4 it is valid in the range of -30^0C to 270^0C) although this does not matter since temperatures beyond 270^0C are never reached.

TABLE 3-2 Information on Best Fitting Curves for the Four Sets of Experimental Data on Ultimate Tensile Strength of Lead (Temperature in ^{0}C, Stress in MPa)

Case	Curve	Parameters
Hofmann (1970)	Exponential I	$E_1 = 15.245$, $E_2 = 0.0075$
ASM (1979)	Exponential II	$E_1 = 22.054$, $E_2 = 0.0080$
Authors' at Strain Rate=0.25/sec	Linear	$L_1 = 7.39 \times 10^{-2}$ $L_2 = 23.61$
Authors' at Strain Rate=0.0075/sec	Bilinear	$L_1 = 1.08 \times 10^{-1}$ and $L_2 = 20.64$ for $T_{Lt} < 100^0 C$ $L_1 = 4.38 \times 10^{-2}$ and $L_2 = 14.32$ for $T_{Lt} > 100^0 C$
Authors' at Strain Rate=0.0075/sec	Exponential III	$E_1 = 20.051$, $E_2 = 0.0069$
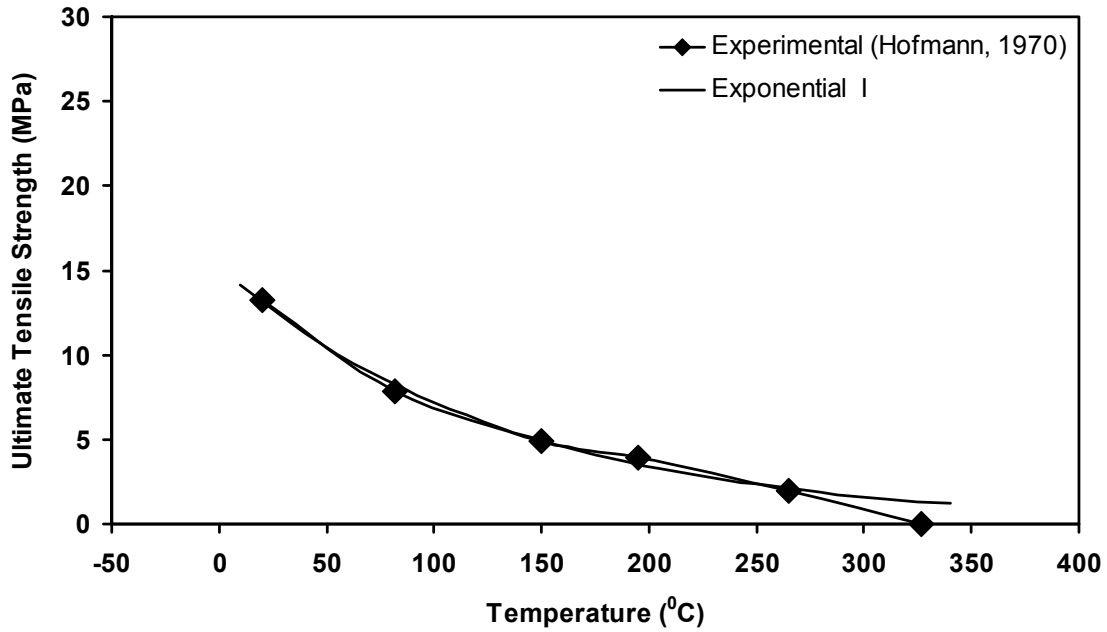
FIGURE 3-1 Relation Between Ultimate Tensile Strength of Lead and Temperature Based on Data of Hofmann (1970)
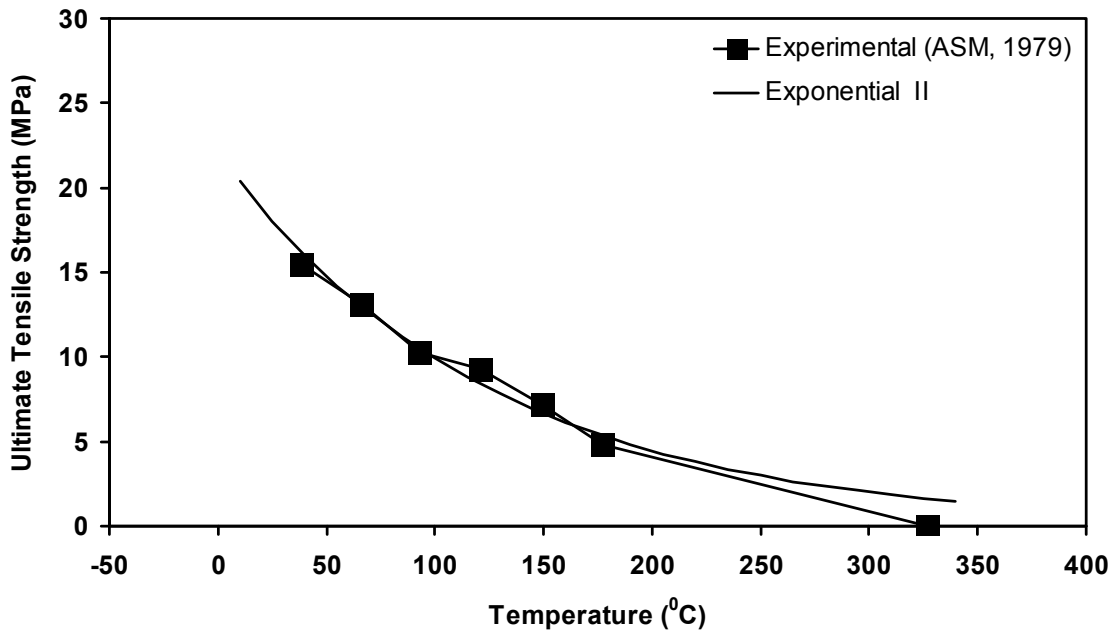
FIGURE 3-2 Relation Between Ultimate Tensile Strength of Lead and Temperature Based on Data of ASM (1979)
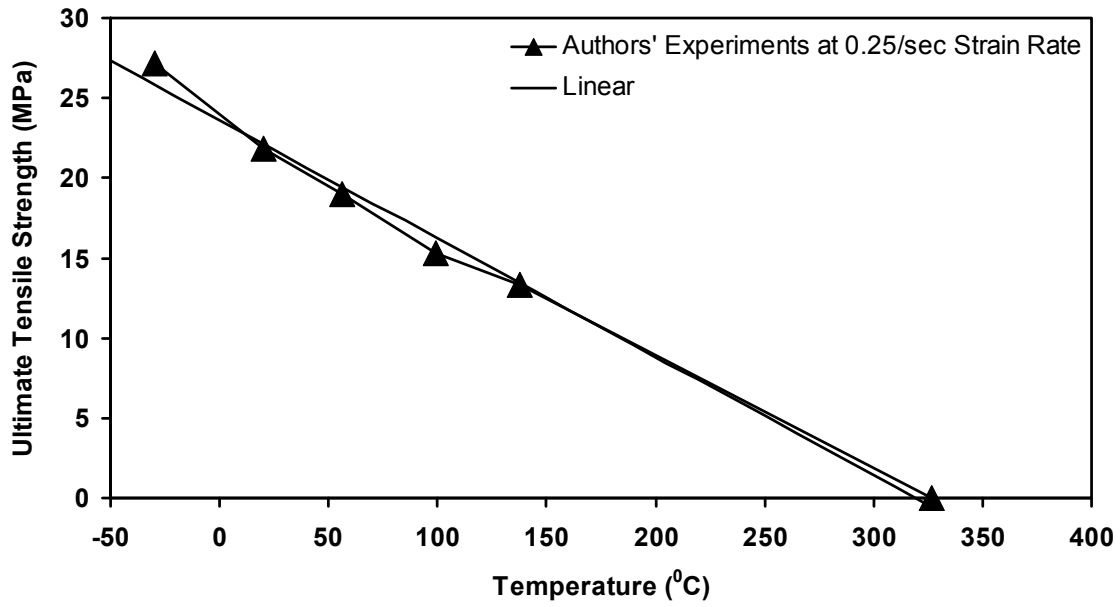
FIGURE 3-3 Relation Between Ultimate Tensile Strength of Lead and Temperature Based on Authors' Experiments at 0.25/sec Strain Rate
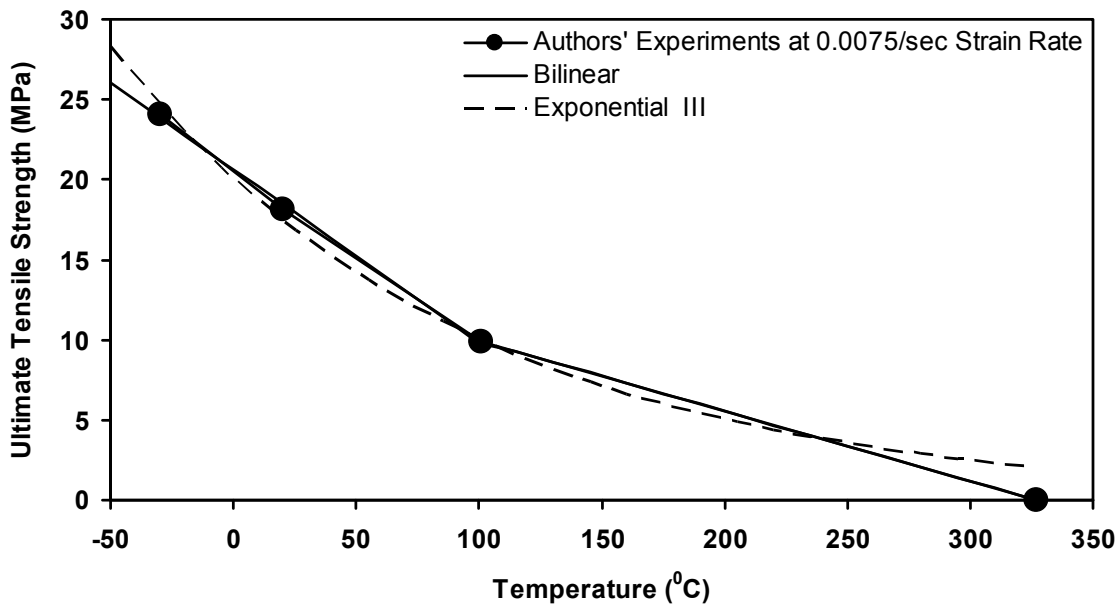
FIGURE 3-4 Relation Between Ultimate Tensile Strength of Lead and Temperature Based on Authors' Experiments at 0.0075/sec Strain Rate

The reference (i.e. initial/at ambient temperature) effective yield stress σ_{YL0} in equation (3-1) cannot be directly obtained in testing. For example consider the bearing of Figure 1-4 and assume that the experiment started when the temperature of the bearing was 20^0C. When the measurement of the energy dissipated per cycle (EDC) was first made after one cycle, the temperature was certainly higher than 20^0C. Therefore, the data of the first cycle cannot be used to estimate σ_{YL0}. However, extrapolation of the EDC data to the hypothetical value of zero cycles provides a useful estimate of σ_{YL0}. From Figure 1-5, the value is EDC=375 kN-m. Based on the bilinear force-displacement relation of Figure 1-3, the EDC is given by

$$EDC = 4 \cdot Q_d \cdot (D - Y) \tag{3-6}$$

where D is the amplitude of motion, Y is the yield displacement and Q_d is the characteristic strength of the bearing defined in (1-1).

Using equations (3-6) and (1-1) with an assumed yield displacement $Y=12$ mm, a value of $\sigma_{YL,0}=12.8$ MPa for the hypothetical "0th" cycle is obtained for the bearing of Figure 1-4 and the testing speed and amplitude given in Figure 1-5. This value corresponds to the "average" value of σ_{YL} during the "0th" cycle while with a similar process we may calculate the "average" value of σ_{YL} during the 1st cycle of motion, $\sigma_{YL,1}$. The sought value of σ_{YL0} at the beginning of testing (end of "0th" cycle and start of 1st cycle) may then be estimated by averaging $\sigma_{YL,0}$ and $\sigma_{YL,1}$.

3.3 Modeling

We seek either a closed-form solution or explicit formulations that can be numerically solved to compute the temperature rise in a lead core and the reduction in characteristic strength of lead-rubber bearings under cyclic loadings. Modeling and solutions are presented herein. Two different approaches are considered (energy approach and constant flux approach), followed by an attempt to nondimensionalize the basic equation of the problem and a simplification for cases of insignificant heat conduction.

Analysis of the problem of the temperature rise in lead-rubber bearings requires the solution of the problem of conduction of heat in a composite cylinder. Consider a lead-rubber bearing with bonded rubber radius R, lead core radius a, end plate thickness t_p and total shim plate thickness t_s. An appropriate model would be the one shown in Figure 3-5 with zero initial increase in temperature (i.e., initial temperature equal to the initial temperature, T_{L0}). Heat is generated inside the lead core at a rate of $q'''(t)$ (heat production rate per unit volume of lead) and is conducted outward through the end plates (of thickness t_p each) and the shim plates (of total thickness t_s). Let q_1 be the amount of heat flowing per unit time through one of the end plates and q_2 be the amount of heat flowing per unit time through the shim plates (note that the shims are treated as a unity, being modeled as a hollow cylinder with inner radius equal to a, outer radius equal to R and thickness equal to the combined thickness of all shims, t_s).
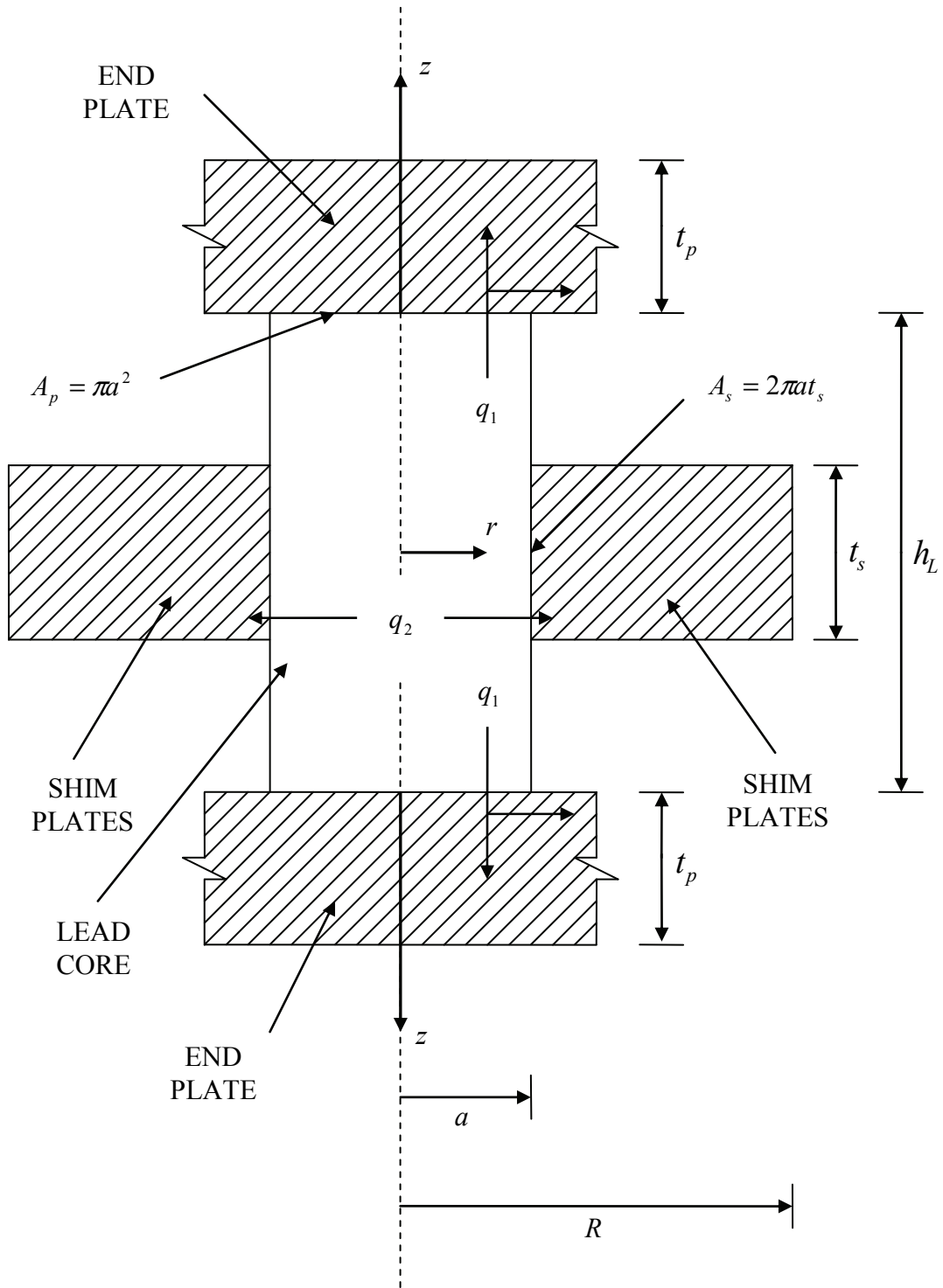
FIGURE 3-5 Model for the Analysis of Heat Conduction in Lead-Rubber Bearings

The heat production rate $q'''(t)$ is given by

$$q'''(t) = \frac{\left| \sigma_{YL} \cdot A_L \cdot \frac{du}{dt} \right|}{V_L} = \frac{\sigma_{YL} \cdot \left| \frac{du}{dt} \right|}{h_L} \qquad (3\text{-}7)$$

where h_L is the height of the lead core, $u(t)$ is the history of motion of the top of the lead core with respect to its bottom (or the history of motion of the lead-rubber bearing), A_L and V_L are the cross-sectional area and volume of the lead core, respectively, and the other terms have already been defined.

The following basic assumptions are made:

a) The increase in the temperature of lead T_L (measured with respect to the initial temperature) is only a function of time (that is, there is no space variability) with the exception of two small transition layers at the end plates-lead core interface and shim plates-lead core interface. The interface temperature increases are assumed to be half the increase in temperature in the bulk of the lead core, T_L. See Figure 3-6 (a definition of T_{ave} is given later in this section).

b) Convection and radiation at the free boundaries are neglected.

c) There is perfect contact between the lead core and the steel plates at their interface; that is, the increase in temperature of the lead core is equal to the increase in temperature of the end plates, T_p, and shim plates, T_s, at their points of contact. This increase in interface temperature is half of the increase in the temperature of lead T_L as mentioned before.

44

d) Conduction is the major mechanism of heat transfer and the solid is treated as stationary with a heat production rate inside the lead core equal to the rate of energy dissipation within the lead core given by (3-7). Heat conduction is through the end plates (one-dimensional in the vertical direction) and shim plates (one-dimensional in the radial direction).

e) There is no conduction of heat through the rubber layers. This is a reasonable assumption given that rubber has a thermal conductivity much lower than that of steel.

f) Both the top and bottom end plates of the bearing are considered to be in contact with a large volume of steel as was, in fact, the case for all the experimental results presented later on. The case of end plates being in contact with concrete needs separate treatment considering different boundary conditions (e.g., insulated outer ends of end plates).

g) The following two types of solutions are considered:

   i. There is no heat conduction through the steel plates, i.e. all the heat which is dissipated by the lead core is consumed in elevating its temperature.

   ii. There is conduction through the steel plates, however there is unlimited volume of steel for the "heat front" to expand in both the end and the shim plates. Then, the quantities t_{pf} and R_f represent the distance of the "heat front" in the end plates from the lead core and in the shim plates from the center of the bearing, respectively.
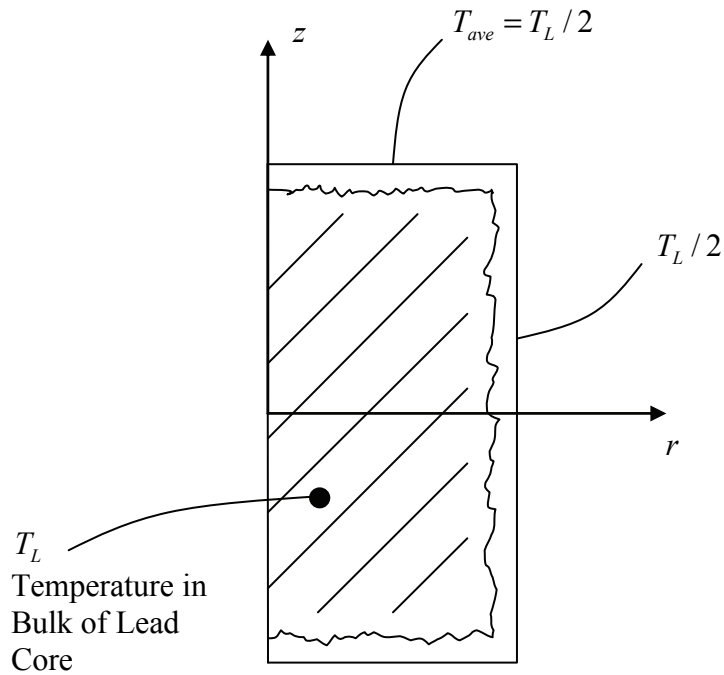
FIGURE 3-6 Assumed Lead Core Temperature Distribution

3.3.1 The Energy Approach

The solution for the problem of the temperature rise of the lead core requires that the position of the heat front in the end plates is determined as a function of time. (Herein, the term "heat front" is used to denote the boundaries of a volume in the end plates and in the shim plates where the temperature increase is non zero. This volume is used in the calculation of energy stored in the plates for the energy approach to the solution of this problem). In the solution presented herein, this position is determined based on energy principles, hence the term "Energy Approach".

The thermal equation for the lead core is

$$\rho_L \cdot c_L \cdot V_L \frac{dT_L}{dt} = q'''(t) \cdot V_L - 2 \cdot q_1(t) - q_2(t) \tag{3-8}$$

where ρ_L is the density of lead and c_L is the specific heat of lead. It is important to note that the density and the specific heat of lead are practically unaffected by the temperature (see Table 3-1). Although the volume V_L of the lead core slightly increases as the lead core is heated, we assume in the analysis that it remains constant.

Heat flux q_1 is given by

$$q_1(t) = -k_S \cdot A_p \cdot \left. \frac{\partial T_p}{\partial z} \right|_{z=0} \tag{3-9}$$

Heat flux q_2 is given by

$$q_2(t) = -k_S \cdot A_s \cdot \left. \frac{\partial T_s}{\partial r} \right|_{r=a} \tag{3-10}$$

In the above equations, $A_p (= \pi a^2)$ is the area of the end plate in contact with the lead plug and $A_s (= 2\pi a t_s)$ is the inside area of the shim plates imaginary hollow cylinder (see Figure 3-5). Solution of (3-8) for the lead core temperature rise T_L requires first that the heat fluxes q_1 and q_2 be obtained by solving the individual problems for the end plates and the shim plates.

The thermal equation for the end plates is

$$\frac{\partial^2 T_p}{\partial z^2} = \frac{1}{\alpha_S} \frac{\partial T_p}{\partial t} \qquad (3\text{-}11)$$

where $T_p(z,t)$ is the increase in temperature of the end plates and α_S is the thermal diffusivity of the end plate material (steel).

The thermal equation for the shim plates is

$$\frac{\partial^2 T_s}{\partial r^2} + \frac{1}{r} \frac{\partial T_s}{\partial r} = \frac{1}{\alpha_S} \frac{\partial T_s}{\partial t} \qquad (3\text{-}12)$$

where $T_s(r,t)$ is the increase in temperature of the shim plates and α_S is the thermal diffusivity of the shim plate material (steel).

Ozisik (1989; 1993) presented solutions to the general problems of the one-dimensional heat conduction through a slab and the one-dimensional heat conduction through a hollow cylinder for all possible combinations of boundary conditions. In both cases the solution may be separated into two parts, a steady-state part and a transient part that decays exponentially with time. Ignoring the transient parts in all cases, we may assume a logarithmic distribution of temperature inside the shim plates and a linear distribution inside the end plates. Also the following boundary and initial conditions are assumed. It should be noted that these conditions imply a non-uniform distribution of temperature in the lead core that is consistent with observations in finite element analyses.

$$T_p(0,t) = \frac{T_L(t)}{2} \qquad (3\text{-}13)$$

48

$$T_p(t_{pf},t) = 0 \qquad\qquad (3\text{-}14)$$

$$T_p(z,0) = 0 \qquad\qquad (3\text{-}15)$$

$$T_s(a,t) = \frac{T_L(t)}{2} \qquad\qquad (3\text{-}16)$$

$$T_s(R_f,t) = 0 \qquad\qquad (3\text{-}17)$$

$$T_s(r,0) = 0 \qquad\qquad (3\text{-}18)$$

where, as already discussed, $t_{pf}(t)$ and $R_f(t)$ are time-dependent variables controlling the location of the heat front in the end and shim plates respectively.

Note that (3-14) and (3-17) presume that the heat front is within the bulk of the steel end plates and shims and did not yet reach the boundaries. Finite element analyses to be reported later in this work confirm this hypothesis. Hence,

$$T_p(z,t) = \left(1 - \frac{z}{t_{pf}(t)}\right) \cdot \frac{T_L(t)}{2} \qquad\qquad (3\text{-}19)$$

$$T_s(r,t) = \left(\frac{\ln(r/R_f(t))}{\ln(a/R_f(t))}\right) \cdot \frac{T_L(t)}{2} \qquad\qquad (3\text{-}20)$$

The thermal energy stored inside each of the end plates, E_1, is

$$E_1 = \int_0^{t_{pf}(t)} \rho_S \cdot c_S \cdot A_p \cdot T_p(z,t) \cdot dz \qquad (3\text{-}21)$$

and the energy stored in the shim plates, E_2, is

$$E_2 = \int_a^{R_f(t)} \rho_S \cdot c_S \cdot t_s \cdot T_s(r,t) \cdot 2\pi r dr \qquad (3\text{-}22)$$

The assumption is made that the ratio of the instantaneous heat fluxes is equal to the ratio of the stored energies; apparently, the validity of this assumption decreases with time:

$$\frac{q_1}{q_2} = \frac{E_1}{E_2} \qquad (3\text{-}23)$$

Combining (3-9), (3-10), (3-19), (3-20), (3-21), (3-22) and (3-23), a relationship connecting the "heat front" parameters $t_{pf}(t)$ and $R_f(t)$ can be evaluated as

$$2 \cdot \left(\frac{t_{pf}}{a}\right)^2 = \left(\frac{R_f}{a}\right)^2 - 1 - 2 \cdot \ln\left(\frac{R_f}{a}\right) \qquad (3\text{-}24)$$

Equation (3-24) is essentially a linear relationship between R_f/a and t_{pf}/a when the latter is in the range of nearly zero to 4. For simplicity, (3-24) is approximated by the simpler expression

$$\left(\frac{R_f}{a}\right) = 1 + 1.2\left(\frac{t_{pf}}{a}\right) \qquad (3\text{-}25)$$

which compares very well with (3-24) as seen in Figure 3-7 particularly for the typical range of 0 to 2 for t_{pf}/a.
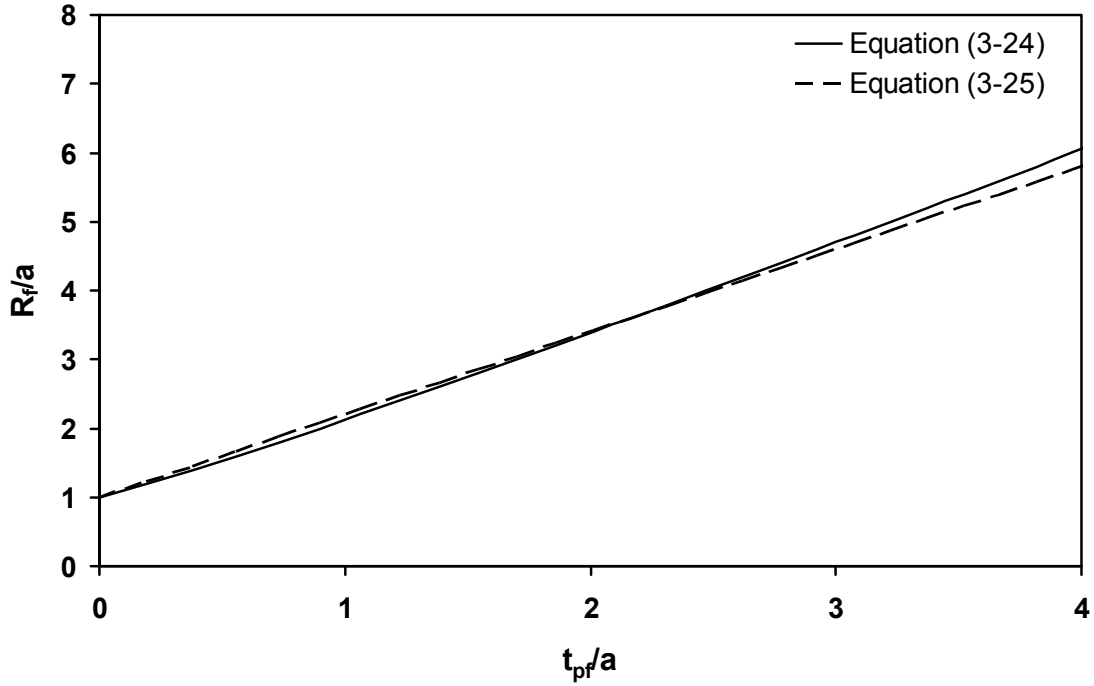
FIGURE 3-7 Relationships Between Heat Front Parameters

An energy balance condition is used for calculating the distance $t_{pf}(t)$ of the heat front in the end plates from the lead core. The thermal energy generated inside the lead core is equal to the sum of the thermal energies stored in the lead core and the steel plates. More specifically, we have

$$\int_0^t \sigma_{YL} \cdot A_L \cdot |v(\tau)| \cdot d\tau = T_L \rho_L c_L V_L + 2 \cdot \int_0^{t_{pf}(t)} \rho_S c_S A_p T_p(z,t)dz + \int_a^{R_f(t)} \rho_S c_S t_s T_s(r,t)2\pi r dr \quad (3\text{-}26)$$

which, in turn, due to Equations (3-19), (3-20), (3-24) and (3-25) gives

51

$$\int_0^t \sigma_{YL} |v(\tau)| d\tau = T_L \left\{ \rho_L c_L h_L + \frac{\rho_S c_S}{2} \left[t_{pf}(t) + t_s \frac{\left(\frac{t_{pf}(t)}{a} \right)^2}{\ln\left(1 + 1.2 \frac{t_{pf}(t)}{a} \right)} \right] \right\} \qquad (3\text{-}27)$$

where $v(t)$ is the velocity history and $|v(t)|$ is its magnitude.

Combining (3-8) with (3-7), (3-9), (3-10), (3-19), (3-20) and (3-25) gives

$$(\rho_L \cdot c_L \cdot h_L) \cdot \frac{dT_L}{dt} = \sigma_{YL} \cdot |v(t)| - \frac{k_S \cdot T_L(t)}{t_{pf}(t)} \cdot \left[1 + \left(\frac{t_s}{a} \right) \cdot \frac{\frac{t_{pf}(t)}{a}}{\ln\left(1 + 1.2 \frac{t_{pf}(t)}{a} \right)} \right] \qquad (3\text{-}28)$$

Considering that t_{pf}/a ranges between 0 and 2, (3-27) and (3-28) may be further simplified as follows:

$$\int_0^t \sigma_{YL} |v(\tau)| d\tau = T_L \left\{ \rho_L c_L h_L + \frac{\rho_S c_S}{2} t_{pf}(t) \left(1 + 1.47 \left(\frac{t_s}{a} \right) \right) \right\} \qquad (3\text{-}29)$$

$$(\rho_L \cdot c_L \cdot h_L) \cdot \frac{dT_L}{dt} = \sigma_{YL} \cdot |v(t)| - \frac{k_S \cdot T_L(t)}{t_{pf}(t)} \cdot \left(1 + \left(\frac{t_s}{a} \right) \cdot \left(0.83 + 0.41 \frac{t_{pf}(t)}{a} \right) \right) \qquad (3\text{-}30)$$

The simplification is based on the function $y = x^2 / \ln(1 + 1.2x)$ being approximately equal to $y = 1.47x$ for x between 0 and 2 (see Figure 3-8). Also, function $y = x / \ln(1 + 1.2x)$ is approximately equal to $y = 0.83 + 0.41x$ for the same range of x (see Figure 3-9).
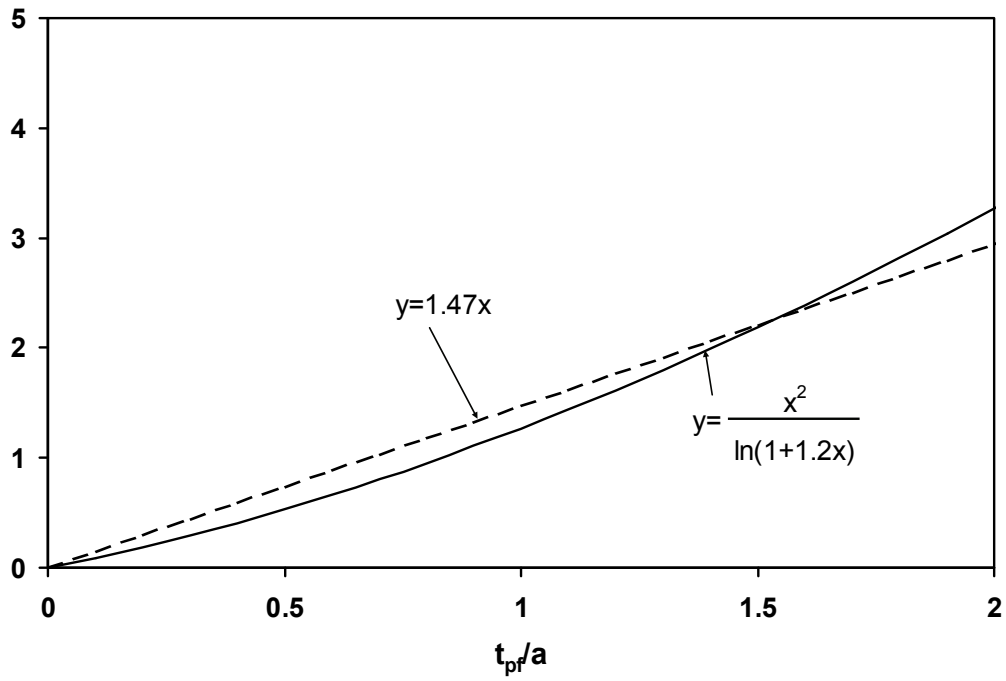
FIGURE 3-8 Simplification Used in Equation (3-27)
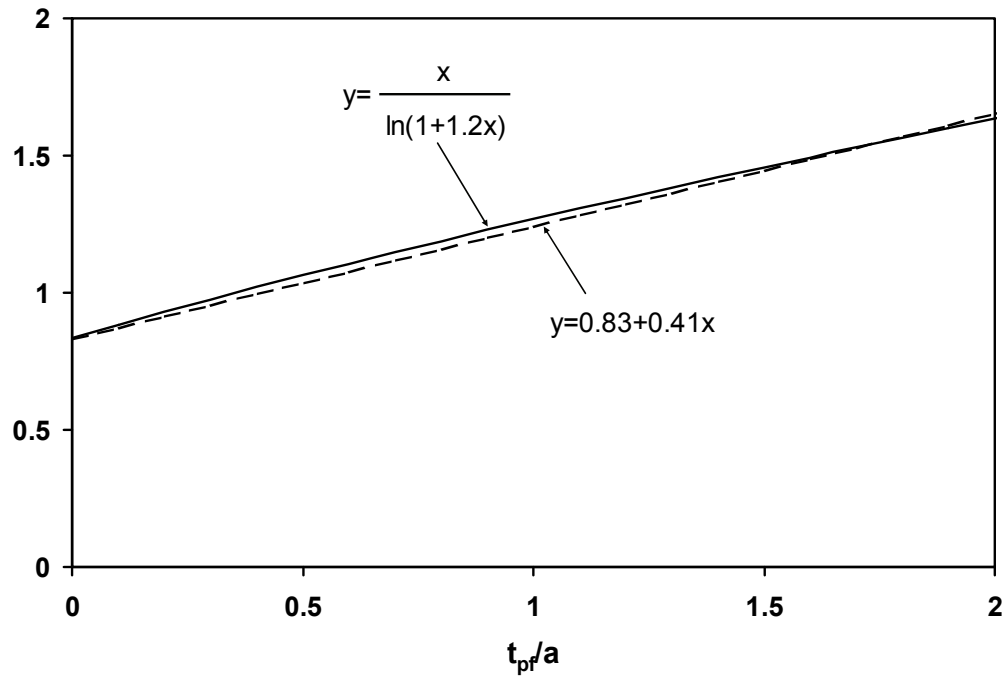
FIGURE 3-9 Simplification Used in Equation (3-28)

53

Equations (3-29) and (3-30) may be used to numerically evaluate the temperature and the strength of the lead core when the lead-rubber bearing undergoes repeated cycling with a velocity history $v(t)$. They also apply for the case of bidirectional motion if one interprets $v(t)$ as the resultant velocity. This is because the yield stress of lead theoretically remains parallel to the instantaneous velocity throughout the cyclic motion of a lead-rubber bearing. The presented theory implies that lead essentially behaves as a rigid-plastic material, i.e. it yields at a very small deformation and the portion of the recoverable elastic energy upon motion reversal is small. Therefore, it is not applicable for very low strains, i.e. when the amplitude is not much larger than the yield displacement of the bearing.

Solution of (3-29) and (3-30) starts with the assumption of an initial small value for the parameter t_{pf}. Equation (3-30) is then used to determine the temperature of the lead core for the next two time steps. Thereafter, at the beginning of each time step the parameter t_{pf} is calculated using (3-29) and then used in (3-30) to calculate the temperature at the end of the step.

For $\Delta t =$ time step, $T_{Lt}(i) =$ temperature of lead, $T_L(i) =$ rise in temperature of lead with respect to the initial temperature T_{L0}, $\sigma_{YL}(i) =$ effective yield stress, $v(i) =$ velocity of motion, $t_{pf}(i) =$ value of the heat front parameter t_{pf}, time $t = (i-1) \cdot \Delta t$ and $i =$ time step, the algorithm proceeds as follows:

a) Assume a small initial value of t_{pf}, say $t_{pf0}=0.01$ m.

b)
$$T_L(1) = 0 \qquad \text{(3-31)}$$

c)
$$T_L(2)=T_L(1)+\left\{\sigma_{YL}(1)\cdot v(1)-\left(\frac{k_S\cdot T_L(1)}{t_{pf0}}\right)\cdot\left(1+\left(\frac{t_s}{a}\right)\cdot\left(0.83+0.41\cdot\frac{t_{pf0}}{a}\right)\right)\right\}\cdot\frac{\Delta t}{\rho_L c_L h_L} \qquad \text{(3-32)}$$

d)
$$T_L(3)=T_L(2)+\left\{\sigma_{YL}(2)\cdot v(2)-\left(\frac{k_S\cdot T_L(2)}{t_{pf0}}\right)\cdot\left(1+\left(\frac{t_s}{a}\right)\cdot\left(0.83+0.41\cdot\frac{t_{pf0}}{a}\right)\right)\right\}\cdot\frac{\Delta t}{\rho_L c_L h_L} \qquad \text{(3-33)}$$

e)
$$t_{pf}(i)=\frac{\dfrac{\displaystyle\sum_{j=1}^{i-1}\sigma_{YL}(j)\cdot v(j)\cdot\Delta t}{T_L(i)}-\rho_L c_L h_L}{0.5\rho_S c_S\left(1+1.47\left(\dfrac{t_s}{a}\right)\right)}, \quad i\geq 3 \qquad \text{(3-34)}$$

f)
$$T_L(i+1)=T_L(i)+\left\{\sigma_{YL}(i)\cdot v(i)-\left(\frac{k_S\cdot T_L(i)}{t_{pf}(i)}\right)\cdot\left(1+\left(\frac{t_s}{a}\right)\cdot\left(0.83+0.41\cdot\frac{t_{pf}(i)}{a}\right)\right)\right\}\cdot\frac{\Delta t}{\rho_L c_L h_L} \qquad \text{(3-35)}$$

where $\sigma_{YL}(i)$ is a function of temperature $T_{Lt}(i)$ (per Equation (3-4) or (3-5)) and

$$T_{Lt}(i)=T_{L0}+T_L(i) \qquad \text{(3-36)}$$

The process described above may be used for any bidirectional input motion as long as the amplitude is much larger than the yield displacement of the bearing. It is noted that the selection of a linear and a logarithmic distribution of temperature for the end and shim plates respectively is not exactly consistent with the nature of the "heat front"

because they do not allow for zero heat flux (i.e. zero temperature gradient) at it. Also, times are usually small to allow for considering the steady-state terms of the solutions by Ozisik (1989; 1993); in other words, we are typically interested in lead core heating for motions that last only a few seconds (a minute at the most). However, this approximation was adopted for simplicity and should give an estimate of the heat conduction (and thus of the solution).

3.3.2 The Constant-Flux – Half-Space Approach

A different approach to the solution of (3-8) is presented herein based on two fundamental problems of heat conduction: the problem of constant heat flux into a semi-infinite half-space through a circular area and the problem of constant heat flux into a semi-infinite hollow cylinder from its inner surface.

3.3.2.1 Constant Flux through a Circular Area into a Semi-Infinite Half-Space

Beck (1979) presented a solution for the determination of temperature of a semi-infinite half-space initially at zero temperature and heated with a constant flux q_p (energy per unit time per unit area) through a circular area of radius a as shown in Figure 3-10. Let the thermal conductivity of the heated material be k and its thermal diffusivity be α.
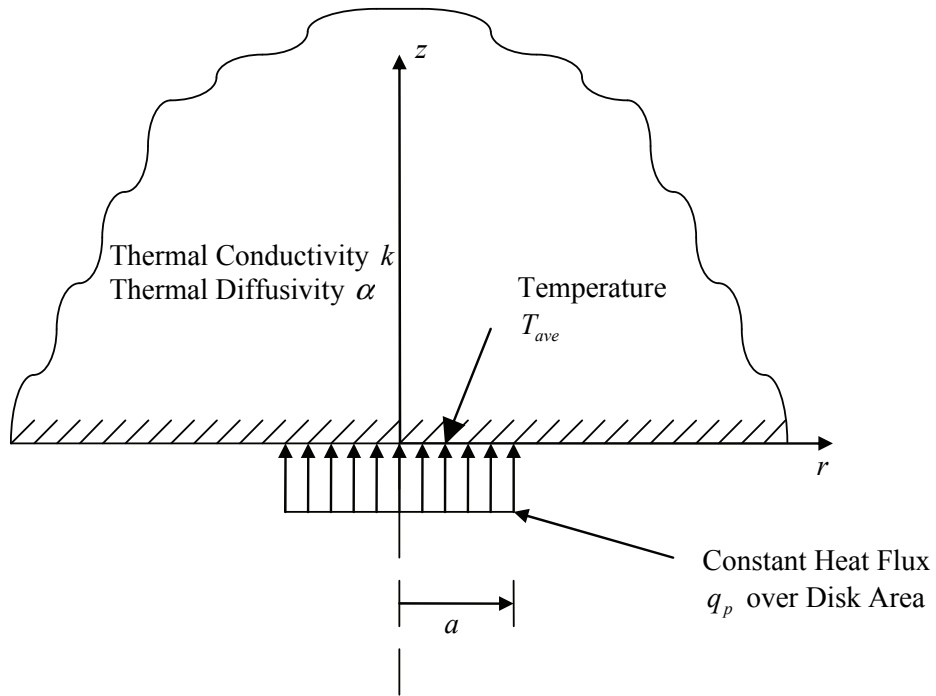
FIGURE 3-10 Semi-Infinite Half-Space Heated Through Circular Area

The solution for the average temperature on the disk surface is given by (Beck, 1979)

$$T^+ = 2 \cdot \left(\frac{t^+}{\pi}\right)^{1/2} - \frac{t^+}{\pi} \cdot \left[2 - \left(\frac{t^+}{4}\right) - \left(\frac{t^+}{4}\right)^2 - \frac{15}{4}\left(\frac{t^+}{4}\right)^3\right], \quad t^+ < 0.6 \qquad (3\text{-}37a)$$

and

$$T^+ = \frac{8}{3\pi} - \frac{1}{2(\pi \cdot t^+)^{1/2}} \cdot \left[1 - \frac{1}{3 \cdot (4t^+)} + \frac{1}{6 \cdot (4t^+)^2} - \frac{1}{12 \cdot (4t^+)^3}\right], \quad t^+ \geq 0.6 \quad (3\text{-}37b)$$

where T^+ is a dimensionless average surface temperature and t^+ is a dimensionless time, respectively, given by

$$T^+ = \frac{k \cdot T_{ave}}{q_p \cdot a} \tag{3-38}$$

$$t^+ = \frac{\alpha \cdot t}{a^2} \tag{3-39}$$

where T_{ave} is the average temperature of the heated disk surface at time t.

Another related problem is that of the semi-infinite half-space uniformly heated at its entire free surface by heat flux q_p (same problem as that of Figure 3-10 but with radius a becoming infinitely large). The solution for the surface temperature is (p. 75 of Carslaw and Jaeger, 1959)

$$T = \frac{2q_p}{k} \cdot \left(\frac{\alpha \cdot t}{\pi} \right)^{1/2} \tag{3-40}$$

which when using the transformations of equations (3-38) and (3-39) may be written as

$$T^+ = 2 \cdot \left(\frac{t^+}{\pi} \right)^{1/2} \tag{3-41}$$

Note that (3-40) does not involve parameter a (radius), whereas in (3-41) this parameter is embedded on both sides of the equation. In this case, parameter a (radius) should be interpreted as an arbitrary length parameter.

The solution given by (3-37) may be approximated by

$$T^+ = 2 \cdot \left(\frac{t^+}{\pi}\right)^{1/2}, \ t^+ \leq 0.1 \qquad (3\text{-}42\text{a})$$

$$T^+ = 0.357 + 0.246 \cdot \log\left(\frac{t^+}{0.1}\right), \ 0.1 \leq t^+ \leq 10 \qquad (3\text{-}42\text{b})$$

$$T^+ = \frac{8}{3\pi}, \ t^+ \geq 10 \qquad (3\text{-}42\text{c})$$

Figure 3-11 presents a comparison of the solutions of the two problems of the heated half-space along with the approximate solution in (3-42). It may be observed that (3-41) approximates well the solution of the heated half-space through a disk for dimensionless time of less than 0.1. This should be expected as (3-41) represents the leading term in the asymptotic expansion solution given by (3-37a). The significance of the observation relates to the problem of heating of the steel end plates of lead-rubber bearings. These steel plates are heated by the lead core which supplies a heat flux over a circular area. The heat flux may be regarded as uniform over the circular area but not constant over time (the solution for intermittent heat flux may be simply obtained by superposition of solutions for the constant heat flux problem). One can conclude that, for short dimensionless time, the heat front in the end steel plates of lead-rubber bearings is sufficiently close to the surface so that the plates of finite dimensions may be treated as semi-infinite half-spaces with uniformly heated surfaces. The question then is what the physical significance of a dimensionless time of less than 0.1 is. Using a thermal diffusivity $\alpha = 1.41 \times 10^{-5}$ m^2/sec for steel and a lead core radius $a = 0.1$ m (typical for large bearings), and using (3-39) the real time is 70.9 sec – a time that typically far

59

exceeds the duration of high speed motion in the testing of bearings and also exceeds the duration of high amplitude seismic motions calculated for seismically isolated structures. However, in cases of quasi-static testing of bearings the dimensionless time may be much longer (see examples in Section 4) in which case solutions valid for large dimensionless times are needed.
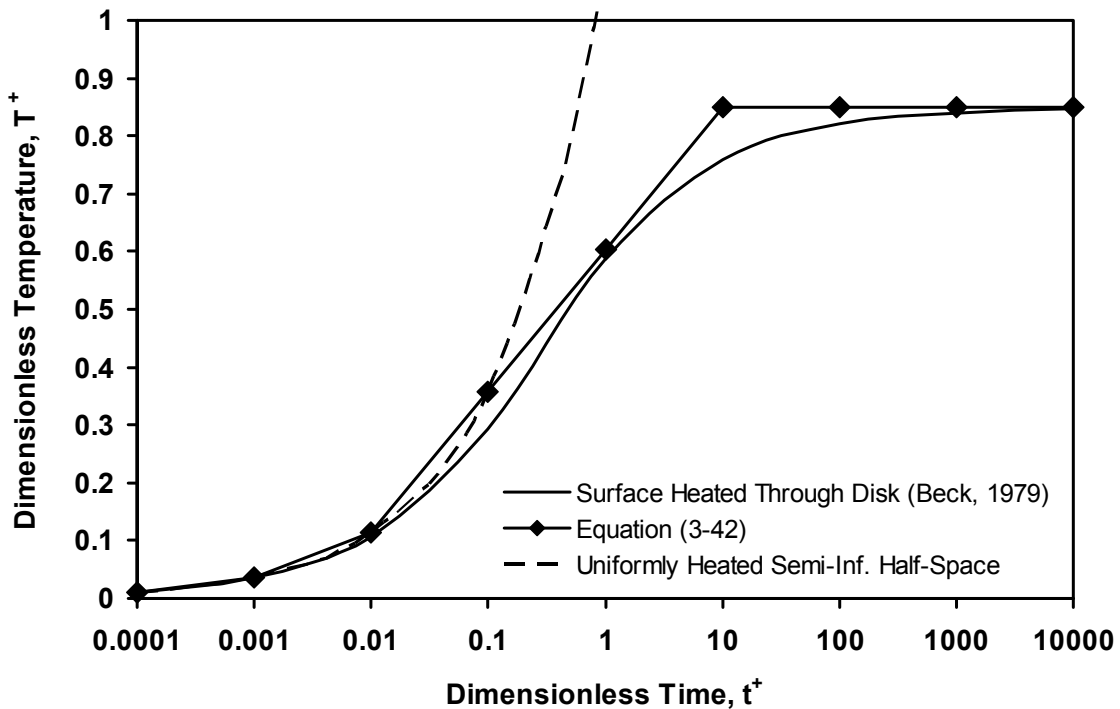
FIGURE 3-11 Surface Dimensionless Temperatures as a Function of Dimensionless Time for the Semi-Infinite Half-Space Uniformly Heated Through a Circular Area

3.3.2.2 Constant Flux into an Infinite Hollow Cylinder

Consider the problem of the surface temperature $T_s(t)$ of a region bounded internally by a circular cylinder of radius a, with zero initial temperature and subjected to constant heat flux q_s at the surface as shown in Figure 3-12. A solution to this problem is presented in Carslaw and Jaeger (1959, p. 338) in terms of an infinite integral of Bessel

60

functions. Also, Carslaw and Jaeger (1959) present a graph of the dimensionless temperature T^+ versus dimensionless time t^+ where t^+ is given by (3-39) and T^+ is given by

$$T^+ = \frac{k \cdot T_s}{q_s \cdot a} \tag{3-43}$$

A simple and good approximation to the dimensionless temperature T^+ is given by

$$T^+ = 0.785 \left(t^+ \right)^{1/3} \tag{3-44}$$

which is plotted in Figure 3-13 for comparison to the exact solution. Carslaw and Jaeger (1959) also provide the following solution valid for small values of the dimensionless time:

$$T^+ \sim 2 \cdot \left(t^+ \right)^{1/2} \cdot \left\{ \frac{1}{\sqrt{\pi}} - \frac{\left(t^+ \right)^{1/2}}{4} \right\} \tag{3-45}$$

A comparison between (3-44) and (3-45) for small values of the dimensionless time is presented in Figure 3-14. We observe a difference between the exact and approximate solutions for short dimensionless times. However, we note that it is more important for the approximate solution (3-44) to be close to the exact solution at large values of t^+ because at that region heat losses are expected to influence the solution much more than at small t^+. In other words, we prefer to have more accuracy of (3-44) at large rather than small t^+.
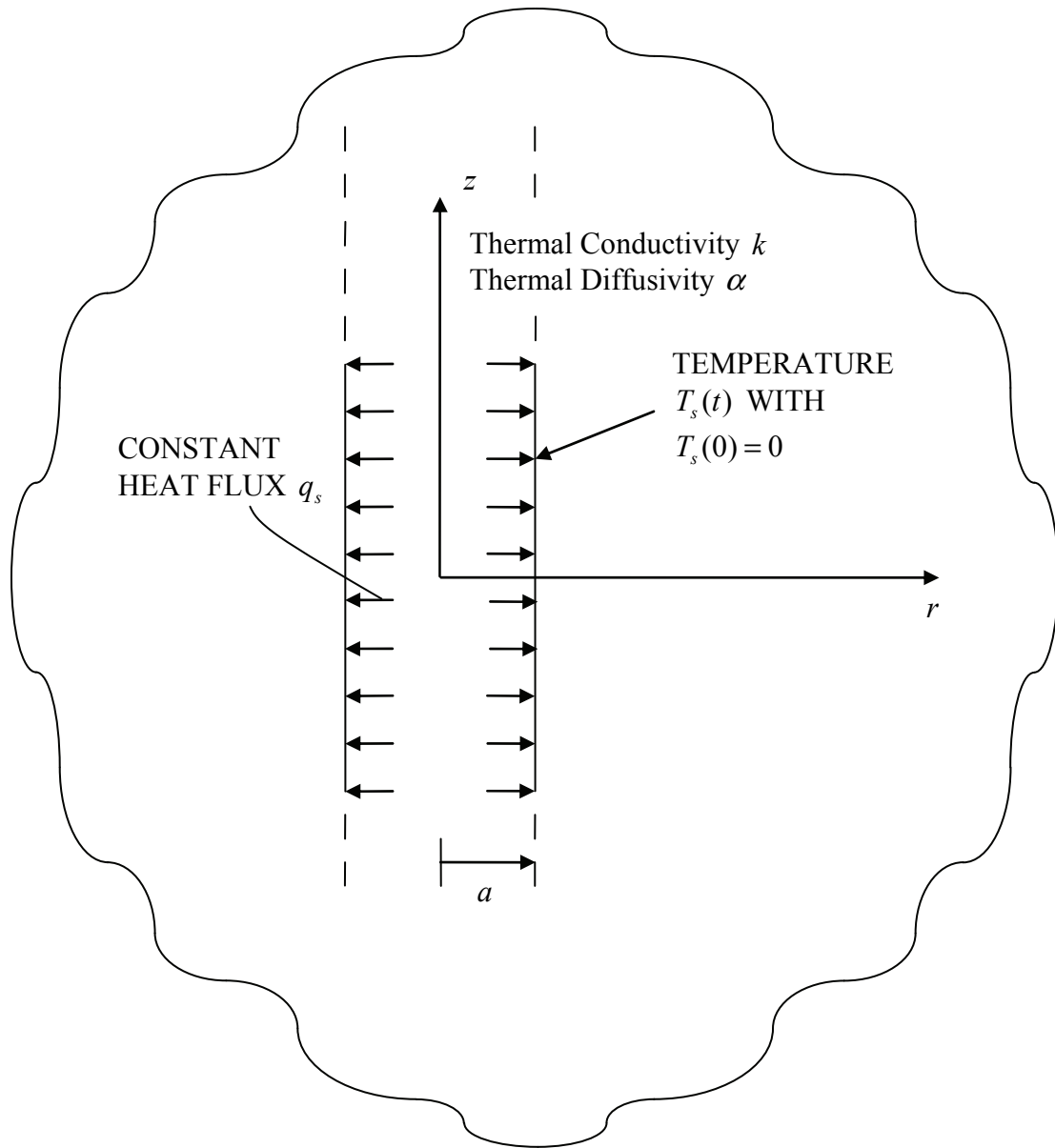
FIGURE 3-12 Infinite Heated Hollow Cylinder
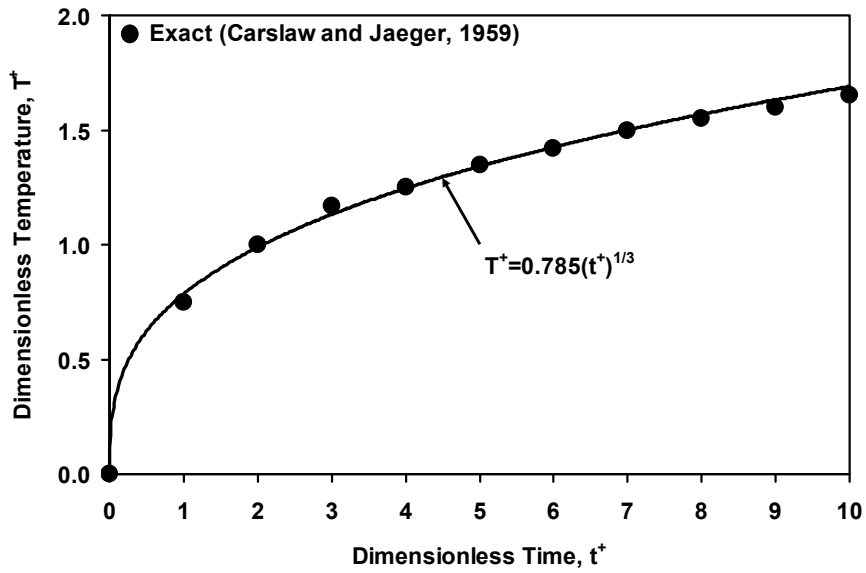
FIGURE 3-13 Exact (Carslaw and Jaeger, 1959) and Approximate (Equation (3-44)) Dimensionless Inner Surface Temperature as a Function of Dimensionless Time for Infinite Heated Hollow Cylinder
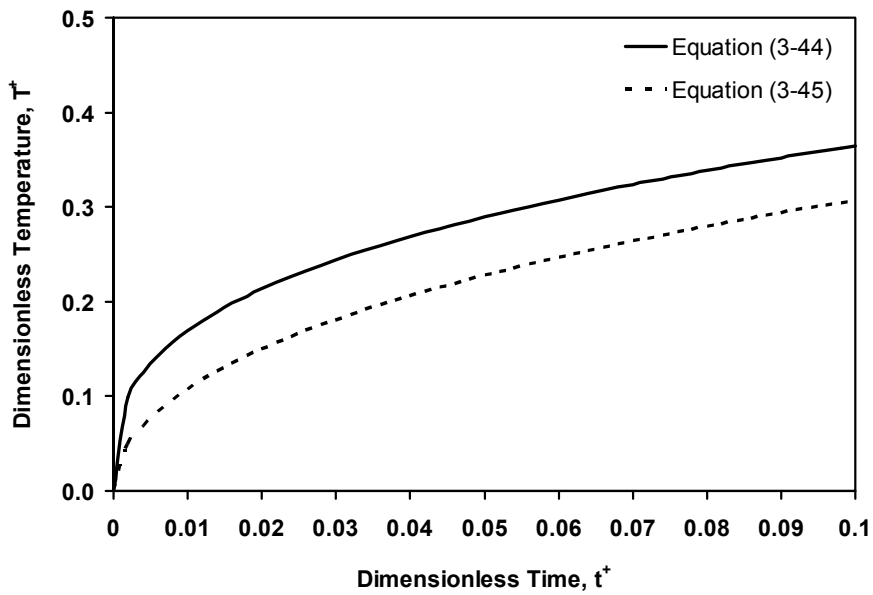
FIGURE 3-14 Comparison Between Exact and Approximate Dimensionless Inner Surface Temperatures for Infinite Heated Hollow Cylinder at Small Values of Dimensionless Time

3.3.2.3 Transformation into an Ordinary Differential Equation

The solutions presented in Sections 3.3.2.1 and 3.3.2.2 provide the tools needed to transform (3-8) to (3-12) into a single ordinary differential equation amenable to solution.

Returning to Figures 3-5 and 3-6, we

(a) Keep the temperature distribution assumption stated in the beginning of Section 3.3 and shown in Figure 3-6.

(b) Treat the end plates as semi-infinite half-spaces subjected to heat per unit time q_1 over circular area of radius a, where

$$q_1 = A_p q_p \tag{3-46}$$

Use of (3-38) with $T_{ave} = T_L / 2$ (where T_L is the lead core temperature increase in the bulk of the core – see Figure 3-6), $k = k_S$, the thermal conductivity of steel, $\alpha = \alpha_S$, the thermal diffusivity of steel, and (3-37) results in

$$q_p = \frac{k_S \cdot T_L}{2a \cdot \left\{ 2 \cdot \left(\dfrac{t^+}{\pi} \right)^{1/2} - \dfrac{t^+}{\pi} \cdot \left[2 - \left(\dfrac{t^+}{4} \right) - \left(\dfrac{t^+}{4} \right)^2 - \dfrac{15}{4} \left(\dfrac{t^+}{4} \right)^3 \right] \right\}} \tag{3-47a}$$

$$q_p = \frac{k_S \cdot T_L}{2a \cdot \left\{ \dfrac{8}{3\pi} - \dfrac{1}{2(\pi \cdot t^+)^{1/2}} \cdot \left[1 - \dfrac{1}{3 \cdot (4t^+)} + \dfrac{1}{6 \cdot (4t^+)^2} - \dfrac{1}{12 \cdot (4t^+)^3} \right] \right\}} \tag{3-47b}$$

These equations hold for $t^+ < 0.6$ and $t^+ \geq 0.6$, respectively, with $t^+ = \alpha_S t / a^2$. Note that (3-47) are presented in terms of the solution (3-37). They could also have been presented in terms of the approximate solution (3-42).

(c) Treat the shim plates as an infinite medium bounded internally by a cylinder of radius a and subjected to heat per unit time q_2 at the cylindrical surface, where

$$q_2 = A_s q_s \tag{3-48}$$

Use of (3-43) with $T_s = T_L / 2$, $k = k_S$, the thermal conductivity of steel, $\alpha = \alpha_S$, the thermal diffusivity of steel, and (3-44) results in

$$q_s = \frac{k_S T_L}{1.57 a \left(t^+ \right)^{1/3}} \tag{3-49}$$

Note that (3-49) has been written in terms of the approximation to the solution (3-44). It could have been written in terms of solution (3-45) but valid only for small dimensionless times.

Note the use of $T_{ave} = T_L / 2$ and $T_s = T_L / 2$ as per Figure 3-6 and beginning of Section 3.3.

Substitution of (3-46) to (3-49) into (3-8), use of (3-7) with $|du / dt|$ replaced by $v(t)$, the velocity, and use of $V_L = A_L h_L$, $A_s = 2\pi a t_s$ and $A_p = A_L = \pi a^2$, results in

$$\frac{dT_L}{dt} = \frac{\sigma_{YL}(T_L) \cdot v(t)}{\rho_L c_L h_L} - \frac{k_S \cdot T_L}{a \cdot \rho_L c_L h_L} \cdot \left(\frac{1}{F} + 1.274 \cdot \left(\frac{t_s}{a} \right) \cdot \left(t^+ \right)^{-1/3} \right) \tag{3-50a}$$

65

$$F = \begin{cases} 2 \cdot \left(\dfrac{t^+}{\pi}\right)^{1/2} - \dfrac{t^+}{\pi} \cdot \left[2 - \left(\dfrac{t^+}{4}\right) - \left(\dfrac{t^+}{4}\right)^2 - \dfrac{15}{4}\left(\dfrac{t^+}{4}\right)^3\right], & t^+ < 0.6 \\[3mm] \dfrac{8}{3\pi} - \dfrac{1}{2(\pi \cdot t^+)^{1/2}} \cdot \left[1 - \dfrac{1}{3 \cdot (4t^+)} + \dfrac{1}{6 \cdot (4t^+)^2} - \dfrac{1}{12 \cdot (4t^+)^3}\right], & t^+ \geq 0.6 \end{cases} \qquad (3\text{-}50\text{b})$$

Equation (3-50) is an ordinary differential equation with input $v(t)$ $(=|du/dt|$, where u is the history of motion of the lead-rubber bearing). It can be numerically solved as an initial value problem.

3.3.3 Dimensional Analysis and Similarity

In this section an attempt is made to identify the minimum number of parameters on which the lead core temperature depends. These parameters may be identified either by formal application of dimensional analysis (e.g., Barenblatt, 1996; 2003) or by casting the solution given by (3-50) in dimensionless form.

Equation (3-4) is used to describe the temperature dependence of the lead effective yield stress. Equation (3-50) may then be written in a more general form in which J and G are functions of the dimensionless time $t^+ = \alpha_S t / a^2$:

$$\left(\rho_L c_L h_L\right) \frac{dT_L}{dt} = \sigma_{YL0} \cdot \exp(-E_2 T_L) \cdot v(t) - \frac{k_S T_L}{a} \left\{ J\left(\frac{\alpha_S t}{a^2}\right) + \left(\frac{t_s}{a}\right) \cdot G\left(\frac{\alpha_S t}{a^2}\right) \right\} \qquad (3\text{-}51)$$

Equation (3-51) may be re-written when using the dimensionless time t^+ (equation (3-39) with thermal diffusivity α_S in place of α) and dimensionless temperature Q given by

$$Q = E_2 T_L \tag{3-52}$$

The dimensionless form of (3-51) is

$$\exp(Q) \cdot \left[\left(\frac{dQ}{dt^+} \right) + Q \cdot \left\{ J\left(t^+\right) + \left(\frac{t_s}{a} \right) \cdot G\left(t^+\right) \right\} \cdot \left(\frac{a\rho_S c_S}{\rho_L c_L h_L} \right) \right] = \frac{E_2 \sigma_{YL0} v}{\rho_L c_L h_L} \frac{a^2}{\alpha_S} \tag{3-53}$$

Equation (3-53) was derived by making use of the following relations among thermal parameters

$$k_S = \alpha_S \rho_S c_S \tag{3-54}$$

Consider now that the lead-rubber bearing undergoes motion of constant velocity so that $v(t) = v_0$. Then equation (3-53) includes the following four dimensionless parameters:

$$\left(\frac{\alpha_S t}{a^2} \right), \ \left(\frac{t_s}{a} \right), \ \left(\frac{a\rho_S c_S}{\rho_L c_L h_L} \right), \ \left(\frac{E_2 \sigma_{YL0} v_0 a^2}{\alpha_S \rho_L c_L h_L} \right) \tag{3-55}$$

The dimensionless parameters in (3-55) do not include the radius R of the bearing and the thickness t_p of the end plates (see Figure 3-5). This is due to the assumption that the heat front did not reach the ends of the steel end plates and shim plates. It will be shown later in Section 4 on the basis of finite element analysis that indeed this is the case.

It may be noted that the dimensionless parameters in (3-55) include particular groupings of parameters with length dimensions (a, h_L and t_s). These groupings could not have

67

been obtained in formal dimensional analysis without the benefit of having a solution derived for the problem.

To demonstrate the utility of the dimensionless parameters in (3-55), consider the two lead-rubber bearings of Figure 3-15 which are assumed constructed of materials of the same properties α_S, ρ_S, c_S, ρ_L, c_L, E_2 and σ_{YL0}. Parameter β is a scalar larger than unity. Each bearing is subjected to the shown histories of constant velocity motion (top of bearing with respect to the bottom). The displacement histories are "sawtooth" and the ratio of amplitude of motion to height of the lead core is the same in the two bearings.

BEARING 2

BEARING 1

βh_L

βt_s

h_L t_s

a

βa

Displacement
u

Amplitude
u_0

v_0

t

Real Time

θ

u

$\dfrac{v_0}{\beta}$

βu_0

t

$\beta^2 \theta$
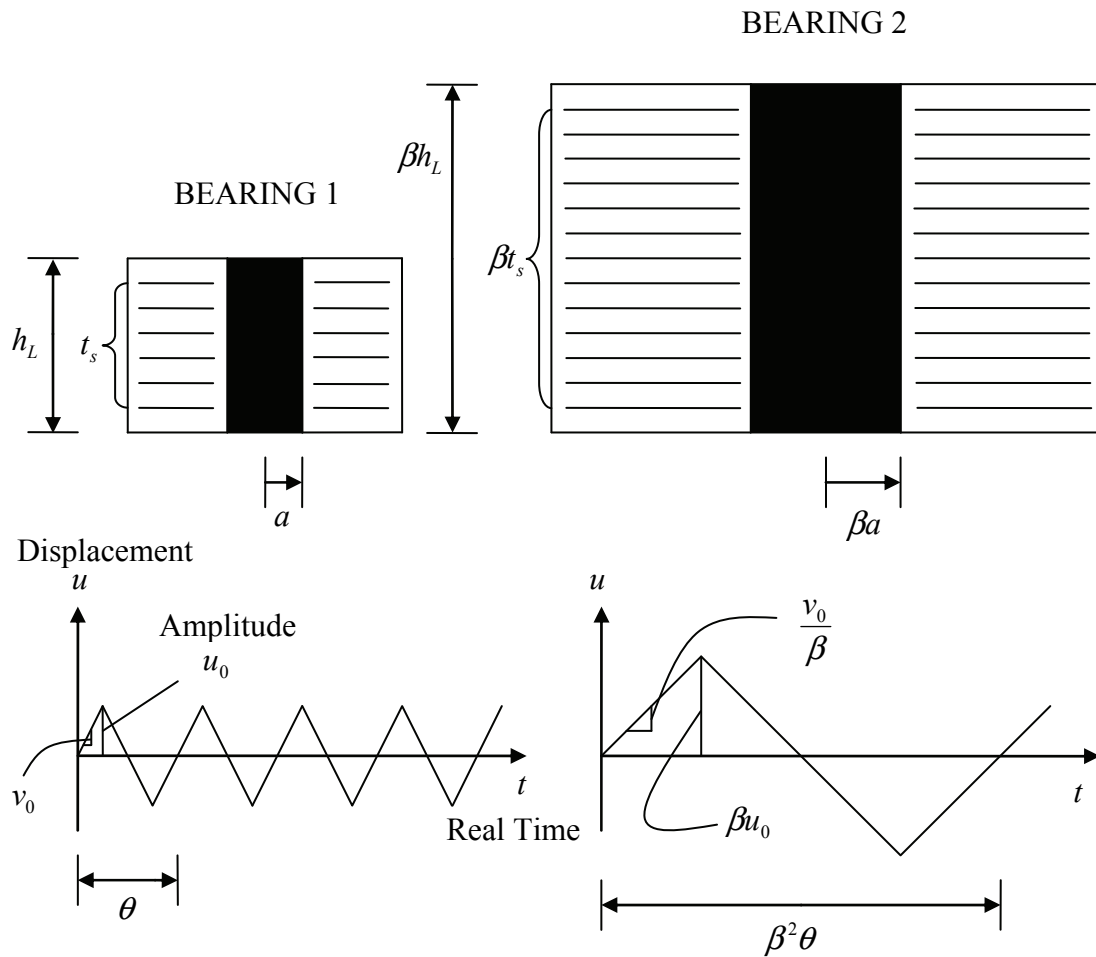
FIGURE 3-15 Similarity in Two Lead-Rubber Bearings

It is easy to verify that the second, third and fourth dimensionless parameters in (3-55) are the same in the two bearings. Consider now the dimensionless temperature Q of the two bearings. Based on (3-52) and since parameter E_2 is the same for the two bearings, temperature T_L in the two bearings is the same at the same dimensionless time t^+. Use of the first dimensionless parameter in (3-55) requires for similarity that $\beta^2 t_1 = t_2$, where t_i is the real time for bearing i ($i = 1,2$). Given that the duration of a cycle of motion of

bearing 2 is β^2 times that of bearing 1 (see Figure 3-15), we conclude that **the dimensionless time histories of the lead core temperature of the two bearings are identical** (e.g., the temperature of the lead core is the same in the two bearings at the end of each cycle of motion).

Moreover, given that E_2 is the same for the two bearings and based on equations (3-4) and (1-1), we conclude that **the characteristic strength Q_d of bearing 2 is β^2 times the characteristic strength of bearing 1 at the same dimensionless time**.

Based on this analysis, the smaller bearing 1 may be tested to obtain the behavior of the larger bearing 2. Note that parameter β is the length scale. For example, β could be 4 so that instead of testing the bearing of Figure 1-4 (for which currently a single facility in the US is capable of testing at high speed) a bearing of 238 mm (9.4 in) diameter and 45 mm (1.75 in) lead core diameter could be tested (which is entirely within the load and displacement capabilities of the small bearing testing machine at the University at Buffalo). However, the velocity of testing of the smaller bearing should be four times larger, which would far exceed the capabilities of the small bearing testing machine; and those of any available machine.

We conclude that while the principles of similarity have been established, we cannot make direct use of them because testing of smaller bearings would require very large velocities. To circumvent this problem, an approximation to similarity is needed in which longer duration and lower velocity motions are used. This problem is briefly addressed in Section 3.3.5 herein.

3.3.4 Simplified Solution – The Case of Insignificant Conduction of Heat

It is reasonable to assume that for a short time interval after the start of an experiment, heat conduction through the steel shim plates and the steel end plates is negligible. Accordingly, the heat generated in the lead core is entirely consumed for the rise of its own temperature. That is, the heat fluxes per unit time through the end plates and shim plates, q_1 and q_2 respectively, are zero. Then, functions J and G in (3-51) are zero and the equation can be integrated to obtain

$$T'_L = \frac{1}{E_2} \cdot \ln\left(1 + \frac{E_2 \sigma_{YL0} S}{\rho_L c_L h_L}\right) \tag{3-56}$$

where S is the distance travelled

$$S = \int v(t)\,dt \tag{3-57}$$

We now attempt to establish a criterion for the validity of (3-56). We start from (3-50) which provides an accurate description of the temperature history of lead. When the negative term on the right-hand side of this equation is neglected, heat conduction through the end and shim plates is neglected and the lead core temperature is given by (3-56). The error in estimating the temperature is then approximately given by

$$\Delta T_L = \int_0^t \frac{k_S T'_L}{a \rho_L c_L h_L}\left(\frac{\pi^{1/2}}{2}\cdot\left(t^+\right)^{-1/2} + 1.274\cdot\left(\frac{t_s}{a}\right)\cdot\left(t^+\right)^{-1/3}\right)d\tau \tag{3-58}$$

Note that in order to be able to evaluate the integral, the approximate expression for temperature in (3-56) was used in (3-58). Also, equation (3-50a) was utilized but using only the leading term (i.e., when (3-37a) is used, only the leading term, valid for small dimensionless times, is used).

Evaluation of the integral in (3-58) is obtained by integration by parts in which the second part of the integration (containing the time derivative of T_L') is neglected. This results in a conservative estimation of the error as

$$\Delta T_L \leq \left(\frac{\rho_S c_S}{\rho_L c_L}\right) \cdot \left(1.772\left(\frac{a}{h_L}\right)\left(t^+\right)^{1/2} + 1.911\left(\frac{t_s}{h_L}\right)\left(t^+\right)^{2/3}\right) \cdot T_L' \qquad (3\text{-}59)$$

Note the approximate nature of the derivation of (3-59). First is the neglect of a part of the equations (term containing the derivative of T_L'), although this results in a conservative estimation of the error. Second is the use of (3-50a), which contains results from two solutions: one from Beck (1979) but valid only for small dimensionless times (use of leading term in (3-37a)) and one described by equation (3-44) which is valid for all times but introduces errors for small dimensionless times.

The simplified solution (3-56) is considered acceptable when ΔT_L is less than an acceptable limit. Herein we take this limit to be 40^0C as that corresponds to an acceptably small error on the prediction of the energy dissipation per cycle as will be demonstrated in Section 4.

72

3.3.5 Scaling Principles for Lead-Rubber Bearing Testing

Testing is essential in many fields of science and engineering for the verification of theories. However, it is often practically impossible or too expensive to conduct tests in full scale. In such cases, scale testing is often performed. That is, instead of testing an appropriate large-size specimen (prototype), a smaller specimen which is considered capable of reliably capturing the behavior of the prototype is tested (model). The behavior of the prototype is then predicted and evaluated based on the results obtained from the testing performed on the model.

Testing in scale is common in structural engineering. Models of real-size structures are constructed and tested in order to reach conclusions regarding the behavior of their prototypes. The design of these models and the selection of the test programs are not straightforward. Rather, they are based on principles of similarity which depend mainly on those aspects of the behavior of the prototype that are under investigation. For example, different similarity rules apply when testing a structure statically from those that apply in dynamic tests. A common method of ensuring similitude in dynamic tests is, for instance, the so-called "artificial mass simulation" where mass is added to the model in order for it to have such dynamic characteristics that it appropriately captures the behavior of the prototype under dynamic conditions.

A common type of experimental procedure in structural engineering aiming at the evaluation of structural behavior under earthquake excitations is shake table testing. In such a test, the model of a real-size structure is mounted on a shake table and appropriately scaled ground motions are applied at its base. Shake table tests of structures

mounted on lead-rubber bearings have been performed by a number of researchers, such as Hwang and Hsu (2000) and Wolff and Constantinou (2004) among others. Testing of lead-rubber bearings in scale is always necessary for shake table testing and is sometimes necessary when only lead-rubber bearings are to be tested (depending on availability of testing machines capable of testing at the required conditions).

Focken (1953), followed by Harris and Sabnis (1999), stated the general principle of dynamic similarity as

$$S_F = \frac{S_L S_M}{S_T^2}$$

(3-60)

where S_F is the force scale factor, S_L is the length scale factor, S_M is the mass scale factor and S_T is the time scale factor. This general principle should ideally hold for all testing processes where a dynamic phenomenon is reproduced in scale. In structural engineering tests, typically three of the above four scale factors are appropriately set and then (3-60) is used to determine the fourth one. With these four scale factors determined, the "required" and "provided" scale factors for all quantities can be calculated and checked. The aforementioned "artificial mass simulation" is exactly the result of this process in shake table test program preparation.

When performing shake table tests on an isolated structure where the isolation system consists of lead-rubber bearings, the similitude requirements are two-fold; those that apply for the superstructure and similar ones that apply for the isolation system. For lead-rubber bearings, similitude requirements should consider lead core heating effects. Both

sets of requirements would have to be met for performing a good shake table test. The superstructure must have a **length scale equal to the square of the time scale** ($S_L = S_T^2$) and artificial mass simulation should be applied for reliable dynamic similitude. This, however, is at odds with the requirements of Section 3.3.3, according to which the **length scale should be equal to the square root of the time scale** ($S_L = \sqrt{S_T}$) in order to have similitude in strength degradation due to lead core heating (i.e., to have same values of temperature in the lead cores of both the model and the prototype bearings at the same dimensionless times). The requirement of Section 3.3.3 is inherent in the heat conduction equation (see (3-11) and (3-12)). It is concluded that only shake table tests where the dynamic/geometric conditions are such that either (a) the lead core temperature of both prototype and model does not increase significantly (i.e., there is essentially no strength degradation in the isolators of either the prototype structure or the model structure) or (b) heat conduction through the steel plates is insignificant in both prototype and model (i.e., the simplified solution is valid for both, thus making every parameter other than $(E_2 \sigma_{YL0} S)/(\rho_L c_L h_L)$ in (3-56) irrelevant. For all other cases ranging between the above two "extremes", a shake table test of a structure mounted on lead-rubber bearings cannot, in theory, reliably capture the strength degradation of the prototype bearings.

Similarly in the testing of individual bearings, complete similarity cannot be achieved and we should resort to what we will refer to as "approximate similarity". The purpose of model testing is still to capture the strength deterioration of the prototype but not necessarily within the same dimensionless/real time. Rather, the model is tested in such a way that the strength of the model deteriorates so that its normalized effective yield stress

at the end of testing equals that of the prototype – for instance, this may be achieved by subjecting the model to a higher number of cycles of motion than the prototype.

In summary, for individual bearing testing, increasing the velocity on the model by the length scale factor should reproduce the cycle-by-cycle strength reduction of the prototype as long as both the model and the prototype have the same initial effective yield stress σ_{YL0}. In cases where the velocity demand for complete similarity on the model is too high for the available testing equipment, the model can be tested at lower velocities and for a larger number of cycles until its lead core temperature reaches that of the prototype (estimated) at the end of prototype testing.

3.4 Finite Element Analysis

Numerical solutions using finite element modeling are complex and time consuming but very useful in verifying the assumptions made in the presented solutions and investigating the accuracy of the derived analytical solutions. Particularly, a finite element solution is useful for (a) investigating the significance of the transient terms in the temperature histories of the steel plates and (b) investigating the validity of the assumptions for the temperature distribution within the lead plug. Accordingly, a finite element model was developed with the intention of investigating the aforementioned items (a) and (b) and also the accuracy and validity of the derived analytical solutions for the histories of temperature rise and characteristic strength.

A finite element model was developed for analyzing many different bearing geometries. The model was developed in computer code ABAQUS (Hibbitt, Karlsson & Sorensen,

Inc., 2002) with all elements being of the type: axisymmetric, 4-node linear diffusive heat transfer element DCAX4 (see Figure 3-16). All free boundaries were modeled as heat-insulated. This means that (a) radiation effects at the free rubber and steel shim ends are neglected, and (b) the steel structures above and below the bearing represent the conditions of the actual bearing installation (in a massive test machine or in structure) where the temperature rise is zero at some distance t_p from the lead core. For the analysis, the heat generation within the lead core was defined as a property of the material. The heat generation rate within the core (thermal energy per time per volume) is given by (3-7). The initial temperature was assumed to be equal to 20^0C unless otherwise specified.
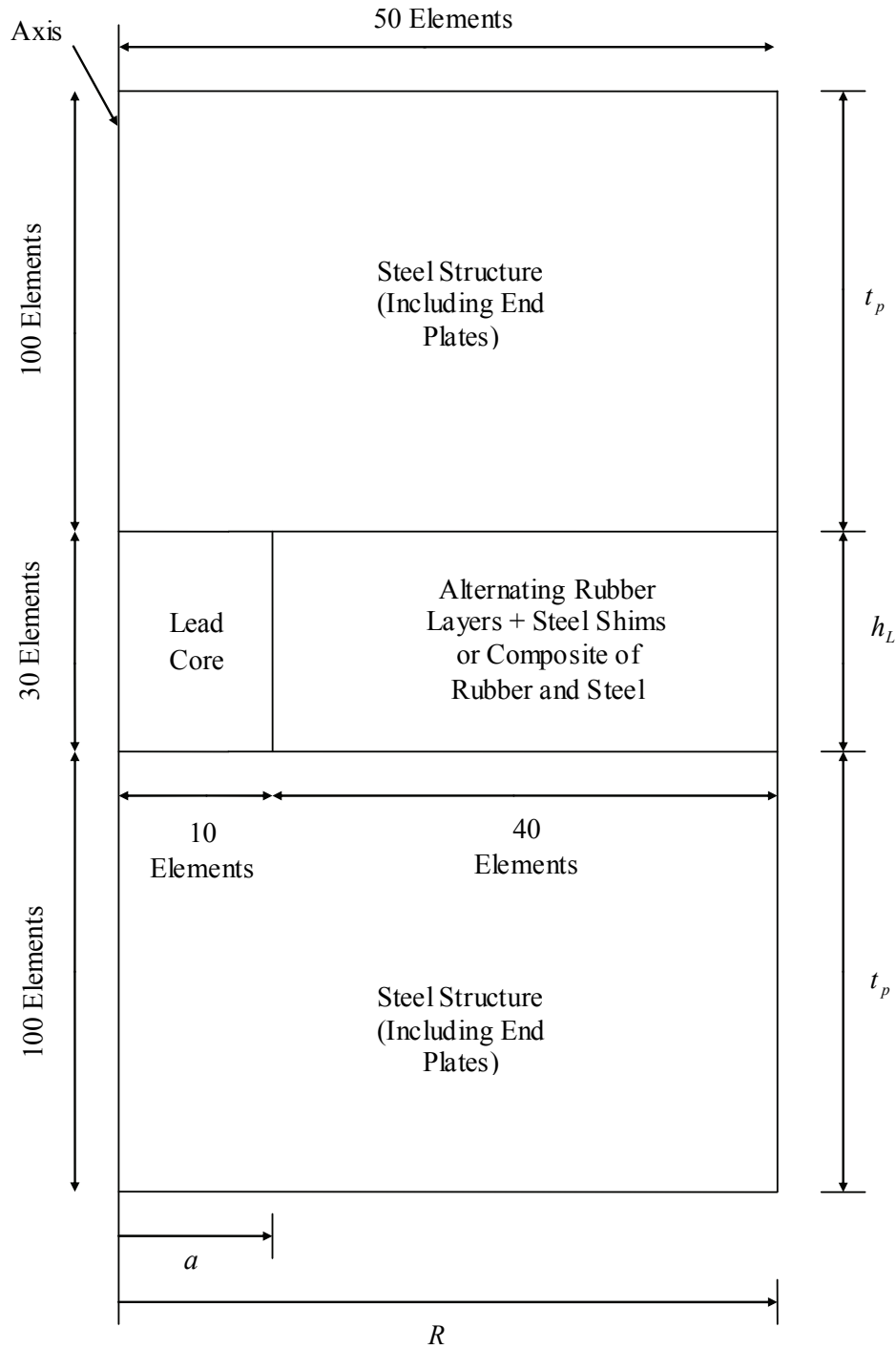
FIGURE 3-16 Axisymmetric Finite Element Model for Lead-Rubber Bearing Heating

Table 3-3 presents the material properties used for the steel end and shim plates, the lead core and the rubber layers. Note that in the finite element model the rubber is not

assumed to be a perfect thermal insulator but is rather modeled as a material with a low thermal conductivity. Moreover, in one example analysis the alternate layers of rubber and shim plates were directly modeled whereas in the other examples they were modeled as anisotropic composite material with two values of thermal conductivity, one radial and one vertical (see Section 4). Salazar (2003) states that for this composite the effective heat capacity is

$$\rho c = V_1 \left(\rho_1 c_1 \right) + V_2 \left(\rho_2 c_2 \right)$$ (3-61)

where V_i is the volume fraction of component i. Also, the effective thermal conductivity parallel to the layers ($k_{eff,radial}$) and that perpendicular to the layers ($k_{eff,vert}$) are given by

$$k_{eff,radial} = V_1 k_1 + V_2 k_2$$ (3-62)

$$\frac{1}{k_{eff,vert}} = \frac{V_1}{k_1} + \frac{V_2}{k_2}$$ (3-63)

For a lead-rubber bearing with a total shim plate thickness t_s and lead core height h_L, the volume fractions for steel and rubber in the composite region are given by

$$V_{steel} = \frac{t_s}{h_L}$$ (3-64)

$$V_{rubber} = 1 - \frac{t_s}{h_L}$$ (3-65)

79

TABLE 3-3 Material Parameters Used in Finite Element Analysis

Parameter	End and Shim Plates (Steel)	Rubber Layers (Rubber)	Lead Core (Lead)
Density, ρ (kg/m^3)	7900	1300	11200
Conductivity, k (W/(m^{0}C))	50	0.16	34
Specific Heat, c (J/(kg^{0}C))	450	1700	130
Diffusivity, α (m^2/s))	1.41×10^{-5}	7.24×10^{-8}	2.34×10^{-5}

3.5 Summary

A theory has been presented that is capable of predicting the temperature rise of the lead core and the associated reduction in characteristic strength and energy dissipation per cycle (EDC) of lead-rubber bearings subjected to cyclic motion. The theory includes a simplification in which an explicit closed-form solution was derived. The closed-form solution is useful in engineering calculations and a validity criterion has been derived. The only input parameter required for the analysis is the absolute value of the instantaneous velocity of motion of the top of the bearing with respect to its bottom. Accordingly, the analytic solutions developed can also be applied in cases of random bidirectional motion, provided that the amplitude is much larger than the yield displacement of the bearing. Moreover, the development of the theory of temperature rise in lead-rubber bearings allowed for the development of principles of scaling and similarity for lead-rubber bearings. These principles can be used in the reduced scale testing of lead-rubber bearings.

SECTION 4

VERIFICATION OF THEORY OF HEATING OF LEAD-RUBBER BEARINGS

4.1 Introduction

In this section we investigate the validity and accuracy of the theory presented in Section 3 for a selection of cases where experimental results are available. All solutions of Section 3, namely the one based on an energy approach, the one based on the constant flux assumption and the simplified, closed-form solution, along with results of limited finite element analyses, are compared against experimental results from the testing of lead-rubber bearings under harmonic or constant velocity motion. A total of 15 cases are presented.

Test data and analysis results for bearings of different sizes, initial temperature conditions and testing conditions (amplitude and speed of motion) are presented. Values of the energy dissipated per cycle (which is directly proportional to the characteristic strength) of lead-rubber bearings over several cycles of motion are compared to (a) predictions of finite element analysis, (b) predictions of the analytical solution obtained by numerical solution of equations (3-29) and (3-30) or (3-50), and (c) predictions of the simplified solution of equation (3-56). In all cases the "exponential III" equation for the relation between effective yield stress and temperature (see Table 3-2) was used.

The experimentally obtained values of energy dissipated per cycle include both the part associated with energy dissipation in the lead core and the part associated with energy dissipation in the rubber. Therefore, before using the experimental data to obtain the

initial effective yield stress σ_{YL0} through the process described in Section 3.2, the portion of the energy dissipated by the rubber should be estimated and then subtracted from the total energy dissipated per cycle. This estimation requires testing of control specimens without lead core. In the absence of such experimental results, the rubber contribution to the energy dissipated per cycle may be estimated by assuming that rubber contributes to the effective damping a specific amount.

The theoretically predicted energy dissipated per cycle was calculated as follows:

a) The temperature of the lead core in the middle of the first cycle was obtained by analysis (analytic or by finite element analysis).

b) Use of (3-4) (or (3-5)) gave the effective yield stress of lead for the first cycle while (3-6) combined with (1-1) gave the energy dissipated in the lead core during the first cycle.

c) The estimated energy dissipated in the rubber was added to the energy dissipated in the lead core, giving the total theoretically predicted dissipated energy to be compared against its experimentally obtained value for the first cycle.

d) The previous steps were repeated for each cycle of motion.

4.2 Examples

A total of 15 examples are presented in the sequel.

4.2.1 Example 1

Consider the bearing of Figure 1-4 with experimental energy dissipated per cycle data shown in Figure 1-5. Figure 4-1 shows the force-displacement loops recorded in that

experiment. Note that for this bearing $a = 0.0889$ m (3.5 in) and time t after 15 cycles of 0.5 Hz frequency is 30 sec. The dimensionless time $t^+ = \alpha_S t / a^2$ is 0.054. A value $\alpha_S = 1.41 \times 10^{-5}$ m^2/s was used in the calculation. (Composite) finite element analysis was performed based on the model shown in Figure 3-16 considering the alternate rubber layers and steel shim plates to behave as a composite material with properties defined by (3-61) through (3-65). For comparison and verification purposes, another (explicit) finite element analysis for the same bearing and harmonic motion was performed; the model for that analysis is shown in Figure 4-2.
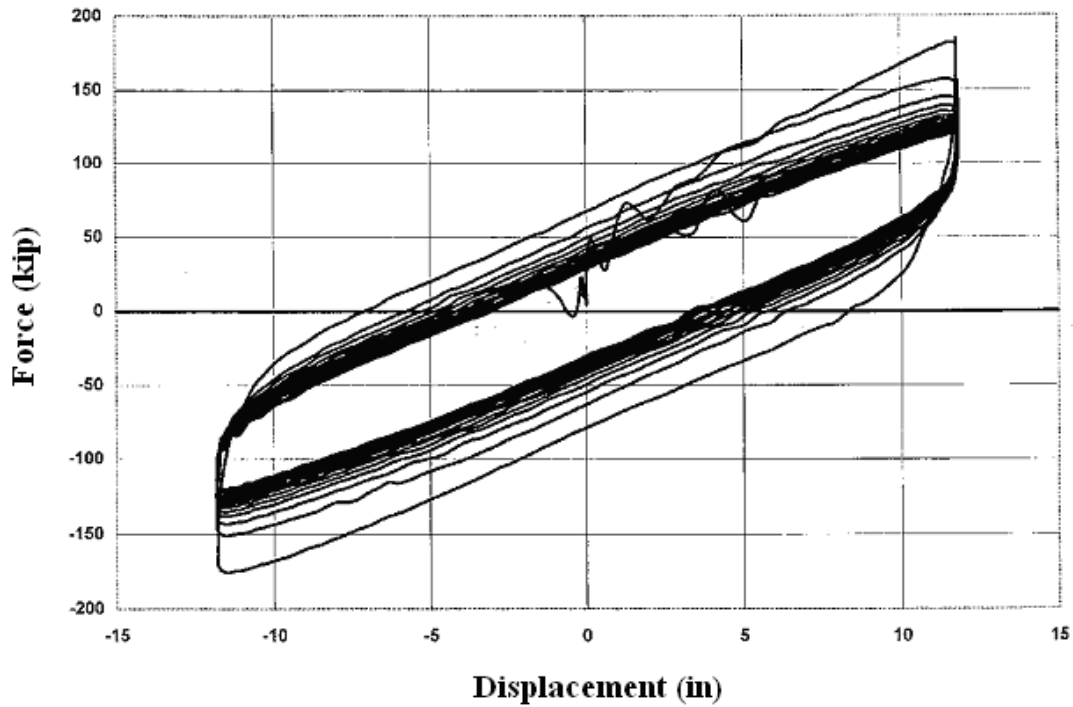
FIGURE 4-1 Force-Displacement Loops of Bearing of Figure 1-4. Load=850 kip (3783 kN), Displacement Amplitude=12 in (305 mm) and Frequency=0.5 Hz (Peak Velocity=37.7 in/s=958 mm/s)
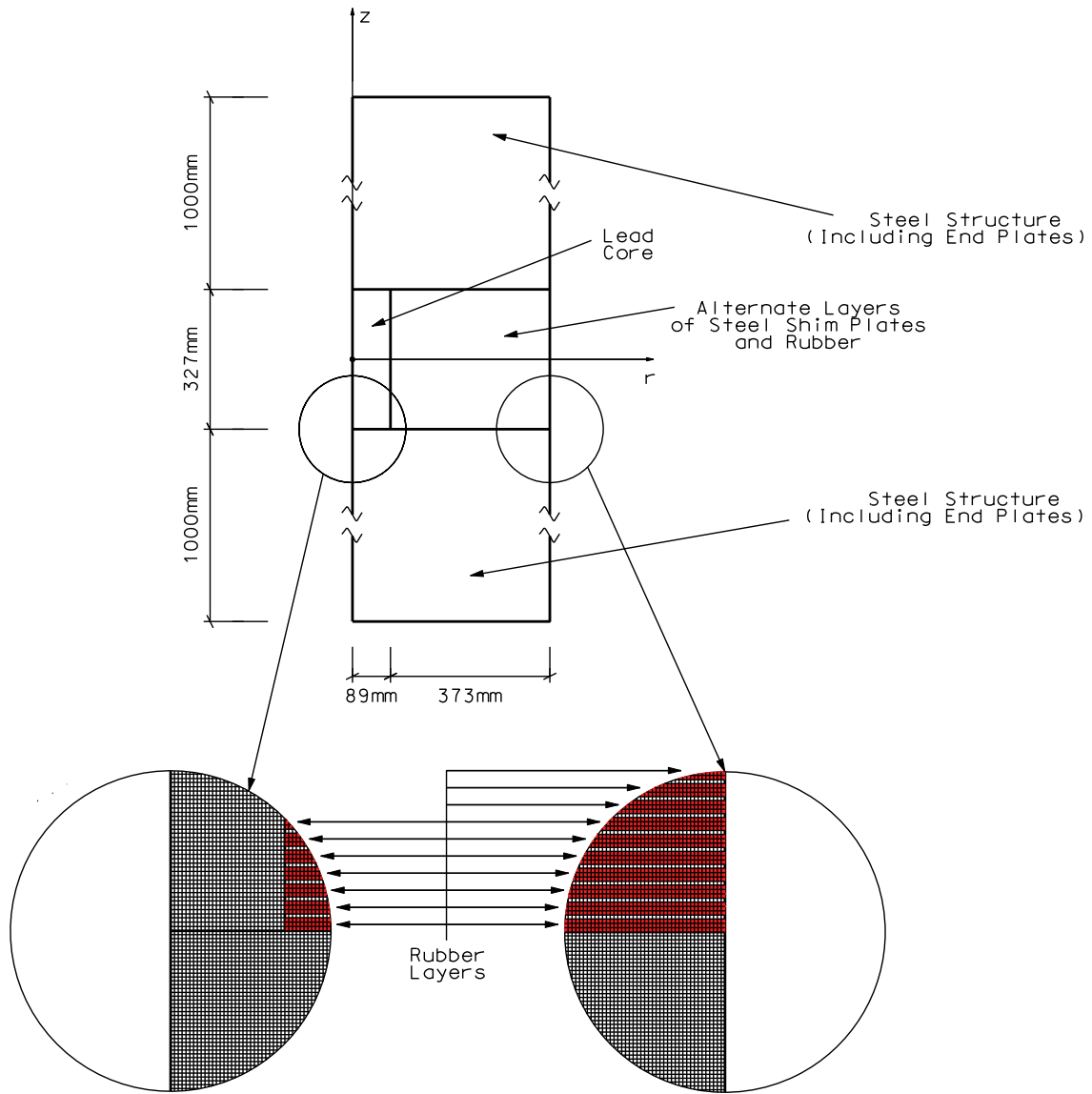
FIGURE 4-2 Explicit Finite Element Model for the Analysis of Temperature Rise in the Bearing of Figure 1-4

This explicit, finely meshed finite element model is only being used in this example for comparison and verification purposes. In the rest of the examples only the model of Figure 3-16 is used. Table 4-1 provides the data used in the analyses. Figure 4-3 presents the calculated histories of temperature and energy dissipated per cycle (EDC), and Figures 4-4 and 4-5 present temperature profiles in the lead core obtained in the

(composite) finite element analysis. Figure 4-6 compares the lead core center temperature obtained in both cases of finite element analysis (explicit & composite). Throughout this section, and with the exception of Figure 4-6, lead core temperatures presented as the output of finite element analyses are local temperatures collected at a point with coordinates $r = 0.7a$ and $z = 0$ (see Figure 3-16). It was observed that temperatures at that point were close to the average lead core temperature.

TABLE 4-1 Data Used in Analysis of Example 1

Vertical Load on Bearing, N	3783 kN
Amplitude of Motion, u_0	305 mm
Period of Motion, T	2.0 sec
Total Thickness of Shims, t_s	73 mm
Thickness of Steel Above and Below Bearing, t_p	1000 mm
Radius of Lead Core, a	89 mm
Bonded Rubber Radius, R	464 mm
Height of Lead Core, h_L	327 mm
Peak Velocity of Sinusoidal Motion, v_{max}	958 mm/s
Initial (Reference) Lead Effective Yield Stress, σ_{YL0}	12.9 MPa
Initial Temperature, T_{L0}	20^0C
Parameter of Exponential Relation of σ_{YL} vs. Temperature, E_2	$0.0069/^0$C
Effective Stiffness for 1st Cycle, $K_{eff,1}$	2.63 kN/mm
Effective Damping for Estimating Rubber Contribution to EDC	0.02
Assumed Yield Displacement, Y	10 mm
Thermal Properties of Rubber, Steel and Lead	Per Table 3-3
Heat Capacity of Rubber and Steel Composite, ρc	2510260 J/(m^3 ^{0}C)
Radial Conductivity of Rubber and Steel Composite, $k_{eff,radial}$	11.3 W/(m ^{0}C)
Vertical Conductivity of Rubber and Steel Composite, $k_{eff,vert}$	0.21 W/(m ^{0}C)

FIGURE 4-3 Temperature and Energy Dissipated per Cycle for Example 1

FIGURE 4-4 Vertical Temperature Distribution at the Center of the Bearing (r =0) of Figure 1-4 Obtained in Finite Element Analysis Based on Model of Figure 3-16

FIGURE 4-5 Horizontal Temperature Distribution (at z =0) of the Bearing of Figure 1-4 Obtained in Finite Element Analysis Based on Model of Figure 3-16
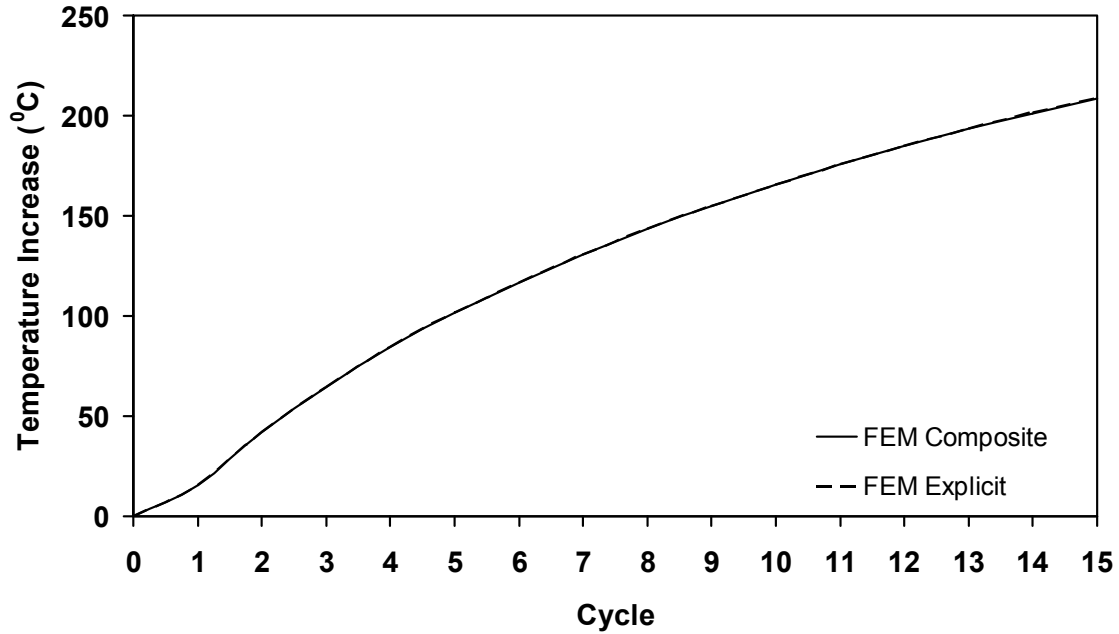
FIGURE 4-6 Comparison of Temperature Histories for the Center of the Lead Core of the Bearing of Figure 1-4 Subjected to a Harmonic Motion with 305 mm Amplitude and 2.0 sec Period as Calculated by FE Model with Explicit and Composite Representation of the Rubber and Steel

The results in Figure 4-3 demonstrate good agreement between experimental results and results of finite element analysis and of the simplified solution. This indicates that in this case heat conduction through the steel plates is very small.

At this point it would be useful to check the error of the simplified solution given by (3-59). We keep in mind that the criterion in (3-59) is conservative (see Section 3). We find that a 10^0C error is obtained after about 3 cycles of motion for this case of motion and bearing geometry. Figure 4-3 shows that a 10^0C error between the simplified solution and the analytical solution is rather obtained after about 8 cycles, when (3-59) yields a 40^0C error. We will confirm later on that using (3-59) with a 40^0C error (instead of a 10^0C one)

provides a more realistic approach when estimating the limit beyond which the simplified solution is not applicable.

The finite element analysis results presented in Figures 4-4 and 4-5 confirm the assumption that the lead core temperature in its bulk is about twice the steel-lead interface temperature, an assumption made in the analytical solutions. Also, the figures demonstrate (a) relatively uniform temperature distribution over the lead core height and (b) minimal extent of temperature increase in the steel shims. Note that there is practically no increase in temperature of the steel shims at distance $r=120$ mm whereas the free boundary of the shims is at $r=464$ mm. This demonstrates that treatment of the shims as a radially infinite medium in the analytical solutions is valid.

In a further study, the results of the explicit finite element model of Figure 4-2 are compared to the results of the simpler composite finite element model (Figure 3-16) in which the rubber layers and steel shims were replaced with a continuous anisotropic medium (termed composite finite element analysis). Results of the predictions using the two finite element models are presented in Figure 4-6. Evidently, the two models predict identical results. This observation indicates that the composite finite element model is sufficiently accurate for use in such analyses. It is, therefore, being exclusively used from this point on.

4.2.2 Example 2

The tested bearing geometry is again that of Figure 1-4. The bearings of examples 1 and 2 are two different bearings of identical construction, subjected to the same vertical load

and same amplitude of motion. However, in example 2 the velocity is 40 times smaller and only five cycles of motion are imposed. The time at the conclusion of the fifth cycle is 240 sec and the corresponding dimensionless time $t^+ = \alpha_S \cdot t / a^2$ is 0.427. Force-displacement loops are shown in Figure 4-7, test data in Table 4-2, data used in the analysis in Table 4-3 and analysis results in Figures 4-8 to 4-10.

The results in Figure 4-8 demonstrate that the two analytic solutions and the finite element solution predict well the experimental history of EDC. However, the simplified solution slightly underpredicts the EDC and substantially overpredicts (by about 40^0C after 5 cycles) the lead core temperature. It should be noted that the overprediction of temperature by the simplified solution (although apparently of no significant practical effect) is due to the neglect of heat conduction in the steel plates and shims. Apparently in this slow test there is sufficient time after about two cycles for heat to conduct through the steel plates and affect the lead core temperature. Equation (3-59) yields an error larger than 40^0C at the third cycle. Nevertheless, the simplified solution predicts well the experimental results at least up to the fourth cycle.

The finite element analysis results in Figures 4-9 and 4-10 that show temperature distribution within the bearing are qualitatively similar to those of example 1 and confirm the interface temperature assumptions made in the analytical solutions. Particularly (a) the lead core temperature increase at its bulk is about twice the temperature increase at the interface of the lead core and steel shims, and (b) the temperature increase in the steel shims is practically zero.

91

A conclusion from the presented results is that an error of up to about 40^0C in the prediction of the lead core temperature can still result in an acceptable error in the prediction of the energy dissipated per cycle.
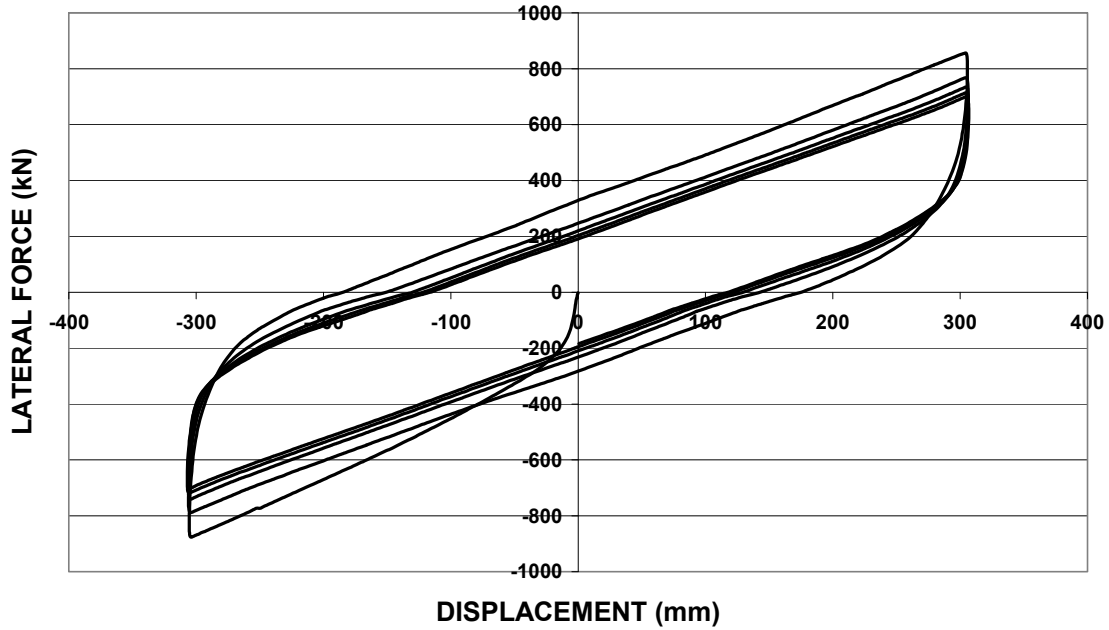
FIGURE 4-7 Force-Displacement Loops of Bearing of Figure 1-4. Load=3695 kN, Displacement Amplitude=12 in (305 mm) and Frequency=0.02 Hz (Constant Velocity=1 in/s=25 mm/s) (Constantinou et al., 2007b)

TABLE 4-2 Test Results for Example 2 (Constantinou et al., 2007b)

Cycle	Effective Stiffness (kN/mm)	Energy Dissipated Per Cycle (kN-mm)	Effective Damping	Effective Yield Stress of Lead (MPa)
1	2.83	358825	0.22	12.2
2	2.54	298218	0.20	9.6
3	2.41	263190	0.19	9.2
4	2.33	245162	0.18	7.9
5	2.28	232491	0.17	7.2

TABLE 4-3 Data Used in Analysis of Example 2

Vertical Load on Bearing, N	3695 kN
Amplitude of Motion, u_0	305 mm
Period of Motion, T	48.0 sec
Total Thickness of Shims, t_s	73 mm
Thickness of Steel Above and Below Bearing, t_p	1000 mm
Radius of Lead Core, a	89 mm
Bonded Rubber Radius, R	464 mm
Height of Lead Core, h_L	327 mm
Constant Velocity, v	25 mm/s
Initial (Reference) Lead Effective Yield Stress, σ_{YL0}	12.7 MPa
Initial Temperature, T_{L0}	20^0C
Parameter of Exponential Relation of σ_{YL} vs. Temperature, E_2	$0.0069/^0$C
Effective Stiffness for 1st Cycle, $K_{eff,1}$	2.84 kN/mm
Effective Damping for Estimating Rubber Contribution to EDC	0.01
Assumed Yield Displacement, Y	10 mm
Thermal Properties of Rubber, Steel and Lead	Per Table 3-3
Heat Capacity of Rubber and Steel Composite, ρc	2510260 J/(m^3 ^{0}C)
Radial Conductivity of Rubber and Steel Composite, $k_{eff,radial}$	11.3 W/(m ^{0}C)
Vertical Conductivity of Rubber and Steel Composite, $k_{eff,vert}$	0.21 W/(m ^{0}C)

FIGURE 4-8 Temperature and Energy Dissipated per Cycle for Example 2

FIGURE 4-9 Vertical Temperature Distribution at the Center of the Bearing (r=0) of Figure 1-4 Obtained in Finite Element Analysis Based on Model of Figure 3-16

FIGURE 4-10 Horizontal Temperature Distribution (at z=0) of the Bearing of Figure 1-4 Obtained in Finite Element Analysis Based on Model of Figure 3-16

4.2.3 Example 3

The tested bearing is that of Figure 4-11. Test data and parameters are presented in Table

4-4, data used in the analysis are presented in Table 4-5 and analysis results are presented

in Figures 4-12 to 4-14. Note that the bearing was subjected to four cycles of 113 mm

amplitude at a frequency of 0.357 Hz (period of 2.8 sec). The duration of testing was 11.2

sec and the corresponding dimensionless time $t^+ = \alpha_S \cdot t / a^2$ was 0.129. In this case a

control specimen without lead core was also tested. This allowed for accurate separation

of lead and rubber contributions to the energy dissipated per cycle.

The results in Figure 4-12 demonstrate that all solutions, including the simplified one,

predict well the history of EDC. It should be noted that there is little change in the EDC

over the four cycles of testing and that the predicted temperature rise over these four

cycles is relatively small.

The results in Figures 4-13 and 4-14 once more provide verification of the validity of the

assumptions of (a) the uniformity of lead core temperature over the height, (b) that the

lead core temperature rise in its bulk is about twice the temperature rise at the lead-steel

shim interface, and (c) the temperature rise in the steel shims vanishes at some point

away from the bearing free boundary.
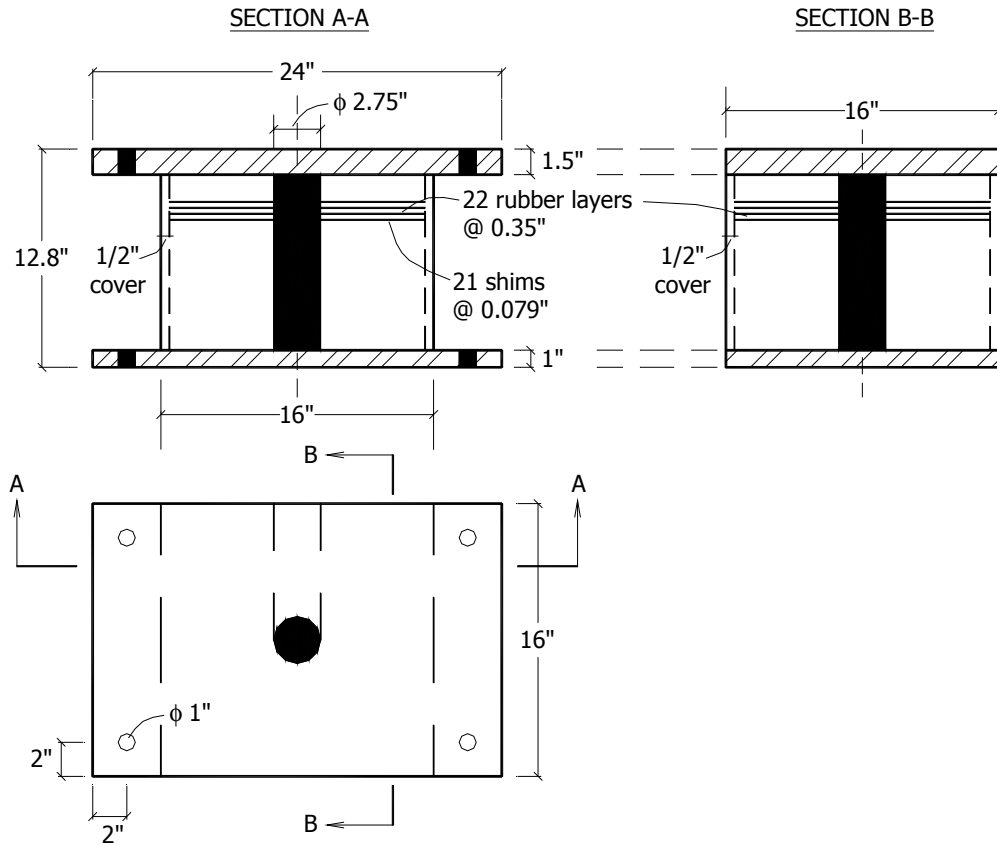
FIGURE 4-11 Tested Bearing with and without Lead Core (1 inch=25.4 mm) (Constantinou et al., 2007b)

TABLE 4-4 Test Data for Example 3 (Constantinou et al., 2007b)

Rubber Bearing (Control Specimen Without Lead Core)				
Cycle	EDC (kN-mm)	Effective Stiffness (kN/mm)	Effective Damping	Effective Shear Modulus (MPa)
1	3436	0.56	0.08	0.75
2	3391	0.54	0.08	0.73
3	3312	0.53	0.08	0.71
4	3278	0.53	0.08	0.71
Lead-Rubber Bearing					
Cycle	EDC (kN-mm)	Effective Stiffness (kN/mm)	Post-elastic Stiffness (kN/mm)	Effective Damping	Lead Yield Stress (MPa)
1	17441	0.88	0.50	0.25	11.2
2	17361	0.86	0.48	0.25	11.1
3	15971	0.81	0.46	0.25	10.3
4	15135	0.79	0.46	0.24	9.7

TABLE 4-5 Data Used in Analysis of Example 3

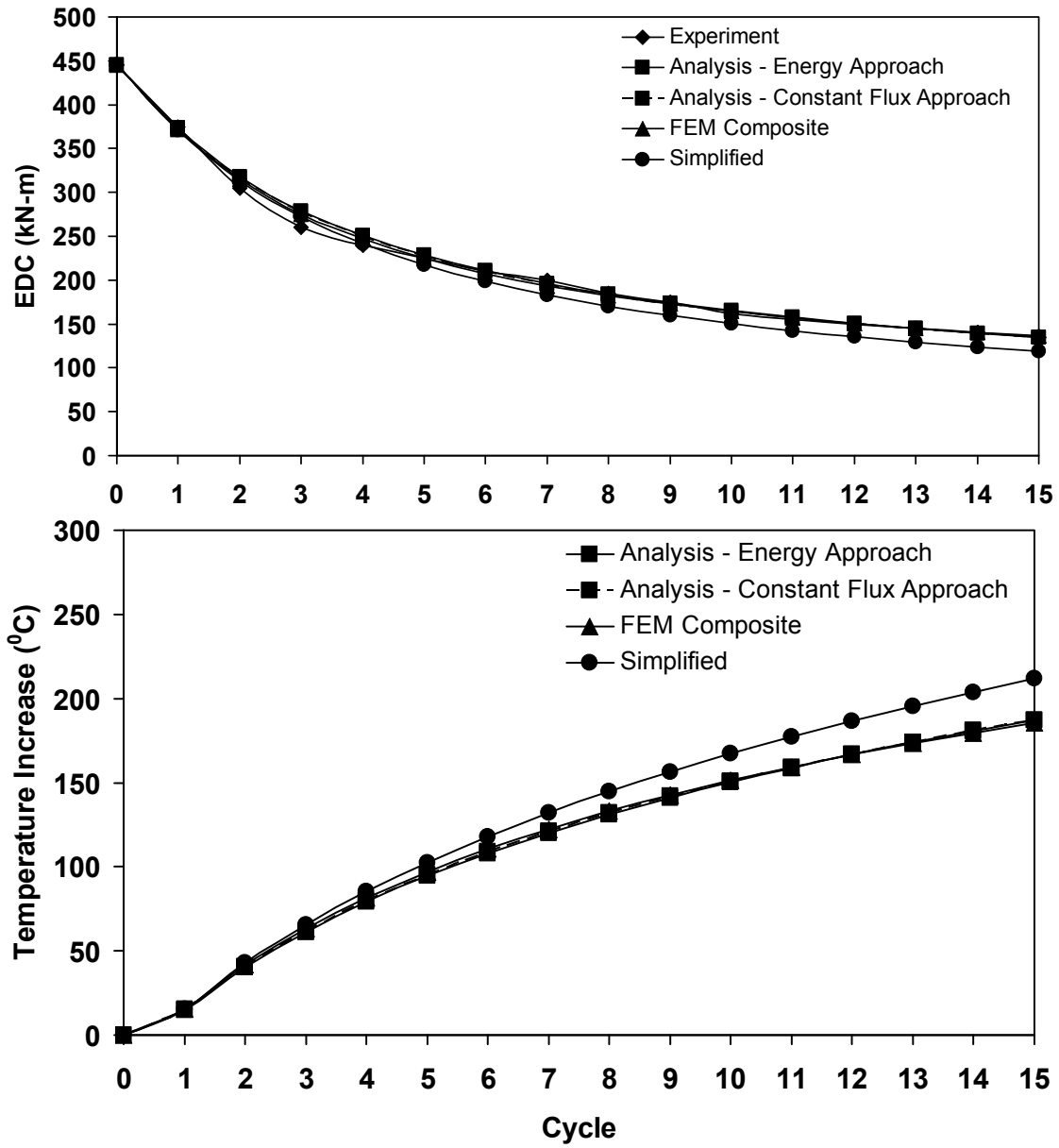|	
Vertical Load on Bearing, N	947 kN
Amplitude of Motion, u_0	113 mm
Period of Motion, T	2.8 sec
Total Thickness of Shims, t_s	42 mm
Thickness of Steel Above and Below Bearing, t_p	700 mm
Radius of Lead Core, a	35 mm
Bonded Rubber Radius, R	191 mm
Height of Lead Core, h_L	262 mm
Peak Velocity of Sinusoidal Motion, v_{max}	250 mm/s
Initial (Reference) Lead Effective Yield Stress, σ_{YL0}	9.0 MPa
Initial Temperature, T_{L0}	20^0C
Parameter of Exponential Relation of σ_{YL} vs. Temperature, E_2	$0.0069/^0$C
Effective Stiffness for 1st Cycle, $K_{eff,1}$	Per Table 4-4
Effective Damping for Estimating Rubber Contribution to EDC	N/A
Assumed Yield Displacement, Y	12 mm
Thermal Properties of Rubber, Steel and Lead	Per Table 3-3
Heat Capacity of Rubber and Steel Composite, ρc	2425611 J/(m^3 ^{0}C)
Radial Conductivity of Rubber and Steel Composite, $k_{eff,radial}$	8.1 W/(m ^{0}C)
Vertical Conductivity of Rubber and Steel Composite, $k_{eff,vert}$	0.19 W/(m ^{0}C)

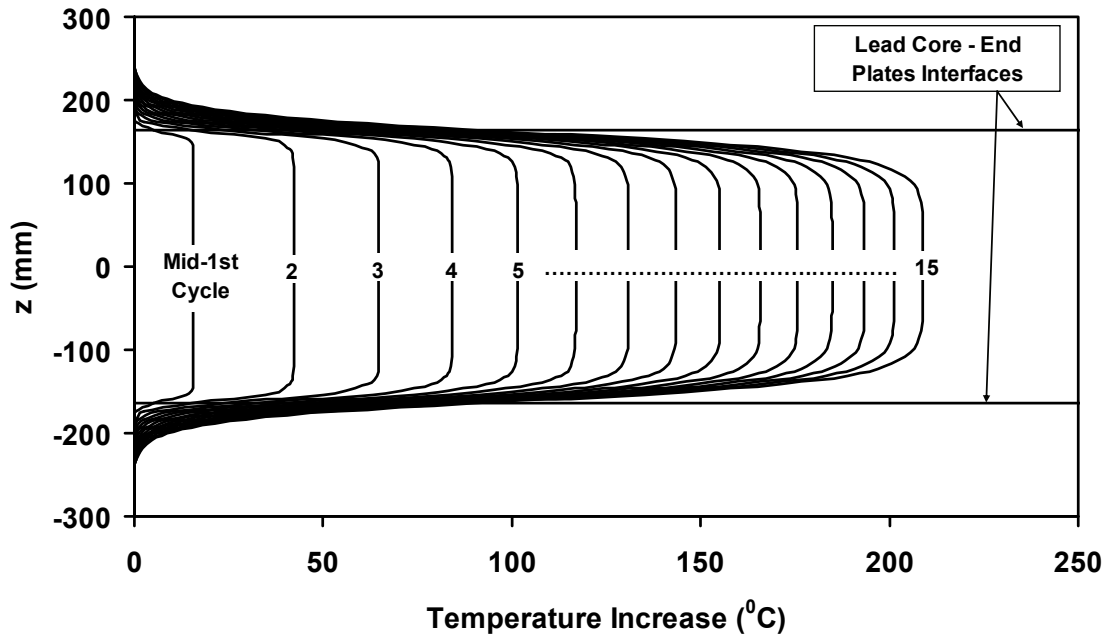**FIGURE 4-12 Temperature and Energy Dissipated per Cycle for Example 3**

FIGURE 4-13 Vertical Temperature Distribution at the Center of the Bearing (r=0) of Figure 4-11 Obtained in Finite Element Analysis Based on Model of Figure 3-16
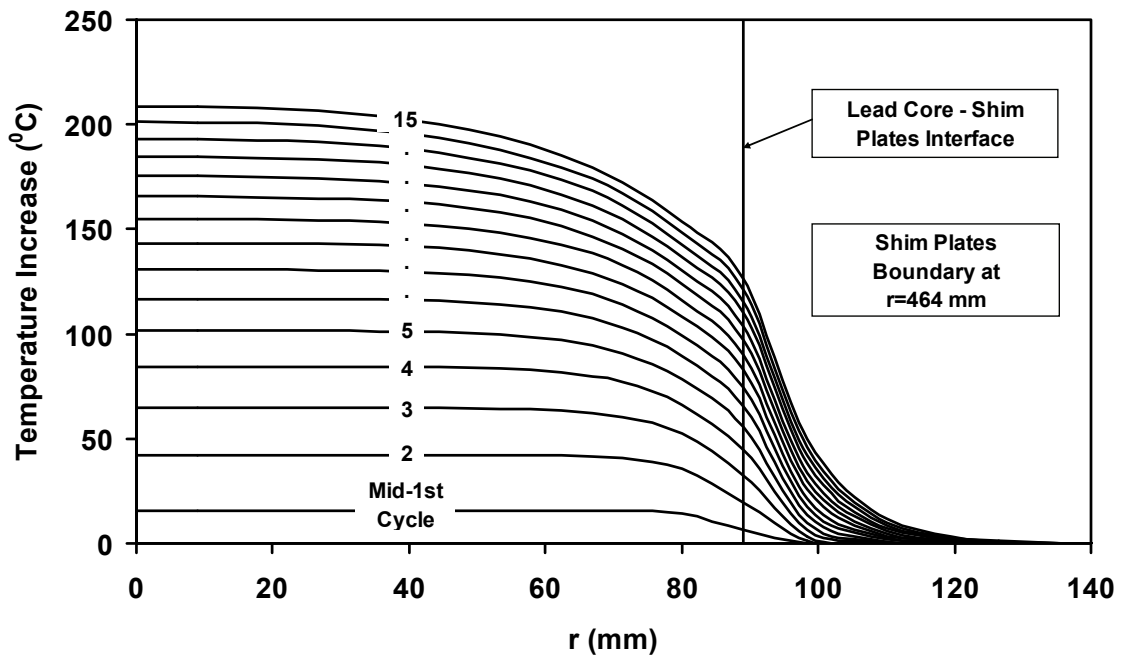

FIGURE 4-14 Horizontal Temperature Distribution (at z=0) of the Bearing of Figure 4-11 Obtained in Finite Element Analysis Based on Model of Figure 3-16

4.2.4 Example 4

The tested bearing is again that of Figure 4-11. Test data and parameters are presented in Table 4-6, data used in the analysis are presented in Table 4-7 and analysis results are presented in Figures 4-15 to 4-17. Note that the only difference from Example 3 is that the initial temperature is -26^0C rather than 20^0C. The dimensionless time at the end of the fourth cycle is again 0.129. The results of this example are qualitatively the same as those of Example 3 with the exception that values of EDC are larger due to the lower initial temperature.

TABLE 4-6 Test Data for Example 4 (Constantinou et al., 2007b)

Rubber Bearing (Control Specimen Without Lead Core)				
Cycle	EDC (kN-mm)	Effective Stiffness (kN/mm)	Effective Damping	Effective Shear Modulus (MPa)
1	8862	0.82	0.14	1.10
2	7833	0.79	0.13	1.06
3	8251	0.77	0.13	1.04
4	8025	0.75	0.13	1.01
Lead-Rubber Bearing				
Cycle	EDC (kN-mm)	Effective Stiffness (kN/mm)	Post-elastic Stiffness (kN/mm)	Effective Damping	Lead Yield Stress (MPa)
1	25635	1.19	0.63	0.27	16.5
2	25274	1.17	0.62	0.27	16.2
3	24030	1.09	0.57	0.27	15.4
4	22889	1.05	0.55	0.27	14.7

TABLE 4-7 Data Used in Analysis of Example 4

Vertical Load on Bearing, N	947 kN
Amplitude of Motion, u_0	113 mm
Period of Motion, T	2.8 sec
Total Thickness of Shims, t_s	42 mm
Thickness of Steel Above and Below Bearing, t_p	700 mm
Radius of Lead Core, a	35 mm
Bonded Rubber Radius, R	191 mm
Height of Lead Core, h_L	262 mm
Peak Velocity of Sinusoidal Motion, v_{max}	250 mm/s
Initial (Reference) Lead Effective Yield Stress, σ_{YL0}	10.9 MPa
Initial Temperature, T_{L0}	$-26\,^0C$
Parameter of Exponential Relation of σ_{YL} vs. Temperature, E_2	$0.0069/^0C$
Effective Stiffness for 1st Cycle, $K_{eff,1}$	Per Table 4-6
Effective Damping for Estimating Rubber Contribution to EDC	N/A
Assumed Yield Displacement, Y	12 mm
Thermal Properties of Rubber, Steel and Lead	Per Table 3-3
Heat Capacity of Rubber and Steel Composite, ρc	2425611 J/(m^3 ^{0}C)
Radial Conductivity of Rubber and Steel Composite, $k_{eff,radial}$	8.1 W/(m ^{0}C)
Vertical Conductivity of Rubber and Steel Composite, $k_{eff,vert}$	0.19 W/(m ^{0}C)

FIGURE 4-15 Temperature and Energy Dissipated per Cycle for Example 4

FIGURE 4-16 Vertical Temperature Distribution at the Center of the Bearing ($r=0$) of Figure 4-11 Obtained in Finite Element Analysis Based on Model of Figure 3-16

FIGURE 4-17 Horizontal Temperature Distribution (at $z=0$) of the Bearing of Figure 4-11 Obtained in Finite Element Analysis Based on Model of Figure 3-16

4.2.5 Example 5

The tested bearing is again that of Figure 4-11. Test data and parameters are presented in Table 4-8, data used in the analysis are presented in Table 4-9 and analysis results are presented in Figures 4-18 to 4-20. Note that the only difference from Example 3 is that the initial temperature is 49^{0}C rather than 20^{0}C. The dimensionless time at the end of the fourth cycle is again 0.129. The results for this example are qualitatively the same as those of Examples 3 and 4 except that values of EDC are smaller due to the higher initial temperature.

TABLE 4-8 Test Data for Example 5 (Constantinou et al., 2007b)

Rubber Bearing (Control Specimen Without Lead Core)				
Cycle	EDC (kN-mm)	Effective Stiffness (kN/mm)	Effective Damping	Effective Shear Modulus (MPa)
1	2701	0.49	0.07	0.66
2	2600	0.49	0.07	0.66
3	2588	0.49	0.07	0.66
4	2622	0.49	0.07	0.66
Lead-Rubber Bearing					
Cycle	EDC (kN-mm)	Effective Stiffness (kN/mm)	Post-elastic Stiffness (kN/mm)	Effective Damping	Lead Yield Stress (MPa)
1	14954	0.77	0.44	0.24	9.6
2	14490	0.74	0.42	0.24	9.3
3	13643	0.70	0.41	0.24	8.8
4	13145	0.70	0.41	0.23	8.4

TABLE 4-9 Data Used in Analysis of Example 5

Vertical Load on Bearing, N	947 kN
Amplitude of Motion, u_0	113 mm
Period of Motion, T	2.8 sec
Total Thickness of Shims, t_s	42 mm
Thickness of Steel Above and Below Bearing, t_p	700 mm
Radius of Lead Core, a	35 mm
Bonded Rubber Radius, R	191 mm
Height of Lead Core, h_L	262 mm
Peak Velocity of Sinusoidal Motion, v_{max}	250 mm/s
Initial (Reference) Lead Effective Yield Stress, σ_{YL0}	8.0 MPa
Initial Temperature, T_{L0}	49^0C
Parameter of Exponential Relation of σ_{YL} vs. Temperature, E_2	$0.0069/^0$C
Effective Stiffness for 1st Cycle, $K_{eff,1}$	Per Table 4-8
Effective Damping for Estimating Rubber Contribution to EDC	N/A
Assumed Yield Displacement, Y	12 mm
Thermal Properties of Rubber, Steel and Lead	Per Table 3-3
Heat Capacity of Rubber and Steel Composite, ρc	2425611 J/(m^3 ^{0}C)
Radial Conductivity of Rubber and Steel Composite, $k_{eff,radial}$	8.1 W/(m ^{0}C)
Vertical Conductivity of Rubber and Steel Composite, $k_{eff,vert}$	0.19 W/(m ^{0}C)

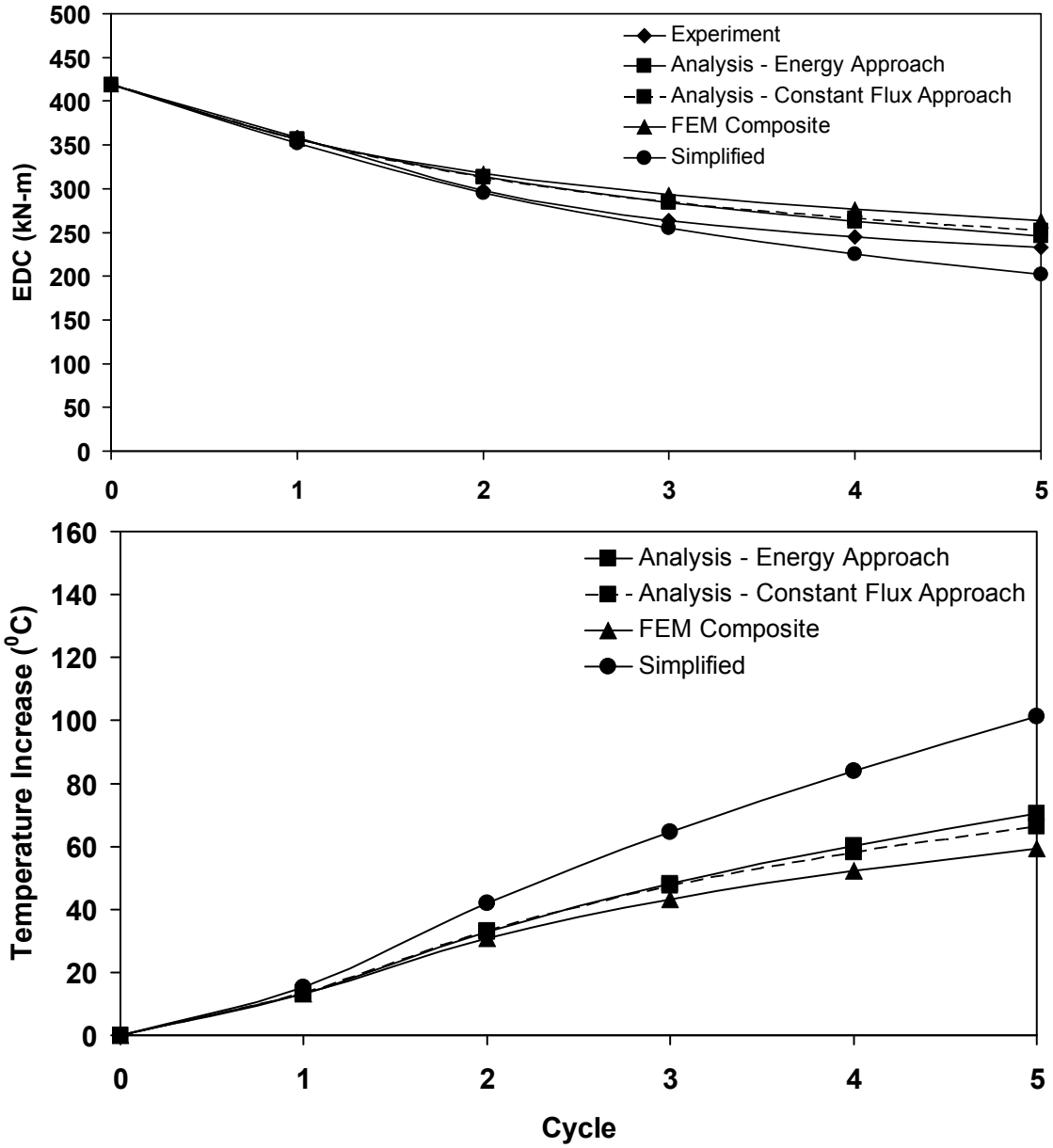**FIGURE 4-18 Temperature and Energy Dissipated per Cycle for Example 5**
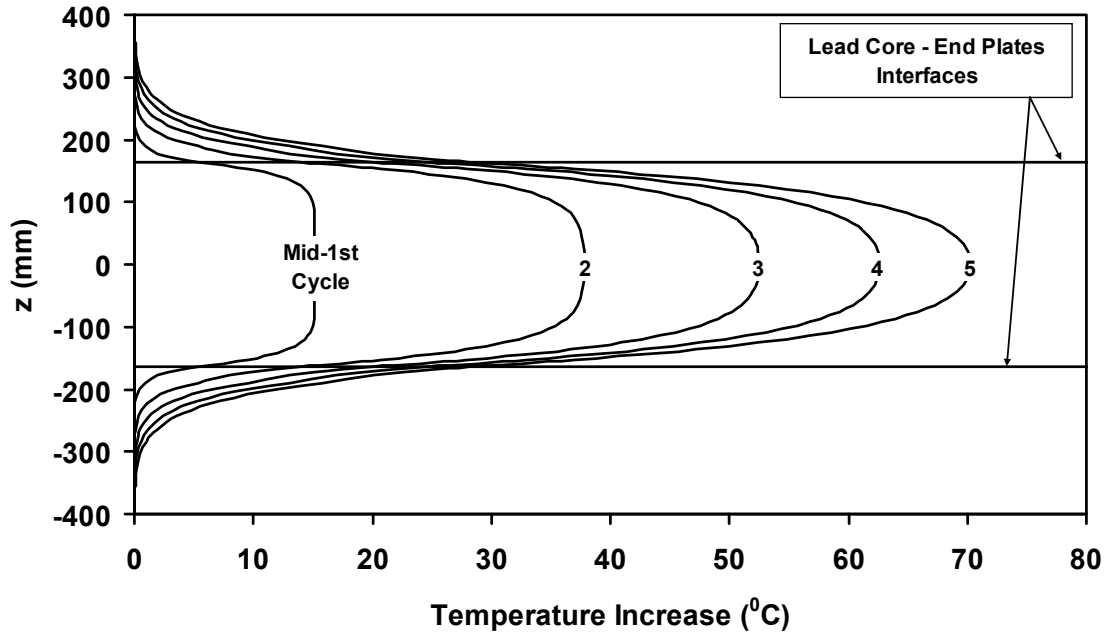
FIGURE 4-19 Vertical Temperature Distribution at the Center of the Bearing (r =0) of Figure 4-11 Obtained in Finite Element Analysis Based on Model of Figure 3-16
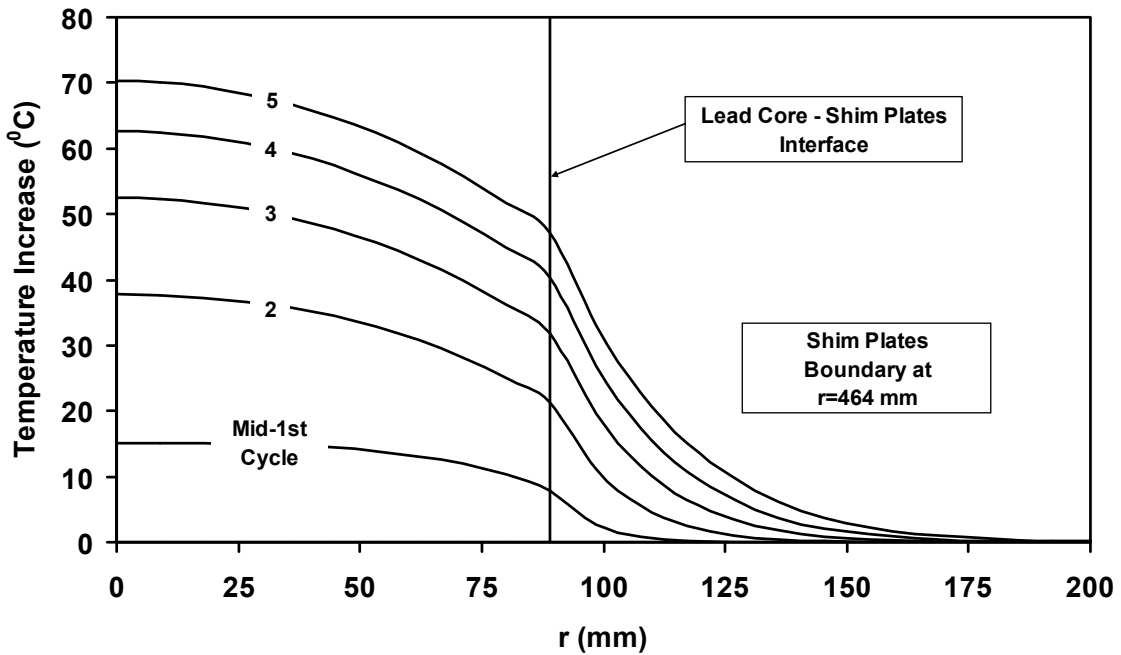

FIGURE 4-20 Horizontal Temperature Distribution (at z =0) of the Bearing of Figure 4-11 Obtained in Finite Element Analysis Based on Model of Figure 3-16

4.2.6 Example 6

The tested bearing is again that of Figure 4-11. Test data and parameters are presented in Table 4-10, data used in the analysis are presented in Table 4-11 and analysis results are presented in Figures 4-21 to 4-23. Note that all parameters in this example are identical to those of Example 3 except that the duration of testing is much larger (28 sec per cycle instead of 2.8 sec per cycle). The dimensionless time at the end of the fourth cycle is 1.295.

The results in Figure 4-21 demonstrate insignificant changes in EDC over the four cycles of testing and that all solutions predict well the experimental EDC. This may be counterintuitive because the test is slow (as characterized by a large dimensionless time at the end of the test) so that heat conduction effects through the end and shim plates should be important. The simplified solution then (which neglects heat conduction) should have underestimated the EDC. Although this is true, the underestimation is very small for practical purpose. This is due to the relatively small increase in temperature of the lead core – a result of the small travel over lead core height experienced by the bearing during the four cycles (this is true for all Examples 3 to 7).

The results in Figures 4-22 and 4-23 show for the first cycle uniform temperature increase over lead core height and validity of the assumption that the lead core temperature in the bulk is about twice that at the interface of lead and steel shims. The validity of these conditions deteriorates as the number of cycles increases (apparently due to heat conduction effects) – a situation that is also true for Example 2 for which also the test was under slow or quasi-static conditions.

111

Also in Figure 4-23 we observe once more that the temperature increase in the steel shims is practically zero at a point far away from the free surface of the bearing – a condition common to all examples presented herein.

TABLE 4-10 Test Data for Example 6 (Constantinou et al., 2007b)

Rubber Bearing (Control Specimen Without Lead Core)				
Cycle	EDC (kN-mm)	Effective Stiffness (kN/mm)	Effective Damping	Effective Shear Modulus (MPa)
1	3007	0.49	0.08	0.66
2	2826	0.49	0.07	0.66
3	2769	0.49	0.07	0.66
4	2735	0.49	0.07	0.66
Lead-Rubber Bearing					
Cycle	EDC (kN-mm)	Effective Stiffness (kN/mm)	Post-elastic Stiffness (kN/mm)	Effective Damping	Lead Yield Stress (MPa)
1	15282	0.70	0.37	0.27	9.8
2	15203	0.65	0.32	0.29	9.8
3	14954	0.65	0.32	0.29	9.6
4	14796	0.65	0.32	0.28	9.5

TABLE 4-11 Data Used in Analysis of Example 6

Vertical Load on Bearing, N	947 kN
Amplitude of Motion, u_0	113 mm
Period of Motion, T	28 sec
Total Thickness of Shims, t_s	42 mm
Thickness of Steel Above and Below Bearing, t_p	700 mm
Radius of Lead Core, a	35 mm
Bonded Rubber Radius, R	191 mm
Height of Lead Core, h_L	262 mm
Peak Velocity of Sinusoidal Motion, v_{max}	25 mm/s
Initial (Reference) Lead Effective Yield Stress, σ_{YL0}	7.9 MPa
Initial Temperature, T_{L0}	20^0C
Parameter of Exponential Relation of σ_{YL} vs. Temperature, E_2	$0.0069/^0$C
Effective Stiffness for 1st Cycle, $K_{eff,1}$	Per Table 4-10
Effective Damping for Estimating Rubber Contribution to EDC	N/A
Assumed Yield Displacement, Y	12 mm
Thermal Properties of Rubber, Steel and Lead	Per Table 3-3
Heat Capacity of Rubber and Steel Composite, ρc	2425611 J/(m^3 ^{0}C)
Radial Conductivity of Rubber and Steel Composite, $k_{eff,radial}$	8.1 W/(m ^{0}C)
Vertical Conductivity of Rubber and Steel Composite, $k_{eff,vert}$	0.19 W/(m ^{0}C)

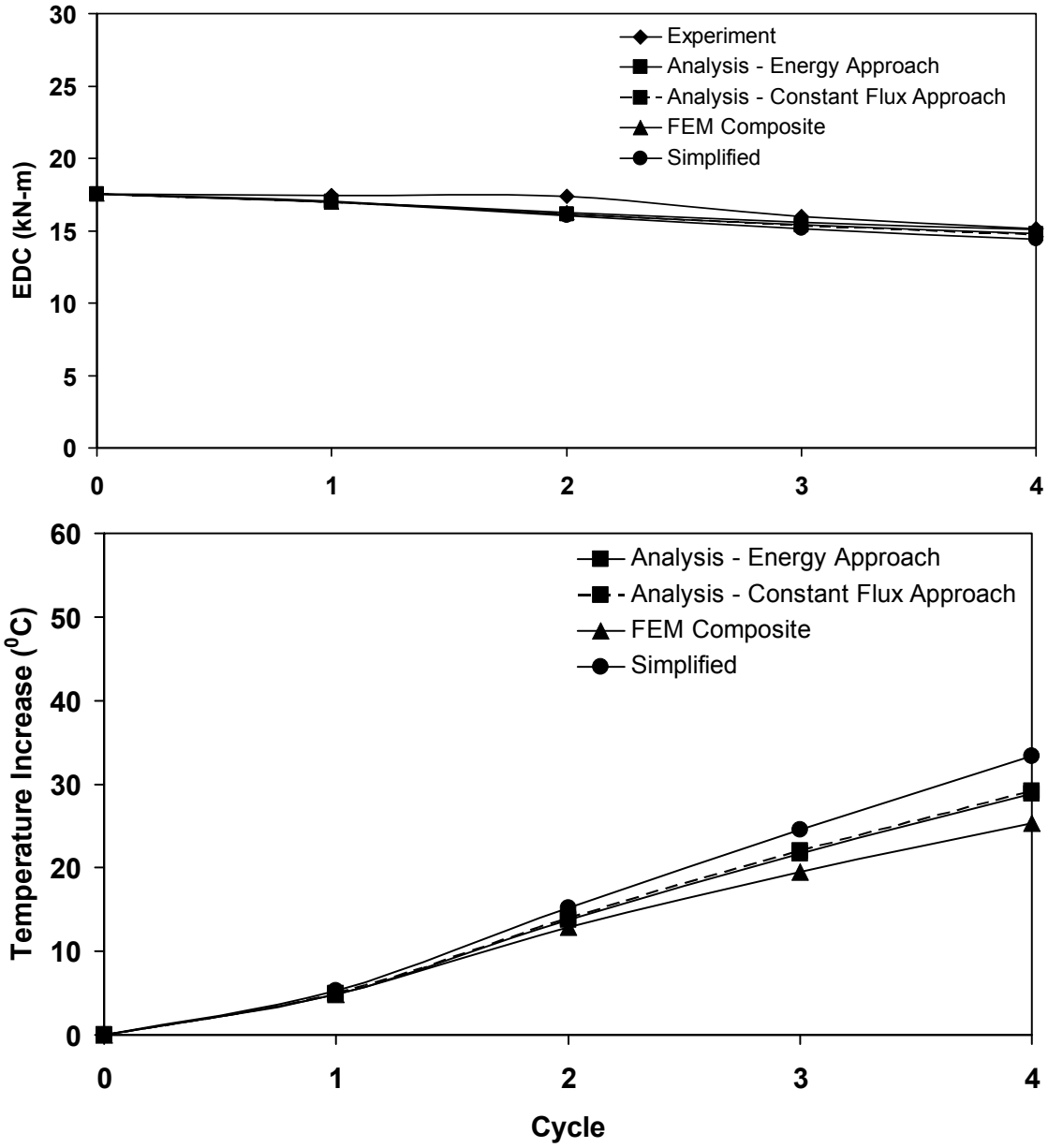**FIGURE 4-21 Temperature and Energy Dissipated per Cycle for Example 6**
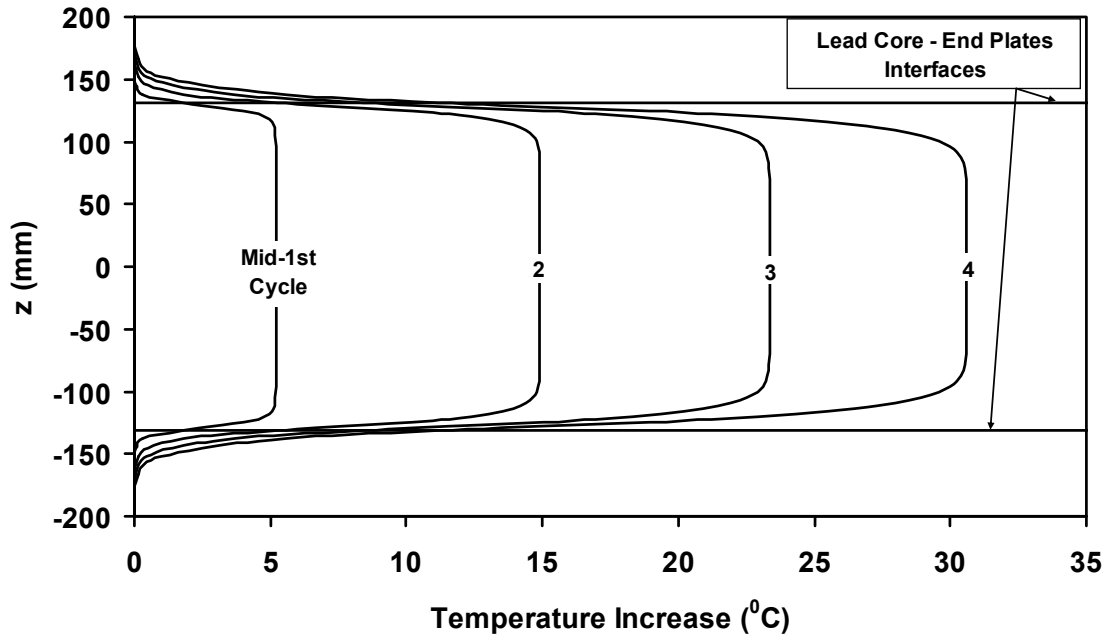
114

FIGURE 4-22 Vertical Temperature Distribution at the Center of the Bearing ($r=0$) of Figure 4-11 Obtained in Finite Element Analysis Based on Model of Figure 3-16
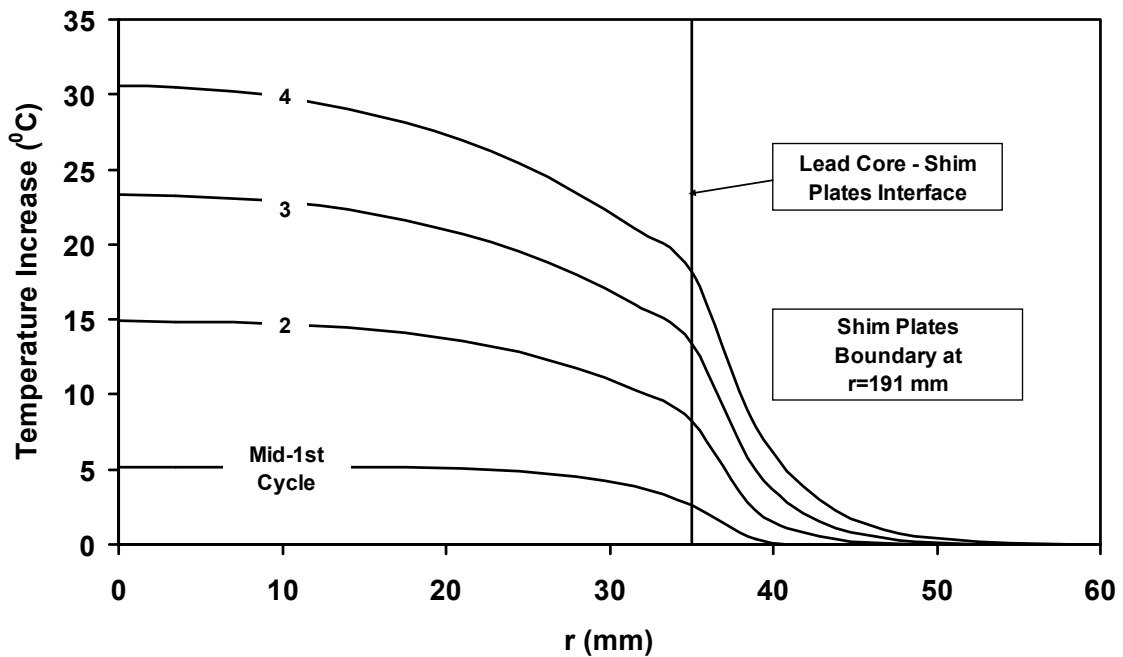

FIGURE 4-23 Horizontal Temperature Distribution (at $z=0$) of the Bearing of Figure 4-11 Obtained in Finite Element Analysis Based on Model of Figure 3-16

4.2.7 Example 7

The tested bearing is again that of Figure 4-11. Test data and parameters are presented in Table 4-12, data used in the analysis are presented in Table 4-13 and analysis results are presented in Figures 4-24 to 4-26. The parameters in this example are identical to those of Examples 3 and 6 except that the duration of testing is in-between that in the other two examples (5.7 sec per cycle). The dimensionless time at the end of the fourth cycle of testing is 0.263.

The results are qualitatively the same as those of Example 3 which was conducted at comparable speed (although twice as much). Thus, the testing speed in this example is half that of Example 3 but still much higher than that of Example 6. Again the predictions of all solutions, including the simplified one, compare very well with the experimental values of EDC. This is due to the heat conduction through the steel plates and shims being very small and its effect on the lead core temperature being insignificant.

TABLE 4-12 Test Data for Example 7 (Constantinou et al., 2007b)

Rubber Bearing (Control Specimen Without Lead Core)				
Cycle	EDC (kN-mm)	Effective Stiffness (kN/mm)	Effective Damping	Effective Shear Modulus (MPa)
1	2939	0.53	0.07	0.71
2	3018	0.53	0.07	0.71
3	3007	0.53	0.07	0.71
4	2973	0.53	0.07	0.71
Lead-Rubber Bearing				
Cycle	EDC (kN-mm)	Effective Stiffness (kN/mm)	Post-elastic Stiffness (kN/mm)	Effective Damping	Lead Yield Stress (MPa)
1	17689	0.81	0.42	0.27	11.4
2	16988	0.74	0.37	0.29	10.9
3	16152	0.72	0.37	0.28	10.4
4	15621	0.72	0.37	0.27	10.0

TABLE 4-13 Data Used in Analysis of Example 7

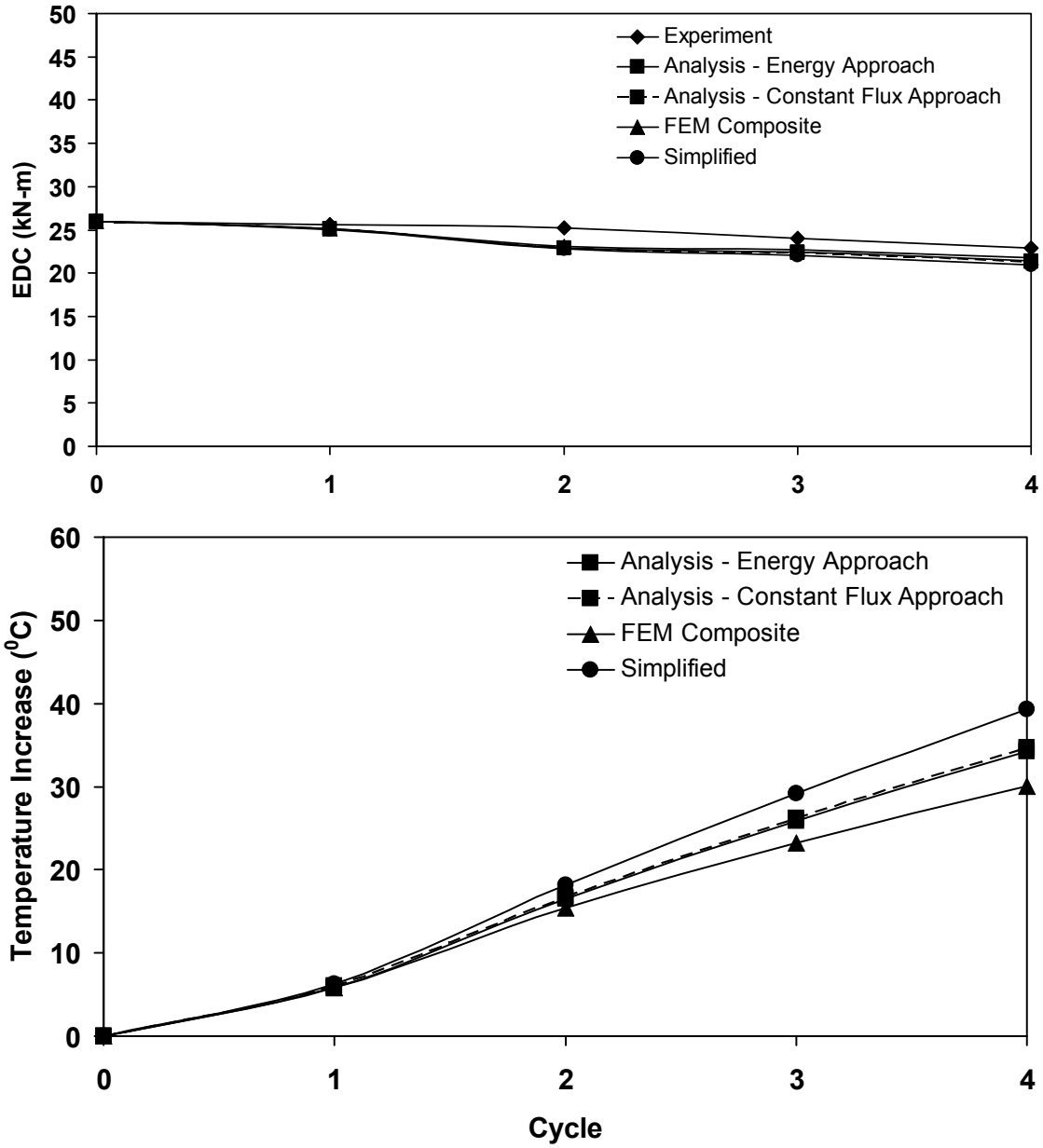|	
Vertical Load on Bearing, N	947 kN
Amplitude of Motion, u_0	113 mm
Period of Motion, T	5.6 sec
Total Thickness of Shims, t_s	42 mm
Thickness of Steel Above and Below Bearing, t_p	700 mm
Radius of Lead Core, a	35 mm
Bonded Rubber Radius, R	191 mm
Height of Lead Core, h_L	262 mm
Peak Velocity of Sinusoidal Motion, v_{max}	125 mm/s
Initial (Reference) Lead Effective Yield Stress, σ_{YL0}	9.7 MPa
Initial Temperature, T_{L0}	20^0C
Parameter of Exponential Relation of σ_{YL} vs. Temperature, E_2	$0.0069/^0$C
Effective Stiffness for 1st Cycle, $K_{eff,1}$	Per Table 4-12
Effective Damping for Estimating Rubber Contribution to EDC	N/A
Assumed Yield Displacement, Y	12 mm
Thermal Properties of Rubber, Steel and Lead	Per Table 3-3
Heat Capacity of Rubber and Steel Composite, ρc	2425611 J/(m^3 ^{0}C)
Radial Conductivity of Rubber and Steel Composite, $k_{eff,radial}$	8.1 W/(m ^{0}C)
Vertical Conductivity of Rubber and Steel Composite, $k_{eff,vert}$	0.19 W/(m ^{0}C)

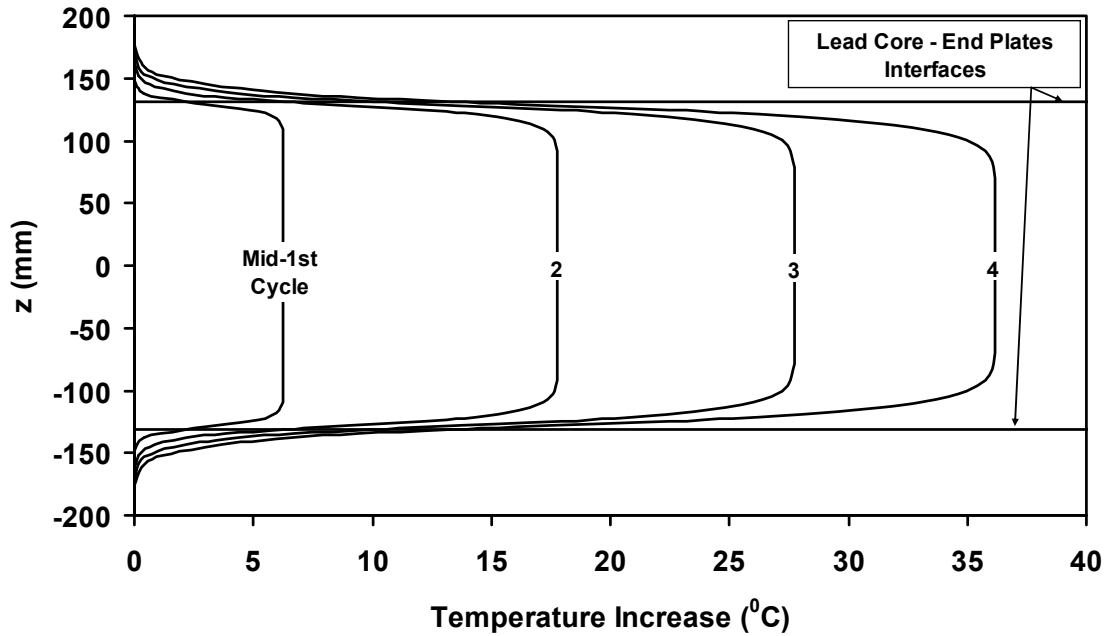**FIGURE 4-24 Temperature and Energy Dissipated per Cycle for Example 7**
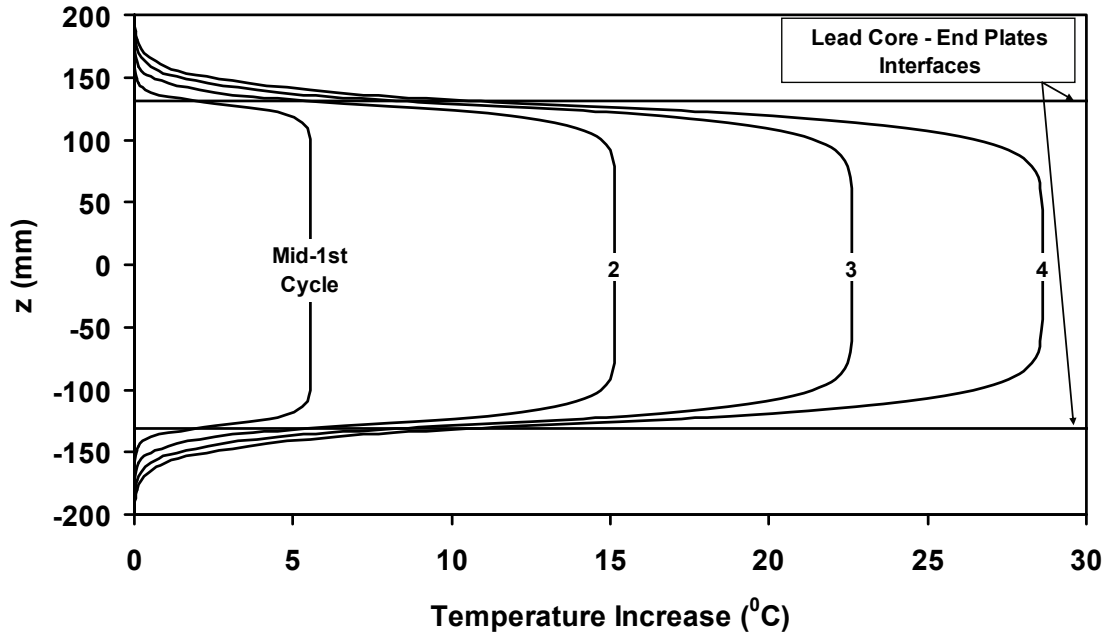
FIGURE 4-25 Vertical Temperature Distribution at the Center of the Bearing ($r=0$) of Figure 4-11 Obtained in Finite Element Analysis Based on Model of Figure 3-16
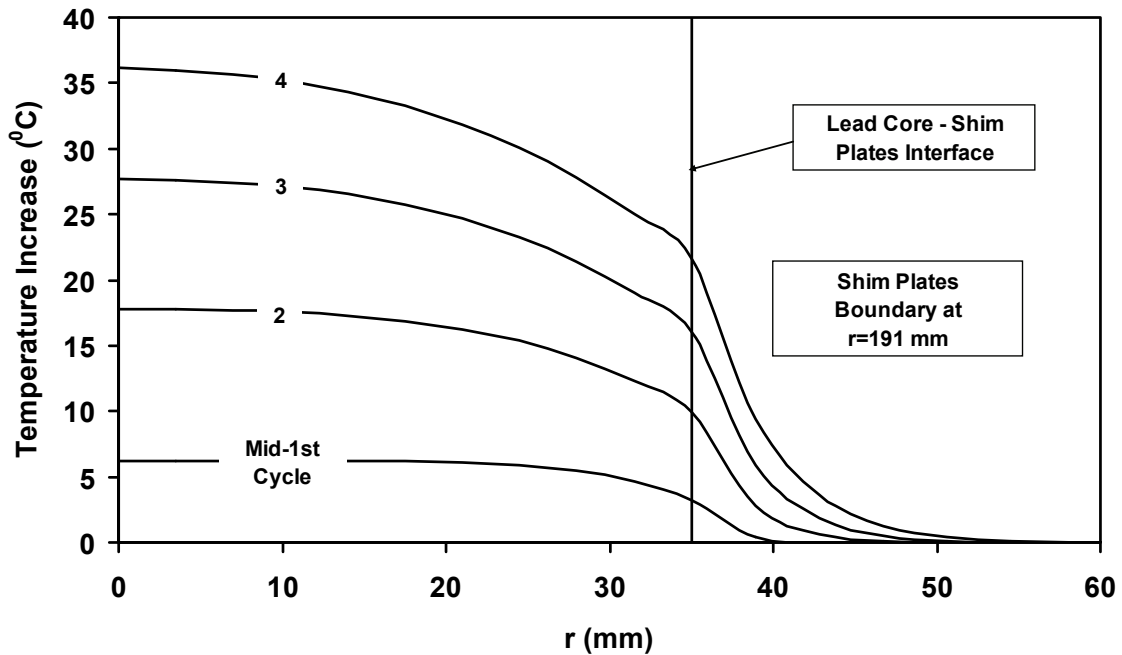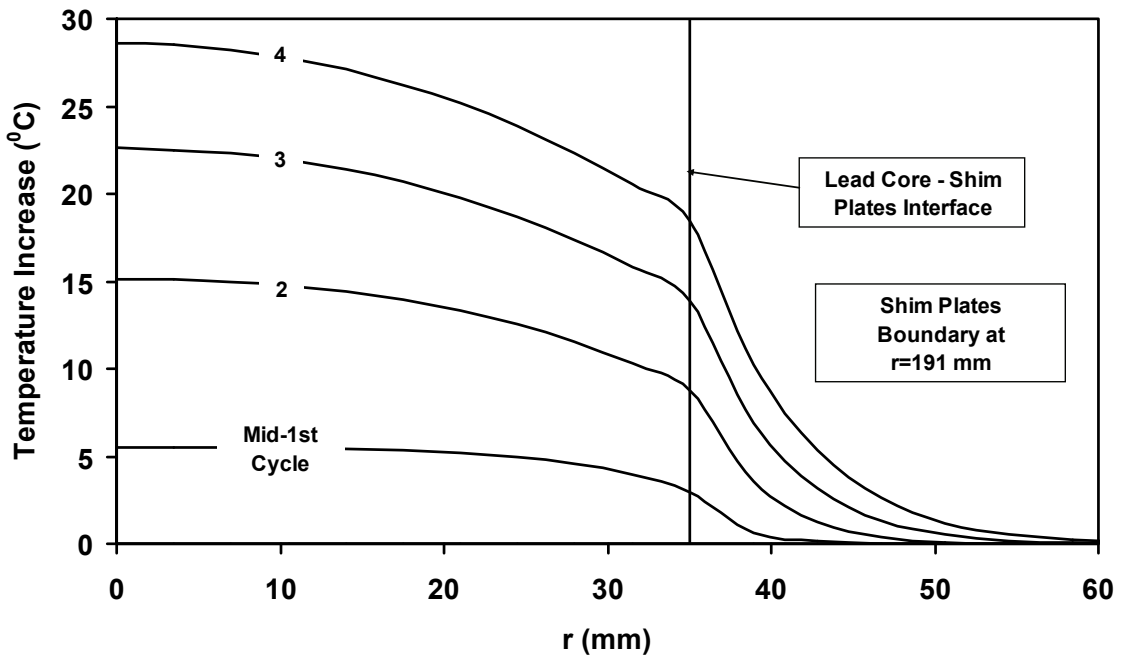

FIGURE 4-26 Horizontal Temperature Distribution (at $z=0$) of the Bearing of Figure 4-11 Obtained in Finite Element Analysis Based on Model of Figure 3-16

4.2.8 Example 8

The tested bearing is that of Figure 4-27 with recorded force-displacement loops shown in Figure 4-28. Data and parameters of testing are presented in Table 4-14, data used in the analysis are presented in Table 4-15 and analysis results are presented in Figures 4-29 to 4-31. The dimensionless time at the end of the third cycle of testing is 0.005, a very short dimensionless time.

Figure 4-29 shows good prediction of the reduction in the EDC by all analytical solutions (including the simplified solution). In this case, (3-59) yields an error much smaller than 40^0C for the 3 cycles of motion, a condition for the validity of the simplified solution. Figures 4-30 and 4-31 confirm the interface temperature assumptions and also show relatively uniform lead temperature distributions over height of the lead core.
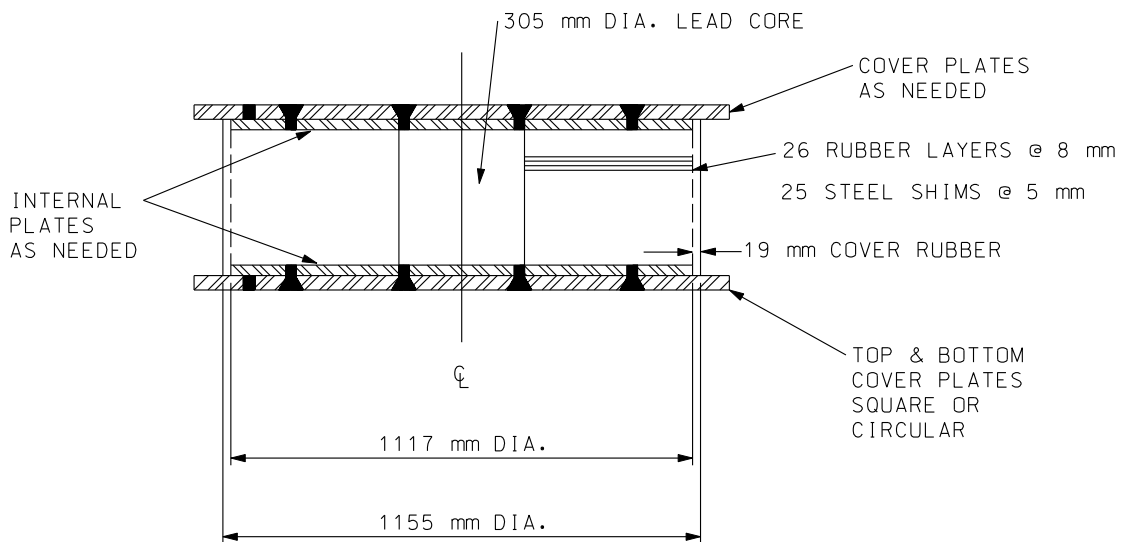
FIGURE 4-27 Large-Scale Tested Lead-Rubber Bearing (Constantinou et al., 2007b)

FIGURE 4-28 Force-Displacement Loops of Bearing of Figure 4-27. Load=10266 kN, Displacement Amplitude=483 mm and Frequency=0.333 Hz (Peak Velocity=1000 mm/s) (Constantinou et al., 2007b)

TABLE 4-14 Test Data for Example 8 (Constantinou et al., 2007b)

Cycle	Peak Velocity (mm/s)	Effective Stiffness (kN-mm)	EDC (kN-m)	Effective Damping	Effective Yield Stress of Lead (MPa)
1	1000	4.67	2059.1	0.30	15.4
2	1000	3.45	1389.8	0.27	10.4
3	1000	3.12	1117.1	0.24	8.4

122

TABLE 4-15 Data Used in Analysis of Example 8

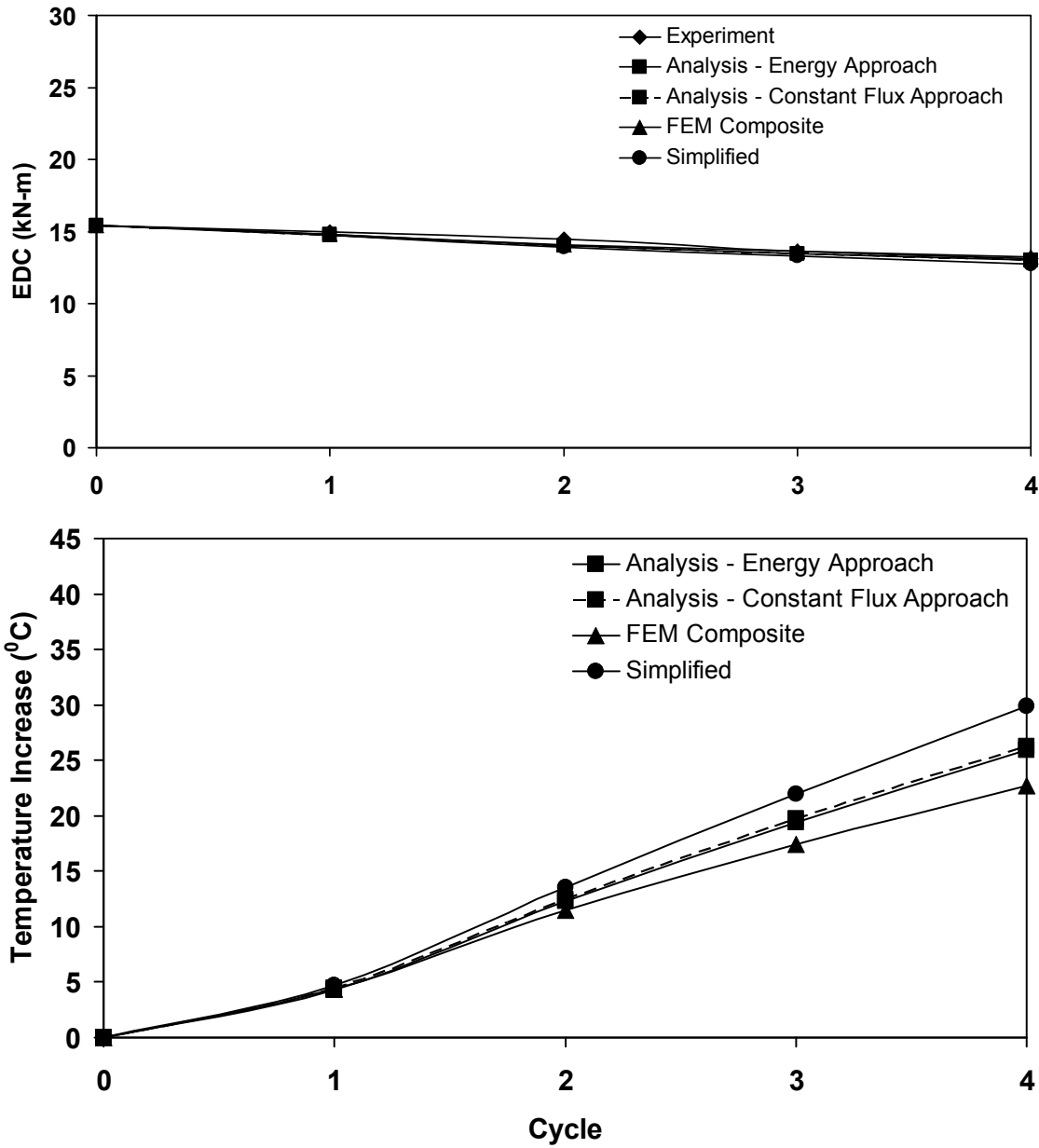|	
Vertical Load on Bearing, N	10266 kN
Amplitude of Motion, u_0	483 mm
Period of Motion, T	3.0 sec
Total Thickness of Shims, t_s	125 mm
Thickness of Steel Above and Below Bearing, t_p	1250 mm
Radius of Lead Core, a	153 mm
Bonded Rubber Radius, R	559 mm
Height of Lead Core, h_L	333 mm
Peak Velocity of Sinusoidal Motion, v_{max}	1000 mm/s
Initial (Reference) Lead Effective Yield Stress, σ_{YL0}	16.9 MPa
Initial Temperature, T_{L0}	20^0C
Parameter of Exponential Relation of σ_{YL} vs. Temperature, E_2	$0.0069/^0$C
Effective Stiffness for 1st Cycle, $K_{eff,1}$	4.66 kN/mm
Effective Damping for Estimating Rubber Contribution to EDC	0.02
Assumed Yield Displacement, Y	30 mm
Thermal Properties of Rubber, Steel and Lead	Per Table 3-3
Heat Capacity of Rubber and Steel Composite, ρc	2714880 J/(m^3 ^{0}C)
Radial Conductivity of Rubber and Steel Composite, $k_{eff,radial}$	18.9 W/(m ^{0}C)
Vertical Conductivity of Rubber and Steel Composite, $k_{eff,vert}$	0.26 W/(m ^{0}C)

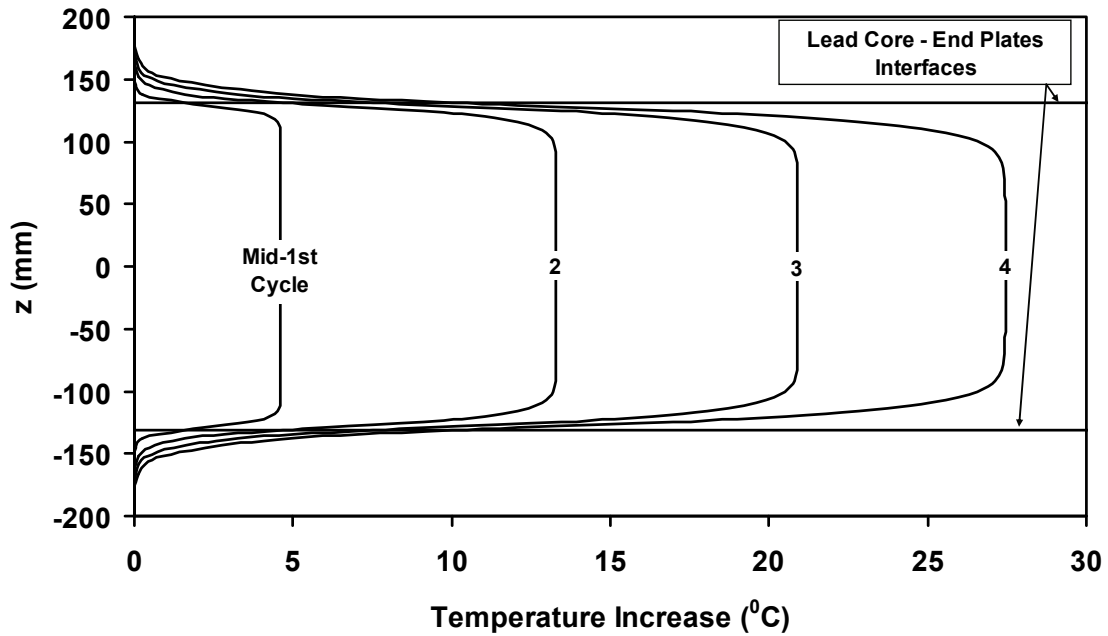**FIGURE 4-29 Temperature and Energy Dissipated per Cycle for Example 8**

FIGURE 4-30 Vertical Temperature Distribution at the Center of the Bearing (r=0) of Figure 4-27 Obtained in Finite Element Analysis Based on Model of Figure 3-16
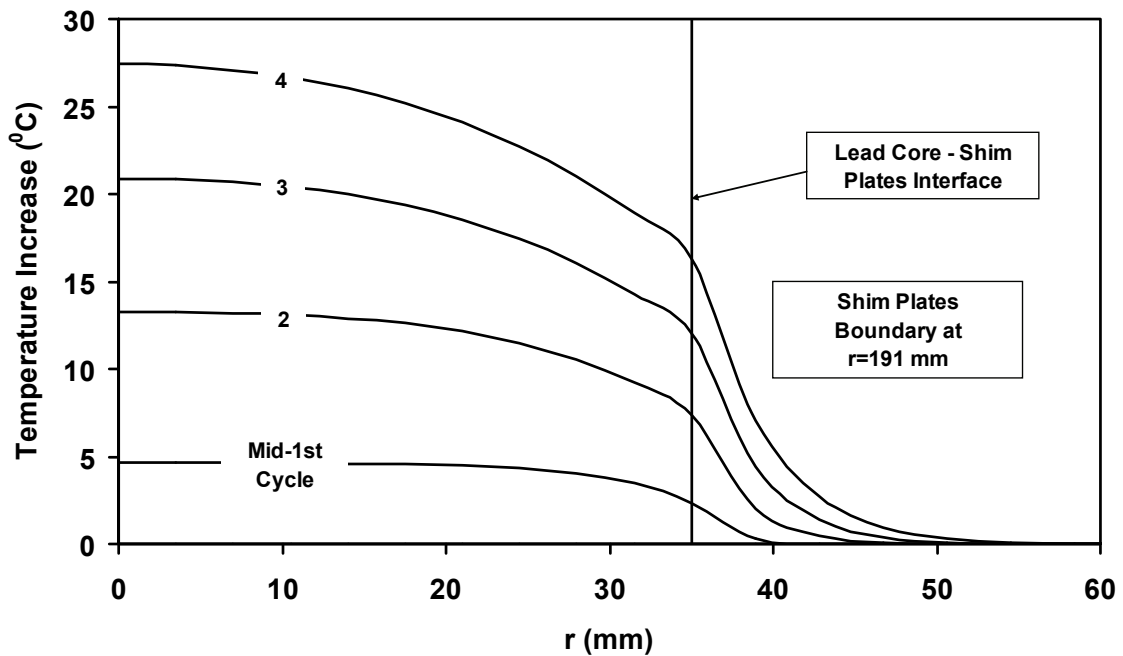

FIGURE 4-31 Horizontal Temperature Distribution (at z=0) of the Bearing of Figure 4-27 Obtained in Finite Element Analysis Based on Model of Figure 3-16

125

4.2.9 Example 9

The tested bearing is again that of Figure 4-27 with recorded force-displacement loops shown in Figure 4-32. Test data and parameters from testing are presented in Table 4-16, data used in the analysis are presented in Table 4-17 and analysis results are presented in Figures 4-33 to 4-35. This test differs from that of Example 8 only in the duration of the test. The three cycles were imposed over a time of 231 sec instead of 9 sec, leading to a dimensionless time of 0.140. Moreover, the two bearings, while of identical construction and materials, were actually two different bearings.

Figure 4-33 shows good prediction of the reduction in the EDC by the two analytical solutions and the simplified solution. In this case, (3-59) yields an error of 48^0C for the first two cycles of motion, yet the prediction of the simplified solution is acceptable in accuracy. The results in Figures 4-34 and 4-35 are qualitatively similar to those observed in other slow tests (e.g., Example 6) and the same conclusions as those of Example 6 apply.
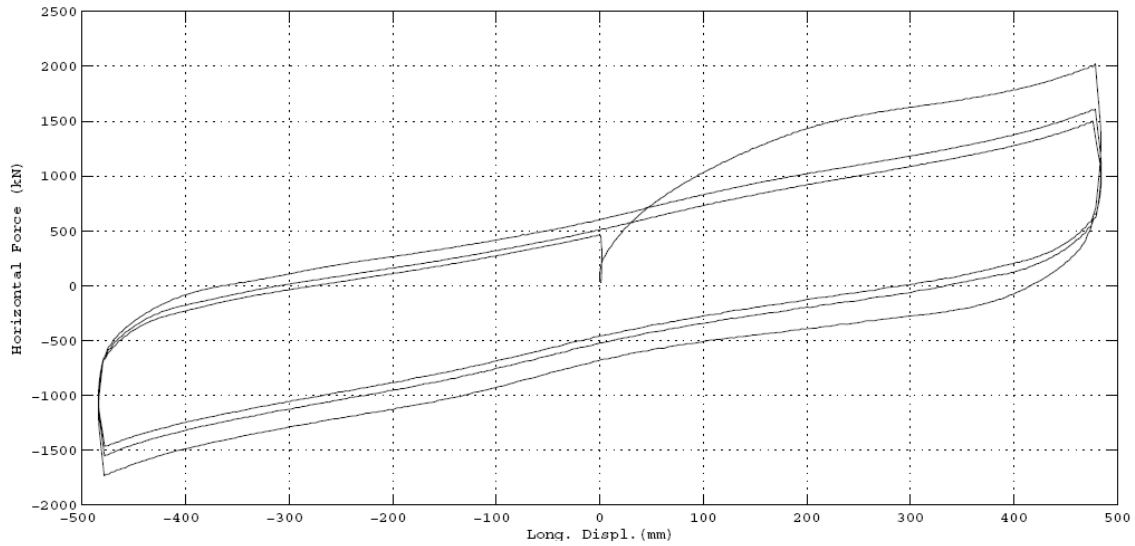
FIGURE 4-32 Force-Displacement Loops of Bearing of Figure 4-27. Load=10266 kN, Displacement Amplitude=483 mm and Frequency=0.013 Hz (Constant Velocity=25 mm/s) (Constantinou et al., 2007b)

TABLE 4-16 Test Data for Example 9 (Constantinou et al., 2007b)

Cycle	Peak Velocity (mm/s)	Effective Stiffness (kN-mm)	EDC (kN-m)	Effective Damping	Effective Yield Stress of Lead (MPa)
1	25	3.89	1471.7	0.26	11.0
2	25	3.27	1109.6	0.23	8.3
3	25	3.07	973.2	0.22	7.3

TABLE 4-17 Data Used in Analysis of Example 9

Vertical Load on Bearing, N	10266 kN
Amplitude of Motion, u_0	483 mm
Period of Motion, T	77 sec
Total Thickness of Shims, t_s	125 mm
Thickness of Steel Above and Below Bearing, t_p	1250 mm
Radius of Lead Core, a	153 mm
Bonded Rubber Radius, R	559 mm
Height of Lead Core, h_L	333 mm
Constant Velocity, v	25 mm/s
Initial (Reference) Lead Effective Yield Stress, σ_{YL0}	12.0 MPa
Initial Temperature, T_{L0}	20^0C
Parameter of Exponential Relation of σ_{YL} vs. Temperature, E_2	$0.0069/^0$C
Effective Stiffness for 1st Cycle, $K_{eff,1}$	3.88 kN/mm
Effective Damping for Estimating Rubber Contribution to EDC	0.01
Assumed Yield Displacement, Y	30 mm
Thermal Properties of Rubber, Steel and Lead	Per Table 3-3
Heat Capacity of Rubber and Steel Composite, ρc	2714880 J/(m^3 ^{0}C)
Radial Conductivity of Rubber and Steel Composite, $k_{eff,radial}$	18.9 W/(m ^{0}C)
Vertical Conductivity of Rubber and Steel Composite, $k_{eff,vert}$	0.26 W/(m ^{0}C)

FIGURE 4-33 Temperature and Energy Dissipated per Cycle for Example 9

129

FIGURE 4-34 Vertical Temperature Distribution at the Center of the Bearing ($r=0$) of Figure 4-27 Obtained in Finite Element Analysis Based on Model of Figure 3-16

FIGURE 4-35 Horizontal Temperature Distribution (at $z=0$) of the Bearing of Figure 4-27 Obtained in Finite Element Analysis Based on Model of Figure 3-16

4.2.10 Example 10

The tested bearing is that of Figure 4-36 with recorded force-displacement loops shown in Figure 4-37. Test data and parameters used in the analysis are presented in Table 4-18 and analysis results are presented in Figures 4-38 to 4-40. This is a long duration (25 cycles), relatively high speed test. The dimensionless time at the end of the 25th cycle is 0.210.
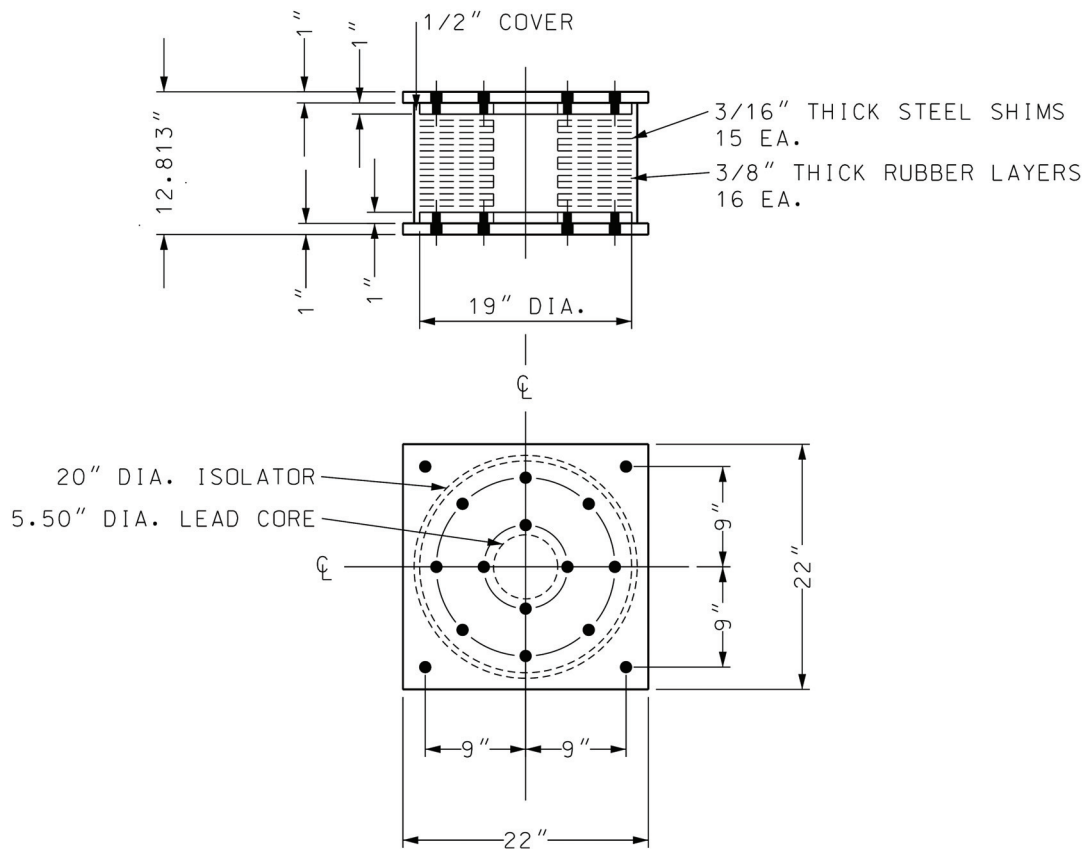
FIGURE 4-36 Large-Scale Tested Lead-Rubber Bearing (1 inch=25.4 mm) (Constantinou et al., 2007b)

131
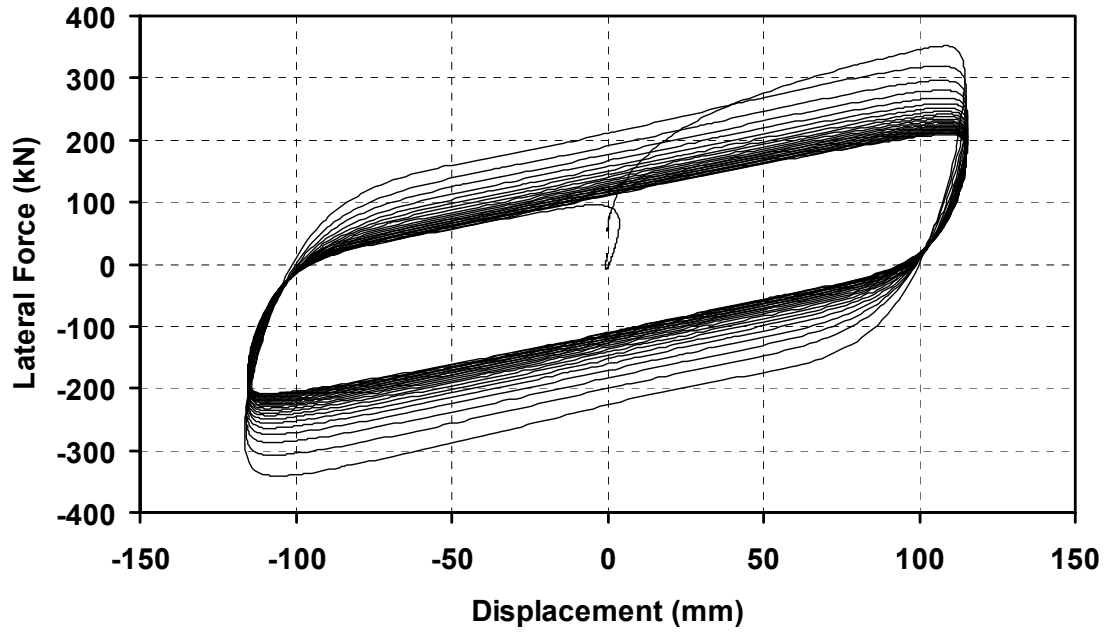
FIGURE 4-37 Force-Displacement Loops of Bearing of Figure 4-36. Load=1441 kN, Displacement Amplitude=114 mm and Frequency=0.35 Hz (Peak Velocity=250 mm/s)

TABLE 4-18 Data Used in Analysis of Example 10

Vertical Load on Bearing, N	1441 kN
Amplitude of Motion, u_0	114 mm
Period of Motion, T	2.9 sec
Total Thickness of Shims, t_s	71 mm
Thickness of Steel Above and Below Bearing, t_p	500 mm
Radius of Lead Core, a	70 mm
Bonded Rubber Radius, R	241 mm
Height of Lead Core, h_L	224 mm
Peak Velocity of Sinusoidal Motion, v_{max}	250 mm/s
Initial (Reference) Lead Effective Yield Stress, σ_{YL0}	13.0 MPa
Initial Temperature, T_{L0}	$20\,^0C$
Parameter of Exponential Relation of σ_{YL} vs. Temperature, E_2	$0.0069/^0C$
Effective Stiffness for 1st Cycle, $K_{eff,1}$	2.78 kN/mm
Effective Damping for Estimating Rubber Contribution to EDC	0.05
Assumed Yield Displacement, Y	7 mm
Thermal Properties of Rubber, Steel and Lead	Per Table 3-3
Heat Capacity of Rubber and Steel Composite, ρc	2636317 J/(m^3 ^{0}C)
Radial Conductivity of Rubber and Steel Composite, $k_{eff,radial}$	16.0 W/(m ^{0}C)
Vertical Conductivity of Rubber and Steel Composite, $k_{eff,vert}$	0.23 W/(m ^{0}C)

FIGURE 4-38 Temperature and Energy Dissipated per Cycle for Example 10
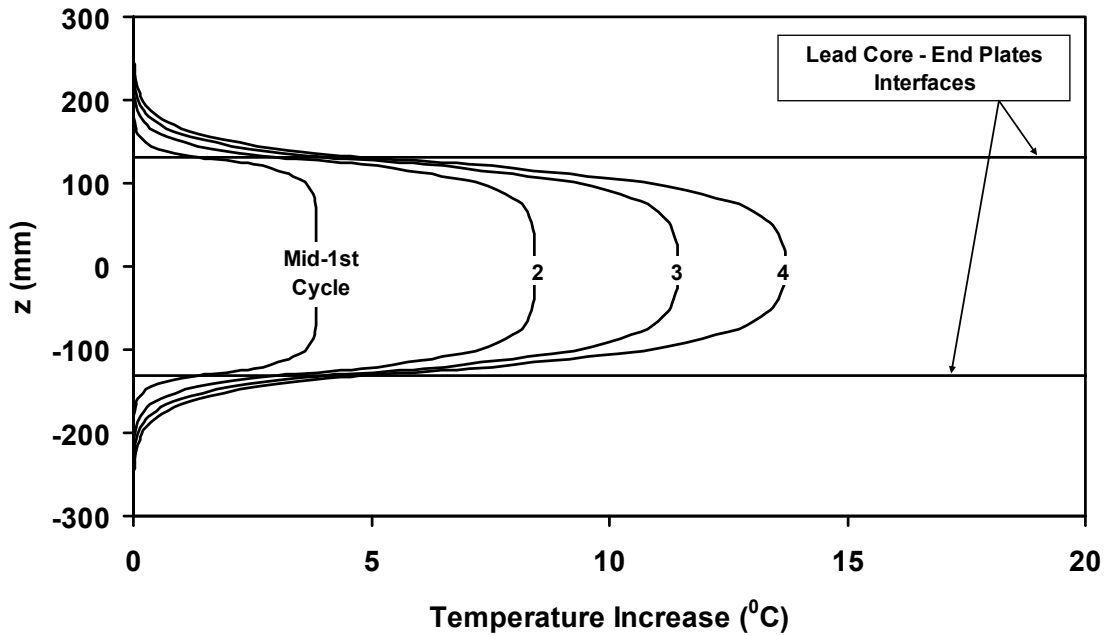
134

FIGURE 4-39 Vertical Temperature Distribution at the Center of the Bearing (r=0) of Figure 4-36 Obtained in Finite Element Analysis Based on Model of Figure 3-16
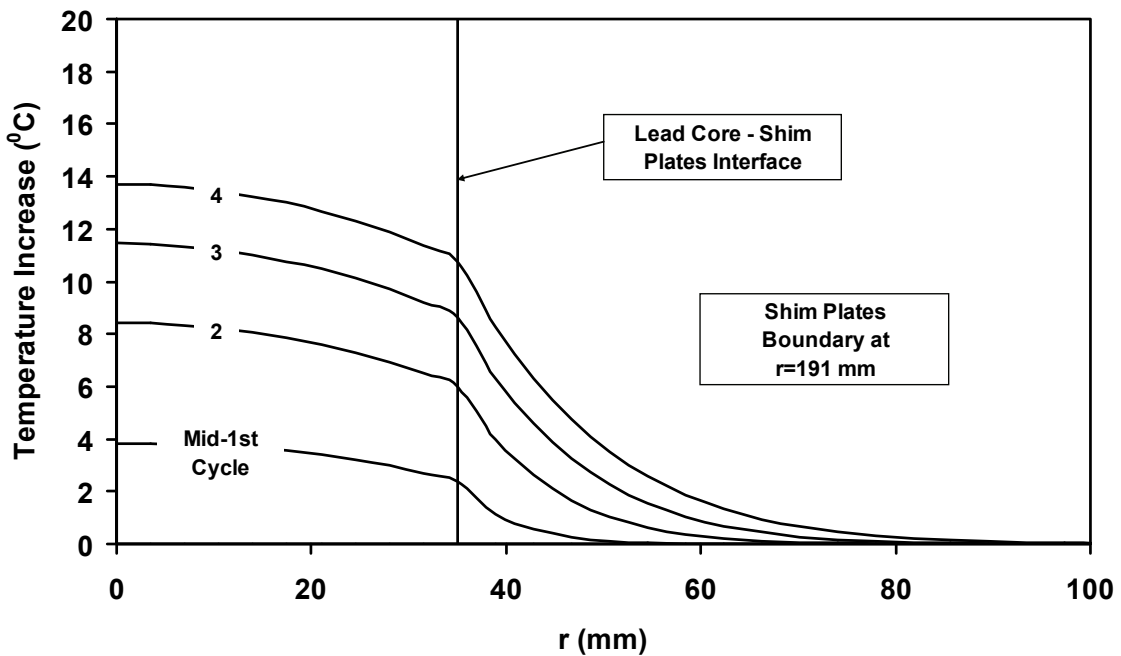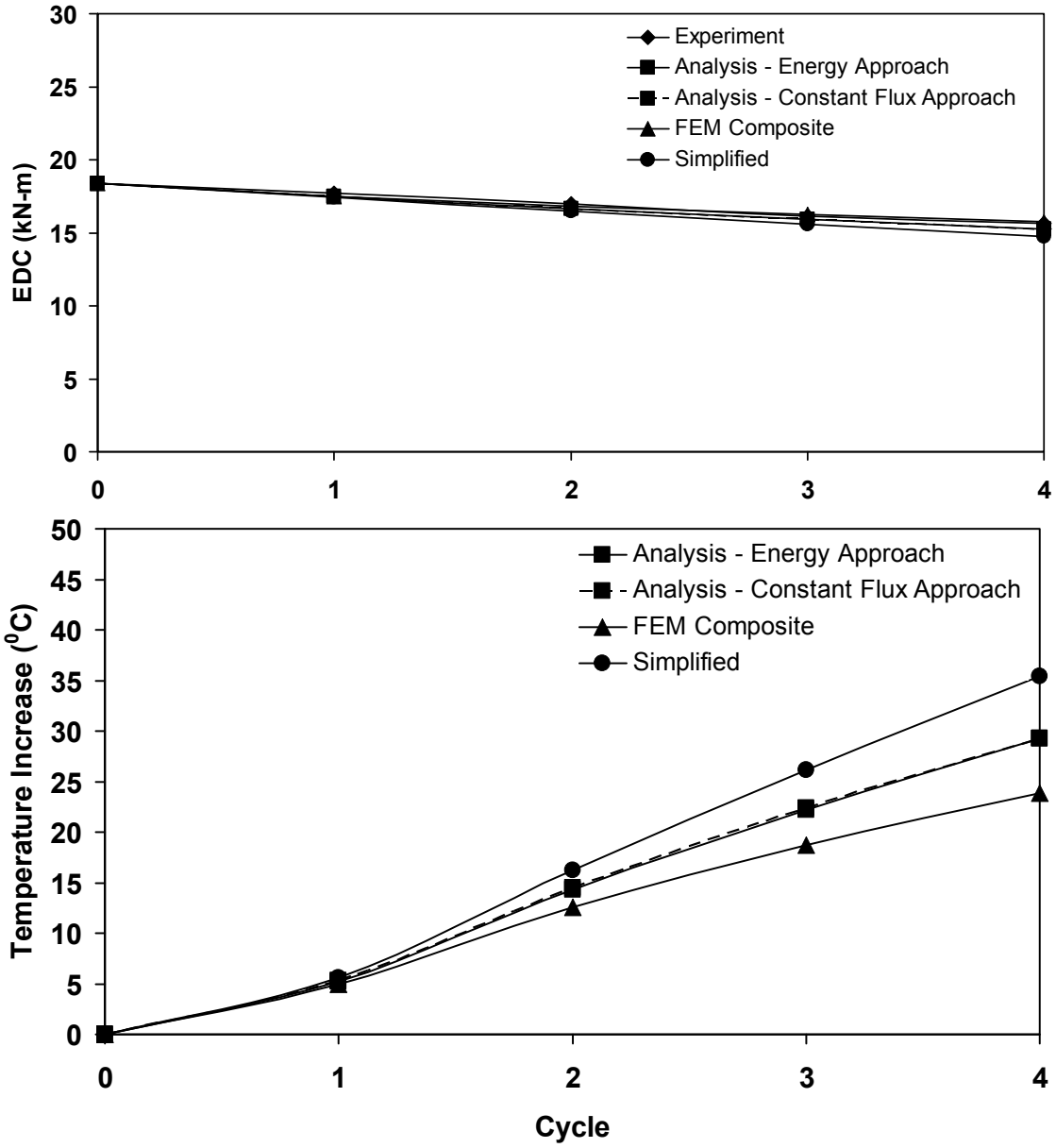

FIGURE 4-40 Horizontal Temperature Distribution (at z=0) of the Bearing of Figure 4-36 Obtained in Finite Element Analysis Based on Model of Figure 3-16

The results in Figure 4-38 demonstrate good prediction of the EDC history over the 25 cycles by the two analytical methods and the finite element analysis. The simplified method predicts acceptably the EDC history up to about the seventh cycle. On the basis of (3-59) the error at the seventh cycle is 48^0C, verifying thus the limit of about 40^0C in (3-59) for the validity of the simplified solution.

Figures 4-39 and 4-40 demonstrate for the initial few cycles the uniformity of temperature increase in the lead core and that the temperature increase at the lead-shim plates interface is about half of that at the bulk of the lead core. These conditions deteriorate with increasing number of cycles due to heat conduction through the end and shim plates.

Also, Figure 4-40 demonstrates that the temperature increase in the steel shims is practically zero at a point far away from the bearing free boundary. That is, the heat front in the steel shims did not reach the end of the bearing – an assumption made in the analytical solutions.

However, it may be observed in Figure 4-39 that the temperature increase in the top and bottom end plates is practically zero at a distance of about 150 mm from the lead core; the actual bearing in the test had about 150 mm of steel plates (50 mm of bearing end plates plus about 100 mm of backing plates in the test machine). Note that the analytical solutions assume infinite depth for the end plates (half space). Also, the finite element analysis (model of Figure 3-16) utilized a generic depth of 500 mm for the end plates. This implies that (relatively small) errors in the prediction of EDC history by the two

analytical methods and the finite element method are primarily due to the modeling of the end plates.

4.2.11 Example 11

The tested bearing is again that of Figure 4-36 with recorded force-displacement loops shown in Figure 4-41. Test data and parameters used in the analysis are presented in Table 4-19 and analysis results are presented in Figures 4-42 to 4-44. The tested bearing is the same (physically) as that of Example 10 with the only difference being the duration of testing. In Example 11 the duration of one cycle is twice that in Example 10 resulting in a dimensionless time at the end of the 25-cycle test equal to 0.420.

The results in Figures 4-42 to 4-44 are qualitatively the same as those for Example 10 and the same observations apply. However, due to the fact that in Example 11 the speed of testing is smaller (whereas all other test parameters are the same), heat conduction effects are greater and the result is a larger difference between the experimental and analytical EDC histories. Nevertheless, the analytical constant flux method underpredicts the experimental EDC by less than 15% at the 25th cycle, which is very good. By comparison the finite element method underpredicts the experimental EDC at the 25th cycle by about 10%. The main reason for the underprediction of the EDC by the finite element method is the use of a large thickness end steel plate (500 mm). As seen in the results in Figure 4-43, the heat front at the 25th cycle has reached approximately 170 mm depth in the end plates, whereas the actual steel depth was about 150 mm.

The simplified method in this example does not produce acceptable results for the EDC except for the first five cycles or so. Use of (3-59) yields an error on temperature of 40^0C at the fifth cycle – a limit considered acceptable for the prediction of EDC by the simplified method.

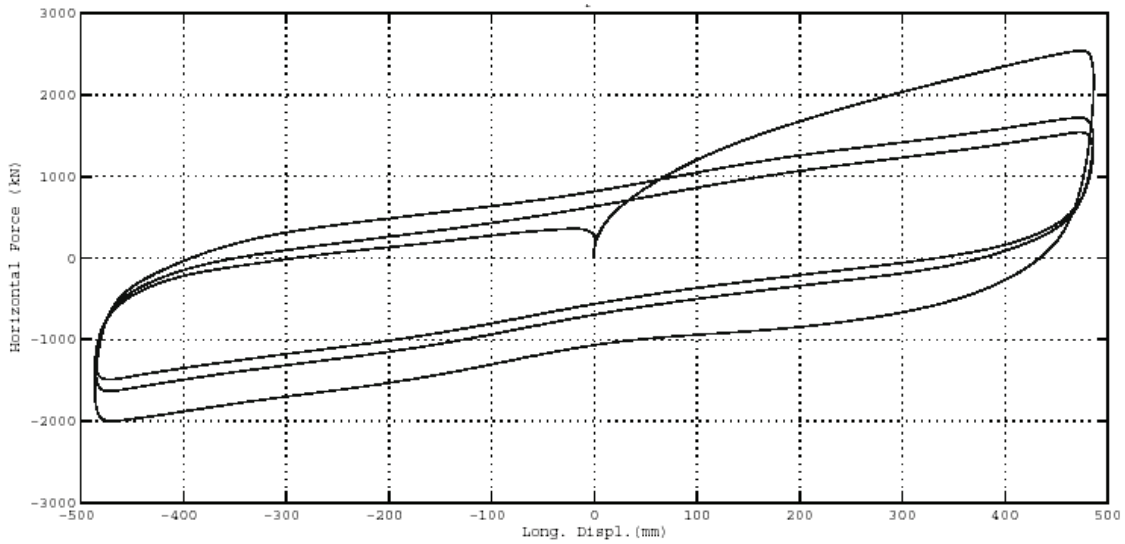**FIGURE 4-41 Force-Displacement Loops of Bearing of Figure 4-36. Load=1410 kN, Displacement Amplitude=114 mm and Frequency=0.18 Hz (Peak Velocity=125 mm/s)**

TABLE 4-19 Data Used in Analysis of Example 11

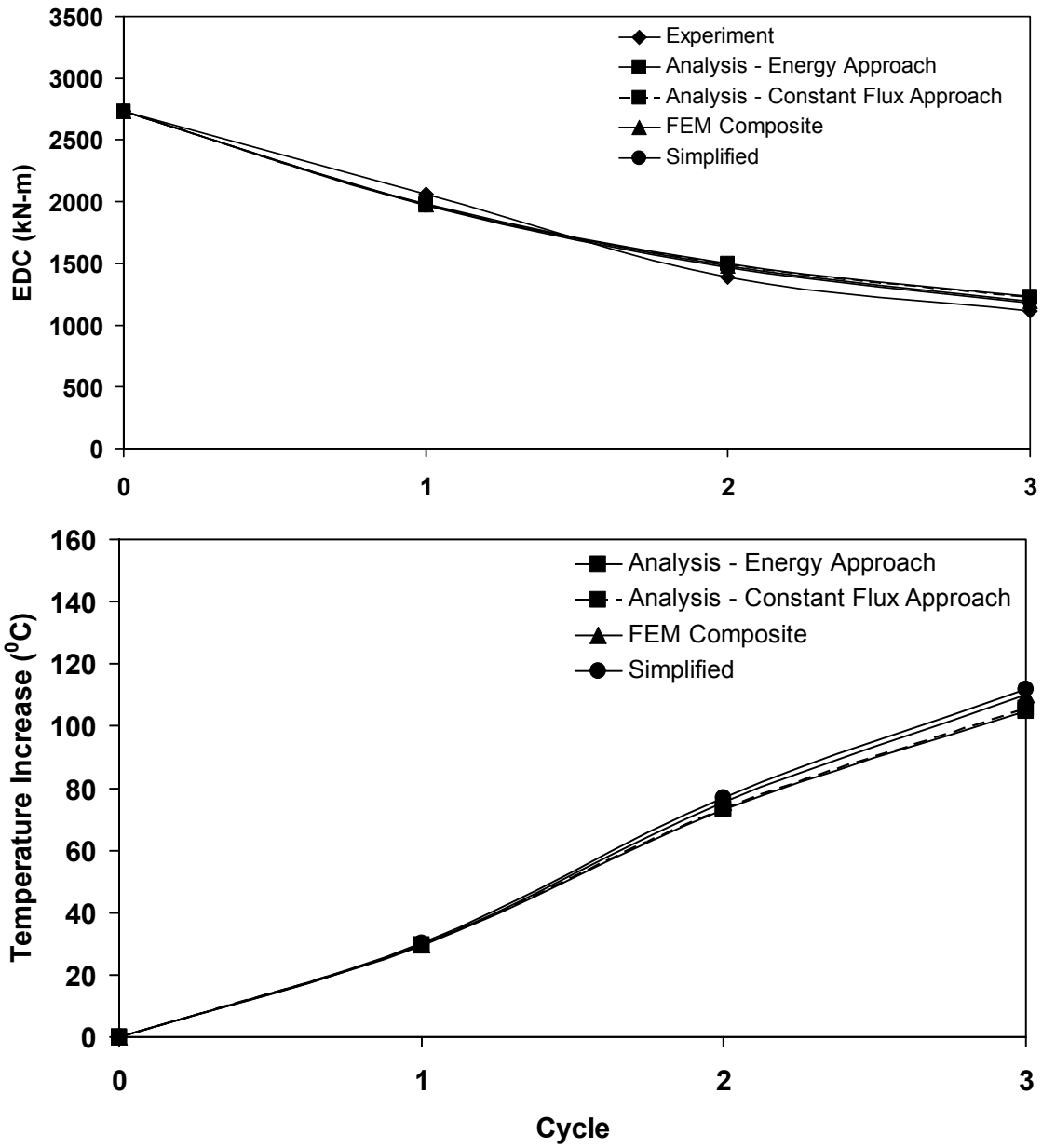|	
Vertical Load on Bearing, N	1410 kN
Amplitude of Motion, u_0	114 mm
Period of Motion, T	5.7 sec
Total Thickness of Shims, t_s	71 mm
Thickness of Steel Above and Below Bearing, t_p	500 mm
Radius of Lead Core, a	70 mm
Bonded Rubber Radius, R	241 mm
Height of Lead Core, h_L	224 mm
Peak Velocity of Sinusoidal Motion, v_{max}	125 mm/s
Initial (Reference) Lead Effective Yield Stress, σ_{YL0}	11.7 MPa
Initial Temperature, T_{L0}	20^0C
Parameter of Exponential Relation of σ_{YL} vs. Temperature, E_2	$0.0069/^0$C
Effective Stiffness for 1st Cycle, $K_{eff,1}$	2.67 kN/mm
Effective Damping for Estimating Rubber Contribution to EDC	0.05
Assumed Yield Displacement, Y	7 mm
Thermal Properties of Rubber, Steel and Lead	Per Table 3-3
Heat Capacity of Rubber and Steel Composite, ρc	2636317 J/(m^3 ^{0}C)
Radial Conductivity of Rubber and Steel Composite, $k_{eff,radial}$	16.0 W/(m ^{0}C)
Vertical Conductivity of Rubber and Steel Composite, $k_{eff,vert}$	0.23 W/(m ^{0}C)

FIGURE 4-42 Temperature and Energy Dissipated per Cycle for Example 11
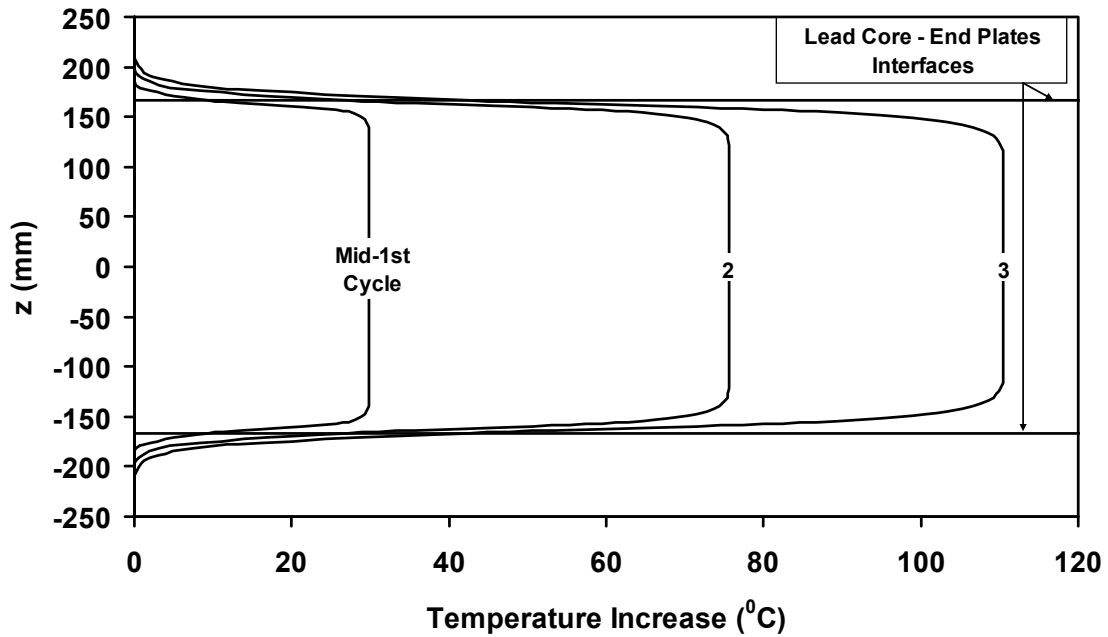
140

FIGURE 4-43 Vertical Temperature Distribution at the Center of the Bearing (r =0) of Figure 4-36 Obtained in Finite Element Analysis Based on Model of Figure 3-16
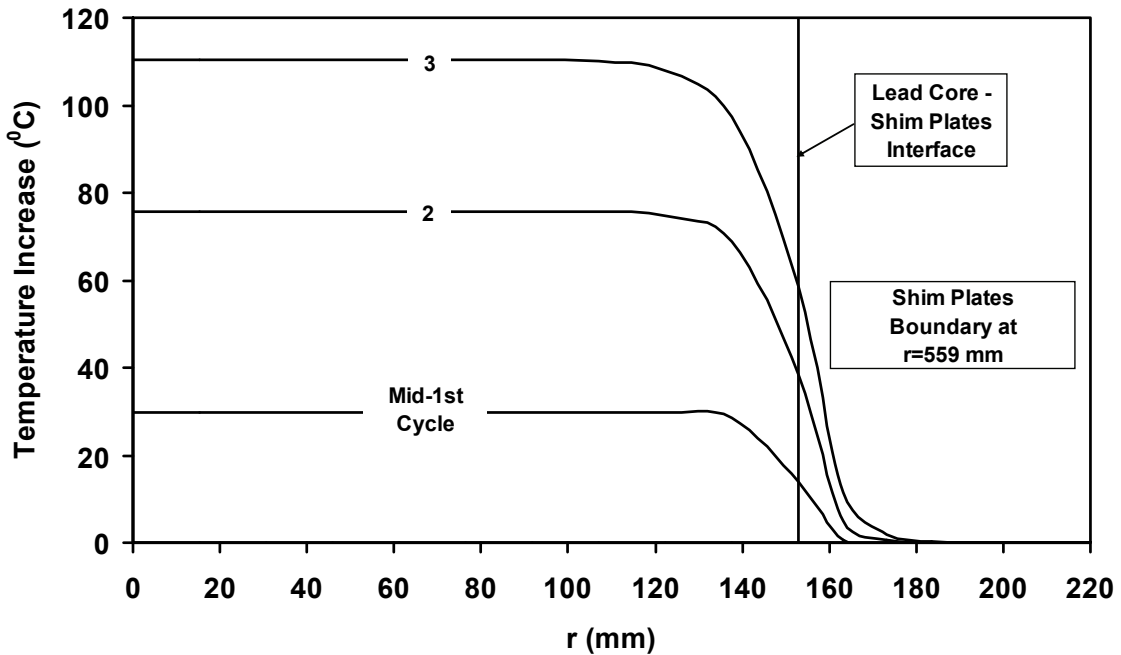

FIGURE 4-44 Horizontal Temperature Distribution (at z =0) of the Bearing of Figure 4-36 Obtained in Finite Element Analysis Based on Model of Figure 3-16

4.2.12 Example 12

The bearing of Example 12 was used at the Coronado Bridge in San Diego, California. Data on the geometry and behavior of the bearing were provided by Dynamic Isolation Systems, Inc. (see Figure 4-45). Test data and parameters used in the analysis are presented in Table 4-20 and analysis results are presented in Figures 4-46 to 4-48. The dimensionless time at the end of the third cycle of testing was 0.004.
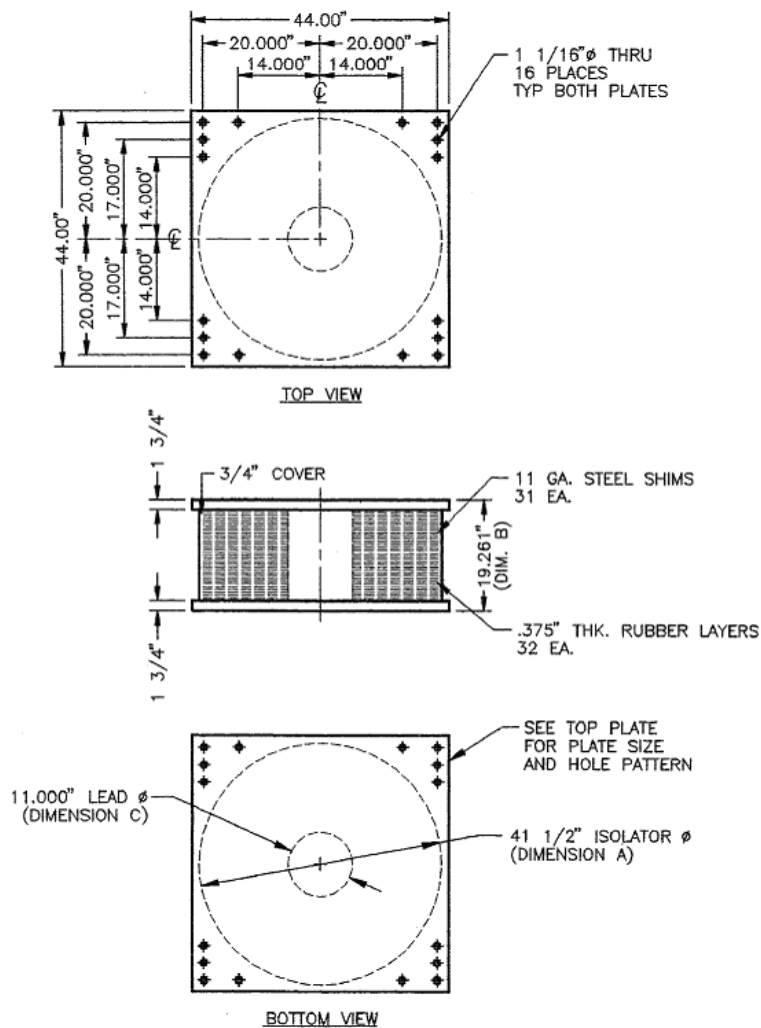
FIGURE 4-45 Large-Scale Tested Coronado Bridge Lead-Rubber Bearing (1 inch=25.4 mm) (Courtesy of DIS, Inc.)

142

TABLE 4-20 Data Used in Analysis of Example 12

Vertical Load on Bearing, N	2482 kN
Amplitude of Motion, u_0	584 mm
Period of Motion, T	2.0 sec
Total Thickness of Shims, t_s	95 mm
Thickness of Steel Above and Below Bearing, t_p	1250 mm
Radius of Lead Core, a	140 mm
Bonded Rubber Radius, R	508 mm
Height of Lead Core, h_L	400 mm
Peak Velocity of Sinusoidal Motion, v_{max}	1835 mm/s
Initial (Reference) Lead Effective Yield Stress, σ_{YL0}	9.7 MPa
Initial Temperature, T_{L0}	20^0C
Parameter of Exponential Relation of σ_{YL} vs. Temperature, E_2	$0.0069/^0$C
Effective Stiffness for 1st Cycle, $K_{eff,1}$	1.76 kN/mm
Effective Damping for Estimating Rubber Contribution to EDC	0.01
Assumed Yield Displacement, Y	30 mm
Thermal Properties of Rubber, Steel and Lead	Per Table 3-3
Heat Capacity of Rubber and Steel Composite, ρc	2529438 J/(m^3 ^{0}C)
Radial Conductivity of Rubber and Steel Composite, $k_{eff,radial}$	12.0 W/(m ^{0}C)
Vertical Conductivity of Rubber and Steel Composite, $k_{eff,vert}$	0.21 W/(m ^{0}C)

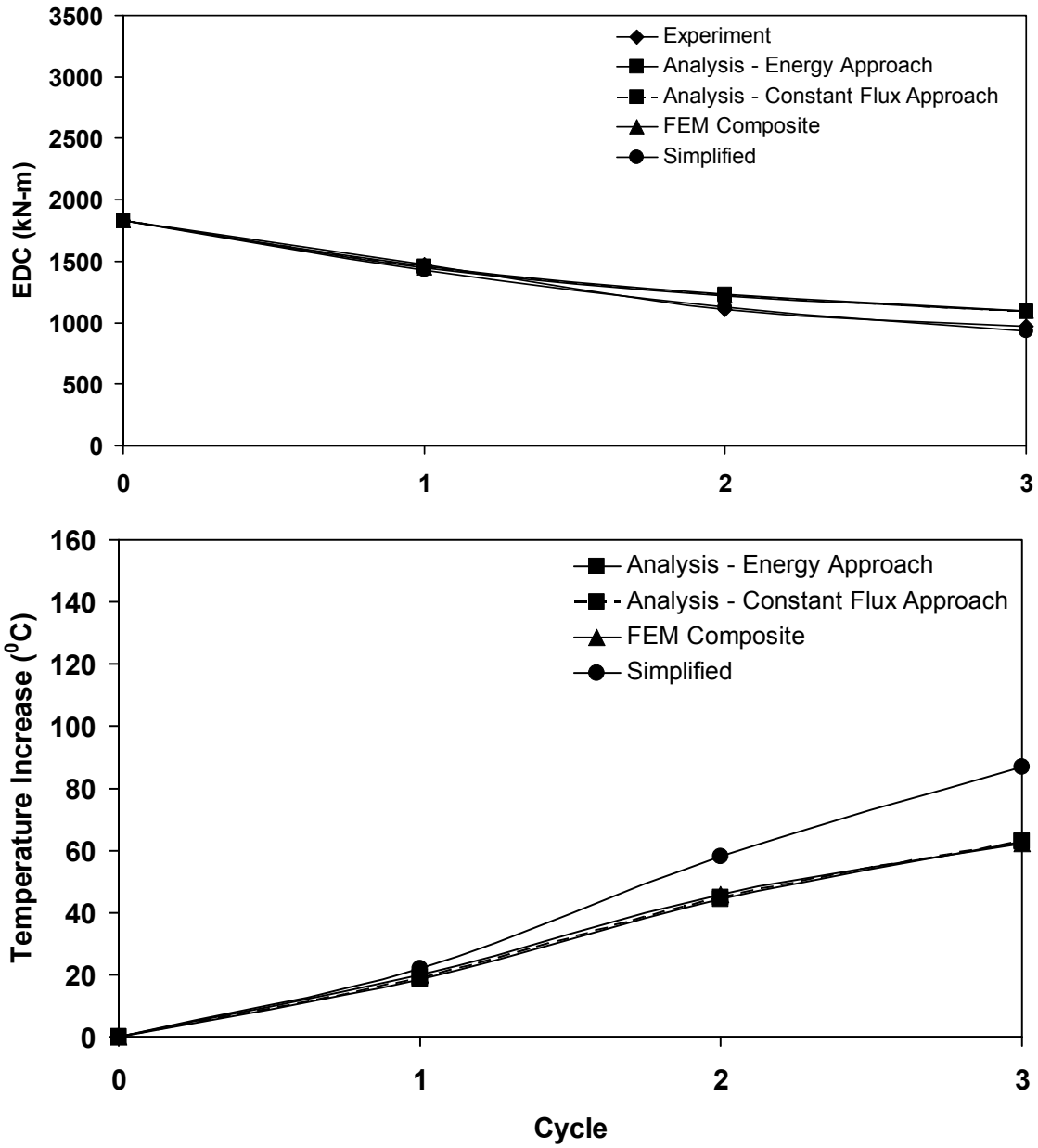**FIGURE 4-46 Temperature and Energy Dissipated per Cycle for Example 12**
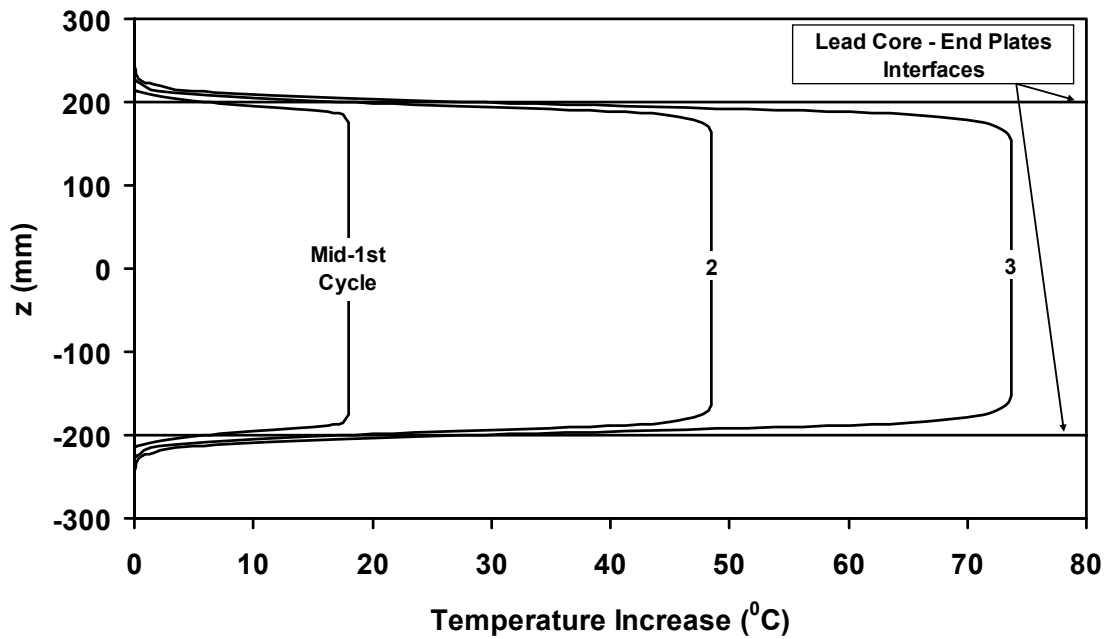
FIGURE 4-47 Vertical Temperature Distribution at the Center of the Bearing ($r=0$) of Figure 4-45 Obtained in Finite Element Analysis Based on Model of Figure 3-16
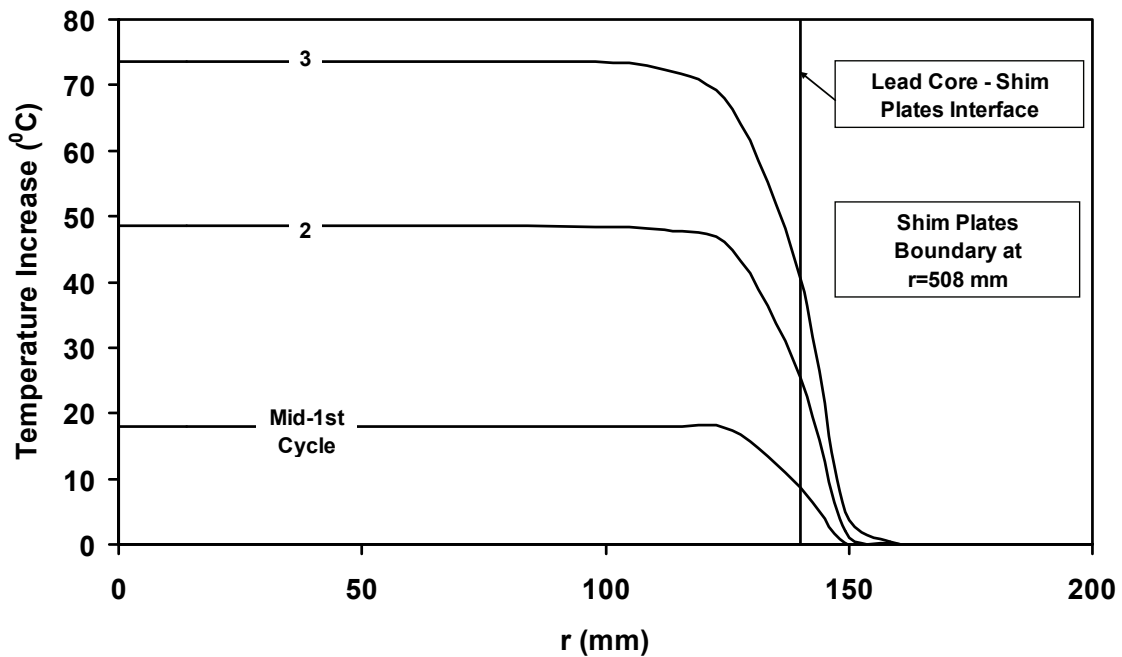
FIGURE 4-48 Horizontal Temperature Distribution (at $z=0$) of the Bearing of Figure 4-45 Obtained in Finite Element Analysis Based on Model of Figure 3-16

145

The results in Figure 4-46 demonstrate excellent prediction of the EDC history by all methods of analysis, including the simplified method. Figures 4-47 and 4-48 demonstrate the validity of the basic assumptions in the analytical solutions. The validity criterion of equation (3-59) yields an error of 9^0C at the third cycle – which demonstrates the validity of the simplified solution for this case (acceptable if less than 40^0C).

4.2.13 Example 13

The bearing is the same as that of Example 12 (Figure 4-45) except that five cycles of motion are imposed at a smaller amplitude. Test data and parameters used in the analysis are presented in Table 4-21 and analysis results are presented in Figures 4-49 to 4-51. The dimensionless time at the end of the fifth cycle was 0.007.

The results in Figure 4-49 show excellent prediction of the EDC history by all methods of analysis. Also, the results in Figures 4-50 and 4-51 again confirm the validity of the assumptions in the analytical solutions. Use of the criterion of equation (3-59) yields an error of 18^0C for the five cycles of motion, confirming thus the acceptable accuracy of the simplified solution (error less than 40^0C).

TABLE 4-21 Data Used in Analysis of Example 13

Vertical Load on Bearing, N	2482 kN
Amplitude of Motion, u_0	490 mm
Period of Motion, T	2.0 sec
Total Thickness of Shims, t_s	95 mm
Thickness of Steel Above and Below Bearing, t_p	1250 mm
Radius of Lead Core, a	140 mm
Bonded Rubber Radius, R	508 mm
Height of Lead Core, h_L	400 mm
Peak Velocity of Sinusoidal Motion, v_{max}	1540 mm/s
Initial (Reference) Lead Effective Yield Stress, σ_{YL0}	11.6 MPa
Initial Temperature, T_{L0}	20^0C
Parameter of Exponential Relation of σ_{YL} vs. Temperature, E_2	$0.0069/^0$C
Effective Stiffness for 1st Cycle, $K_{eff,1}$	2.35 kN/mm
Effective Damping for Estimating Rubber Contribution to EDC	0.01
Assumed Yield Displacement, Y	30 mm
Thermal Properties of Rubber, Steel and Lead	Per Table 3-3
Heat Capacity of Rubber and Steel Composite, ρc	2529438 J/(m^3 ^{0}C)
Radial Conductivity of Rubber and Steel Composite, $k_{eff,radial}$	12.0 W/(m ^{0}C)
Vertical Conductivity of Rubber and Steel Composite, $k_{eff,vert}$	0.21 W/(m ^{0}C)

FIGURE 4-49 Temperature and Energy Dissipated per Cycle for Example 13
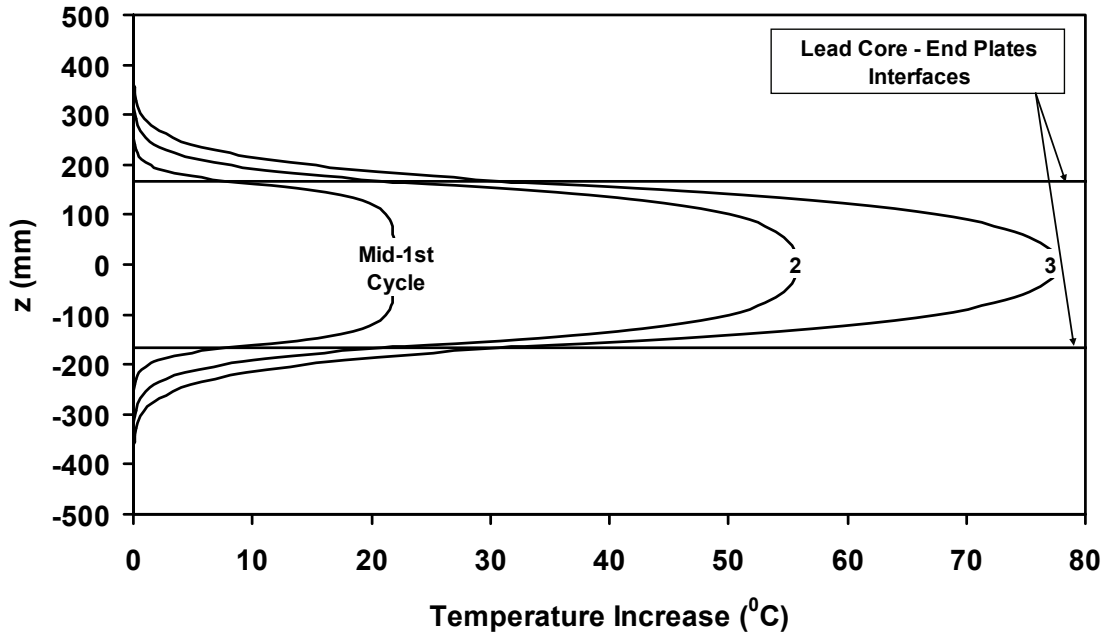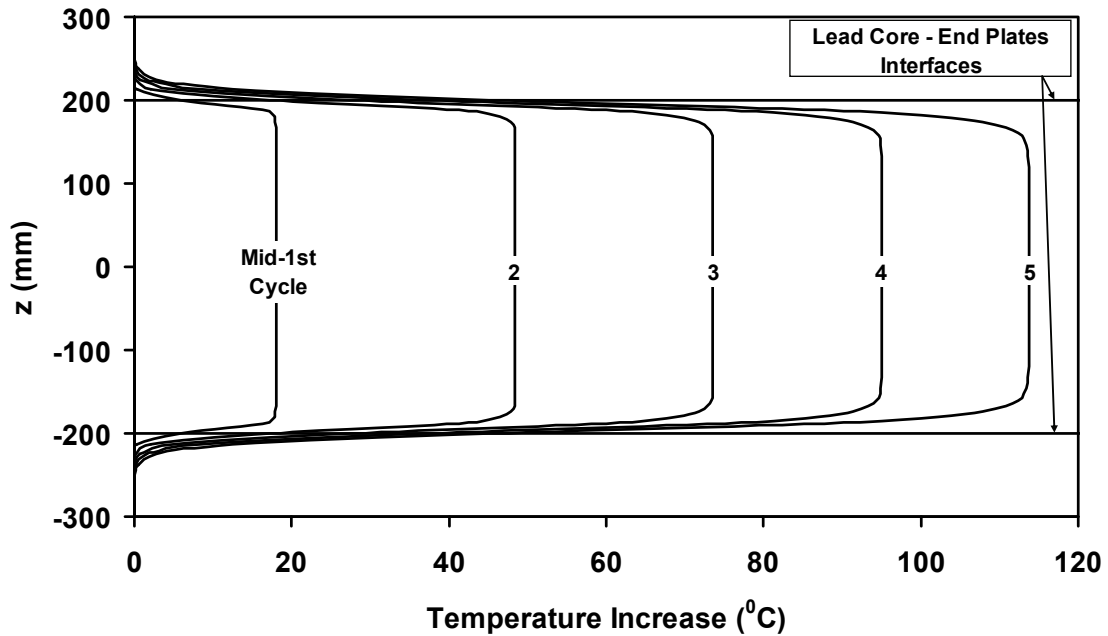
FIGURE 4-50 Vertical Temperature Distribution at the Center of the Bearing ($r=0$) of Figure 4-45 Obtained in Finite Element Analysis Based on Model of Figure 3-16
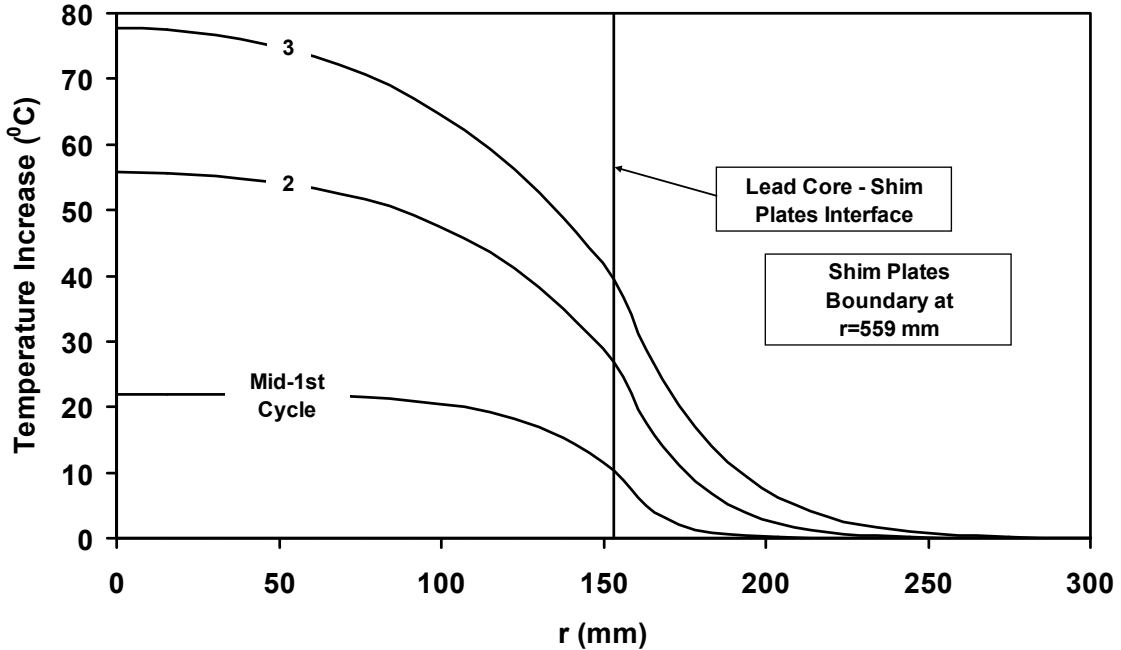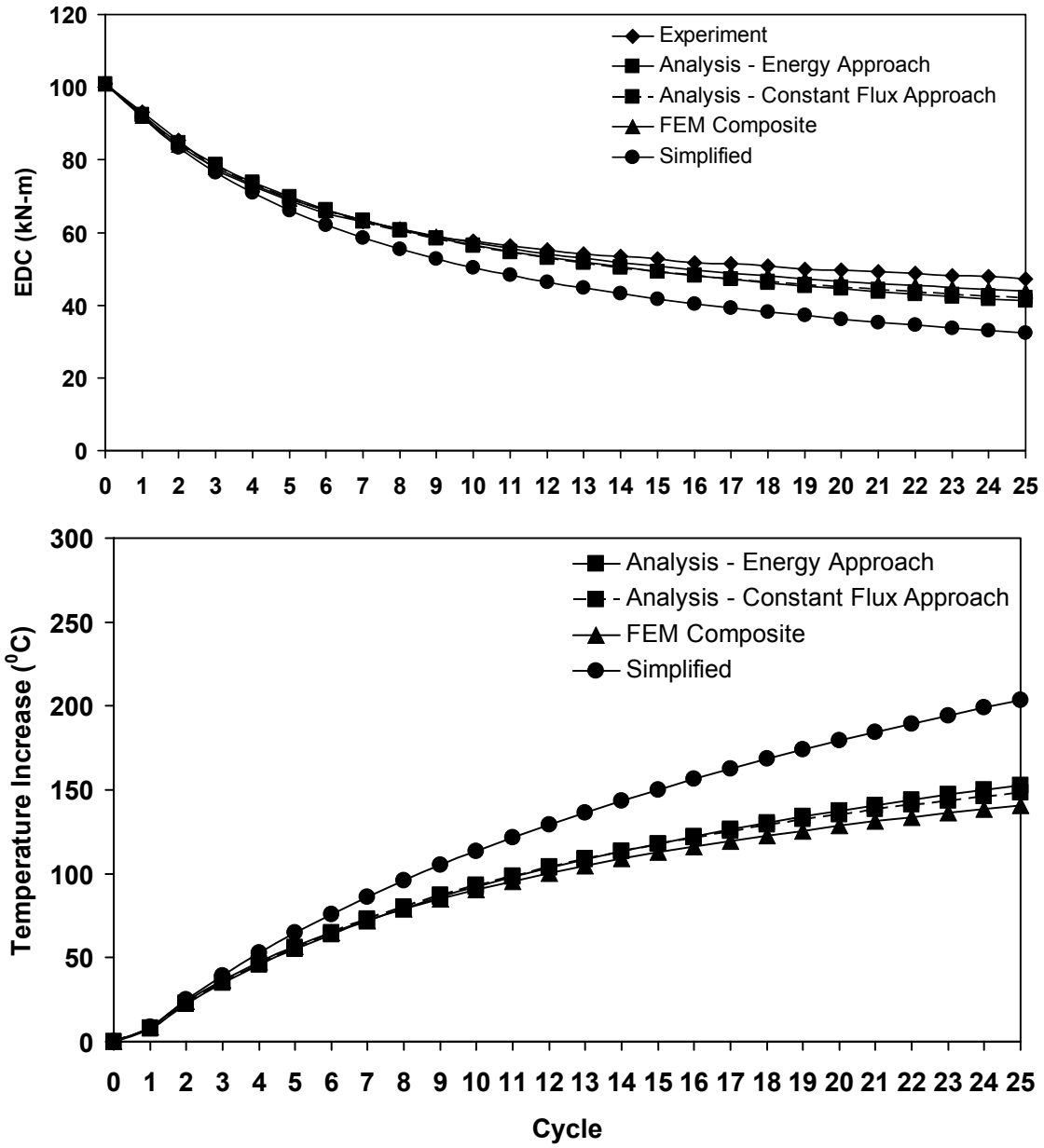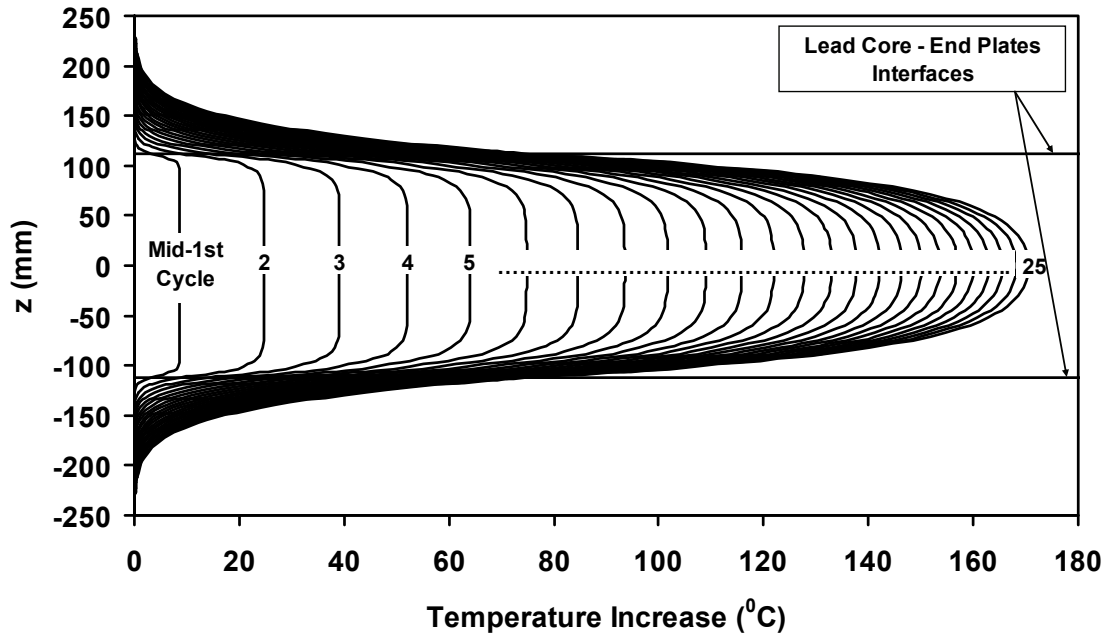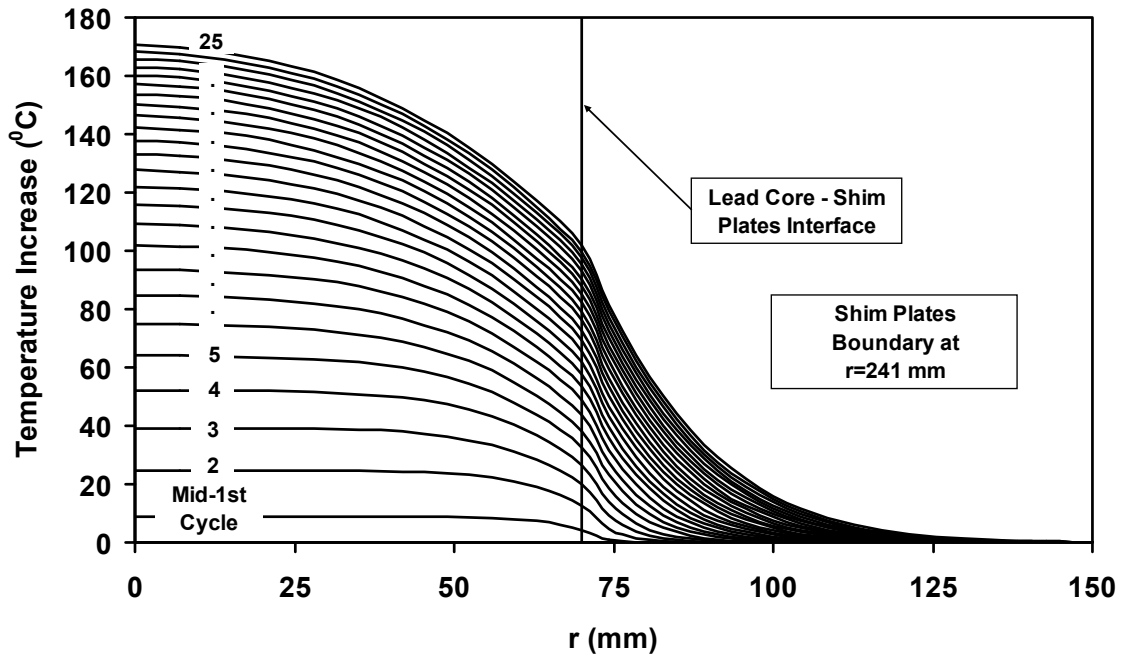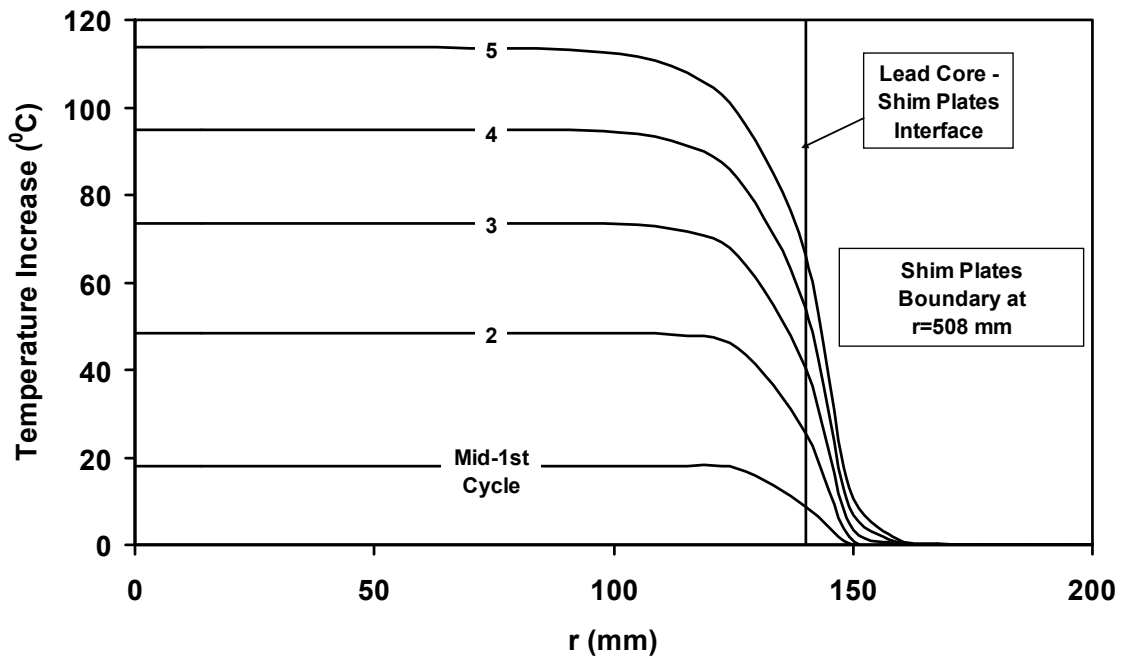

FIGURE 4-51 Horizontal Temperature Distribution (at $z=0$) of the Bearing of Figure 4-45 Obtained in Finite Element Analysis Based on Model of Figure 3-16

149

4.2.14 Example 14

The bearing of Example 14 is shown in Figure 4-52. It is a small scale bearing used for shake table testing by Wolff and Constantinou (2004). The bearing was again tested in the small test machine at the University at Buffalo. The recorded force-displacement loops are presented in Figure 4-53. Test data and parameters used in the analysis are presented in Table 4-22 and analysis results are presented in Figures 4-54 to 4-56. Note that ten cycles of high speed motion were imposed. The dimensionless time at the end of the 10th cycle was 0.902. Also note that the small scale bearing has significantly more thickness of steel shims as compared to rubber thickness than full size bearings. For example, for the full size bearing of Figure 4-45, $t_s / t_r = 0.31$, whereas for the small size bearing of Figure 4-52, $t_s / t_r = 0.56$. This large shim plate thickness raises the expected significance of heat conduction effects.

The experimentally obtained values of EDC presented in Figure 4-54 increase from cycles 2 to 4 – this is not a measurement error or the result of some unusual behavior. Rather it is caused by unsteady amplitude of motion in the first few cycles of testing. As seen in Figure 4-54, the finite element method provides excellent prediction of the EDC (excluding discrepancies due to the unsteady amplitude). Also, the two analytical methods provide acceptable predictions of the EDC for all 10 cycles, whereas the simplified method provides acceptable results for only the first three cycles. Application of the criterion of (3-59) yields an error of 49^0C at the third cycle – therefore, confirming the validity of the simplified solution up to the third cycle for this case.

The results in Figures 4-55 and 4-56 confirm the basic assumptions of the analytical solutions. However, as also noted in the other examples, the validity of these assumptions deteriorates with increasing number of cycles as heat conduction effects become more prevalent.
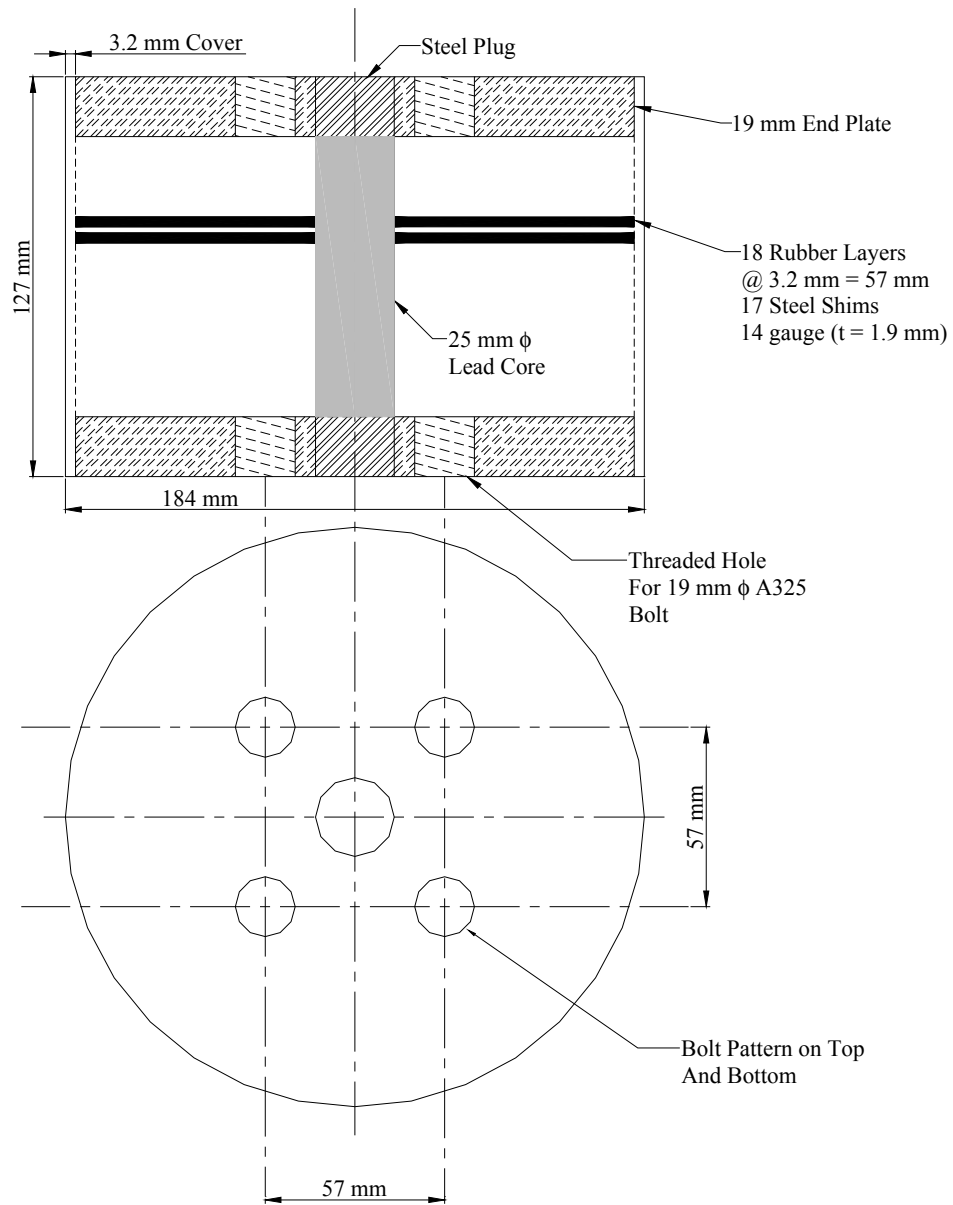
FIGURE 4-52 Tested Small-Scale Lead-Rubber Bearing (Wolff and Constantinou, 2004)
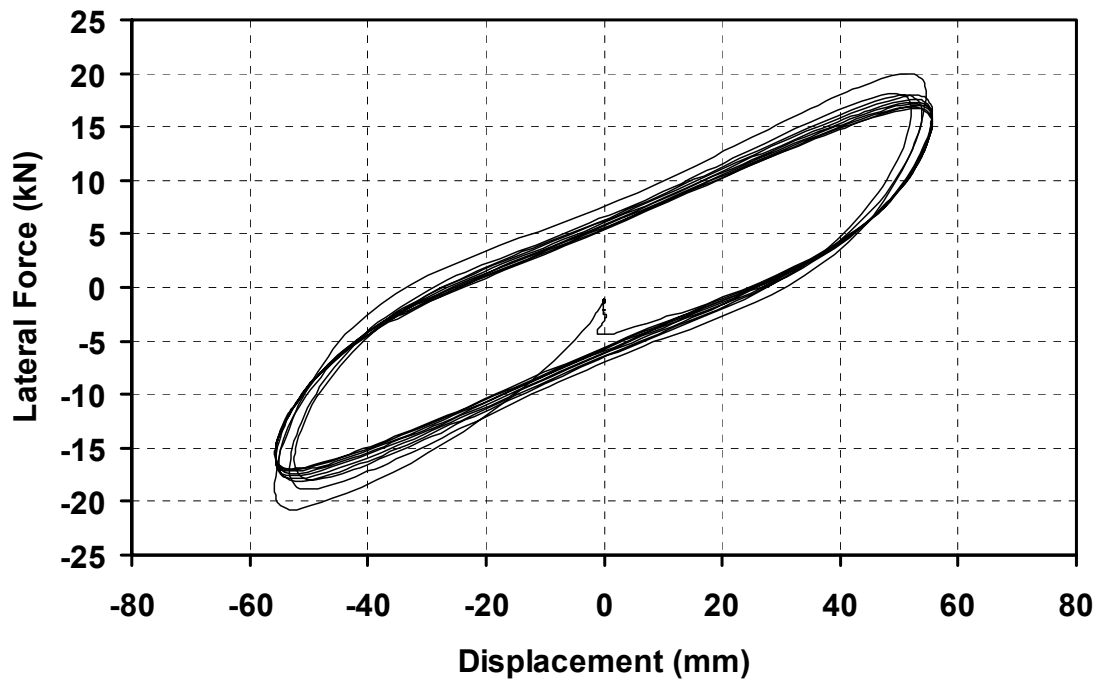
FIGURE 4-53 Force-Displacement Loops of Bearing of Figure 4-52. Load=67 kN, Displacement Amplitude=57 mm and Frequency=1 Hz (Peak Velocity=358 mm/s)

TABLE 4-22 Data Used in Analysis of Example 14

Vertical Load on Bearing, N	67 kN
Amplitude of Motion, u_0	57 mm
Period of Motion, T	1.0 sec
Total Thickness of Shims, t_s	32 mm
Thickness of Steel Above and Below Bearing, t_p	300 mm
Radius of Lead Core, a	12.5 mm
Bonded Rubber Radius, R	89 mm
Height of Lead Core, h_L	89 mm
Peak Velocity of Sinusoidal Motion, v_{max}	358 mm/s
Initial (Reference) Lead Effective Yield Stress, σ_{YL0}	14.8 MPa
Initial Temperature, T_{L0}	20^0C
Parameter of Exponential Relation of σ_{YL} vs. Temperature, E_2	$0.0069/^0$C
Effective Stiffness for 1st Cycle, $K_{eff,1}$	0.37 kN/mm
Effective Damping for Estimating Rubber Contribution to EDC	0.02
Assumed Yield Displacement, Y	5 mm
Thermal Properties of Rubber, Steel and Lead	Per Table 3-3
Heat Capacity of Rubber and Steel Composite, ρc	2693596 J/(m^3 ^{0}C)
Radial Conductivity of Rubber and Steel Composite, $k_{eff,radial}$	18.1 W/(m ^{0}C)
Vertical Conductivity of Rubber and Steel Composite, $k_{eff,vert}$	0.25 W/(m ^{0}C)

FIGURE 4-54 Temperature and Energy Dissipated per Cycle for Example 14
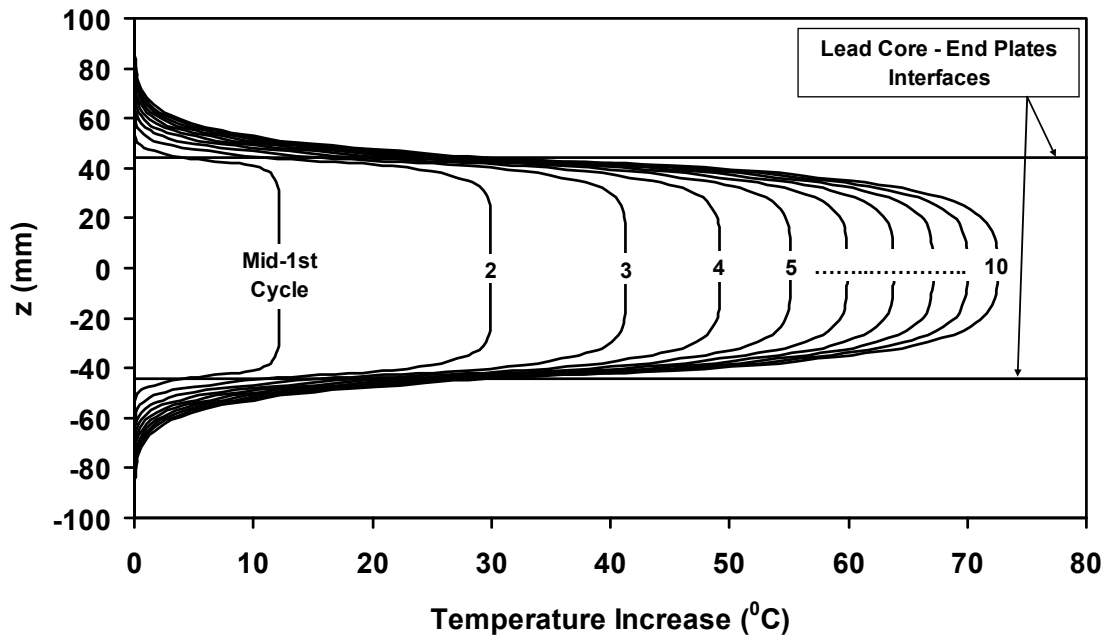
FIGURE 4-55 Vertical Temperature Distribution at the Center of the Bearing ($r=0$) of Figure 4-52 Obtained in Finite Element Analysis Based on Model of Figure 3-16
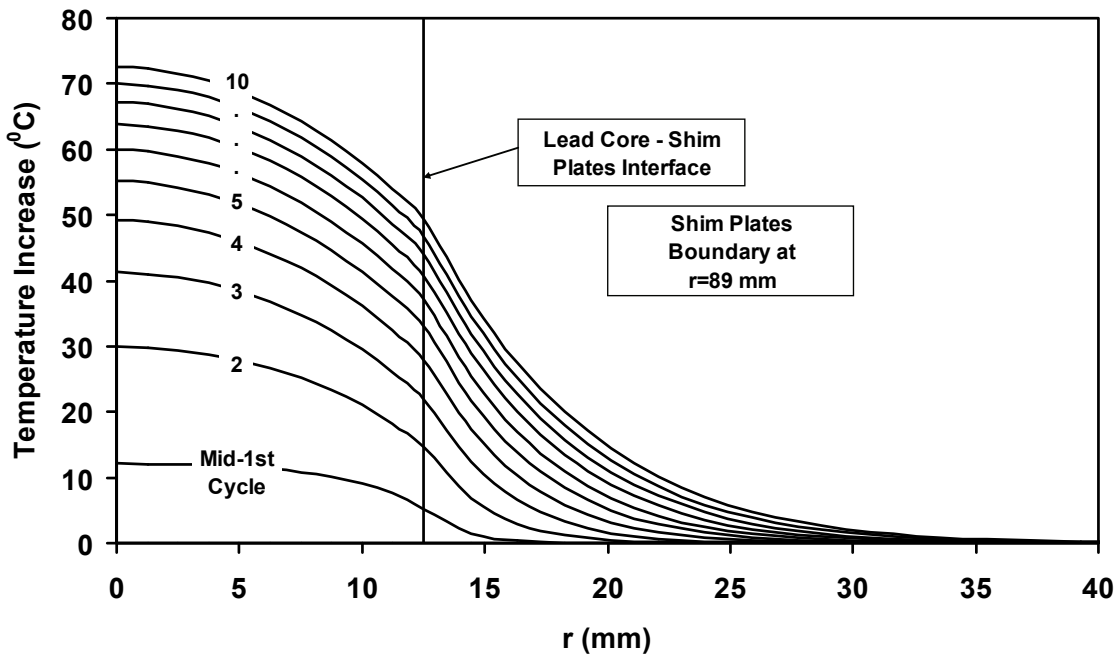
FIGURE 4-56 Horizontal Temperature Distribution (at $z=0$) of the Bearing of Figure 4-52 Obtained in Finite Element Analysis Based on Model of Figure 3-16

4.2.15 Example 15

Example 15 involves the bearing of Example 14 but tested at twice the amplitude and half the frequency (Figure 4-52). Recorded force-displacement loops are presented in Figure 4-57. Test data and parameters used in the analysis are presented in Table 4-23 and analysis results are presented in Figures 4-58 to 4-60. Note that the peak velocity in this test was the same as that of Example 14, but the dimensionless time (1.804) and distance travelled were twice as much.
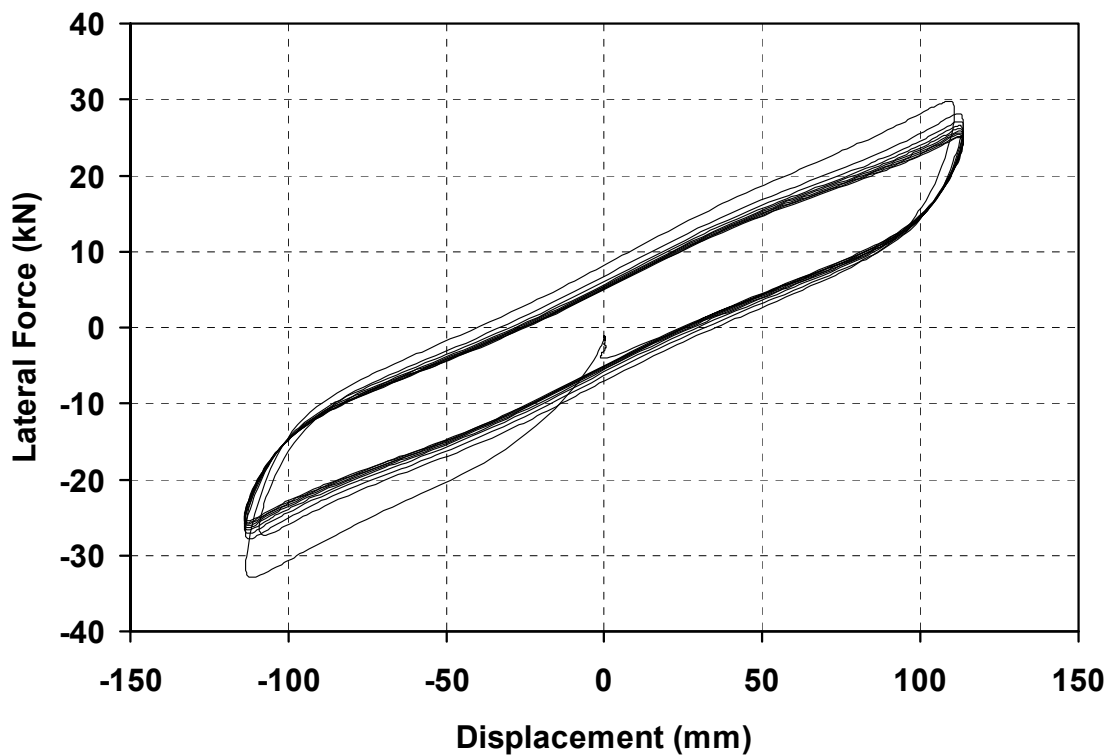
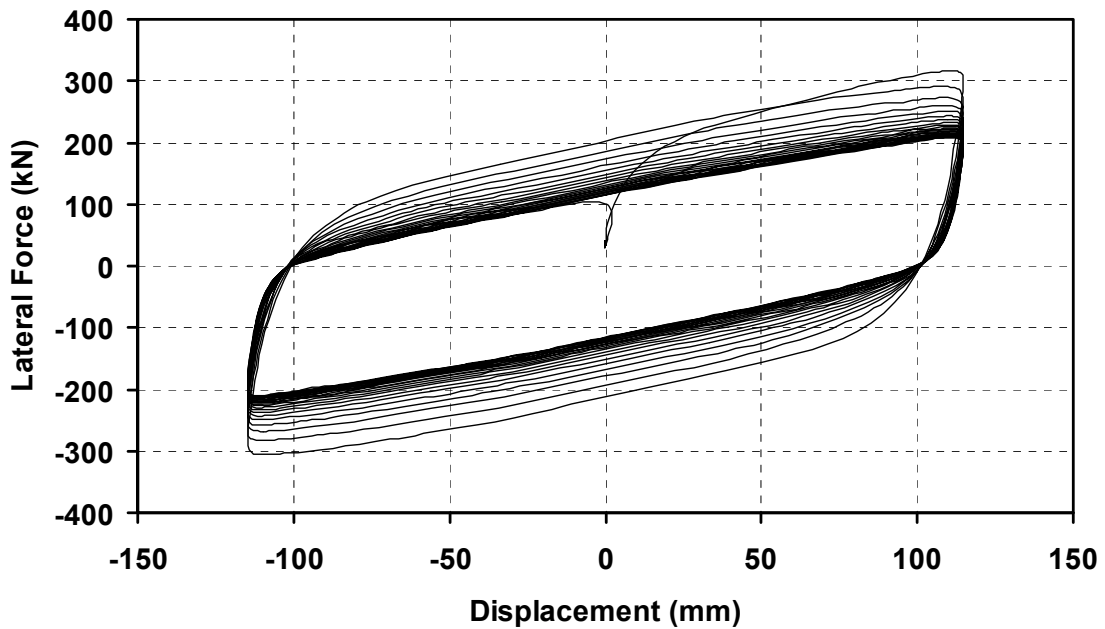**FIGURE 4-57 Force-Displacement Loops of Bearing of Figure 4-52. Load=67 kN, Displacement Amplitude=114 mm and Frequency=0.5 Hz (Peak Velocity=358 mm/s)**

TABLE 4-23 Data Used in Analysis of Example 15

Vertical Load on Bearing, N	67 kN
Amplitude of Motion, u_0	114 mm
Period of Motion, T	2.0 sec
Total Thickness of Shims, t_s	32 mm
Thickness of Steel Above and Below Bearing, t_p	300 mm
Radius of Lead Core, a	12.5 mm
Bonded Rubber Radius, R	89 mm
Height of Lead Core, h_L	89 mm
Peak Velocity of Sinusoidal Motion, v_{max}	358 mm/s
Initial (Reference) Lead Effective Yield Stress, σ_{YL0}	16.2 MPa
Initial Temperature, T_{L0}	20^0C
Parameter of Exponential Relation of σ_{YL} vs. Temperature, E_2	0.0069/^{0}C
Effective Stiffness for 1st Cycle, $K_{eff,1}$	0.28 kN/mm
Effective Damping for Estimating Rubber Contribution to EDC	0.02
Assumed Yield Displacement, Y	5 mm
Thermal Properties of Rubber, Steel and Lead	Per Table 3-3
Heat Capacity of Rubber and Steel Composite, ρc	2693596 J/(m^3 ^{0}C)
Radial Conductivity of Rubber and Steel Composite, $k_{eff,radial}$	18.1 W/(m ^{0}C)
Vertical Conductivity of Rubber and Steel Composite, $k_{eff,vert}$	0.25 W/(m ^{0}C)

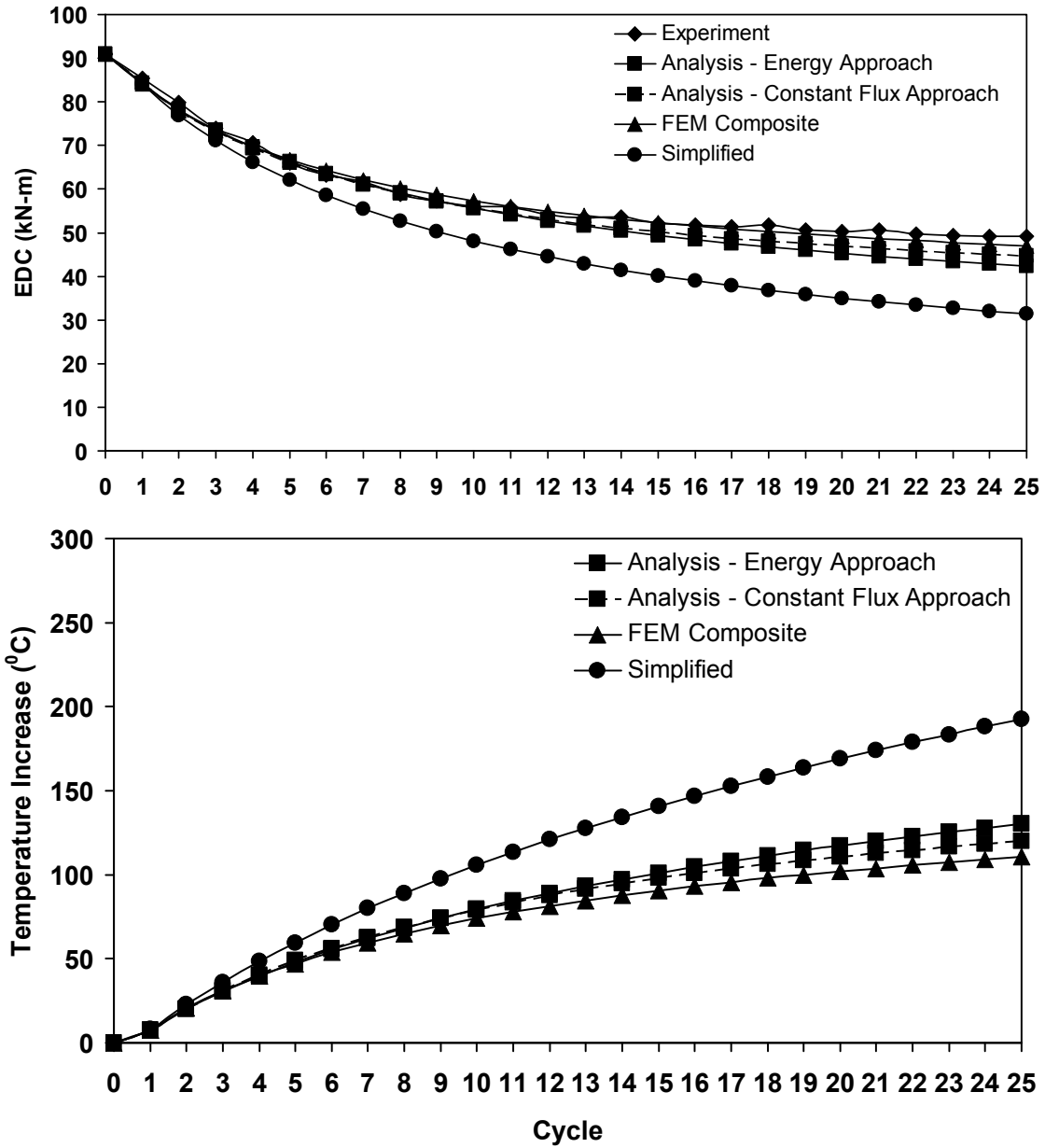**FIGURE 4-58 Temperature and Energy Dissipated per Cycle for Example 15**
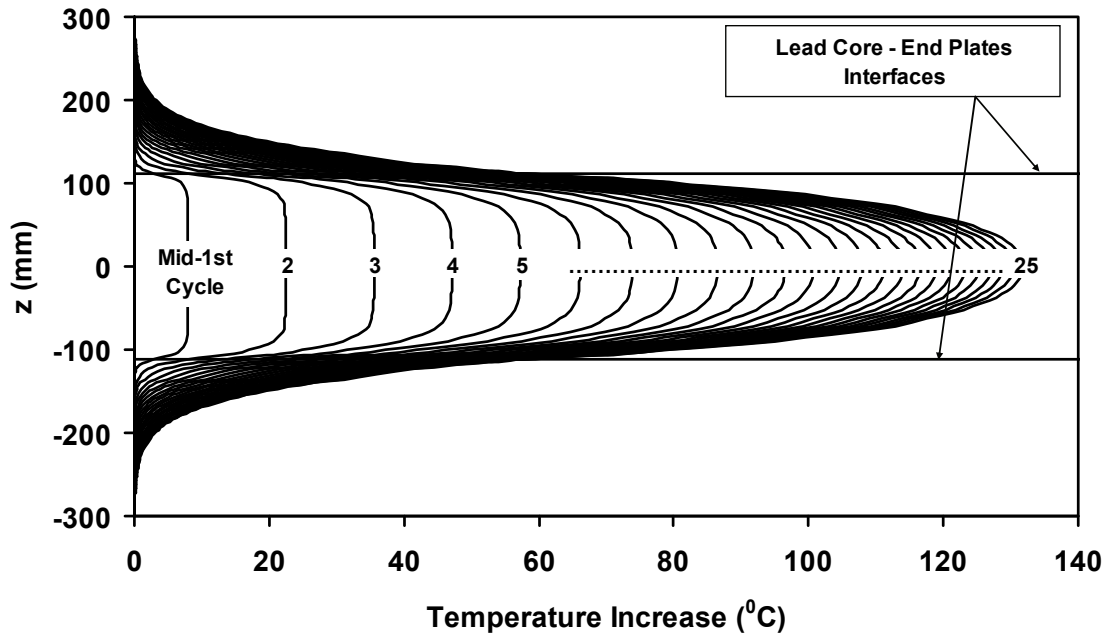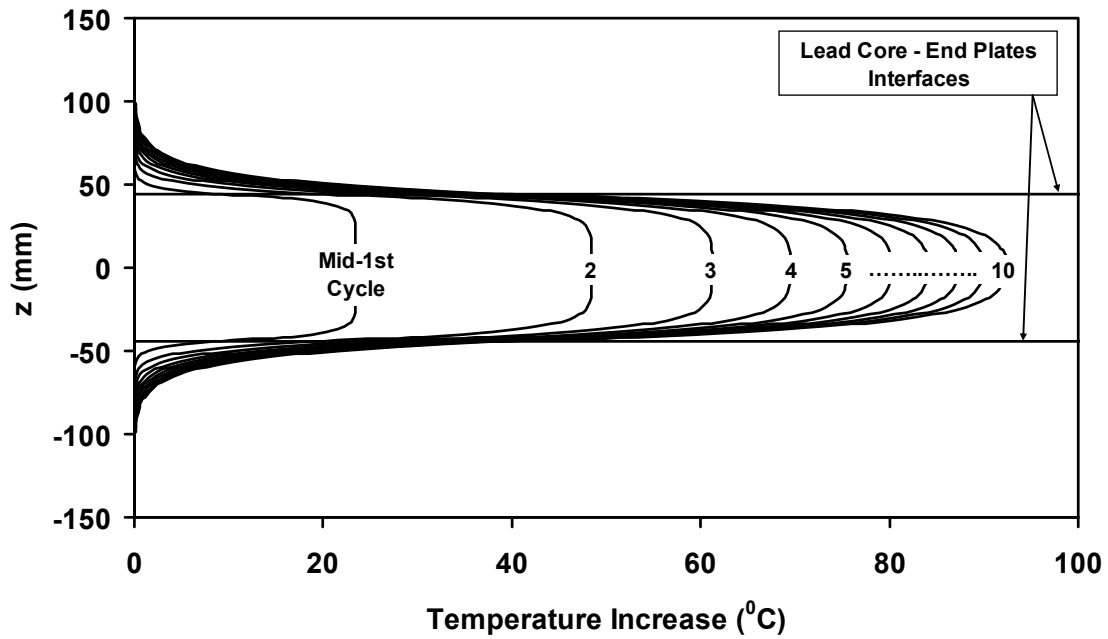
FIGURE 4-59 Vertical Temperature Distribution at the Center of the Bearing (r=0) of Figure 4-52 Obtained in Finite Element Analysis Based on Model of Figure 3-16
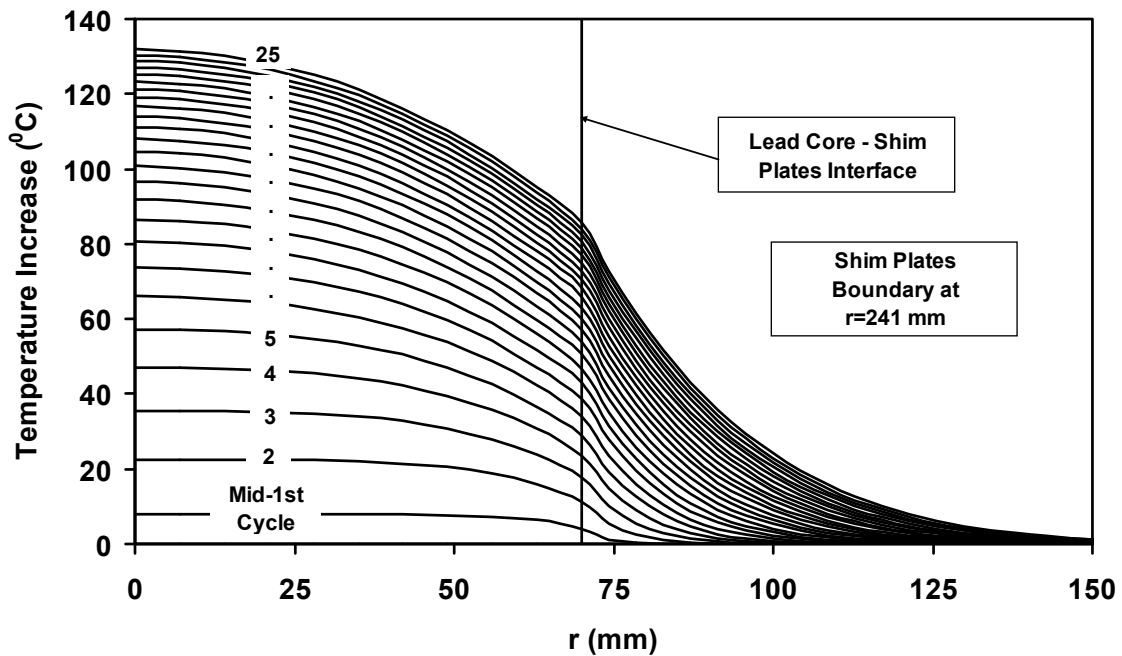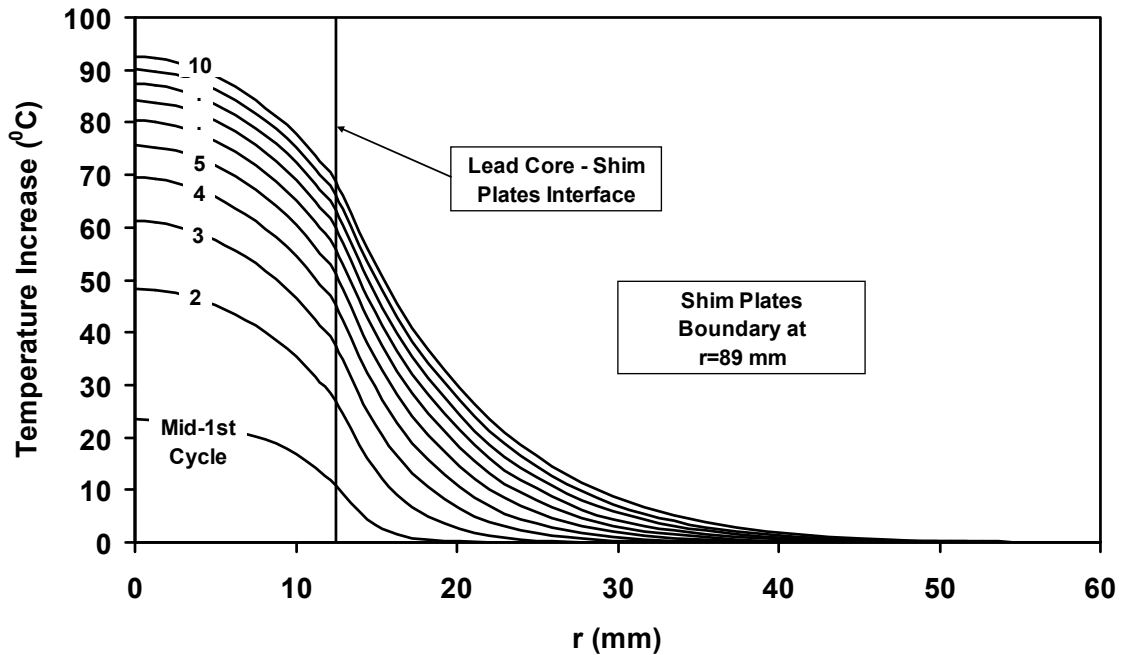

FIGURE 4-60 Horizontal Temperature Distribution (at z=0) of the Bearing of Figure 4-52 Obtained in Finite Element Analysis Based on Model of Figure 3-16

In discussing the results of this test we note that two processes with counteracting effects are involved. On one hand, the test is of longer duration than the test of Example 14 and therefore one should expect greater heat conduction and thus lower lead core temperatures. Indeed, a comparison of Figures 4-59 and 4-60 to 4-55 and 4-56, respectively, reveals that the heat fronts in the test of Example 15 penetrated further into the steel shims and end plates than in the test of Example 14. On the other hand, the distance travelled in each cycle in Example 15 is larger and therefore we should expect more heat generation and higher lead core temperatures. The temperature history predictions in Figure 4-58 demonstrate that the second process dominates resulting in higher lead core temperatures than in the test of Example 14 (Figure 4-54).

The EDC histories predicted by the two analytical methods and the finite element method are in very good agreement with the experimentally measured EDC. As seen in Figure 4-58, the constant flux method predicts the experimental EDC almost exactly, whereas the finite element method slightly overpredicts the EDC. One would expect the finite element method to provide a better prediction, although the differences between the various solutions are too small to be able to identify the reason for the discrepancy.

The simplified method does not provide good prediction of the EDC except in the first cycle. Indeed, a check of the criterion of (3-59) results in an error of 68^0C at the second cycle, which is much larger than the limit of 40^0C. The inability of the simplified method to predict correctly the EDC was expected given the significant heat conduction effects (although in a conceptual sense – only use of equation (3-59) would provide some definitive measure for the validity of the simplified solution).

4.3 Concluding Remarks

The validity of the theory for predicting the temperature rise and the associated reduction in characteristic strength of lead-rubber bearings, and the basic assumptions of the theory have been confirmed by limited finite element analyses and comparison to experimental results in fifteen examples. The analytic solutions and the finite element analyses predicted well the energy dissipated per cycle measured in the experiments. Moreover, on the basis of the presented results, it is concluded that testing at quasi-static conditions (as often done due to limited availability of high speed testing machines), results in a lesser increase in the lead core temperature and in a lesser reduction of EDC.

SECTION 5

MODEL OF LEAD-RUBBER BEARING HYSTERETIC BEHAVIOR

5.1 Introduction

Numerous mathematical models of behavior of elastomeric bearings have been proposed. These models may be classified in two broad categories:

(1) Finite element formulations using models of material behavior for rubber-like materials and plasticity (e.g. Seki et al., 1987; Ali and Abdel-Ghaffar, 1995).

(2) Hysteretic models of various complexities that include (a) bilinear hysteretic models that have been widely used in dynamic analysis programs such as the 3D-BASIS class (Nagarajaiah et al., 1989; Tsopelas et al., 2005) and the SAP2000 (Computers and Structures, Inc., 2007), and (b) improved formulations of hysteretic models based on phenomenological constructions that require calibration on the basis of experimental data (e.g. Kikuchi and Aiken, 1997; Grant et al., 2004; Abe et al., 2004).

While these models may account for complex displacement-dependent (such as elastomer hardening) and rate-dependent behavior, none account for lead core heating effects on the characteristic strength of lead-rubber bearings. Moreover, models based on phenomenological constructions rely for calibration on experimental data obtained in the testing of bearings. Accordingly, the validity of these models is limited to bearing configurations that are "similar" to the tested bearings. Statements on "similarity" or proportionality (geometric similarity) are often included in works of development of phenomenological models (e.g., Abe et al., 2004). It is known from the work presented in Section 3 herein that geometric similarity cannot be used in extrapolating to other

geometries experimental data related to the effect of lead core heating on the behavior of lead-rubber bearings.

This section presents a mathematical model of mechanical behavior of lead-rubber bearings that accounts for lead core heating effects. The model is based on the verified theory of Section 3 and does not require calibration on the basis of experimental data. It simply predicts the instantaneous value of the strength of a lead-rubber bearing based on calculation of the instantaneous temperature of the lead core and is presented as one- and two- dimensional formulations of the smooth bilinear hysteretic model that is currently employed in computer programs 3D-BASIS and SAP2000. Moreover, a discussion is presented on the application of the model in finite element formulations of the behavior of lead-rubber bearings based on thermo-mechanical analysis with temperature-dependent lead properties.

This section also presents comparisons of experimental force-displacement loops to predictions of the presented model in sinusoidal and random motion of lead-rubber bearings. The comparisons provide validation of the model and also further demonstrate the validity of the theory on lead core heating addressed in Section 4 herein. Finally, Section 6 utilizes the now validated model for lead-rubber bearing behavior to study the response of a seismically isolated structure and compare to results obtained using the standard bilinear hysteretic model for lead-rubber bearings within the context of bounding analysis (Constantinou et al., 2007a; 2007b).

5.2 One-Dimensional Lead-Rubber Bearing Model

The proposed model of lead-rubber bearing behavior is a smooth bilinear hysteretic model with characteristic strength that is dependent on the instantaneous lead core temperature. Figure 5-1 illustrates the model. The parameters of the model are: characteristic strength Q_d, yield force F_Y, yield displacement Y, elastic stiffness K_{el} and post-elastic stiffness K_d. These parameters are interrelated as follows:

$$K_{el} = \frac{F_Y}{Y} \tag{5-1}$$

$$F_Y = Q_d + K_d \cdot Y = \frac{Q_d}{1-r} \tag{5-2}$$

$$r = \frac{K_d}{K_{el}} \tag{5-3}$$
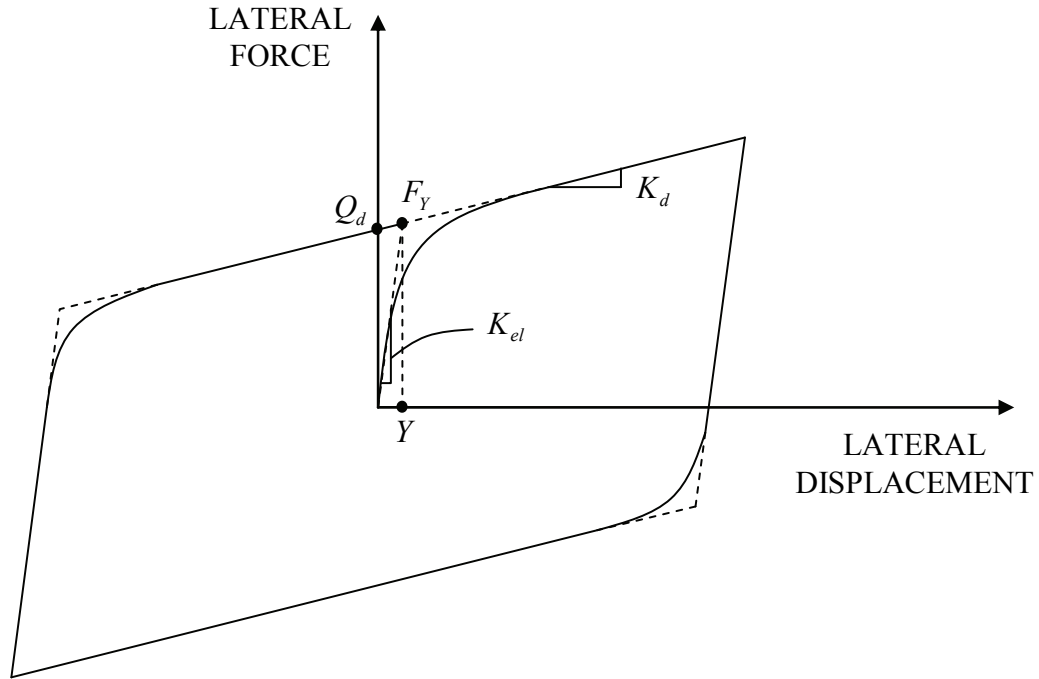
FIGURE 5-1 Bilinear Hysteretic Model for Lead-Rubber Bearings

The formulation described herein is a variant of the one utilized in program 3D-BASIS (Nagarajaiah et al., 1989) and also in program SAP2000 (Computers and Structures, Inc., 2007). The lateral force F_b is related to the lateral displacement u by

$$F_b = K_d u + \sigma_{YL}(T_L)A_L Z + F_d \tag{5-4}$$

$$Y \cdot \dot{Z} = \left(A - |Z|^2 B \cdot (1 + \text{sgn}(\dot{u}Z))\right) \cdot \dot{u} \tag{5-5}$$

where σ_{YL} is the temperature-dependent effective yield stress of lead and A_L is the cross-sectional lead core area. Note that for proper behavior $A/(2B)$ must equal unity (Constantinou and Adnane, 1987). Herein, the values $A=1$, $B=0.5$ are being used.

In equation (5-4), the contributions to dissipative force from the lead core ($\sigma_{YL} A_L Z$) and rubber ($F_d + K_d u$) are separated so that they can be properly considered. Force F_d may either be considered to be of hysteretic nature or of viscoelastic nature. It should be noted that the contribution of force F_d is dependent on the ambient temperature of rubber (see Constantinou et al., 2007b) but is practically independent of the lead core temperature. Herein, the simplest form for force F_d is used:

$$F_d = c_d \dot{u} \tag{5-6}$$

where parameter c_d is selected such that a value of effective damping β is provided by the rubber part of the bearing:

$$c_d = 2\beta \left(\frac{WK_d}{g} \right)^{1/2} \tag{5-7}$$

where W is the weight carried by the bearing. When experimental data on control specimens without lead core are available, parameter c_d may be obtained by relating to the energy dissipated per cycle.

The yield stress is described by (see Section 3)

$$\sigma_{YL} = \sigma_{YL0} \exp\left(- E_2 T_L \right) \tag{5-8}$$

where T_L is the lead core temperature increase, σ_{YL0} is the effective yield stress of lead at the reference (starting) temperature and parameter $E_2 = 0.0069/^0C$. The lead core

167

temperature increase is given by equations (3-50), which are reproduced below after some substitutions:

$$\dot{T}_L = \frac{\sigma_{YL0}\exp(-E_2 T_L)|Z\dot{u}|}{\rho_L c_L h_L} - \frac{k_S T_L}{a\cdot\rho_L c_L h_L}\cdot\left[\frac{1}{F}+1.274\left(\frac{t_s}{a}\right)\left(\frac{\alpha_S t}{a^2}\right)^{-1/3}\right] \qquad (5\text{-}9)$$

$$F=\begin{cases} 2\cdot\left(\dfrac{t^+}{\pi}\right)^{1/2} - \dfrac{t^+}{\pi}\cdot\left[2-\left(\dfrac{t^+}{4}\right)-\left(\dfrac{t^+}{4}\right)^2 - \dfrac{15}{4}\left(\dfrac{t^+}{4}\right)^3\right], & t^+ < 0.6 \\[4mm] \dfrac{8}{3\pi} - \dfrac{1}{2(\pi\cdot t^+)^{1/2}}\cdot\left[1-\dfrac{1}{3\cdot(4t^+)}+\dfrac{1}{6\cdot(4t^+)^2}-\dfrac{1}{12\cdot(4t^+)^3}\right], & t^+ \geq 0.6 \end{cases} \qquad (5\text{-}10)$$

$$t^+ = \frac{\alpha_S t}{a^2} \qquad (5\text{-}11)$$

Note that in (5-9) to (5-11) we have made use of the constant flux solution of Section 3. Moreover, the following parameters appear in (5-9) to (5-11): ρ_L is the density of lead, c_L is the specific heat of lead, h_L is the height of the lead core, a is the radius of the lead core, α_S is the thermal diffusivity of steel, k_S is the thermal conductivity of steel and t_s is the total shim plate thickness.

It should be noted that (5-9) contains the following modification by comparison to Sections 3 and 4: the effective yield stress is multiplied by the term $|Z\dot{u}|$ instead of just the magnitude of the velocity $|\dot{u}|$. Note that the term $|Z\dot{u}|$ equals to $|\dot{u}|$ when the bearing undergoes inelastic action (displacement exceeding yield displacement Y) and otherwise is less than $|\dot{u}|$. This modification has minor effects when the bearings undergo large

deformations but is important in cases of low displacement amplitude because it properly accounts (does not overestimate) for energy dissipation in the lead core.

Equations (5-4) to (5-11) describe the proposed lead-rubber bearing model. Parameters in the model are K_d, σ_{YL0}, Y, A_L, h_L, t_s, a, ρ_L, c_L, k_S, α_S and c_d, whereas parameters $A=1$, $B=0.5$ and $E_2=0.0069/^0C$ have prescribed values. Note that in this model the yield displacement is constant so that the elastic stiffness varies as the yield force reduces with increasing lead core temperature.

5.3 Two-Dimensional Lead-Rubber Bearing Model

The two-dimensional smooth bilinear hysteretic model in program 3D-BASIS (also SAP2000) was originally constructed by Park et al. (1986) and has been shown to produce acceptable results on the behavior of isolators in bi-directional motion (e.g. Nagarajaiah et al., 1989; Mokha et al., 1993). In its isotropic formulation, which is appropriate for describing the behavior of lead-rubber bearings, the model in terms of forces F_x, F_y and displacements U_x, U_y along orthogonal directions x and y is:

$$\begin{Bmatrix} F_x \\ F_y \end{Bmatrix} = r \cdot \begin{bmatrix} \dfrac{F_Y}{Y} & 0 \\ 0 & \dfrac{F_Y}{Y} \end{bmatrix} \cdot \begin{Bmatrix} U_x \\ U_y \end{Bmatrix} + (1-r) \cdot \begin{bmatrix} F_Y & 0 \\ 0 & F_Y \end{bmatrix} \cdot \begin{Bmatrix} Z_x \\ Z_y \end{Bmatrix} \tag{5-12}$$

$$Y \cdot \begin{Bmatrix} \dot{Z}_x \\ \dot{Z}_y \end{Bmatrix} = (A \cdot [I] - B \cdot [\Omega]) \cdot \begin{Bmatrix} \dot{U}_x \\ \dot{U}_y \end{Bmatrix} \tag{5-13}$$

$$[\Omega] = \left\{ \begin{array}{cc} Z_x^2 \cdot \left[\text{sgn}(\dot{U}_x Z_x) + 1\right] & Z_x Z_y \cdot \left[\text{sgn}(\dot{U}_y Z_y) + 1\right] \\ Z_x Z_y \cdot \left[\text{sgn}(\dot{U}_x Z_x) + 1\right] & Z_y^2 \cdot \left[\text{sgn}(\dot{U}_y Z_y) + 1\right] \end{array} \right\} \tag{5-14}$$

where $[I]$ is an identity matrix and $A=1$, $B=0.5$. Equations (5-12) to (5-14) together with (5-6) to (5-11) describe the two-dimensional model for lead-rubber bearings.

5.4 Modifications to Account for Other Behaviors

The model of equations (5-4) to (5-14) only accounts for the effect of heating of the lead core on the characteristic strength of the bearings. It does not account for strain rate effects on the strength and post-elastic stiffness nor does it account for strain effects on stiffness. Although some information on the strain rate effects on strength may be found in Constantinou et al. (2007b), it appears that there is insufficient data to allow for the development of a model based on first principles.

The models described in Sections 5.2 and 5.3 can be easily modified to account for displacement-dependent post-elastic stiffness and for rate-dependent stiffness and strength. Although such modifications are entirely phenomenological, they can provide for complex behavior as demonstrated by Demetriades et al. (1993), Kikuchi and Aiken (1997) and Abe et al. (2004). The interested reader is referred to these studies for further details.

5.5 Thermo-Mechanical Finite Element Analysis

Detailed finite element modeling of lead-rubber bearings is useful primarily in analysis of single bearings in order to predict behavior in lieu of testing or prior to testing. For

example, Ali and Abdel-Ghaffar (1995) and Doudoumis et al. (2005) reported elaborate finite element formulations for rubber, steel and lead in lead-rubber bearings, however restricted to only mechanical behavior. In order to capture the changing characteristics of the bearings due to heating of the lead, coupled thermo-mechanical analysis is required. Important aspect of this analysis is the specification of temperature-dependent mechanical properties for lead. The data presented in Section 2 herein on the behavior of lead indicate that a simple model for lead would be that of elastoplastic behavior with temperature independent elastic modulus (e.g., see Figure 2-5) and yield stress described by (5-8) with E_2=0.0069/^{0}C.

5.6 Verification of Model in Sinusoidal Motion

Two examples from Section 4 are revisited, the lead-rubber bearings are modeled using the one-dimensional model of equations (5-4) to (5-11) and analytical force-displacement loops are constructed for comparison to experimental results. These examples are 8 and 10 in Sections 4.2.8 and 4.2.10, respectively. Parameters for modeling are presented in Table 5-1. Furthermore, for both bearings the following parameters were used: ρ_L=11200 kg/m^3, c_L=130 J/(kg^{0}C), k_S=50 W/(m^{0}C), α_S=1.41x10^{-5} m^2/s, E_2=0.0069/^{0}C.

Figures 5-2 and 5-3 compare analytically predicted and experimental loops for the two bearings. It should be noted that solution of equations (5-4) to (5-11) requires as input the time histories of displacement u and velocity $\dot{u}$ of the top of the bearing with respect to its bottom. The results in Figures 5-2 and 5-3 demonstrate that the model is capable of predicting well the changes in strength of lead-rubber bearings but it does not capture

well the ascending branch of the loop on first loading nor does it capture well the portion of the loop at each reversal of motion. The shape of the ascending branch of the loop on initial loading is likely markedly affected by unrealistic rate effects (and likely measurement errors) as the test started at rest with the test machine attempting to impose an instantaneous velocity of 1 m/sec. These effects are much less pronounced in low speed testing as seen in Example 9 of Section 4 (Figure 4-32). Nevertheless, part of the difference between experimental and analytical results on the ascending initial part of the loop are due to the bilinear hysteretic model employed, which is based on a fixed value of yield displacement. As also seen in the shapes of the loops on each reversal of motion, the actual behavior justifies use of a variable yield displacement. Such behavior can only be captured with phenomenological adjustments of the presented model as, for example, described in Kikuchi and Aiken (1997) and Abe et al. (2004).

TABLE 5-1 Parameters in Model of Lead-Rubber Bearings

Example	c_d (Ns/mm)	σ_{YL0} (MPa)	Y (mm)	K_d (N/mm)	A_L (mm^2)	h_L (mm)	a (mm)	t_s (mm)
8	89	16.9	30	2000	73542	333	153	125
10	128	13.0	7	1080	15394	224	70	71
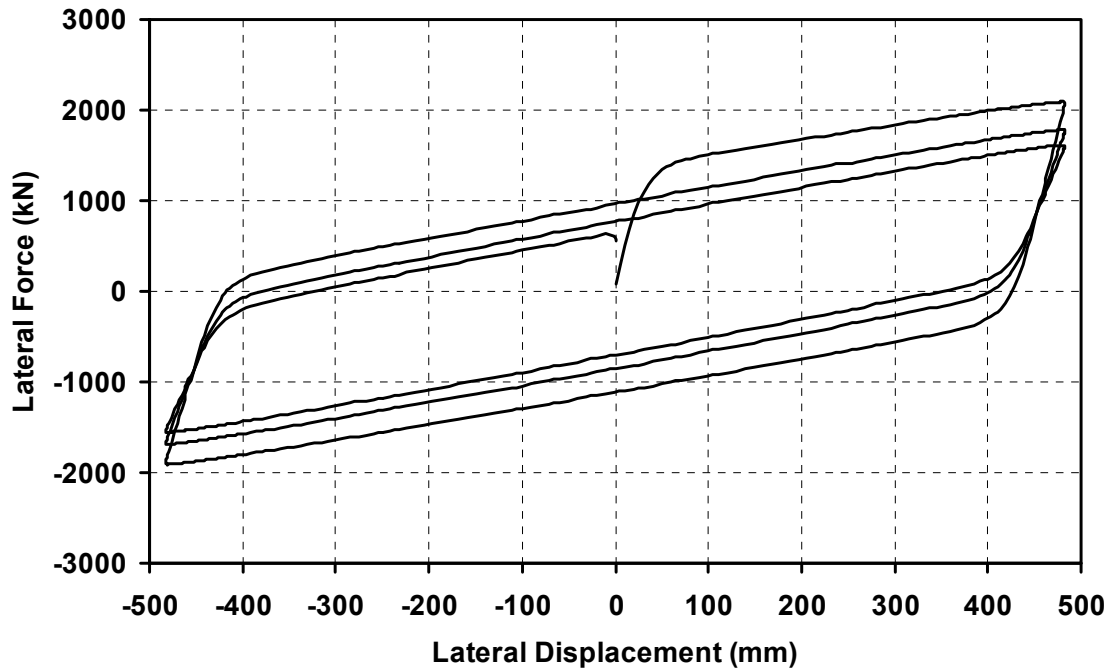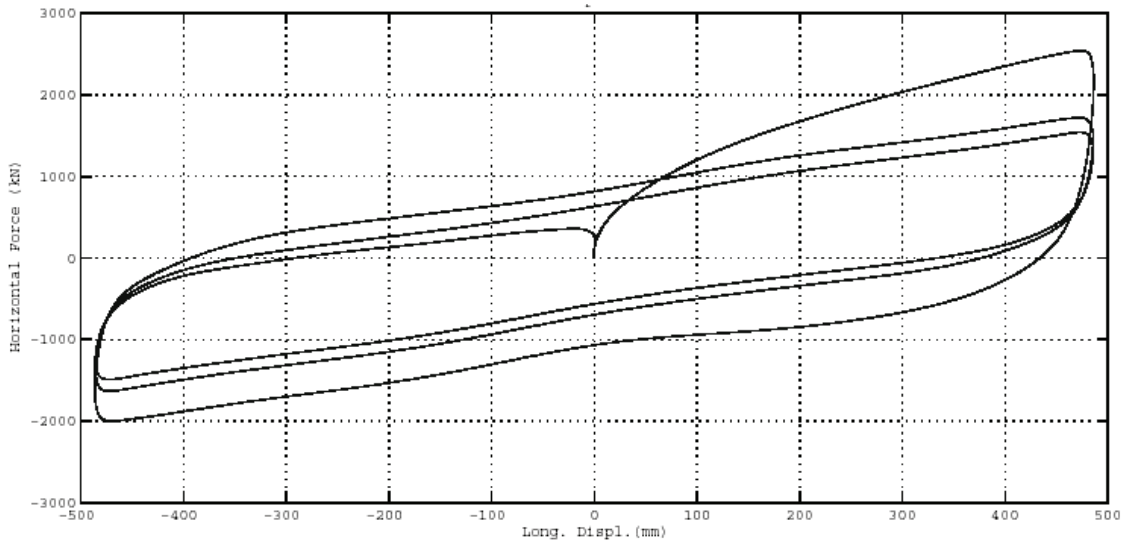
FIGURE 5-2 Comparison of Analytically Predicted (bottom graph) and Experimentally Obtained (top graph) Force-Displacement Loops for the Bearing of Example 8 (Section 4.2.8)
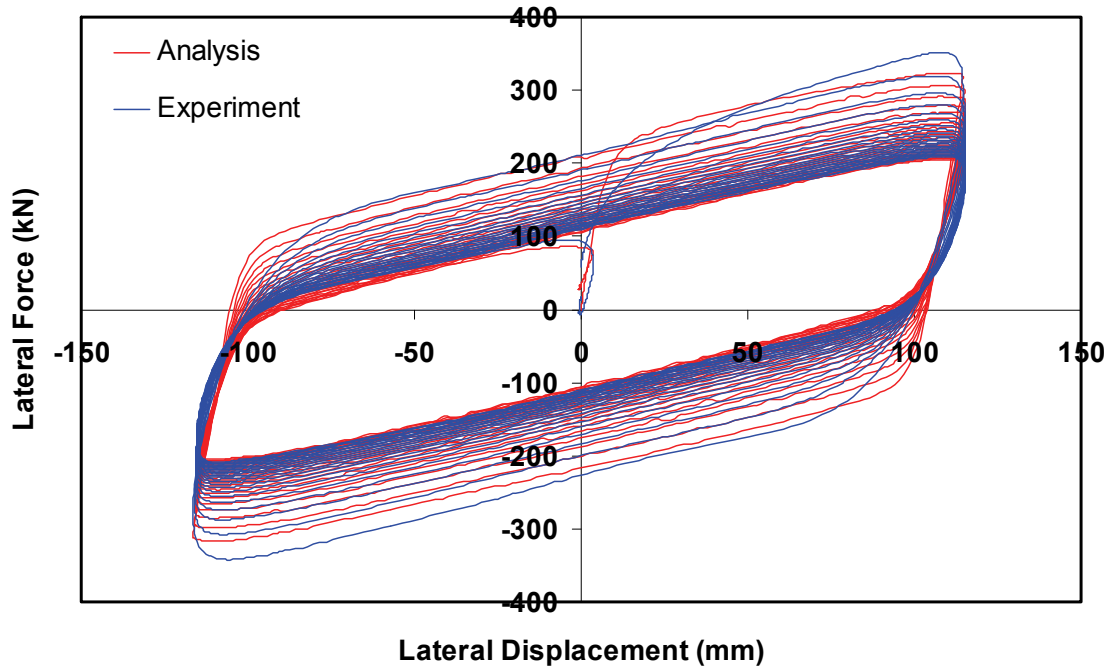
FIGURE 5-3 Comparison of Analytically Predicted and Experimentally Obtained Force-Displacement Loops for the Bearing of Example 10 (Section 4.2.10)

5.7 Verification of Model in Random Motion

The small size bearing of Figure 4-52 (see Examples 14 and 15 in Section 4) was tested by subjecting it to a compressive load of 89 kN and imposing the histories of lateral displacement shown in Figures 5-4 and 5-5. These histories are termed "Motion 1" and "Motion 2", respectively.

Table 5-2 presents values of parameters of the model of the lead-rubber bearing. Moreover, the following values of other parameters were used: ρ_L=11200 kg/m^3, c_L=130 J/(kg^{0}C), k_S=50 W/(m^{0}C), α_S=1.41x10^{-5} m^2/s, E_2=0.0069/^{0}C. Figures 5-6 and 5-7 compare analytically constructed and experimentally measured force-displacement loops of the bearing for the two cases of random motion. Furthermore, Figures 5-8 and 5-

9 present calculated and measured histories of the dissipated energy in the two tests. Finally, Figure 5-10 presents calculated histories of the lead core temperature rise in the two tests. It should be noted that the tested bearing has a small lead core, heating effects are not significant and neither analysis nor experiments show any important strength deterioration.

Overall, the prediction by the model of the force-displacement loops and the dissipated energy histories of the bearing is good. Nevertheless, we still observe differences in the loop shape on reversal of motion at small amplitudes of motion. This is due to inability of the model to describe the hysteretic behavior of the bearings at all amplitudes of motion, a problem that could be corrected by incorporating displacement-dependent post-elastic stiffness.
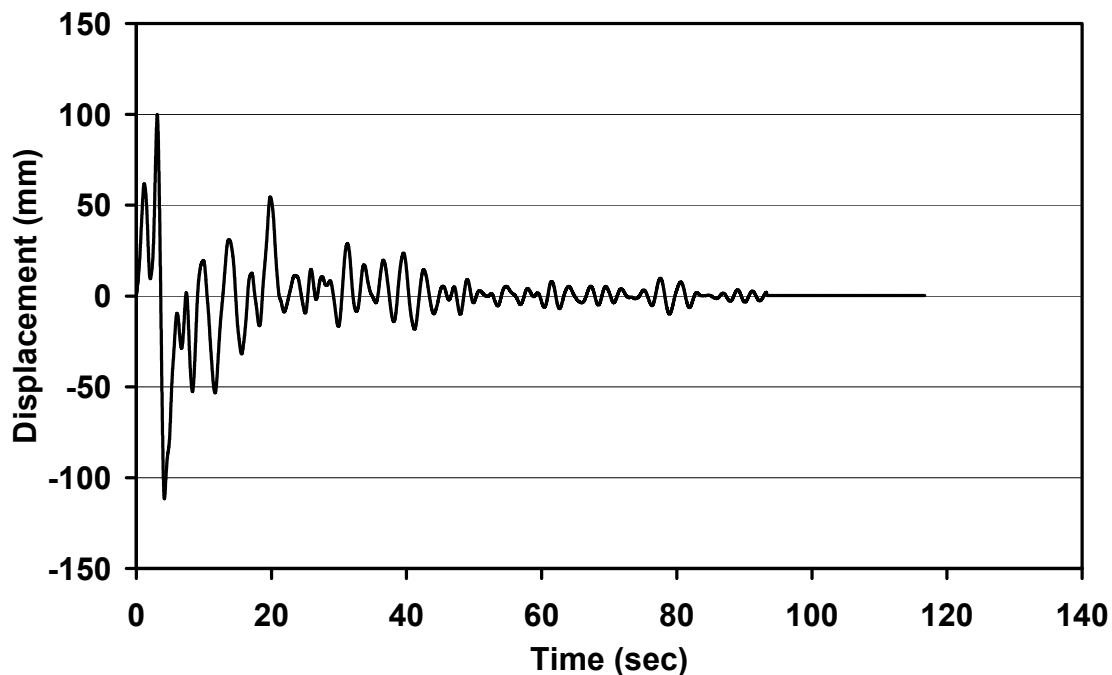
FIGURE 5-4 Motion 1 Displacement History
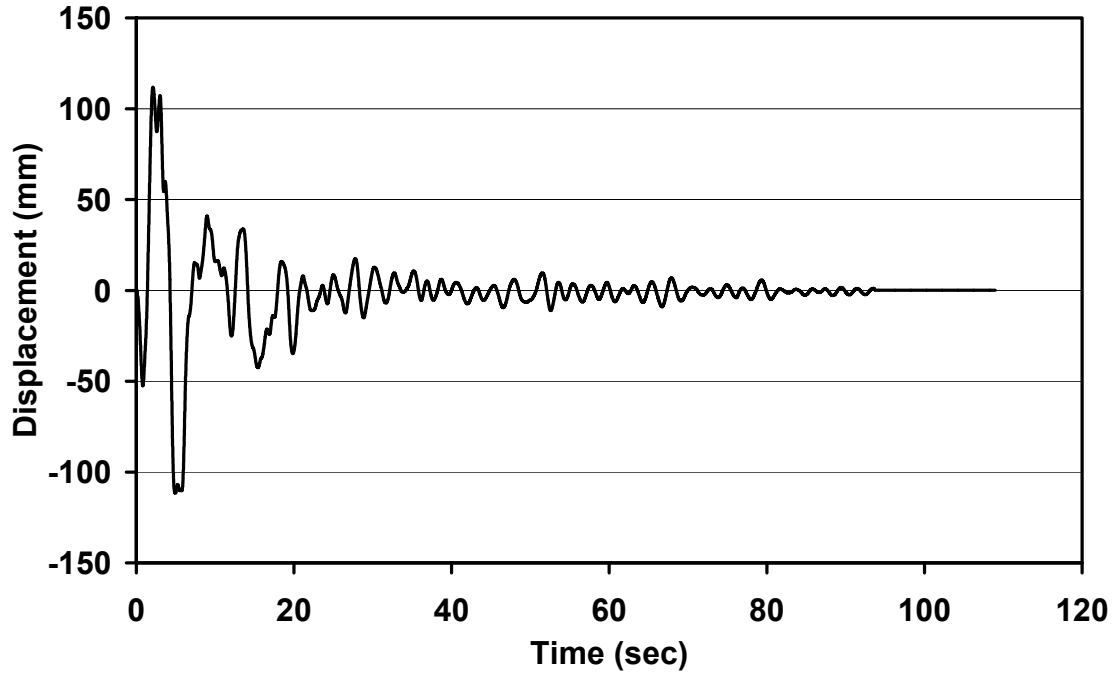
FIGURE 5-5 Motion 2 Displacement History

TABLE 5-2 Parameters in Model of Small-Size Lead-Rubber Bearing

c_d (Ns/mm)	σ_{YL0} (MPa)	Y (mm)	K_d (N/mm)	A_L (mm^2)	h_L (mm)	a (mm)	t_s (mm)
3.6	16.2	5	190	491	89	12.5	32
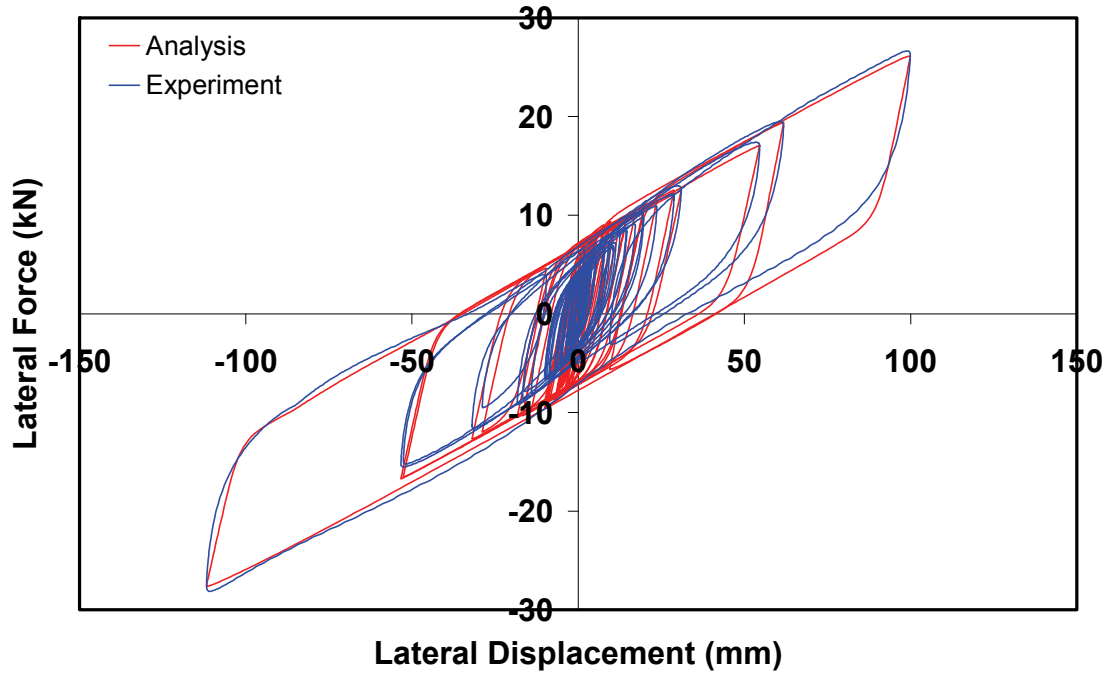
FIGURE 5-6 Analytical and Experimental Force-Displacement Loops of Lead-Rubber Bearing in Random Motion 1
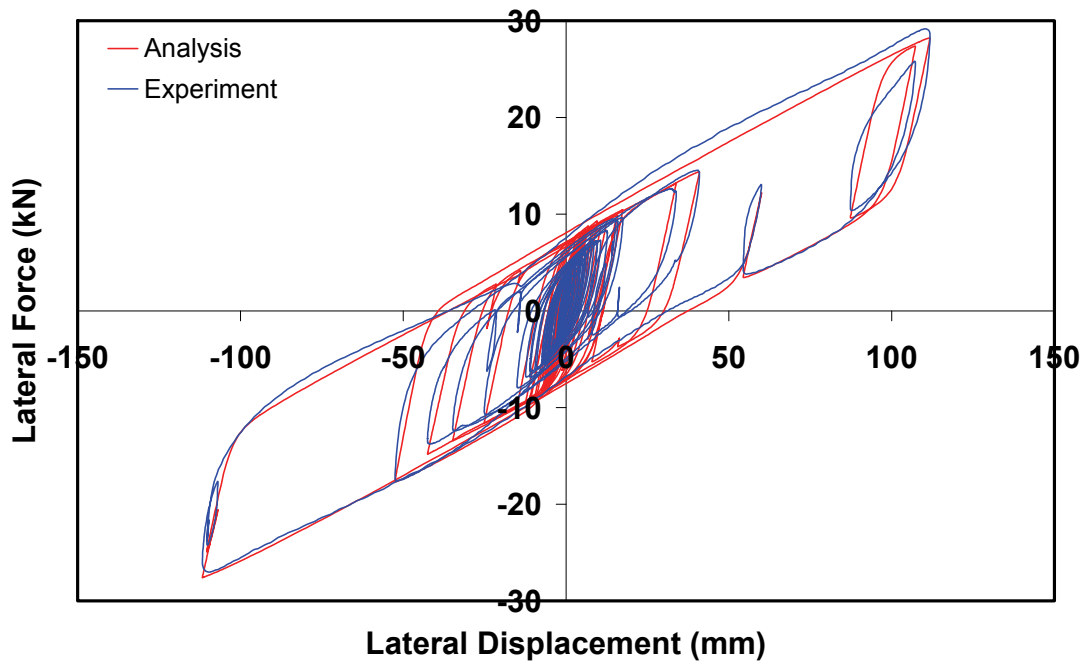
FIGURE 5-7 Analytical and Experimental Force-Displacement Loops of Lead-Rubber Bearing in Random Motion 2
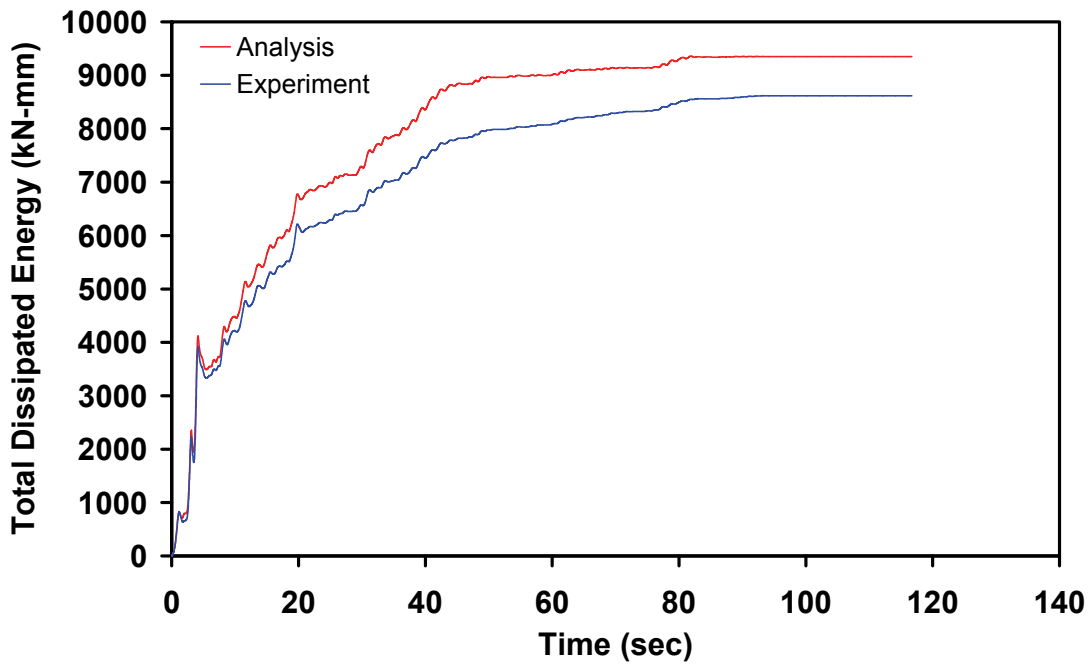
FIGURE 5-8 Analytically Predicted and Experimentally Measured Dissipated Energy Histories in Random Motion 1
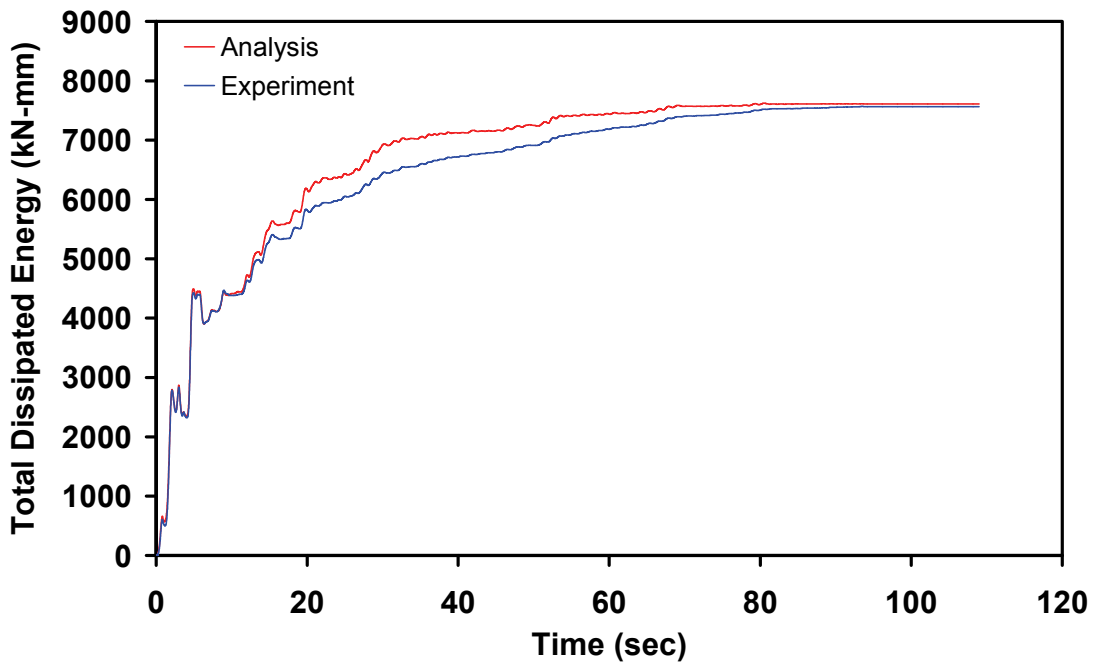
FIGURE 5-9 Analytically Predicted and Experimentally Measured Dissipated Energy Histories in Random Motion 2

178
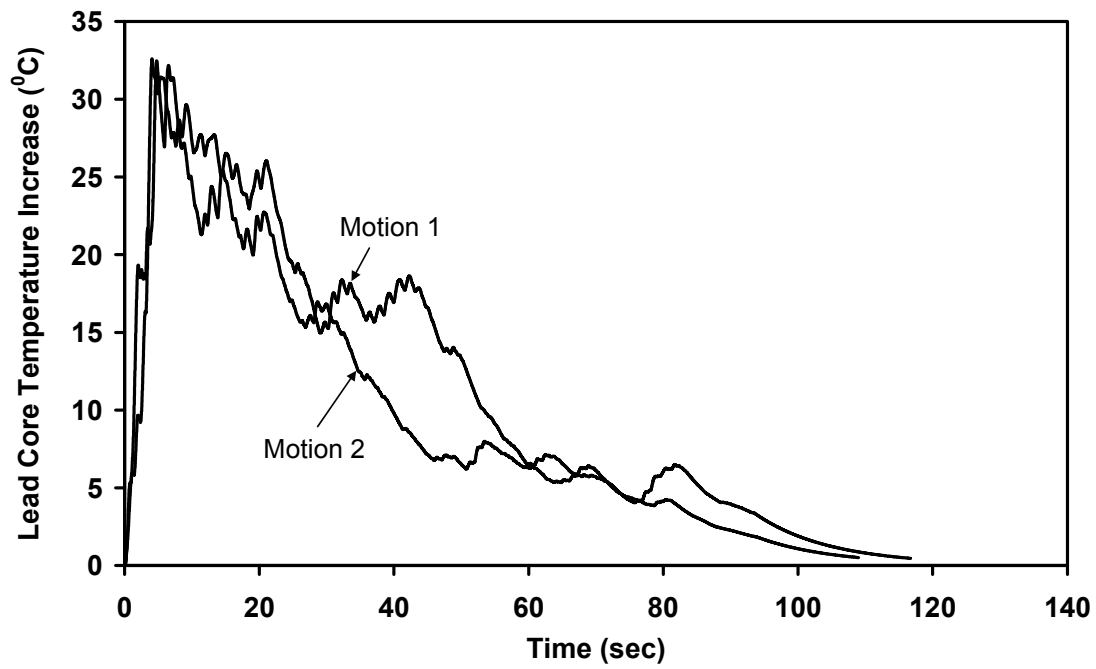
FIGURE 5-10 Calculated Histories of Lead Core Temperature Increase in Tests with Random Motion

SECTION 6

LEAD CORE HEATING EFFECTS ON THE RESPONSE OF ISOLATED STRUCTURES

6.1 Introduction

This section investigates the significance of accounting for lead core heating in the prediction of the dynamic response of seismically isolated structures. The current state-of-practice in the analysis of seismically isolated structures is to perform bounding analysis. In this analysis, changes in the mechanical properties of the isolators due to effects of history of loading, aging and environmental conditions, and due to uncertainties, are accounted for by conducting two analyses, one using lower bound and one using upper bound properties.

For lead-rubber bearings, a significant portion of the difference between the upper and lower bound values of the characteristic strength results from heating effects, which are most often conservatively estimated on the basis of available experimental results. For example, Constantinou et al. (2007a) presented analysis and design examples in which the lower bound value of the characteristic strength is based on the average value of the effective yield stress of lead in three cycles, σ_{L_3}, whereas the upper bound value is based on the yield stress in the first cycle, σ_{L_1}. Proposed values to use were σ_{L_3} =10 to 12 MPa (range to account for uncertainties) and σ_{L_1} =1.35 σ_{L_3}. This leads to lower and upper bound values of strength, excluding any effects of low temperature and aging, that are based on lead yield stress values of 10 MPa and 1.35 x 12 = 16.2 MPa, respectively. This

significant range of values is based on experimental data for bearings with large lead core area and undergoing large shear strains in the lead core at high speeds for a number of cycles. While these conditions are appropriate for applications in areas of high seismicity with at least three cycles of large amplitude motion, they likely lead, when used for applications in areas of lower seismicity and for motions that result in a smaller number of cycles (such as for near-fault high velocity pulses), to conservative estimation of displacement demands and isolation shear forces.

In this section a seismically isolated structure is analyzed by first utilizing the lead-rubber bearing model described in Section 5 and then by utilizing a bilinear hysteretic model with upper and lower bound values of characteristic strength. Comparisons of responses calculated for a number of earthquake motions reveal the significance of accounting for the lead core heating effects.

6.2 Description of Analyzed Structure and Earthquake Ground Motions

The analyzed structure is represented as a two-degree-of-freedom system with one degree describing the structural drift and another describing the isolation system displacement. Figure 6-1 illustrates the system. The structure weighs W =1,026,600 kN, distributed as superstructure weight $W_s = 0.8W$ and basemat weight $W_b = 0.2W$. The stiffness k_s was selected such that the fundamental period of the structure ($T = 2\pi\sqrt{W_s/(gk_s)}$) is 0.5 sec and the structural damping ratio β_s =0.05.

The isolation system consists of 100 lead-rubber bearings of the geometry shown in Figure 4-27 and with force-displacement loops (for vertical load of 10,266 kN) presented

in Figures 4-28 and 4-32. The mathematical model of the lead-rubber bearing is as described by equations (5-4) to (5-11) with parameters presented in Section 5.6 and in Table 5-1 (for Example 8). Note that in this model the effective yield stress of lead at the reference temperature (start of motion) is 16.9 MPa.
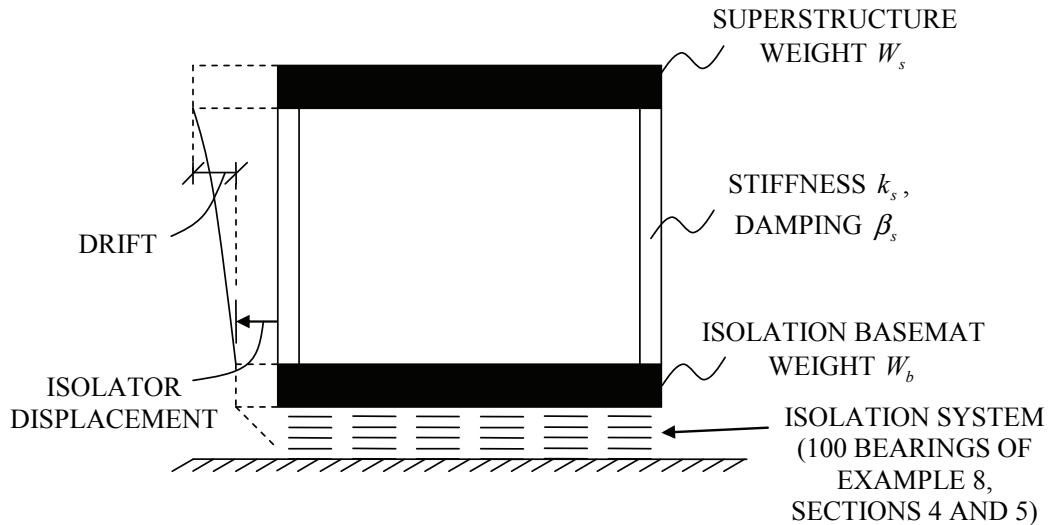
FIGURE 6-1 Analyzed Seismically Isolated Structural System

Upper and lower bound analyses are performed using a temperature independent bilinear hysteretic model (described by (5-1) to (5-6) but with constant σ_{YL}) with the parameters as follows.

Upper bound: Q_d =1243 kN, K_d =2.0 kN/mm, Y =30 mm (based on total yield strength of 16.9 MPa).

Lower bound: Q_d =735 kN, K_d =2.0 kN/mm, Y =30 mm (based on total yield strength of 10 MPa).

Effective properties of the isolated structure at the representative isolator displacement of 500 mm and characteristic properties are presented in Table 6-1.

TABLE 6-1 Characteristic and Effective Properties of Isolated Structure

Condition	Characteristic Strength/W	Period Based on Post-Elastic Stiffness (sec)	Effective Period at Displacement of 500 mm (sec)	Effective Damping at Displacement of 500 mm
Upper Bound (also initial condition in temperature-dependent model)	0.12	4.54	3.03	0.33
Lower Bound	0.07	4.54	3.45	0.25

The motions were selected from a study of Warn and Whittaker (2004) who performed response history analyses using a large number of ground motions organized into eight bins. Motions with large peak ground acceleration from two out of these bins are used for this study, namely: bin 1 (near-field) and bin 2M (large-magnitude small-distance). Table 6-2 provides information on the ground motions used in the analyses. It is noted that these records were modified by ignoring the first few seconds (where the acceleration is nearly zero and no motion and heating occurs). This is theoretically necessary because the model is based on the dimensionless time t^+ defined to start at initiation of heating. Although this is of minor importance, it is suggested that one should perform some representative analyses with the full record and the modified one, compare the results and conclude on the significance of the start time for response history analysis.

TABLE 6-2 Ground Motions Used in Analyses (for more details see Warn and Whittaker, 2004)

Bin	Record	Event	Year	Station	Orientation	PGA (g)	PGV (m/s)
1	NF17	Kobe	1995	JMA	FN	1.09	1.60
2M	BOL090	Duzce, Turkey	1999	Bolu	90	0.82	0.67
1	NF02	Tabas, Iran	1978	Tabas	FN	0.98	1.06
1	NF13	Northridge	1994	Rinaldi	FN	0.89	1.74
1	TCU065-N	Chi Chi, Taiwan	1999	TCU065	North	0.60	0.79

6.3 Results of Analysis

The seismically isolated structure was analyzed for each of the motions of Table 6-2 utilizing three models of analysis: upper bound bilinear hysteretic, lower bound bilinear hysteretic and the proposed lead-rubber bearing model with heating effects considered. Table 6-3 presents the following peak response quantities for each analyzed case: (a) isolator displacement, (b) isolation system shear force normalized by total weight, (c) structural shear normalized by structural weight, (d) structural drift, (e) structural acceleration, and (f) lead core temperature increase. Moreover, Figures 6-2 to 6-11

present comparisons of isolation system force-displacement loops in the five ground motion cases and calculated histories of lead core temperature increase.

The results presented in Table 6-3 and Figures 6-2 to 6-11 clearly demonstrate that use of bounding analysis typically results in conservative estimation of the peak isolator displacement and the peak isolation shear force. Particularly important is the case of earthquake motions with dominant near-fault characteristics, such as the NF02 motion. In this case, the lower bound model significantly overpredicts the displacement demand because it is based on assumptions for lead core heating (several cycles of large amplitude motion) that result in low value for the lower bound characteristic strength. The actual conditions primarily consist of a single large amplitude cycle without significant lead core heating effects so that the characteristic strength of the isolation system remains large and marginally affected by heating. It should be noted that the significance of the strength of isolation systems on the response of seismically isolated structures has been known for near-fault ground motions (Makris and Chang, 2000).

TABLE 6-3 Peak Response of Analyzed Isolated Structure

Motion	Analysis Model	Isolator Displ. (mm)	Isolation Shear/W	Structural Shear/W_s	Struct. Drift (mm)	Struct. Acc. (g)	Lead Core Temp. Increase (^{0}C)
NF17	Upper	466	0.21	0.26	16	0.27	NA
	Lower	553	0.18	0.20	12	0.20	NA
	Proposed	539	0.19	0.23	15	0.24	87
BOL090	Upper	115	0.14	0.18	11	0.18	NA
	Lower	126	0.10	0.11	7	0.11	NA
	Proposed	115	0.14	0.16	10	0.16	34
NF02	Upper	355	0.19	0.20	12	0.20	NA
	Lower	455	0.16	0.16	10	0.16	NA
	Proposed	399	0.17	0.17	11	0.17	66
NF13	Upper	376	0.20	0.20	13	0.20	NA
	Lower	484	0.17	0.17	11	0.17	NA
	Proposed	381	0.19	0.19	12	0.19	54
TCU065-N	Upper	379	0.20	0.21	13	0.21	NA
	Lower	474	0.16	0.17	11	0.17	NA
	Proposed	447	0.17	0.18	11	0.18	115
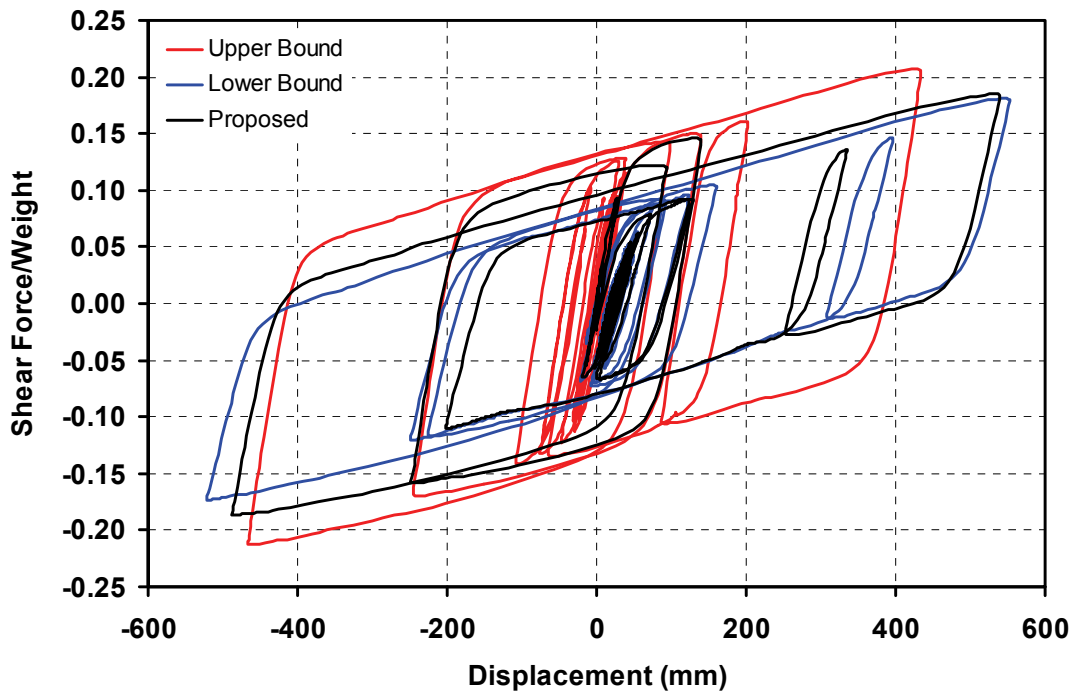
FIGURE 6-2 Isolation System Force-Displacement Loops for Motion NF17
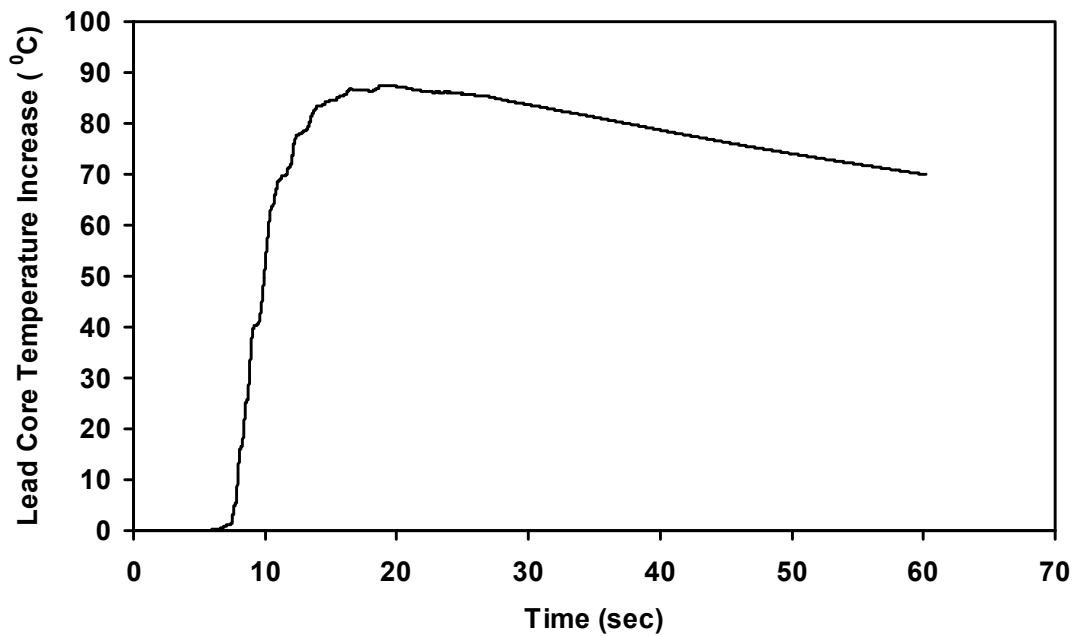
FIGURE 6-3 Lead Core Temperature Increase History for Motion NF17
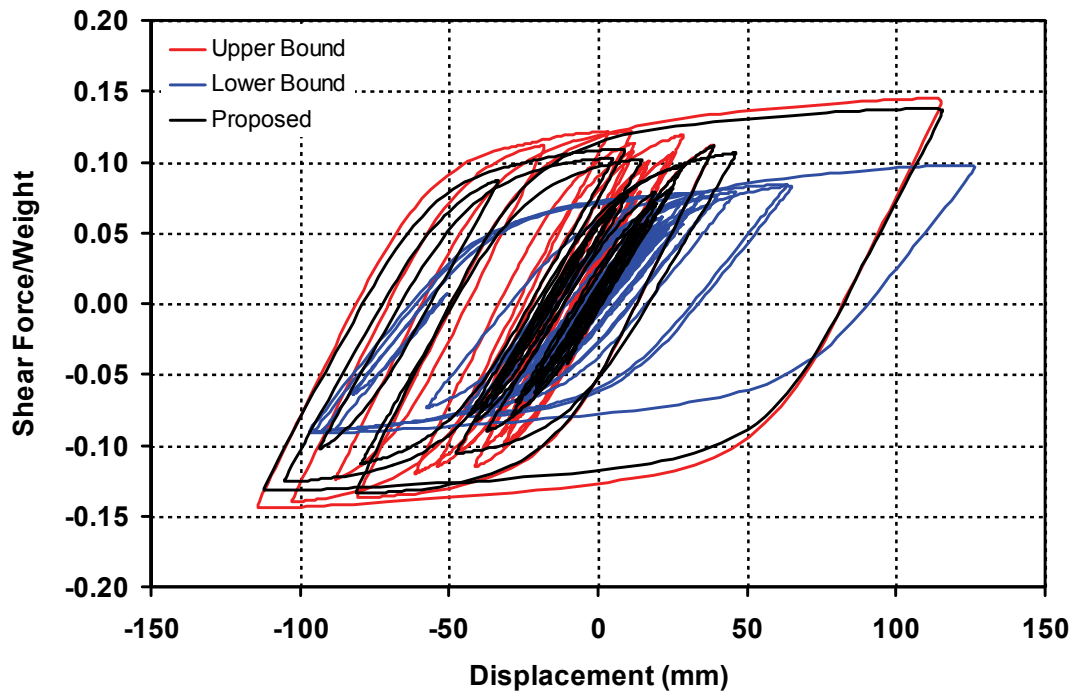
FIGURE 6-4 Isolation System Force-Displacement Loops for Motion BOL090
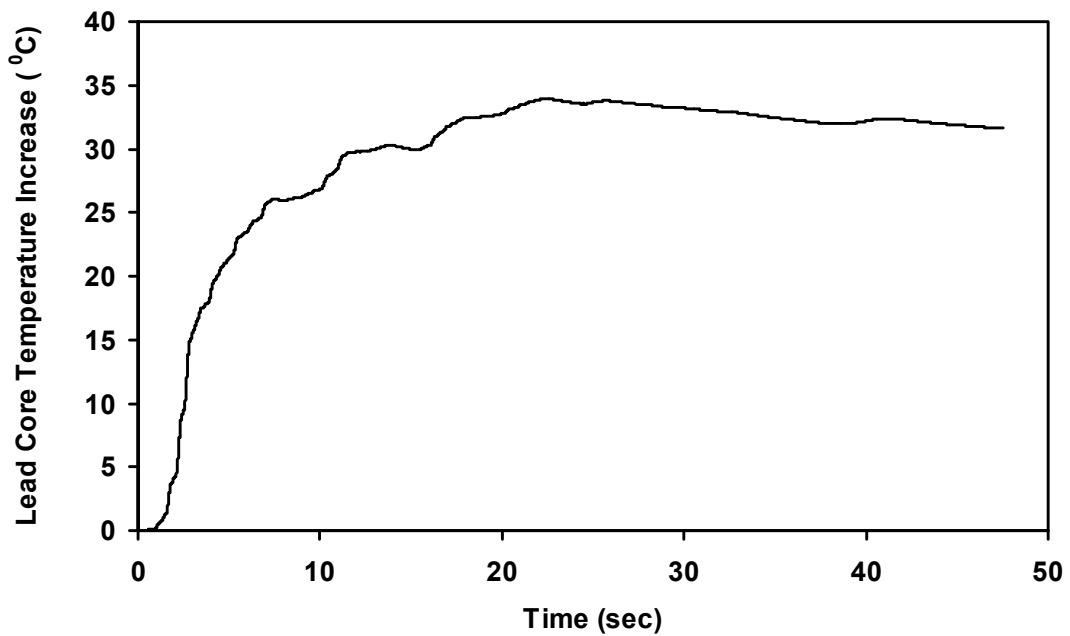
FIGURE 6-5 Lead Core Temperature Increase History for Motion BOL090
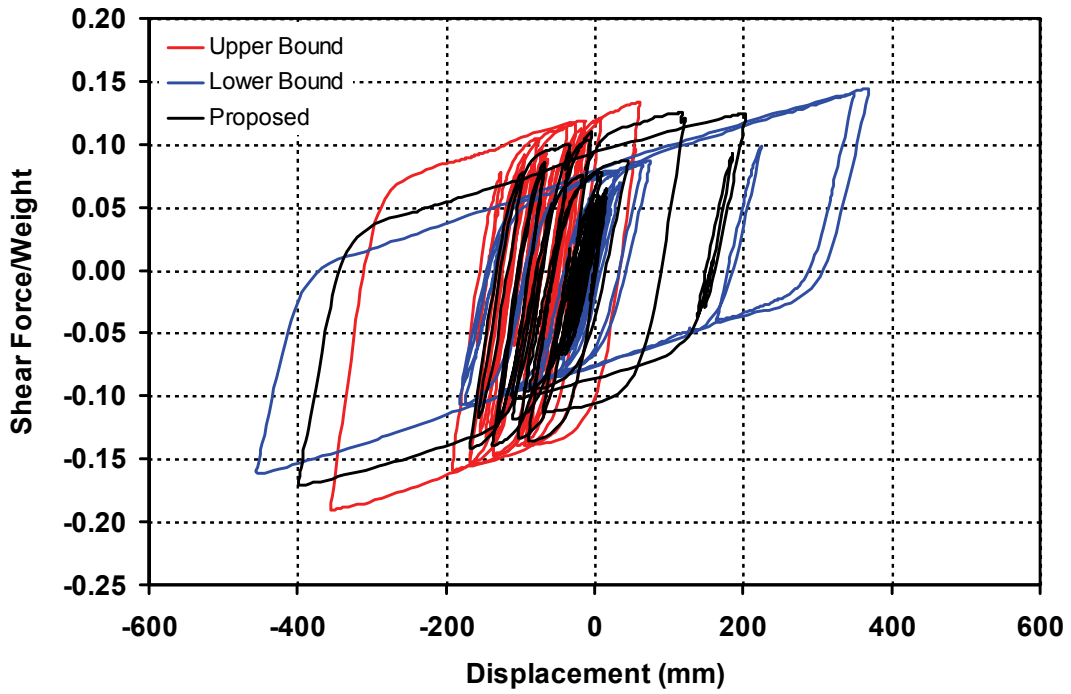
FIGURE 6-6 Isolation System Force-Displacement Loops for Motion NF02
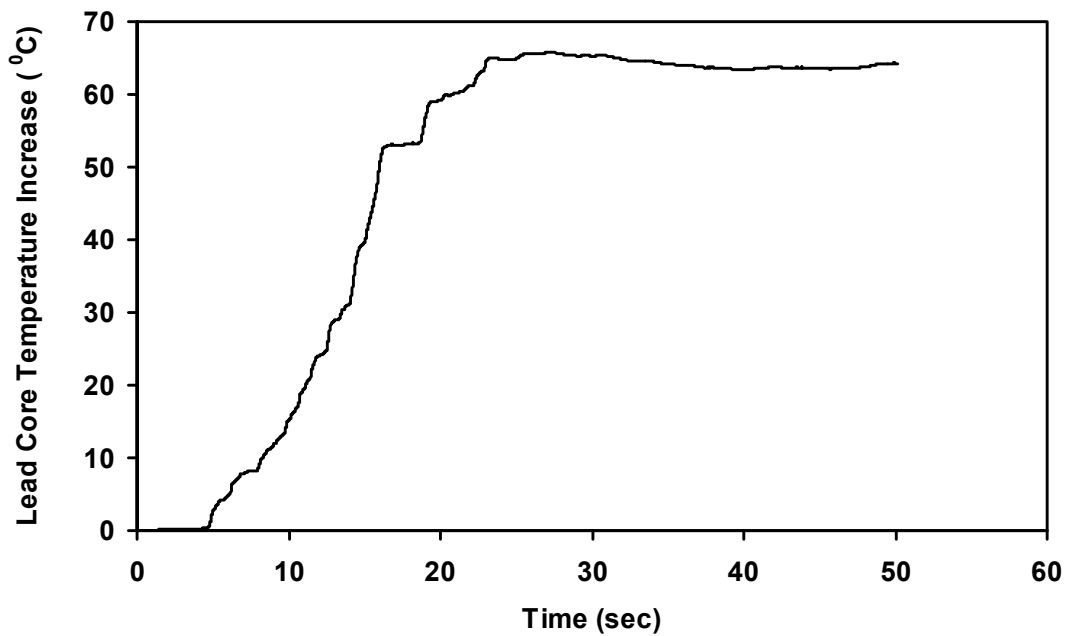
FIGURE 6-7 Lead Core Temperature Increase History for Motion NF02
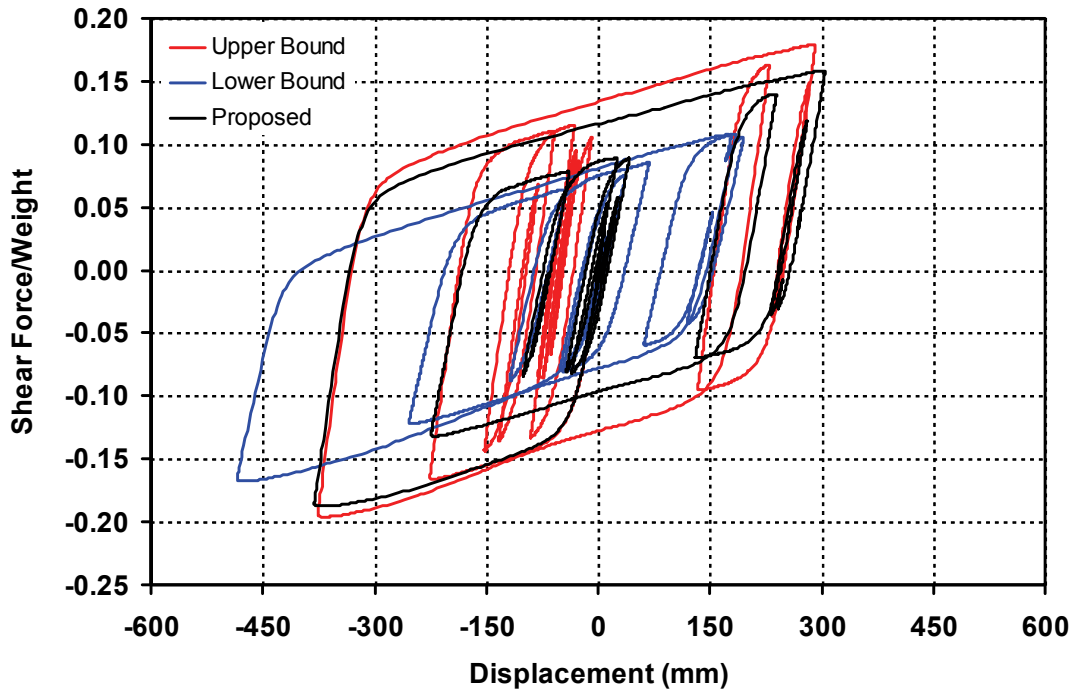
FIGURE 6-8 Isolation System Force-Displacement Loops for Motion NF13
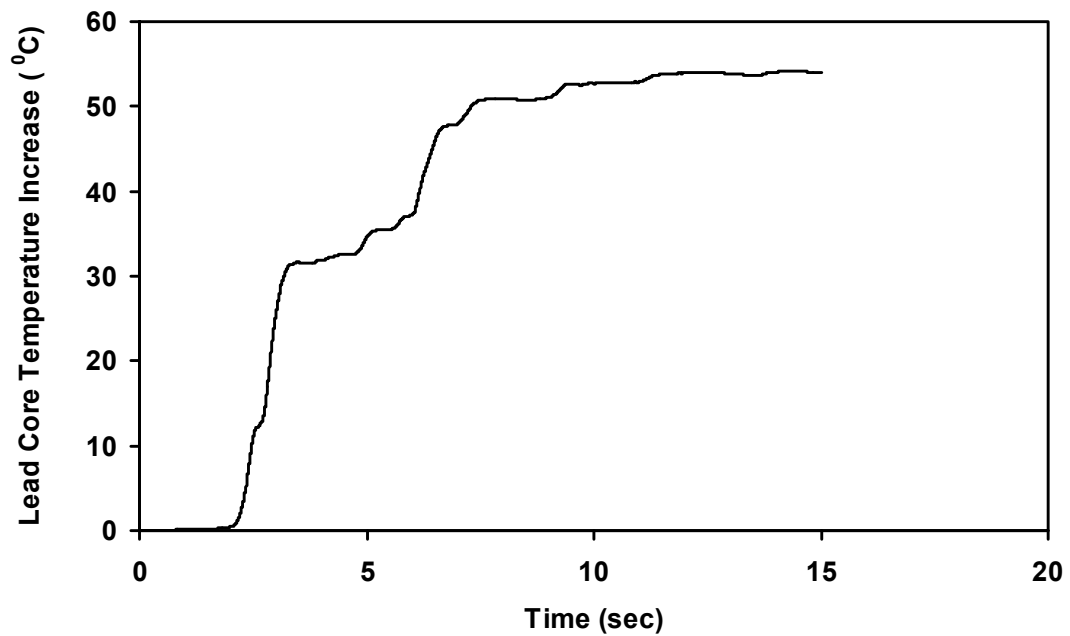
FIGURE 6-9 Lead Core Temperature Increase History for Motion NF13

191
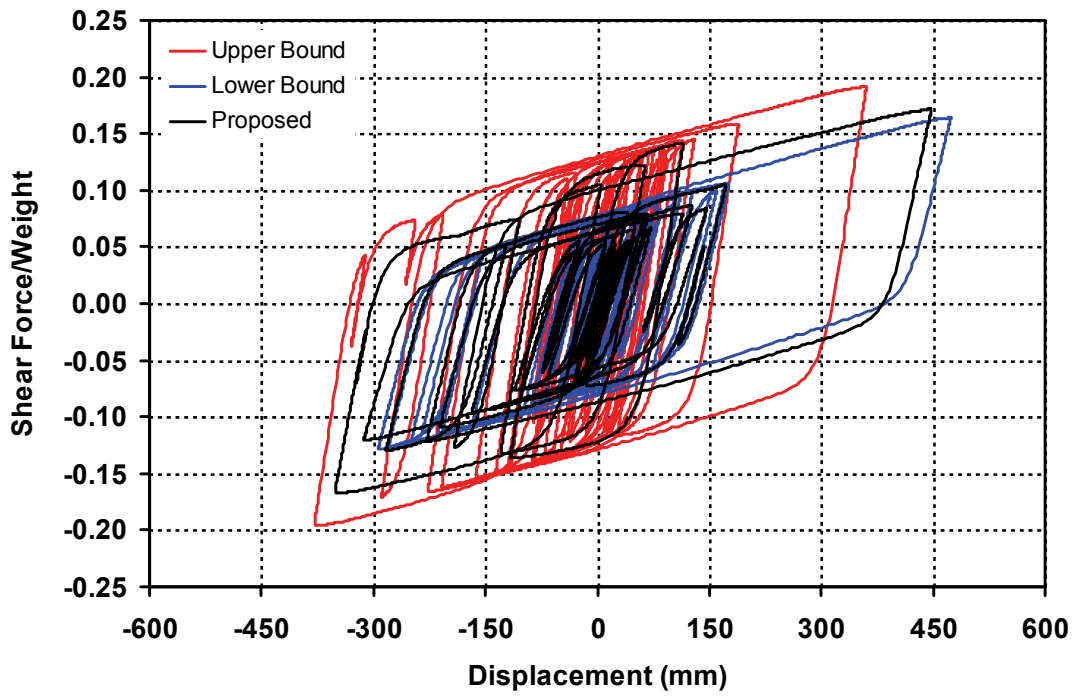
FIGURE 6-10 Isolation System Force-Displacement Loops for Motion TCU065-N
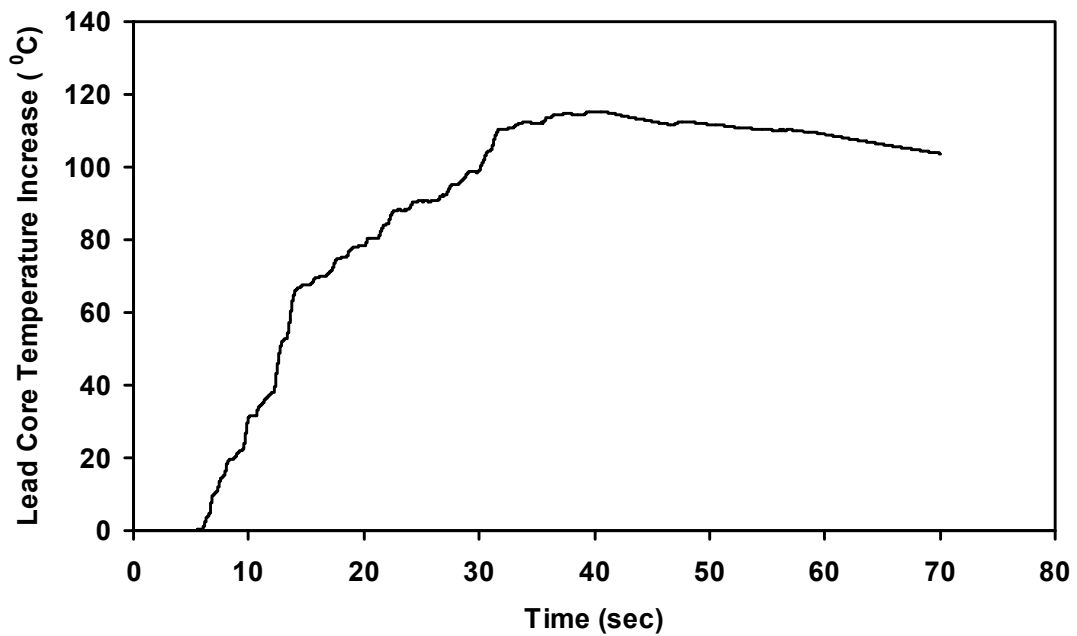
FIGURE 6-11 Lead Core Temperature Increase History for Motion TCU065-N

192

SECTION 7

EFFECT OF LOAD HISTORY ON THE MECHANICAL PROPERTIES OF

LEAD-RUBBER BEARINGS

7.1 Background

Bearings in bridges are subjected to continuous movement due to traffic and temperature effects. The result of this cumulative movement on sliding bearings is wear and some effect on the frictional properties, which have been described in Constantinou et al. (2007b). There is very little data on the effect of cumulative movement on the mechanical properties of elastomeric bearings.

Two lead-rubber bearings were tested at the University at Buffalo in 2003 at low speeds that are representative of service loading (thermal expansion and contraction) and high speeds representative of seismic loading prior to and following a cumulative low speed test of 1.6 km (1 mile) (Constantinou et al., 2007b).

Figure 7-1 presents drawings of the bearings; the ratio of the lead core diameter to the bonded diameter was 0.29. The bearings were tested individually as shown in Figure 7-2 to obtain their mechanical properties under thermal and dynamic loads and as a pair in the low speed, 1.6 km cumulative movement test – see Figure 7-3 (Constantinou et al., 2007b).

Figures 7-4 and 7-5 present the recorded lateral force-displacement loops for lead-rubber bearings No. 1 and No. 2, respectively, for a dynamic sinusoidal test (amplitude of 114 mm, peak velocity of 250 mm/sec) and a thermal loading test (amplitude of 75 mm,

constant velocity of 0.15 mm/sec) prior to the 1.6 km cumulative travel test. The average axial load on bearings No. 1 and No. 2 was 1425 kN and 1363 kN, respectively, in the dynamic test and was 1863 kN and 1800 kN, respectively, in the slow test. The significant increase (factor of 2.5) in the effective yield stress of lead due to dynamic loading is clearly seen in these figures.

After these tests the two bearings were subjected to an axial load of 1825 kN and 15,840 cycles of lateral movement with an amplitude of 25 mm at a constant velocity of 3.4 mm/sec. The total travel was 1584 m. The movement was intended to represent the effect of traffic loading – and the velocity of motion was higher than that expected under thermal loading. Ideally the velocity should have been about 1 mm/sec (see Constantinou et al., 2007b) but time constraints required the use of a higher speed. The testing was conducted over a period of 19 days with 8 to 10 hours of testing per day. The bearings were cooled during testing with large fans that maintained a temperature on the central moving steel plate of 29^0C after stabilization (at the start of test the temperature was 23^0C). The internal temperature in the lead core was not recorded. Figure 7-6 presents the recorded loops (the force is from two specimens tested as a pair) in the first 5 cycles (1 to 5) and cycles 15,823 to 15,828. There is little difference in the behavior of the bearings between the start and the end of testing. There is a small change in the hysteresis loop in the first five cycles due to an increase in the temperature of the lead core. Once the temperature of the lead core stabilized, the loop shape did not change (Constantinou et al., 2007b).
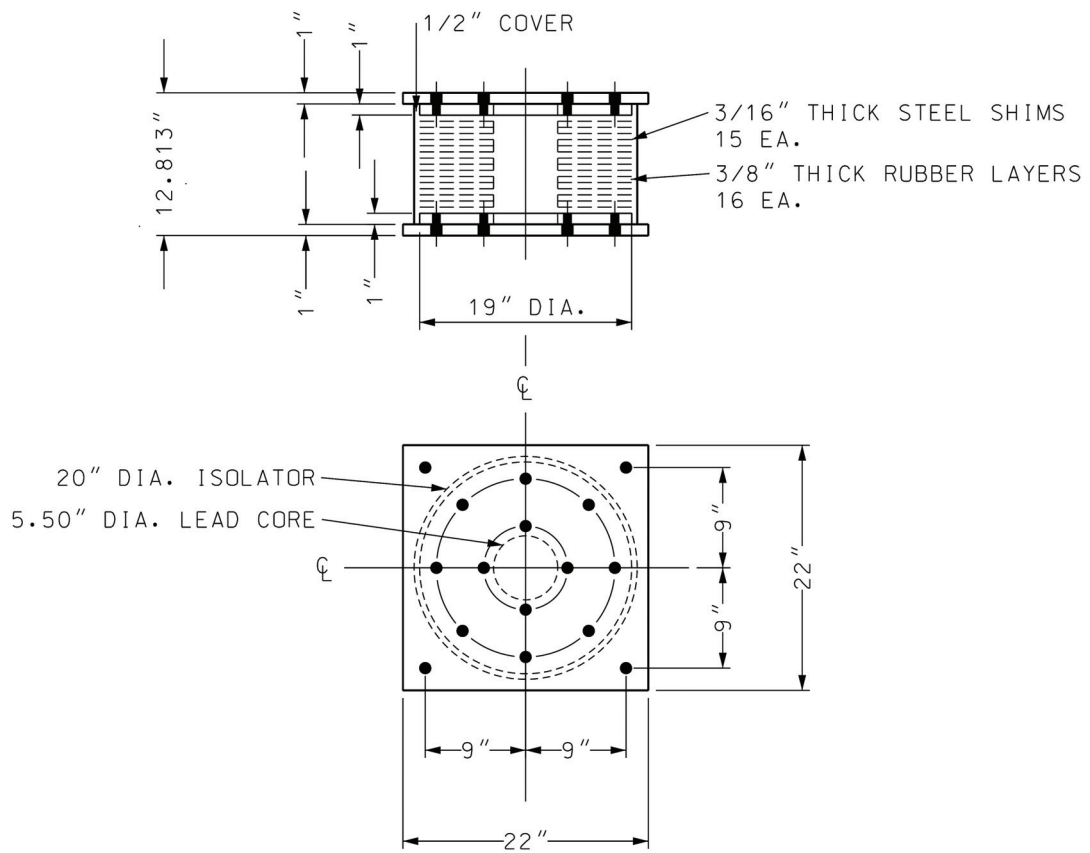
FIGURE 7-1 Large Scale Lead-Rubber Bearing Tested for 1.6 km of Cumulative Travel (1 inch=25.4 mm) (Constantinou et al., 2007b)

FIGURE 7-2 Lead-Rubber Bearing During High Speed Testing (Constantinou et al., 2007b)

FIGURE 7-3 Lead-Rubber Bearings Tested in Pair in the 1.6km Cumulative Travel Test (Constantinou et al., 2007b)

BEARING No. 1, BEFORE 1.6km CUMULATIVE TRAVEL TEST
(5 cycles, peak velocity 250mm/sec)
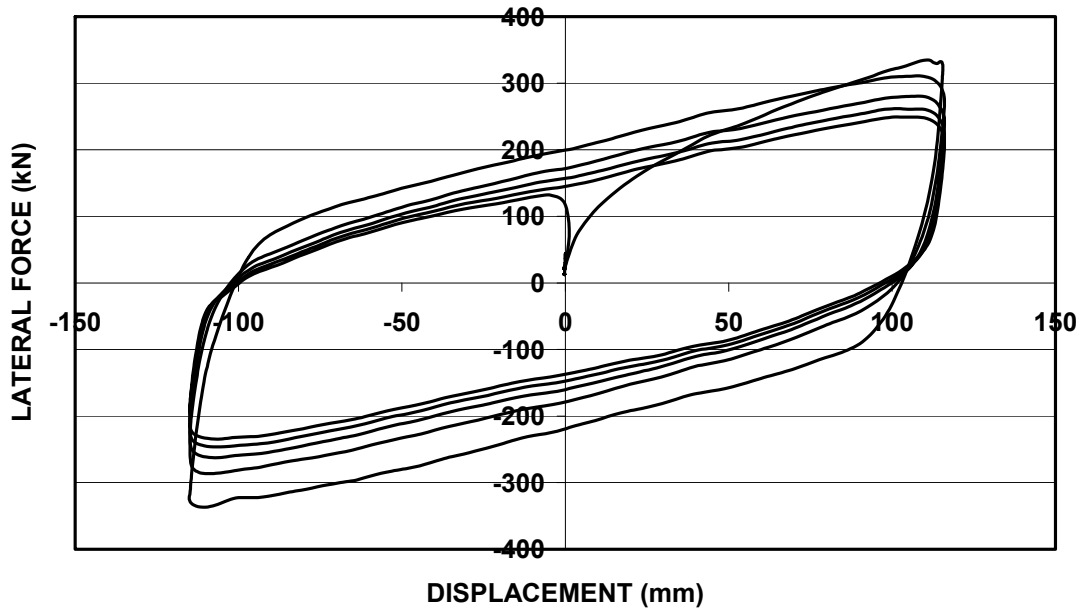
BEARING No. 1, BEFORE 1.6km CUMULATIVE TRAVEL TEST
(3 cycles, constant velocity 0.15mm/sec)
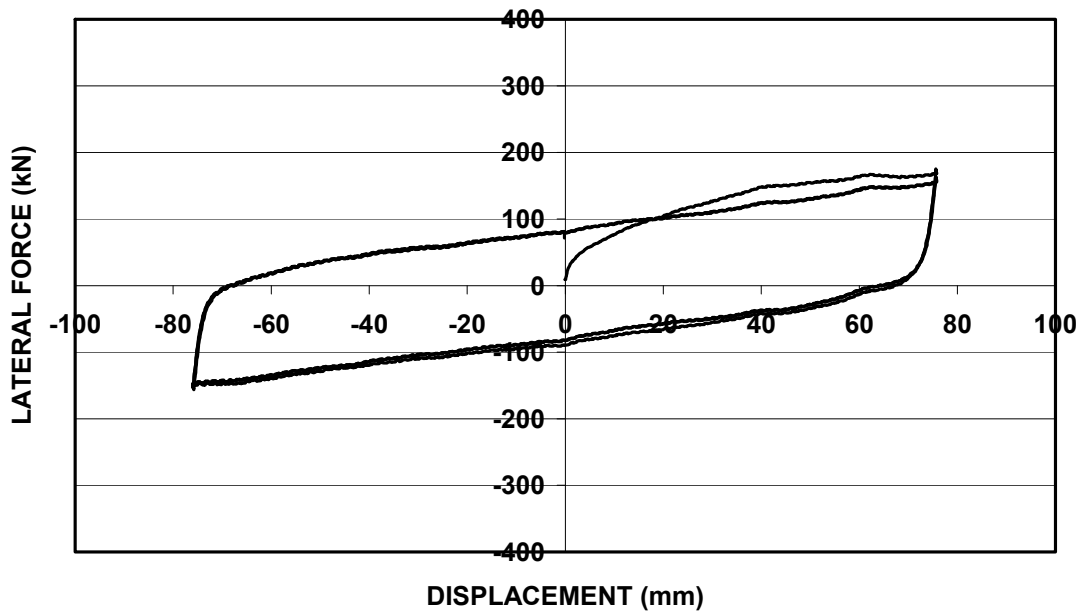
FIGURE 7-4 Force-Displacement Loops of Lead-Rubber Bearing No. 1 Under Seismic and Service Load Conditions Prior to the Cumulative Travel Test

BEARING No. 2, BEFORE 1.6km CUMULATIVE TRAVEL TEST
(5 cycles, peak velocity 250mm/sec)
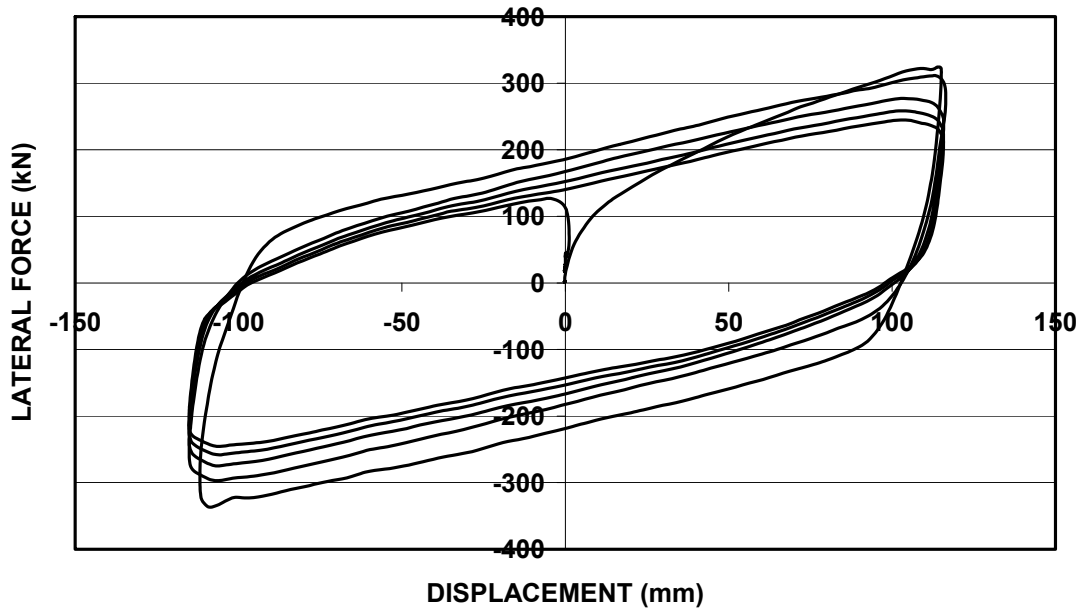
BEARING No. 2, BEFORE 1.6km CUMULATIVE TRAVEL TEST
(3 cycles, constant velocity 0.15mm/sec)
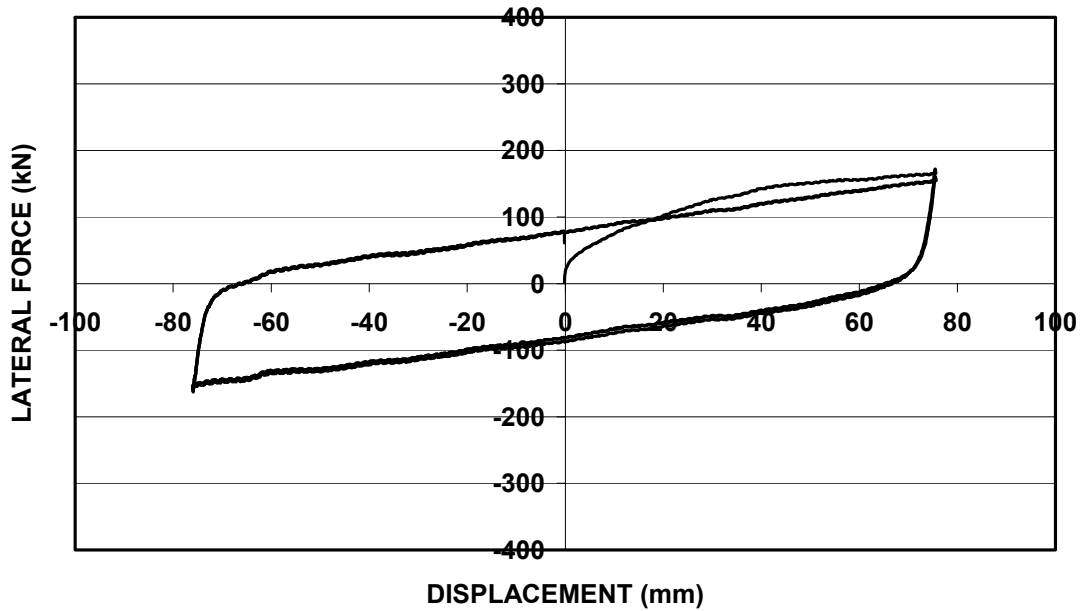
FIGURE 7-5 Force-Displacement Loops of Lead-Rubber Bearing No. 2 Under Seismic and Service Load Conditions Prior to the Cumulative Travel Test

198

CUMULATIVE TRAVEL TEST
CYCLES 1 to 5
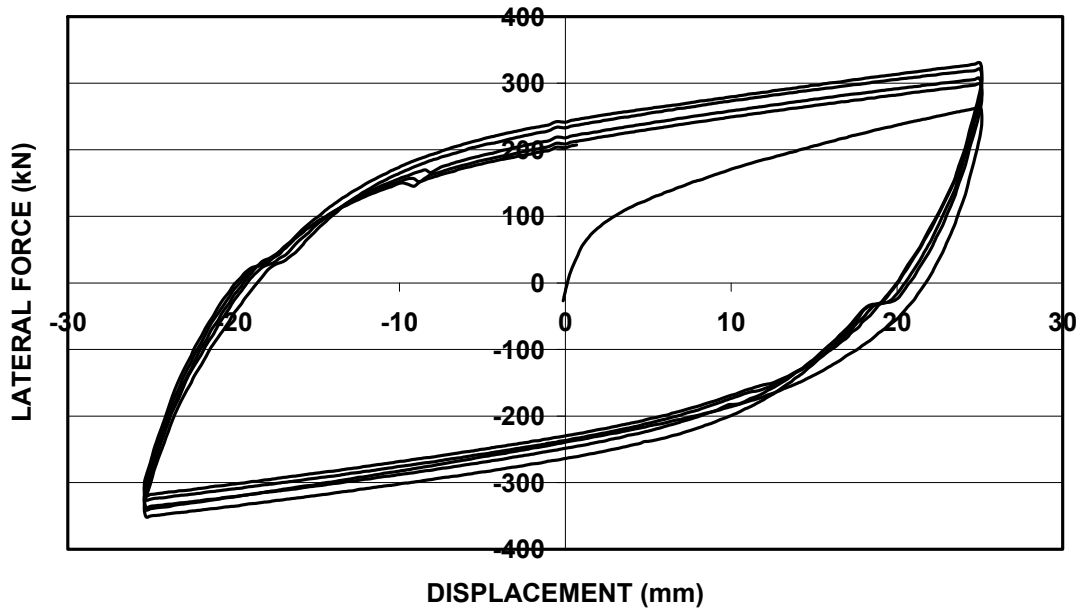
CUMULATIVE TRAVEL TEST
CYCLES 15823 to 15828
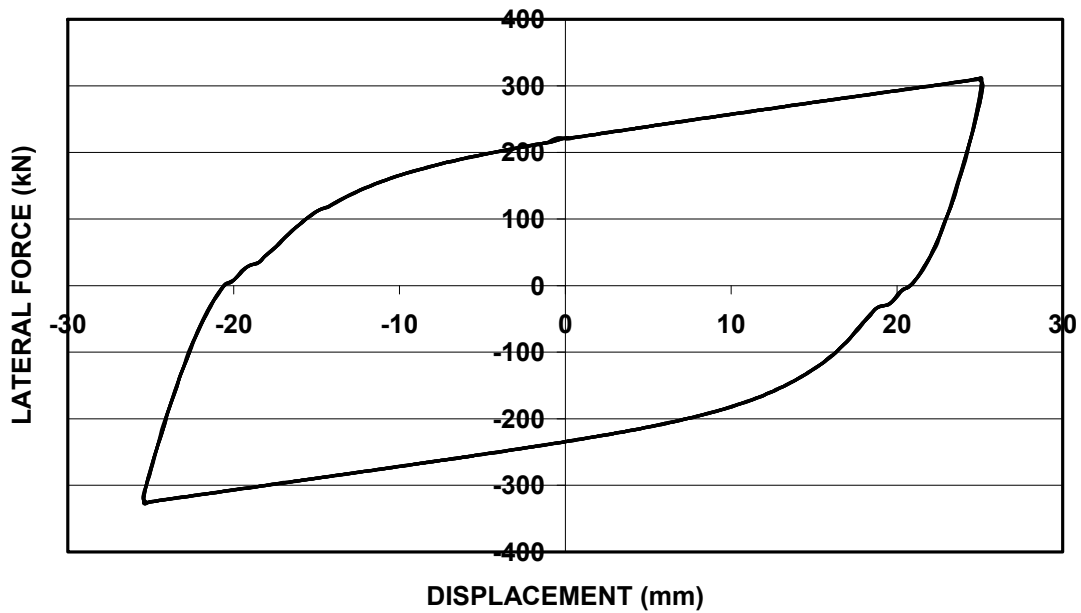
FIGURE 7-6 Force-Displacement Loops of the Pair of Lead-Rubber Bearings in the Cumulative Travel Test (Constantinou et al., 2007b)

199

Figures 7-7 and 7-8 present the recorded lateral force-displacement loops for lead-rubber bearings No. 1 and No. 2, respectively, for a dynamic sinusoidal test (amplitude of 114 mm, peak velocity of 250 mm/sec) and a thermal loading test (amplitude of 75 mm, constant velocity of 0.15 mm/sec), which were conducted after the 1.6 km cumulative travel test. The axial load on bearings No. 1 and No. 2 was 1848 kN and 1806 kN, respectively, for the dynamic test and 1980 kN and 1802 kN, respectively, for the thermal loading test (Constantinou et al., 2007b). The difference in axial load on the two bearings in the dynamic tests compared with the tests conducted prior to the cumulative travel test (1848 kN and 1806 kN versus 1425 kN and 1363 kN) was the result of error; they should have been the same.

BEARING No. 1, AFTER 1.6km CUMULATIVE TRAVEL TEST
(5 cycles, peak velocity 250mm/sec)
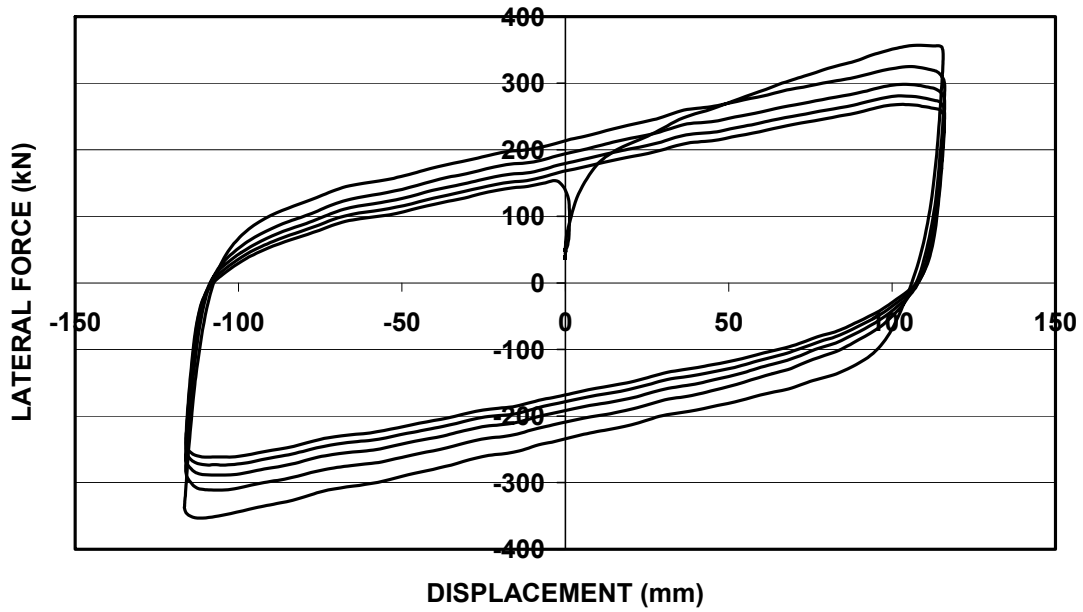
BEARING No. 1, AFTER 1.6km CUMULATIVE TRAVEL TEST
(3 cycles, constant velocity 0.15mm/sec)
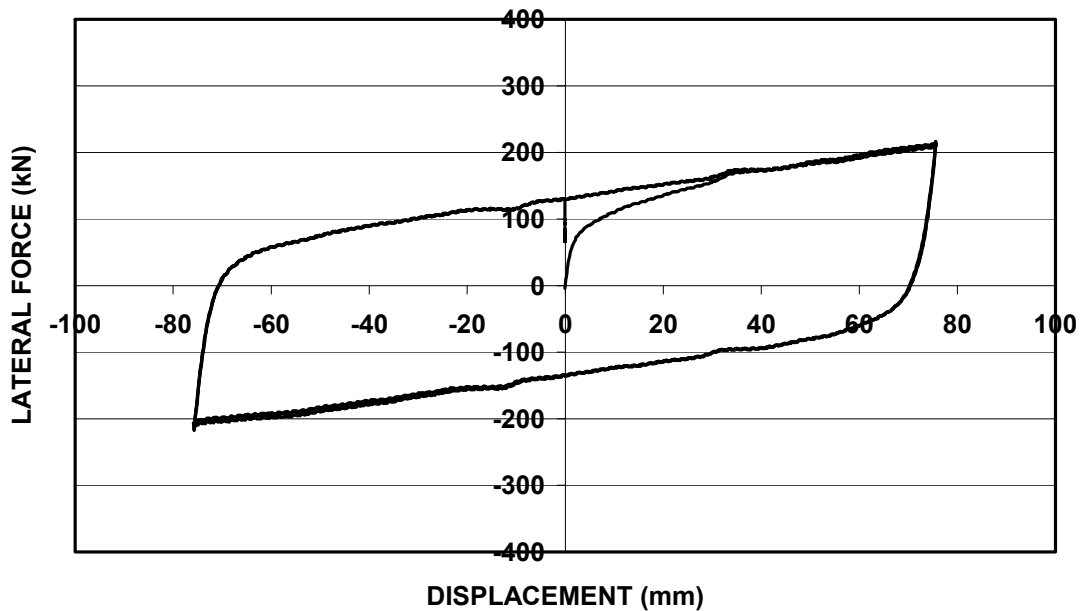
FIGURE 7-7 Force-Displacement Loops of Lead-Rubber Bearing No. 1 Under Seismic and Service Load Conditions After the Cumulative Travel Test

BEARING No. 2, AFTER 1.6km CUMULATIVE TRAVEL TEST
(5 cycles, peak velocity 250mm/sec)

BEARING No. 2, AFTER 1.6km CUMULATIVE TRAVEL TEST
(3 cycles, constant velocity 0.15mm/sec)
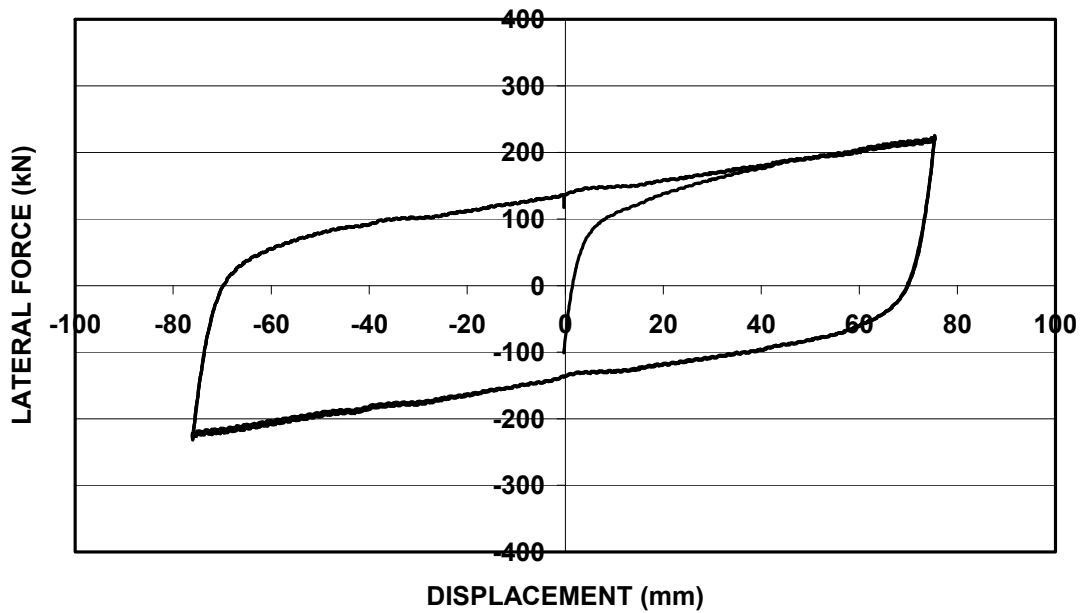
FIGURE 7-8 Force-Displacement Loops of Lead-Rubber Bearing No. 2 Under Seismic and Service Load Conditions After the Cumulative Travel Test

A comparison of the results in Figures 7-4 and 7-5 (prior to the cumulative travel test) with those in Figures 7-7 and 7-8 (after the cumulative travel test) reveals a minor increase in the characteristic strength in the dynamic test and a major increase in the characteristic strength in the service load test. The increase in the characteristic strength is by a factor of approximately 1.75. Such change is substantial and warrants consideration in analysis and design (Constantinou et al., 2007b).

Bearing No.2 was also subjected to two slower tests after the cumulative travel test. The bearing was subjected to axial loads of 1806 kN and 1930 kN, respectively, in the two tests, and one cycle of lateral movement at a constant velocity of 0.05 mm/sec and 0.00353 mm/sec, respectively. Figures 7-9 and 7-10 present the recorded force-displacement loops. There is an insignificant change in characteristic strength as the velocity reduces from 0.15 mm/sec (Figure 7-8) to 0.05 mm/sec and then to 0.00353 mm/sec. The duration of one-cycle motion was 0.6, 1.8 hours and 24 hours, respectively, in these tests – velocities representative of thermal loading.

BEARING No. 2, AFTER 1.6km CUMULATIVE TRAVEL TEST
(1 cycle, constant velocity 0.05mm/sec)
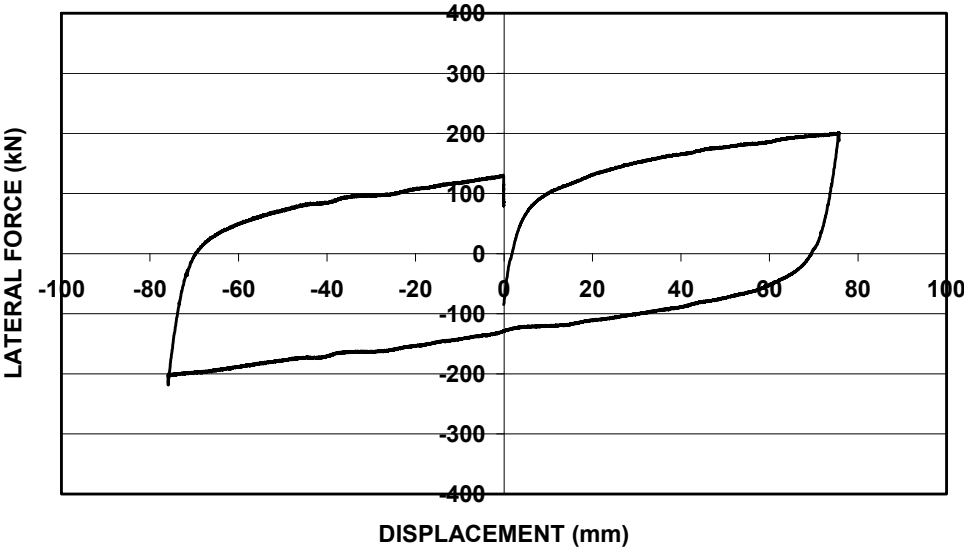
FIGURE 7-9 Force-Displacement Loops of Lead-Rubber Bearing No. 2 Under Thermal Load Conditions After the Cumulative Travel Test

BEARING No. 2, AFTER 1.6km CUMULATIVE TRAVEL TEST
(1 cycle, constant velocity 0.00353mm/sec)
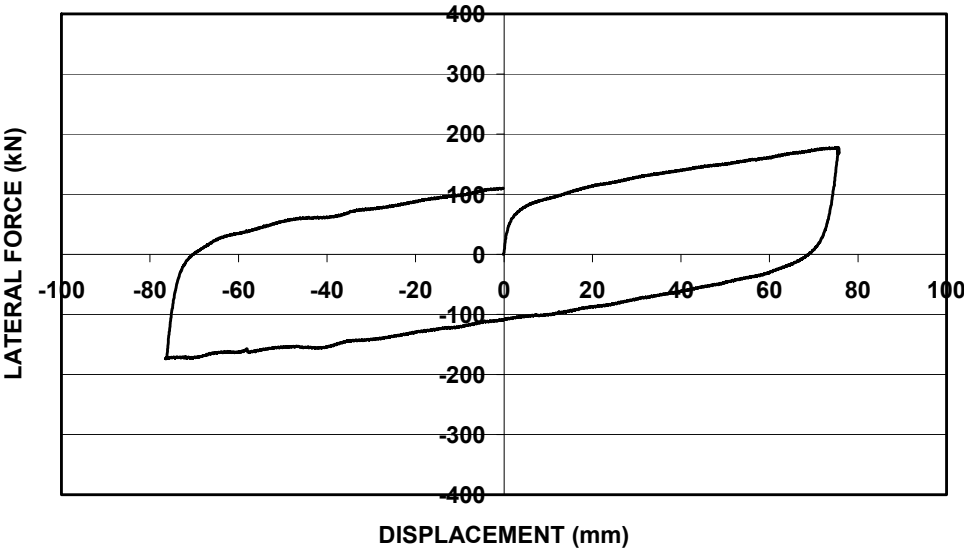
FIGURE 7-10 Force-Displacement Loops of Lead-Rubber Bearing No. 2 Under Extremely Slow Thermal Load Conditions After the Cumulative Travel Test

Two possible mechanisms that contributed to the observed increase in strength of the lead-rubber bearings were considered:

a) The origin is due to increased confinement of lead, possibly due to the elevated temperature in the cumulative travel testing. It should be noted that the testing was conducted accelerated both in the speed of motion and in the continuity of the motion. Actual conditions involve lower speeds and interrupted motion so that temperature in the lead core is unlikely to change.

b) The origin is due to strain hardening effects induced by repeated plastic deformation. In this case the elevated temperature of the test would have accelerated the process of recrystallization and subsequent grain growth which would have actually reduced the strain hardening effect. That is, had the cumulative travel test been conducted at speeds that do not cause heating of lead, the increase in strength would have been larger. Conversely, the imposed 25 mm amplitude of deformation (much larger than that expected in service – about 1 mm) could have magnified the strain hardening effect.

7.2 Investigation of Confinement Effects

To investigate the origin of the observed increase in strength, the two bearings were kept unloaded (so that any confinement effects relax) for a period of nearly 3.5 years and re-tested in April 2007 at high speed and low speed motions – conditions identical to those in the tests prior to the cumulative travel test. Results from these tests are shown in Figures 7-11 and 7-12. The average normal load on bearings No. 1 and No. 2 in the dynamic test was 1345 kN and 1441 kN, respectively, and in the low speed test it was 1902 kN and 1903 kN, respectively. A comparison of the results in Figures 7-7 and 7-8

with those in Figures 7-11 and 7-12 demonstrates no change in the strength of the bearings. Therefore, a mechanical origin for the effect (increased confinement) could not have occurred. Rather, most likely explanation for the observed increase in strength is strain hardening due to plastic deformation with a likely reduction of the effects due to accelerated recrystallization of lead resulting from the increased temperature.

BEARING No. 1, 3.5 YRS AFTER 1.6km CUMULATIVE TRAVEL TEST
(5 cycles, peak velocity 250mm/sec)
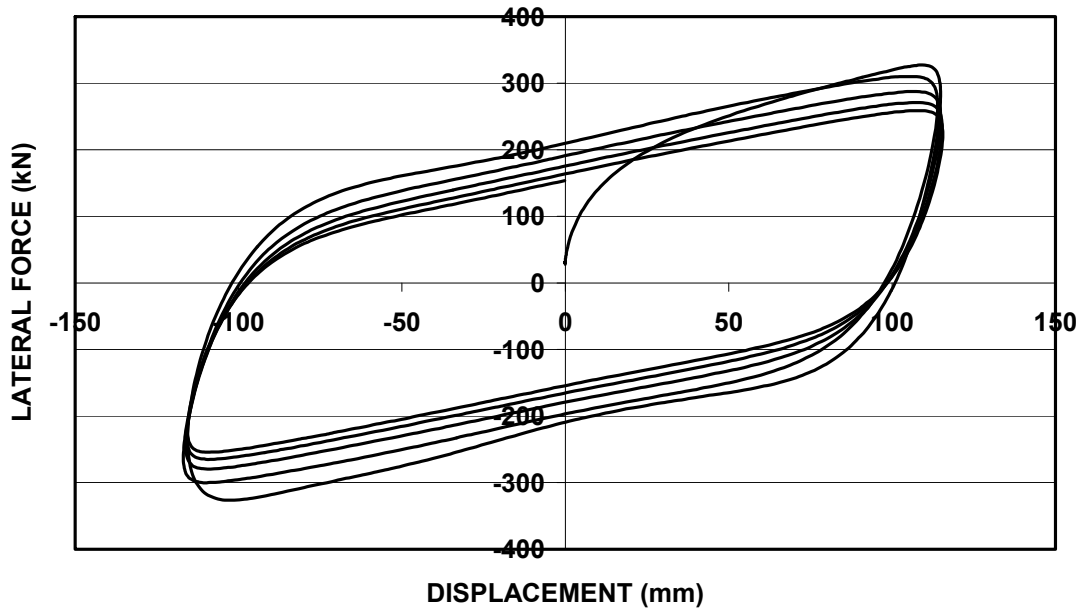
BEARING No. 1, 3.5 YRS AFTER 1.6km CUMULATIVE TRAVEL TEST
(3 cycles, constant velocity 0.15mm/sec)
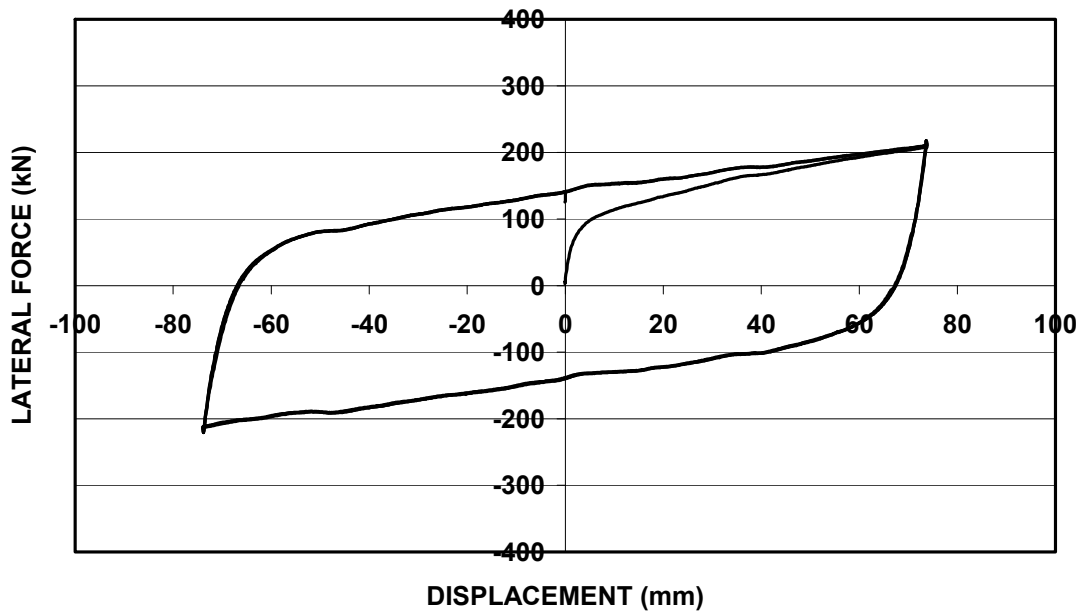
FIGURE 7-11 Force-Displacement Loops of Lead-Rubber Bearing No. 1 Under Seismic and Service Load Conditions 3.5 Years After the Cumulative Travel Test

BEARING No. 2, 3.5 YRS AFTER 1.6km CUMULATIVE TRAVEL TEST
(5 cycles, peak velocity 250mm/sec)

BEARING No. 2, 3.5 YRS AFTER 1.6km CUMULATIVE TRAVEL TEST
(3 cycles, constant velocity 0.15mm/sec)
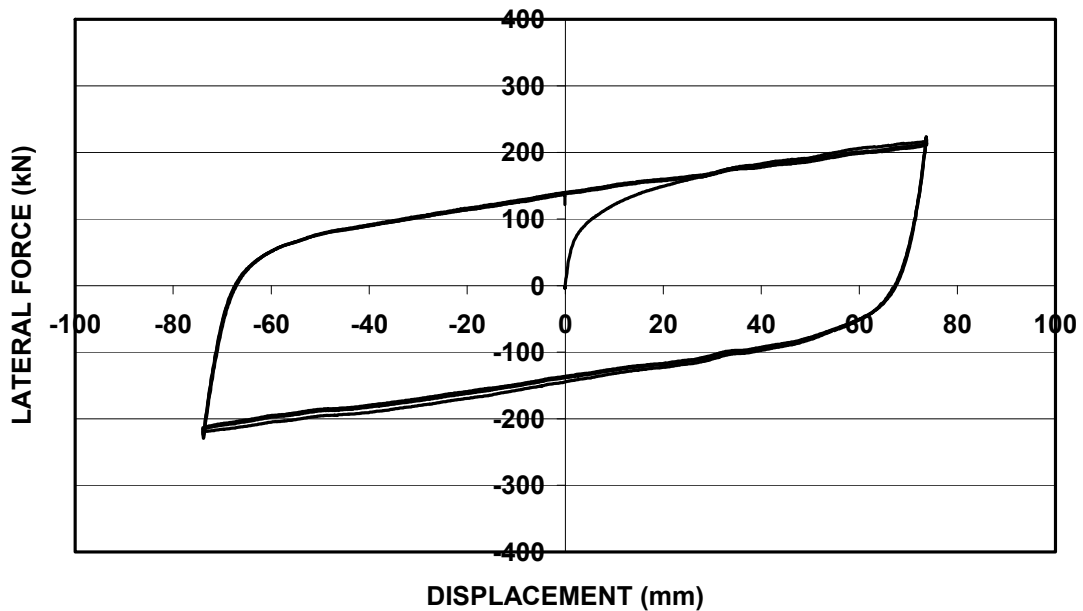
FIGURE 7-12 Force-Displacement Loops of Lead-Rubber Bearing No. 2 Under Seismic and Service Load Conditions 3.5 Years After the Cumulative Travel Test

7.3 Investigation of Effect of Plastic Deformation

In order to further investigate the effects of travel on the strength of lead-rubber bearings, testing was performed on two small-scale bearings of the geometry shown in Figure 4-52 using the machine shown in Figure 7-13. The two bearings were subjected to the same cumulative travel of 500 m but at different amplitudes of motion in order to investigate the effect of plastic deformation on the characteristic strength. In all tests presented in this section, the vertical load on the bearing was 89 kN.

The testing conditions for these bearings were selected by consideration of the similarity principles presented in Section 3 herein and consideration of the actual conditions of operation of the bearings. In general under service load conditions, bearings are subjected to motions of amplitude and speed of the order of 1 mm and 1 mm/sec, respectively. The motion may accumulate to a large travel but is intermittent so that heating effects in the lead core are insignificant.

The two small-scale bearings were designated to have a scale factor of 2.5 as the bearing dimensions, other than the lead core diameter, were approximately 2.5 times smaller than the full-size bearing of Figure 7-1. Bearing A was subjected to 125000 cycles of 1 mm amplitude and 2.5 mm/sec constant velocity motion for a total travel of 500 m. Based on the principles of similarity established in Section 3, this corresponds to prototype motion of 2.5 mm amplitude, 1 mm/s velocity and travel of 1250 m. These are representative conditions of motion under service conditions of full-size bearings. Bearing B was subjected to 12500 cycles of 10 mm amplitude and 2.5 mm/s constant velocity motion for

a total travel of 500 m. These conditions correspond to prototype motion of 25 mm amplitude, 1 mm/s velocity and travel of 1250 m.

The main difference in the testing of the two bearings is the amplitude of motion, which is expected to cause minimal inelastic action in the lead core of bearing A and substantial inelastic action in bearing B. Moreover, as a result of differences in inelastic action in the two bearings, the temperature of the lead core of bearing B is expected to further increase than that of bearing A. Actual conditions in the field would not result in any significant temperature increase as service load effects are intermittent. Such conditions cannot be generated in the laboratory because of the limited available time to conduct the testing. Specifically, the testing was conducted continuously over periods of about 7 hours each day, followed by a pause and re-start on the next day. Each test required 10 days of testing. During testing the temperature on the free boundary of the bearings was monitored and found to increase only on bearing B (subjected to the 10 mm amplitude) by about 5^0C at the conclusion of testing each day. The temperature of the lead core in the two bearings should have been different by at least 5^0C. Although this difference in temperature is small, it is sufficient to accelerate recrystallization in bearing B by comparison to bearing A. Therefore, any differences in the characteristic strength of the two bearings following the cumulative travel test would be due to strain hardening effects (because of the significant yielding in bearing B) but somehow mitigated by beneficial recrystallization in bearing B.
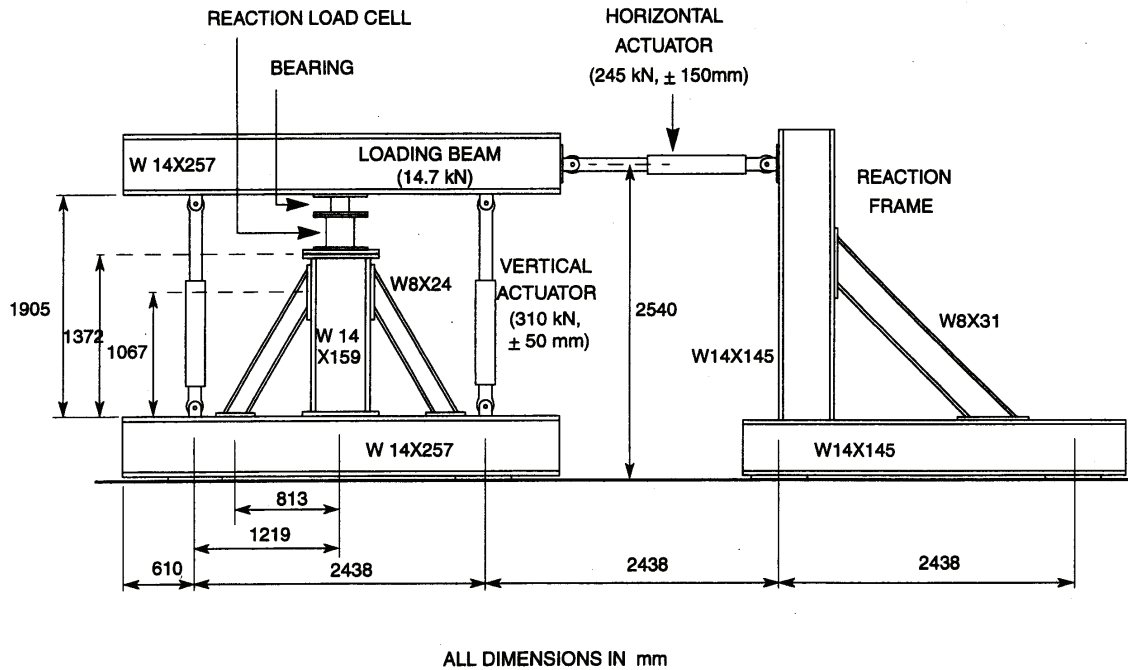
FIGURE 7-13 Small Bearing Testing Machine

The cumulative travel test of each bearing was preceded and followed by a fast and a slow large amplitude test in order to investigate the effect of travel on the characteristic strength for conditions of high and low strain rates. The high speed tests were conducted at an amplitude of 114 mm and at the highest speed the machine of Figure 7-13 could provide (358 mm/sec). The low speed tests were conducted at a constant speed of 0.05 mm/sec and an amplitude of 50 mm.

The testing of bearing A at an amplitude of 1 mm required that an instrument is used to specifically measure the deformation of the bearing as use of the displacement transducer of the horizontal actuator (see Figure 7-13) could not provide sufficient accuracy. An extensometer was mounted as shown in Figure 7-14 and used to measure the imposed deformation of the top of the bearing relative to its bottom for verifying the accuracy of the horizontal actuator displacement output.

211

Figures 7-15 to 7-17 present force-displacement loops for bearing A before the cumulative travel test, during the travel test and after the travel test, respectively. Figures 7-18 to 7-21 present force-displacement loops for bearing B before the travel test, during the travel test, after the travel test and after the travel test, respectively. The loops in Figure 7-16 of bearing A lack clear hysteretic characteristics that would indicate yielding of the lead core. However, measurement of the effective damping gave values of about 0.15 which are unlikely to be entirely due to energy dissipation in the rubber. We conclude that bearing A was actually subjected to some yielding of its lead core. By comparison, Figure 7-19 for bearing B shows clear hysteretic characteristics due to yielding of the lead core.

It may be noted in Figures 7-16 and 7-19 that the hysteresis loops at the start and at the end of the cumulative travel tests of both bearings are stable without any changes from cycle to cycle (note that the first few cycles of bearing A have amplitude of 0.8 mm instead of 1 mm – this was later corrected as control of the testing machine was established). The stability of the loops indicates stable temperature of the lead core. As noted earlier, the temperature on the free boundary of bearing A was equal to the ambient during the entire test, leading to the conclusion that the lead core temperature increase was very small. Bearing B had a measured temperature of about 5^0C above ambient on its free boundary during the duration of the test. In this test, the buildup of temperature in the lead core is expected to be slow due to the low rate of heat generation. The temperature is then expected to stabilize due to heat conduction effects. As seen in Figure 7-19, the strength of the bearing in the last few cycles is constant but slightly lower than the

strength in the first few cycles. This demonstrates that the temperature is slightly higher but stable in the last few cycles.

Comparing the results in Figures 7-15 and 7-17 of the tests conducted prior to and following the cumulative travel test on bearing A, we observe insignificant differences. It may be concluded that cumulative travel does not have any important effect on the characteristic strength of lead-rubber bearings when the amplitude of deformation is small and consistent with the typical effects of traffic load (amplitude of the order of 1 mm).

However, comparing the results in Figures 7-18 and 7-20 of the tests conducted prior to and following the cumulative travel test on bearing B (subjected to large amplitude motion), we observe a large – as much as 45% – increase in the characteristic strength following the cumulative travel test at conditions of very low speed of motion.

It should be noted that the low speed test was conducted twice: (a) 24 hours following the conclusion of the cumulative travel test, and (b) four days following the conclusion of the cumulative travel test. As seen in the results in Figure 7-20, there is a distinct difference in the characteristic strength measured in the two tests, with the strength decreasing as the bearing is allowed to relax for longer time.

To further investigate the observation of reduced strength with increasing relaxation time, the bearing was tested again 43 days following the conclusion of the cumulative travel test. A high speed test and a low speed test were conducted. Results are presented in Figure 7-21. Evidently, there is no further relaxation effect on the characteristic strength

at low speeds. Furthermore, comparing the results of the high speed test prior to (Figure 7-18) and following (Figure 7-21) the cumulative travel test we observe very small and practically negligible differences.

We conclude that for all practical purposes the characteristic strength of lead-rubber bearings at high speed motion is unaffected by the prior cumulative travel. The conclusion is valid for (a) travel of small amplitude of cyclic motion (order of 1 mm and barely causing yielding to the lead core) or (b) travel of large amplitude of cyclic motion (order of 10 mm and clearly causing yielding to the lead core).

Also, we conclude that the characteristic strength of lead-rubber bearings at low speed of motion (as that experienced under thermal loading conditions) is unaffected by the prior cumulative travel provided that the amplitude of cyclic motion during prior travel is small (order of 1 mm and barely causing yielding to the lead core). However, the characteristic strength is markedly affected by the prior cumulative travel provided that the amplitude of cyclic motion during prior travel is large (order of 10 mm and clearly causing yielding to the lead core). It is believed that this effect is the result of strain hardening of lead and that relaxation has some beneficial effect in limiting the extent of the strength increase.

It is recommended that cumulative travel test specifications for lead-rubber bearings include only components of large amplitude deformation, which are typically caused by temperature changes and not traffic loading effects. Cumulative travel caused by thermal loading is typically smaller than that caused by traffic loading. Alternatively, test specifications could specify a test regime with small amplitude and large amplitude components that are respectively caused by the expected traffic and thermal load effects.
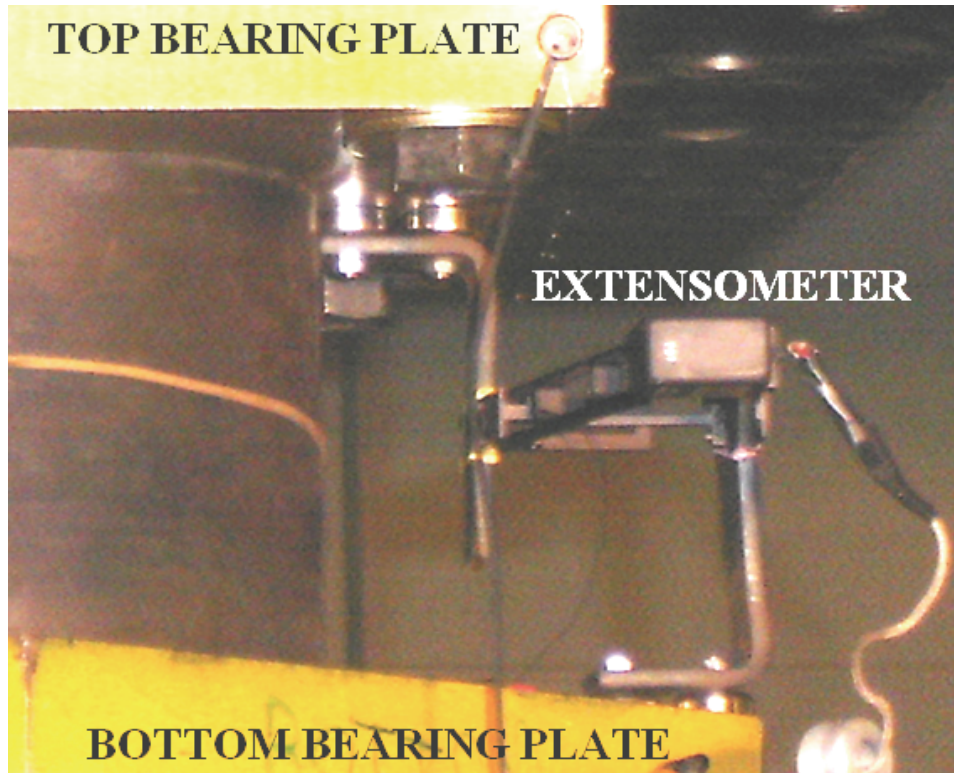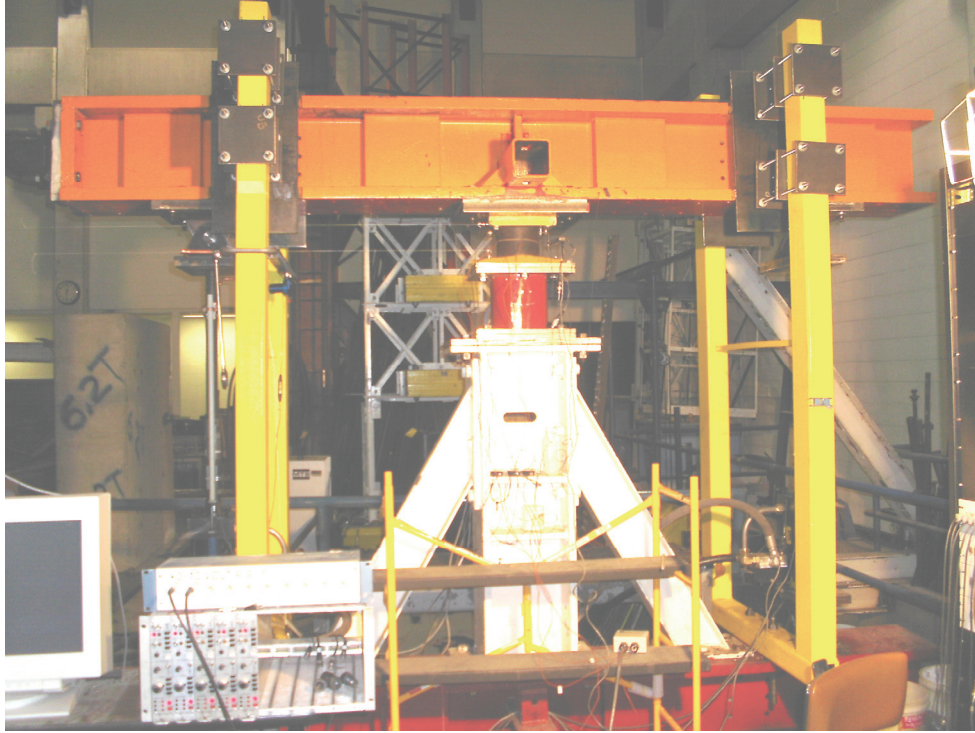
FIGURE 7-14 Bearing A on Testing Machine and Detail of Extensometer Used in Testing

BEARING A, BEFORE 500m CUMULATIVE TRAVEL TEST
(10 cycles, peak velocity 358mm/sec)
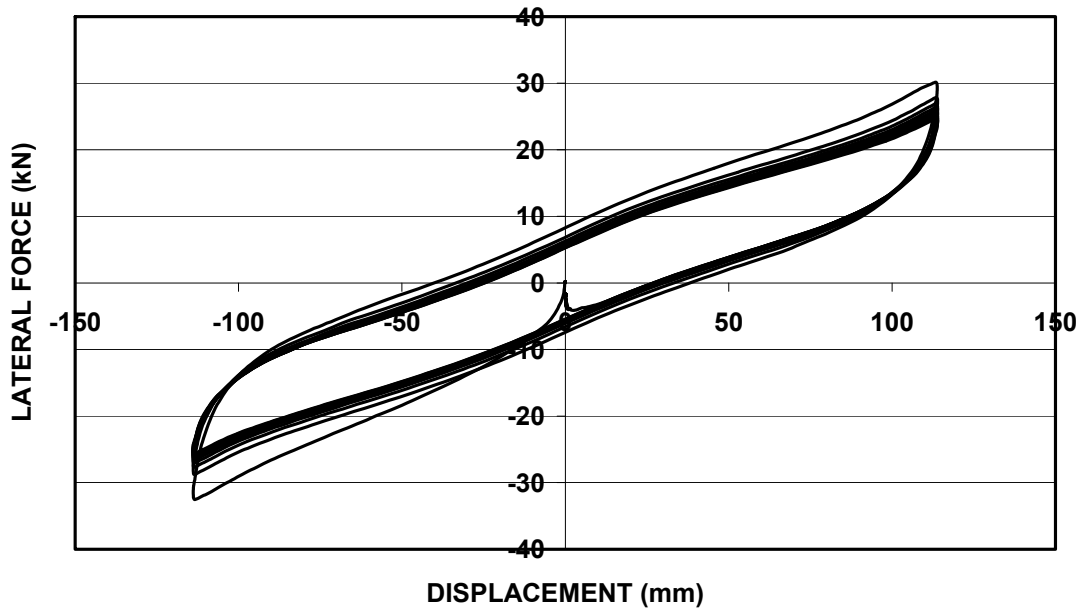
BEARING A, BEFORE 500m CUMULATIVE TRAVEL TEST
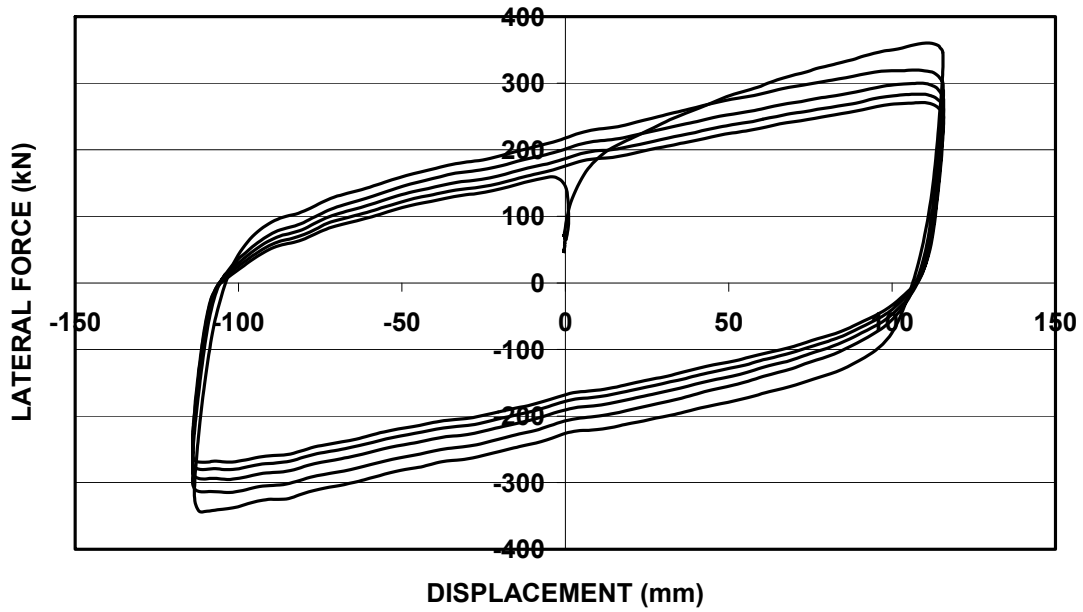**(1 cycle, constant velocity 0.05mm/sec)**
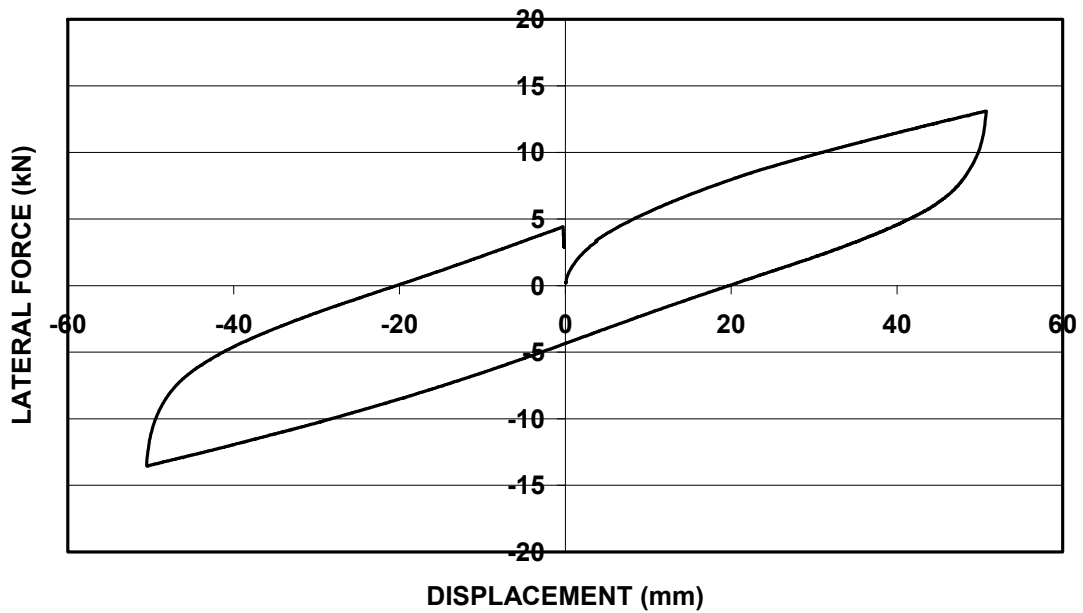
FIGURE 7-15 Force-Displacement Loops of Bearing A Before Cumulative Travel Test Recorded at High and Low Speed

**BEARING A, LOOPS 1-50 OF 500m CUMULATIVE TRAVEL TEST
(constant velocity 2.5mm/sec)**
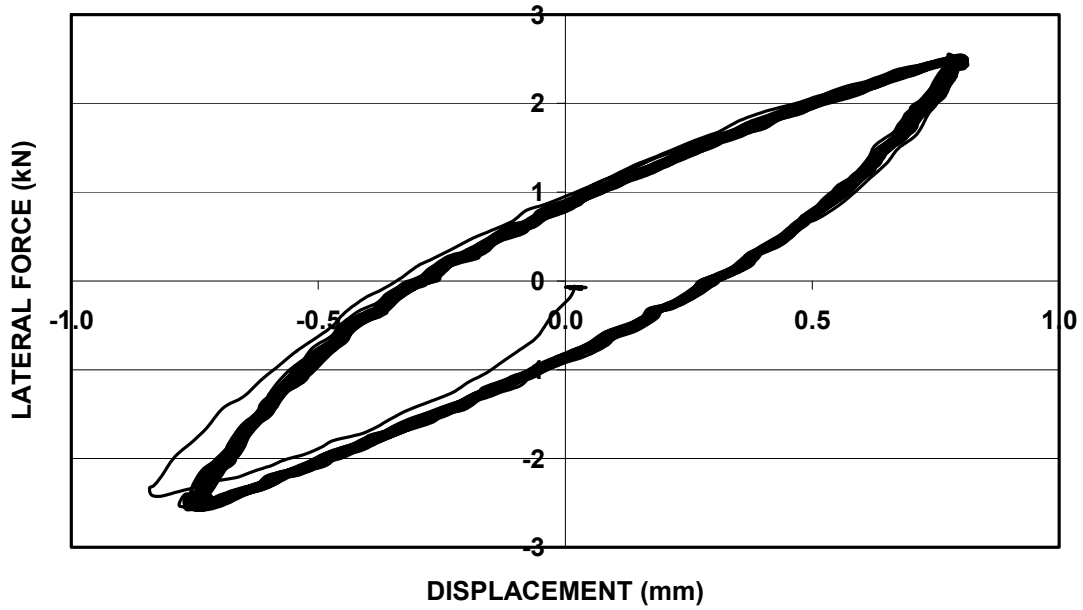
DISPLACEMENT (mm)

**BEARING A, LOOPS 125301-125376 OF 500m CUMULATIVE TRAVEL
TEST (constant velocity 2.5mm/sec)**
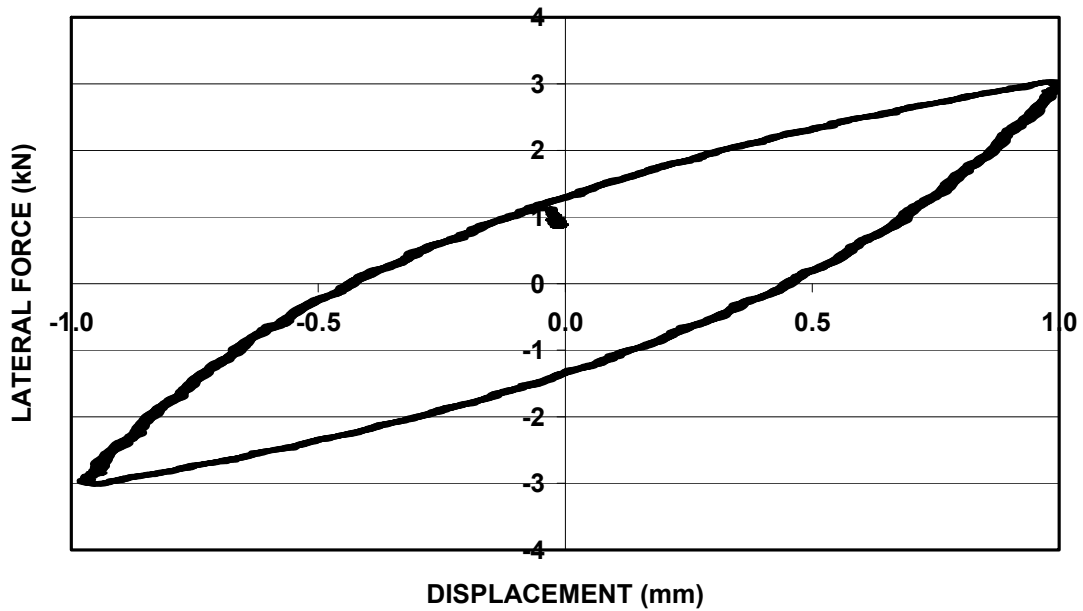
DISPLACEMENT (mm)

FIGURE 7-16 Force-Displacement Loops of Bearing A Recorded During Cumulative Travel Test

BEARING A, AFTER 500m CUMULATIVE TRAVEL TEST
(10 cycles, peak velocity 358mm/sec)
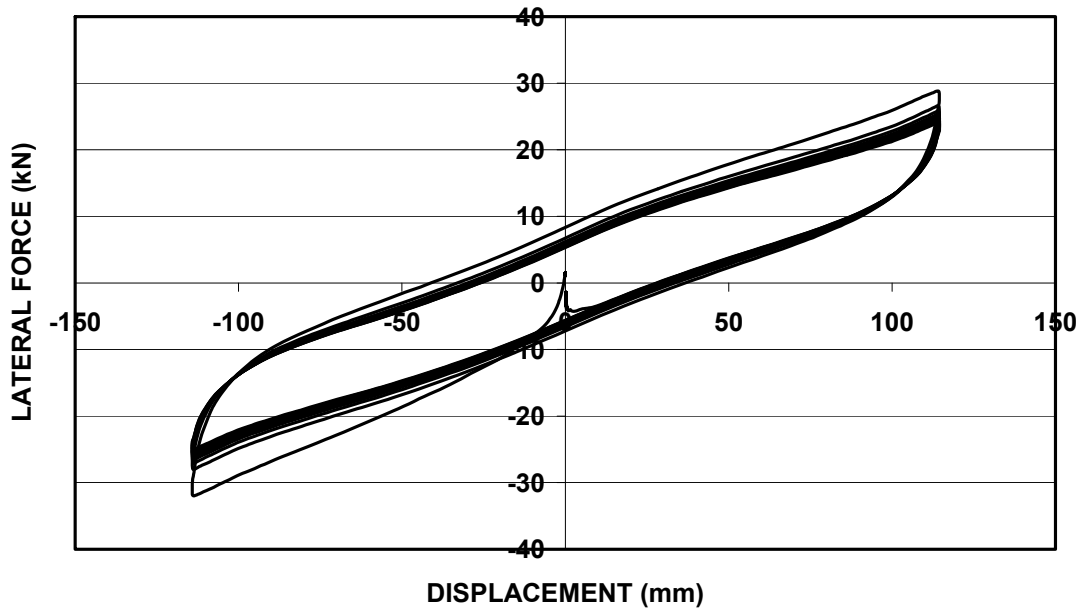
BEARING A, AFTER 500m CUMULATIVE TRAVEL TEST
(1 cycle, constant velocity 0.05mm/sec)
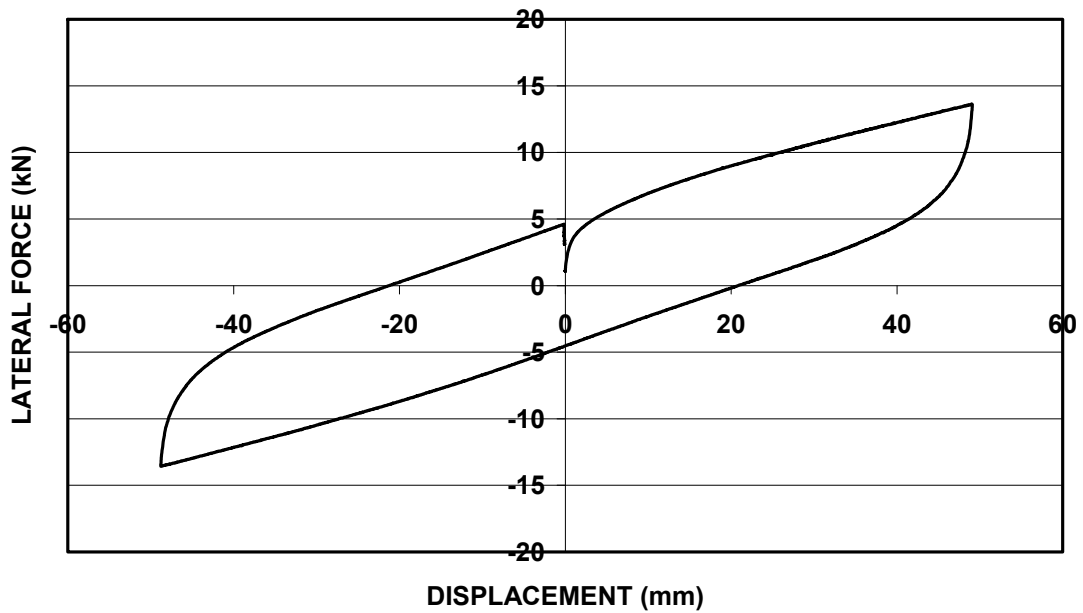
FIGURE 7-17 Force-Displacement Loops of Bearing A After Cumulative Travel Test Recorded at High and Low Speed

218

BEARING B, BEFORE 500m CUMULATIVE TRAVEL TEST
(10 cycles, peak velocity 358mm/sec)

DISPLACEMENT (mm)
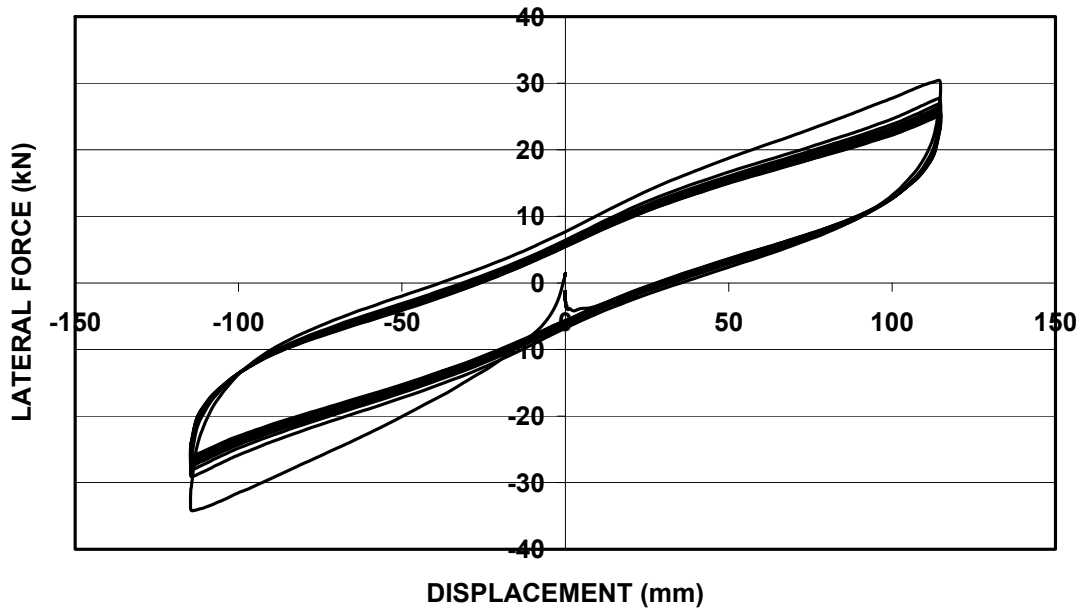
BEARING B, BEFORE 500m CUMULATIVE TRAVEL TEST
(1 cycle, constant velocity 0.05mm/sec)
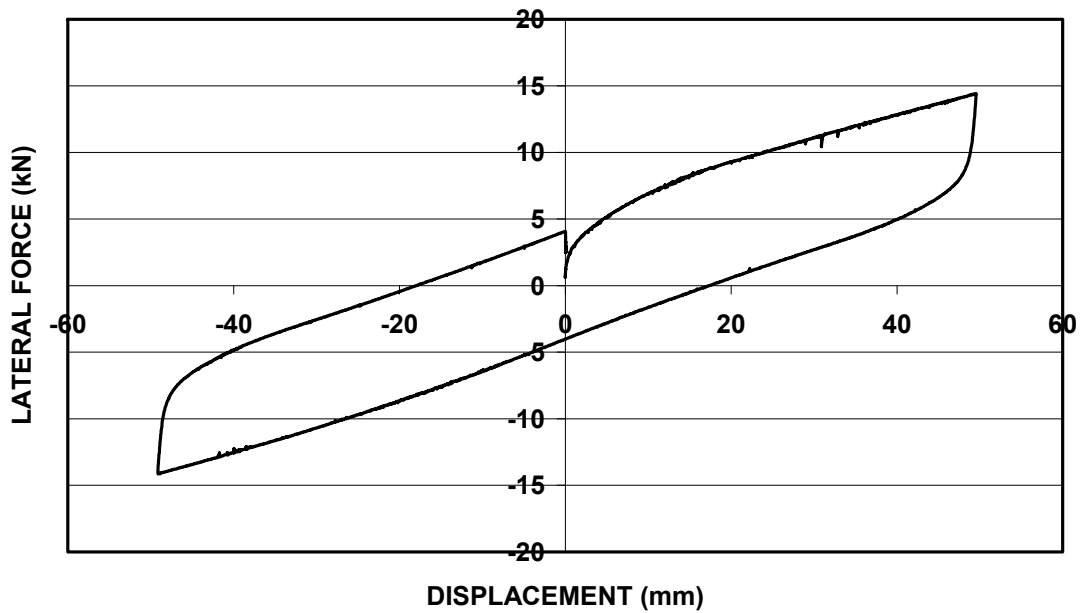
DISPLACEMENT (mm)

FIGURE 7-18 Force-Displacement Loops of Bearing B Before Cumulative Travel Test Recorded at High and Low Speed

BEARING B, LOOPS 1-7 OF 500m CUMULATIVE TRAVEL TEST
(constant velocity 2.5mm/sec)
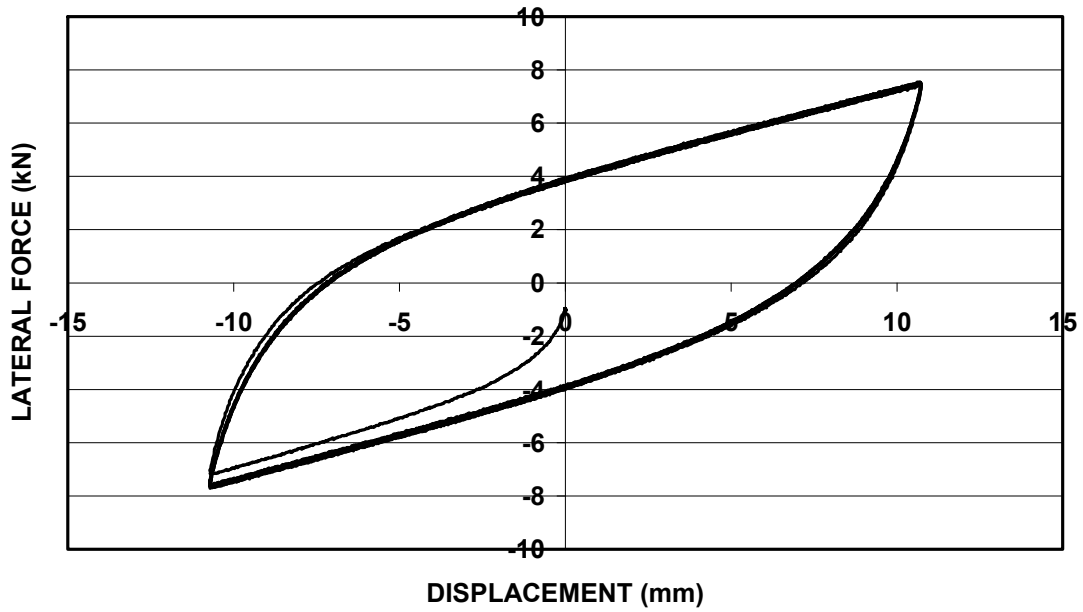
BEARING B, LOOPS 12491-12498 OF 500m CUMULATIVE TRAVEL
TEST (constant velocity 2.5mm/sec)
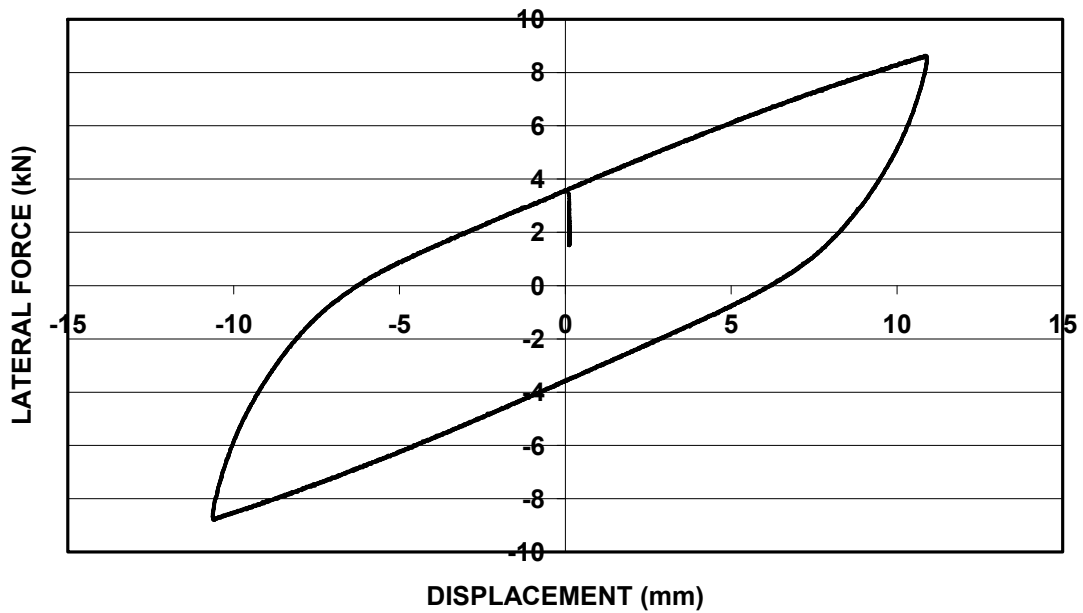
FIGURE 7-19 Force-Displacement Loops of Bearing B Recorded During Cumulative Travel Test

220

BEARING B, 1 DAY AFTER 500m CUMULATIVE TRAVEL TEST
(1 cycle, constant velocity 0.05mm/sec)
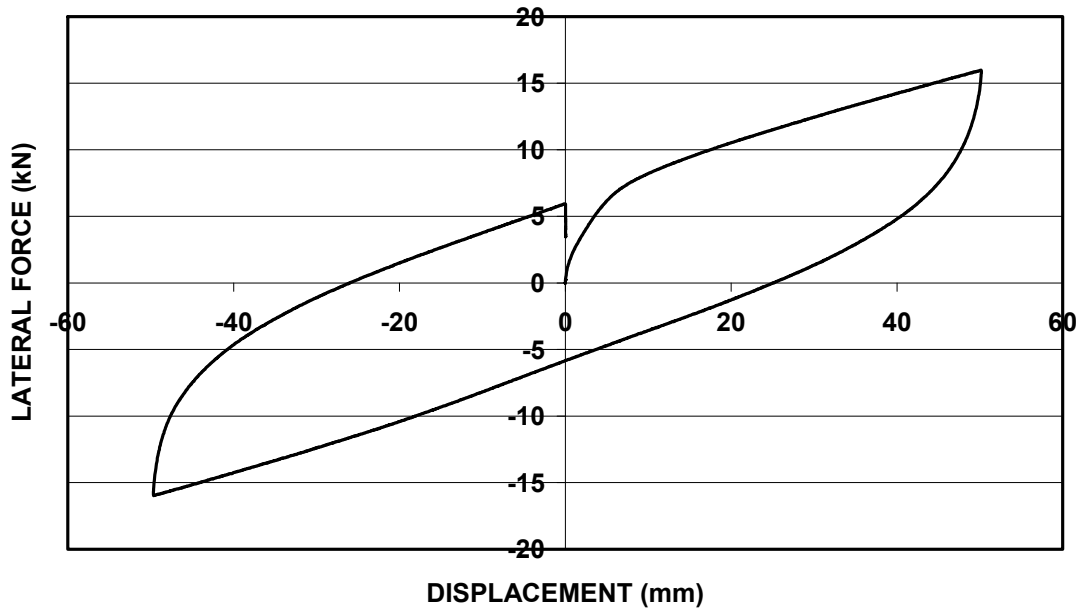
DISPLACEMENT (mm)

BEARING B, 4 DAYS AFTER 500m CUMULATIVE TRAVEL TEST
(1 cycle, constant velocity 0.05mm/sec)
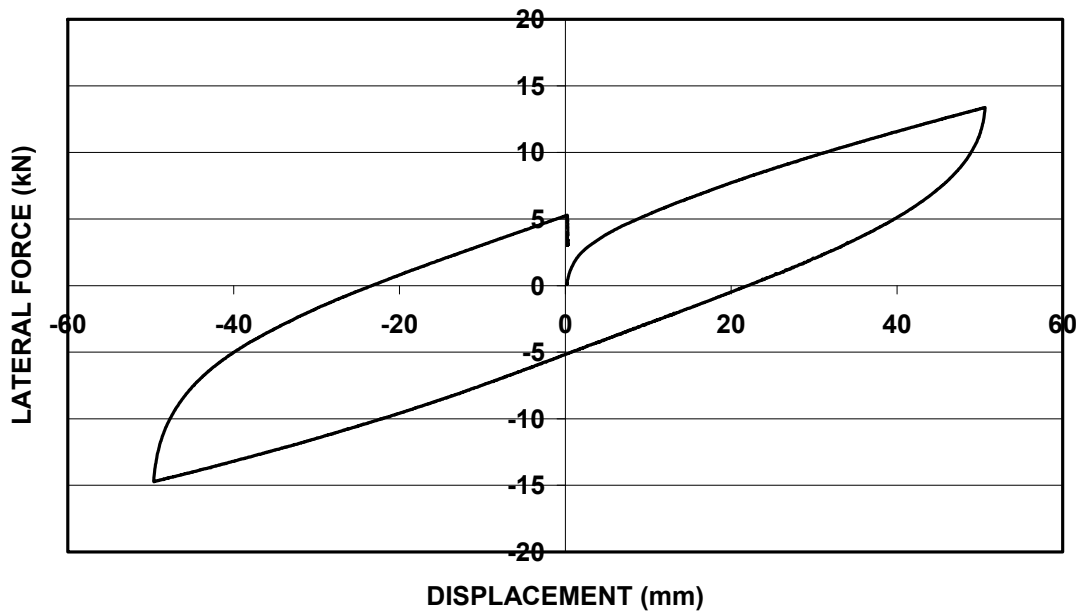
DISPLACEMENT (mm)

FIGURE 7-20 Force-Displacement Loops of Bearing B 1 Day and 4 Days After Cumulative Travel Test Recorded at Low Speed

BEARING B, 43 DAYS AFTER 500m CUMULATIVE TRAVEL TEST
(10 cycles, peak velocity 358mm/sec)
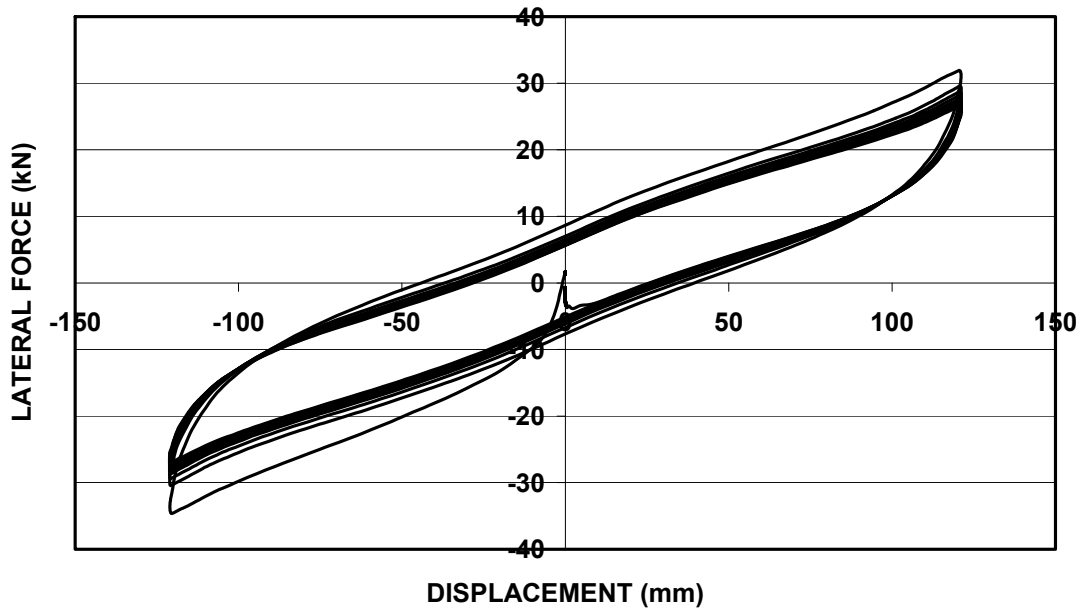
BEARING B, 43 DAYS AFTER 500m CUMULATIVE TRAVEL TEST
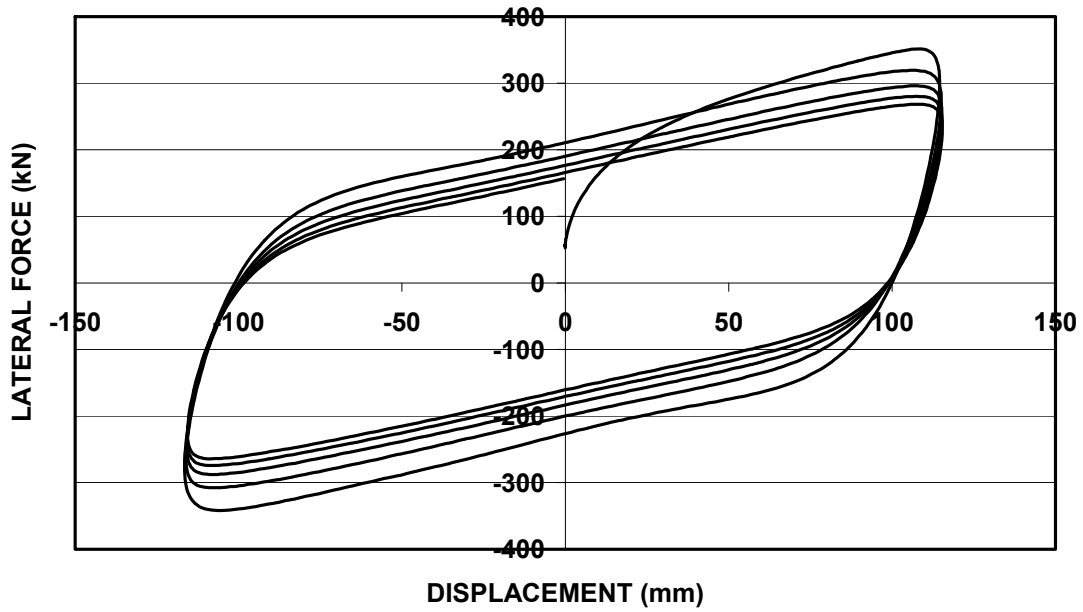**(1 cycle, constant velocity 0.05mm/sec)**
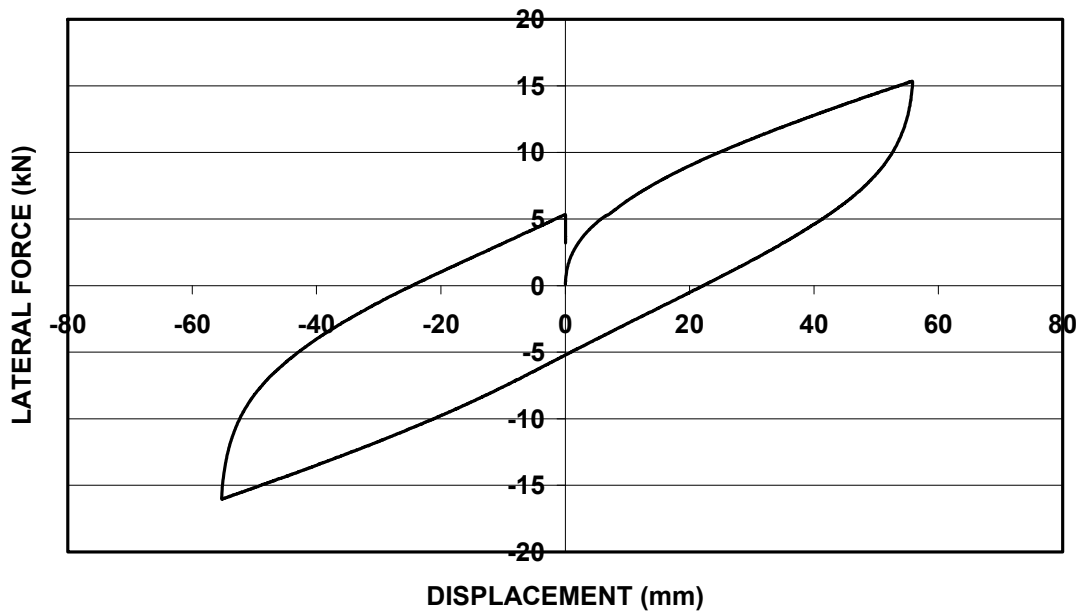
FIGURE 7-21 Force-Displacement Loops of Bearing B 43 Days After Cumulative Travel Test Recorded at High and Low Speed

SECTION 8

SUMMARY AND CONCLUSIONS

The phenomenon of lead core heating causes the strength of a lead-rubber bearing to decrease when cyclically loaded. The main objective of the work described in this report was to understand and predict the effect of this phenomenon on the behavior of a lead-rubber bearing. Moreover, this report presented a description of the behavior of lead-rubber bearings following significant cumulative travel that is caused by thermal and traffic loads.

The report presented a review of available information on the properties and material behavior of lead. Information on the effects of temperature, rate of deformation, crystal structure, impurities etc. on the strength and the general behavior of lead was given in Section 2. In general, the plastic deformation of lead is of a very complex nature with many of the aforementioned factors coming into play and interacting with each other. We have seen, for instance, that even the composition of the impurities can have an important effect on the strength of highly pure lead. Tests on lead specimens in tension were conducted and results were reported for two levels of speed and at various temperatures. The information provided in Section 2 formed a basis upon which a relationship between the temperature and the strength of the lead core of a bearing was established. This relationship was used in the modeling of the phenomenon of lead core heating (Section 3).

Section 3 presented a formulation and solution of the problem of predicting the lead core temperature of lead-rubber bearings and the associated effects on the characteristic

223

strength and dissipated energy. Two approaches were presented, one based on energy balance and another based on a constant flux assumption. On the basis of simplifying assumptions regarding the temperature distributions inside the bearing, the partial differential equations (in time and in two spatial independent variables) governing the problem were reduced to an ordinary differential equation in time which requires numerical solution. The equation has a simple explicit solution in cases where heat losses through the end and shim plates of the bearing are insignificant. The validity of most of the simplifying assumptions gradually deteriorates as time increases and as heat conduction effects become more prevalent.

Section 3 also presented an analysis of the dimensionless parameters of the problem. On the basis of this analysis, principles of scaling and similarity for lead-rubber bearings were presented. These principles demonstrated that reduced scale testing of individual bearing and reduced scale shake-table testing cannot generally capture the effects of lead core heating. There are cases, however, where the presented scaling law can be relaxed. These are cases where (a) there are insignificant heat losses due to heat conduction through the end and shim plates in both the model and the prototype bearings, or (b) both the model and the prototype bearings experience minor increases in temperature.

Section 4 presented a verification study of the presented theory of lead core heating by comparison of analytical, finite element and experimental results for a total of 15 cases involving lead-rubber bearings of various geometries and conditions of loading and motion. It was shown that the presented analytical model predicts well the reduction of the characteristic strength of the tested bearings in cyclic motion. Moreover, results

obtained in finite element thermal analysis of some of the tested bearings confirmed the basic assumptions of the theory that were used in the solution of the problem. The validity of these assumptions was found to be generally satisfactory for all cases that were investigated. Specifically:

(a) The assumption that the lead-steel interface temperatures is equal to one half of the temperature in the bulk of the lead core was found to be approximately valid for short times, which correspond to typical conditions of testing or operation of the bearings in earthquakes (a few cycles). However, at large times these temperatures (especially the one at the steel shim to lead interface) were found to gradually approach the temperature in the bulk of the core. Nevertheless, the time needed to reach that level of interface temperature was observed to be much larger than the typical duration of a cyclic testing or that of an earthquake.

(b) The assumption of the constant temperature distribution in the bulk of the lead core (except for the boundaries) was found to be valid for short times subject to the same constraints mentioned in item (a) above.

(c) The assumptions that the end plates are infinitely deep and that the shim plates are infinitely long were found to be valid as finite element analyses demonstrated that temperature increases of practical significance occurred only within a small volume of the end and shim plates even in cases of large duration of motion.

(d) The assumption that the *instantaneous* heat fluxes are proportional to the *stored* thermal energies in the steel plates is theoretically valid for small times while the

225

assumption that temperature distributions follow a linear/logarithmic law for the end/shim plates is theoretically valid for large times. Despite this discrepancy, the solution based on energy balance has proven itself sufficiently accurate and reliable for predictions of the lead core temperature and the characteristic strength.

Also, it should be noted that the analysis was based on the use of an exponential relation between the lead core effective yield strength and the lead core temperature. This relation was found to be valid in tensile testing of lead specimens at low strain rate. This exponential relation proved to give better predictions of lead core temperatures than a linear relation that was found to be valid in experiments at high strain rates. It is speculated that the reason for this paradox may lie in the difference between a lead core undergoing high speed cyclic motion with its temperature increasing and a lead specimen tested at high speed at a constant temperature. It is possible that the temperature increase taking place inside a lead core during cyclic motion speeds up the recrystallization process and switches the strength-temperature relation from linear to nonlinear (see Figure 2-1). This phenomenon is not expected to occur during a high speed test of a lead specimen because there should not be enough time for recrystallization to commence. Further testing of lead specimens would possibly provide a further insight into this issue.

Section 5 presented a model of hysteretic behavior of lead-rubber bearings that accounts for lead core heating. The model is capable of predicting the instantaneous temperature of the lead core and its instantaneous effect on the characteristic strength of the bearing. Predictions of force-displacement relations of lead-rubber bearings subjected to harmonic and random motions were shown to be in good agreement with experimental results.

Further improvements of the model would require consideration of (a) the effects of strain and of strain rate on the post-elastic stiffness and (b) the effects of strain rate on the characteristic strength. Understanding of these phenomena requires experimental investigations but there is no theoretical complexity in accounting for these effects on the basis of phenomenological models.

Section 6 presented a study of the dynamic response of a representative structure isolated with lead-rubber bearings. The analysis was based on the proposed model that accounts for the instantaneous effects of lead core heating. The results of the analysis were compared to results of analysis based on currently available models of hysteretic behavior of lead-rubber bearings but with consideration of the effects of lead core heating through the use of bounding analysis. Bounding values of characteristic strength are established on the basis of experimental results and tend to be systematically conservative. The results of the study demonstrated that bounding analysis produces conservative results on the prediction of isolation system displacement demand and isolation system peak shear force. The conservatism is particularly pronounced in ground motions with strong near-fault pulses. Under these conditions, the actual heating effects are not substantial and the bearings maintain their strength to substantially benefit the performance of the isolation system.

Section 7 presented a study of the effects of load history on the strength of lead-rubber bearings. The reported work attempted to determine whether the strength of lead-rubber bearings is affected by cumulative travel induced by service load conditions. Testing on large- and small-scale bearings was performed and investigated the effect of large

cumulative travel that consisted of either small amplitude (as those experienced due to traffic loadings in bridges) or large amplitude (as those experienced due to thermal loadings in bridges) cycles of motion. It was concluded that large cumulative travel has a pronounced effect on the characteristic strength of lead-rubber bearings under quasi-static conditions (as those experienced in service loading conditions) provided that the amplitude of motion during the cumulative travel is large enough to cause marked yielding of the lead core. No similar effect was observed when the amplitude of motion was such that no significant yielding occurred in the lead core. The increase in the lead core strength is likely caused by strain hardening of the lead. It is recommended that cumulative travel test specifications for lead-rubber bearings (a) either only include components caused by temperature changes (large amplitude) and not traffic loading effects (small amplitude), or (b) specify a regime of testing that separates the effects of large amplitude thermal and small amplitude traffic effects.

SECTION 9

REFERENCES

Abe, M., Yoshida, J. and Fujino, Y. (2004), "Multiaxial Behaviors of Laminated Rubber Bearings and Their Modeling. II: Modeling", Journal of Structural Engineering, Vol. 130, No. 8, pp. 1133-1144.

Ali, H.-E. M. and Abdel-Ghaffar, A. M. (1995), "Modeling of Rubber and Lead Passive-Control Bearings for Seismic Analysis", Journal of Structural Engineering, Vol. 121, No. 7, pp. 1134-1144.

American Society for Metals (1979), *Properties and Selection: Nonferrous Alloys and Pure Metals*, Metals Handbook, 9th Edition, Vol. 2, American Society for Metals, Metals Park, Ohio.

American Society for Metals (1991), *Properties and Selection: Non-ferrous Alloys and Special-Purpose Materials*, ASM Handbook, Vol. 2, Metals Park, Ohio.

American Society for Metals (1992), *Friction, Lubrication, and Wear Technology*, ASM Handbook, Vol. 18, Metals Park, Ohio.

ASTM International (2005), *Annual Book of ASTM Standards*, Vol. 02.04, ASTM International, West Conshohocken, PA.

ASTM International (2005), *Annual Book of ASTM Standards*, Vol. 03.01, ASTM International, West Conshohocken, PA.

Barenblatt, G. I. (2003), *Scaling*, Cambridge University Press.

Barenblatt, G. I. (1996), *Scaling, Self-similarity, and Intermediate Asymptotics*, Cambridge University Press.

Beck, J. V. (1979), "Average Transient Temperature within a Body Heated by a Disk Heat Source", presented as Paper 79-0175 at the AIAA 17th Aerospace Sciences Meeting, New Orleans, La., Jan. 15-17, 1979.

Callister, W. D. (1999), *Materials Science and Engineering: An Introduction*, 5th Edition, John Wiley and Sons, New York.

Carslaw, H. S. and Jaeger, J. C. (1959), *Conduction of Heat in Solids*, 2nd Edition, Oxford University Press, London, UK.

Computers and Structures, Inc. (2007), *SAP2000, Static and Dynamic Finite Element Analysis of Structures, Version 11.0.8*, Berkeley, California.

Constantinou, M. C., and Adnane, M. A. (1987), "Dynamics of Soil-Base-Isolated Structure Systems: Evaluation of Two Models for Yielding Systems", Report to NSF, Department of Civil Engineering, Drexel University, Philadelphia.

Constantinou, M. C., Whittaker, A. S., Fenz, D. M., and Apostolakis, G. (2007a), "Seismic Isolation of Bridges", Department of Civil, Structural and Environmental Engineering, University at Buffalo, State University of New York, Buffalo, NY 14260.

Constantinou, M. C., Whittaker, A. S., Kalpakidis, Y., Fenz, D. M., and Warn, G. P. (2007b), "Performance of Seismic Isolation Hardware under Service and Seismic Loading", Technical Report MCEER-07-0012, Multidisciplinary Center for Earthquake Engineering Research, University at Buffalo, State University of New York, Department of Civil, Structural and Environmental Engineering, Ketter Hall, Buffalo, NY 14260.

Demetriades, G. F., Constantinou, M. C. and Reinhorn, A. M. (1993), "Study of Wire Rope Systems for Seismic Protection of Equipment in Buildings", Engineering Structures, Vol. 15, No. 5, pp. 321-334.

Doudoumis, I. N., Gravalas, F. and Doudoumis, N. I. (2005), "Analytical Modeling of Elastomeric Lead-Rubber Bearings with the Use of Finite Element Micromodels", 5th GRACM International Congress on Computational Mechanics, Limassol, 29 June-1 July 2005.

Focken, C. M. (1953), *Dimensional Methods and their Applications*, Edward Arnold and Co., London.

Grant, D. N., Fenves, G. L. and Whittaker, A. S. (2004), "Bidirectional Modelling of High-Damping Rubber Bearings", Journal of Earthquake Engineering, Vol. 8, Special Issue 1, pp. 161-185.

Guruswamy, S. (2000), *Engineering Properties and Applications of Lead Alloys*, Marcel Dekker, Inc., New York.

Harris, H. G. and Sabnis, G. M. (1999), *Structural Modeling and Experimental Techniques*, 2nd Edition, CRC Press, Boca Raton, Florida.

Hibbitt, Karlsson and Sorensen, Inc. (2002), *ABAQUS Version 6.3-1*, Pawtucket, Rhode Island.

Hofmann, W. (1970), *Lead and Lead Alloys: Properties and Technology*, Springer-Verlag, Berlin.

Hwang, J.-S. and Hsu, T.-Y. (2000), "Experimental Study of Isolated Building under Triaxial Ground Excitations", Journal of Structural Engineering, Vol. 126, No. 8.

Kikuchi, M. and Aiken, I. D. (1997), "An Analytical Hysteresis Model for Elastomeric Seismic Isolation Bearings", Earthquake Engineering and Structural Dynamics, Vol. 26, pp. 215-231.

Lide, D. R. (1993), editor, *Handbook of Chemistry and Physics*, 74th Edition, CRC Press, Boca Raton, Florida.

Makris, N. and Chang, S-P. (2000), "Effect of Viscous, Viscoplastic and Friction Damping on the Response of Seismic Isolated Structures", Earthquake Engineering and Structural Dynamics, Vol. 29, pp. 85-107.

Mokha, A. S., Constantinou, M. C. and Reinhorn, A. M. (1993), "Verification of Friction Model of Teflon Bearings under Triaxial Load", Journal of Structural Engineering, Vol. 119, No. 1, pp. 240-261.

Nadai, A. (1950), *Theory of Flow and Fracture of Solids*, Engineering Societies Monographs, Vol. 1, 2nd Edition, McGraw-Hill Book Company, Inc., New York.

Nagarajaiah, S., Reinhorn, A. M. and Constantinou, M. C. (1989), Nonlinear Dynamic Analysis of Three-Dimensional Base Isolated Structures (3D-BASIS), Technical Report NCEER-89-0019, National Center for Earthquake Engineering Research, State University of New York at Buffalo, Red Jacket Quadrangle, Buffalo, NY 14261.

Ozisik, M. N. (1989), *Boundary Value Problems of Heat Conduction*, Dover Publications, Inc., New York.

Ozisik, M. N. (1993), *Heat Conduction*, 2nd Edition, John Wiley and Sons, Inc., New York.

Park, Y. J., Wen, Y. K. and Ang, A. H-S. (1986), "Random Vibration of Hysteretic Systems Under Bi-Directional Ground Motions", Earthquake Engineering and Structural Dynamics, Vol. 14, pp. 543-557.

Rollason, E. C. (1973), *Metallurgy for Engineers*, 4th Edition, Edward Arnold (Publishers) Ltd..

Salazar, A. (2003), "On Thermal Diffusivity", European Journal of Physics, Vol. 24, pp. 351-358.

Seki, W., Fukahori, Y., Iseda, Y. and Matsunaga, T. (1987), "A Large-Deformation Finite-Element Analysis for Multilayer Elastomeric Bearings", Rubber Chemistry and Technology, Vol. 60, No. 5, pp. 856-869.

Skinner, R. I., Robinson, W. H. and McVerry, G. H. (1993), *An Introduction to Seismic Isolation*, John Wiley and Sons, Chichester, England.

Tsopelas, P. C., Roussis, P. C., Constantinou, M. C., Buchanan, R. and Reinhorn, A. M. (2005), "3D-BASIS-ME-MB: Computer Program for Nonlinear Dynamic Analysis of Seismically Isolated Structures", Technical Report MCEER-05-0009, Multidisciplinary Center for Earthquake Engineering Research, University at Buffalo, State University of New York.

Tyler, R. G. and Robinson, W. H. (1984), "High-Strain Tests on Lead-Rubber Bearings for Earthquake Loadings", Bulletin of the New Zealand National Society for Earthquake Engineering, Vol. 17, No. 2, pp. 90-105.

Van Vlack, L. H. (1980), *Elements of Materials Science & Engineering*, 4th Edition, Addison-Wesley Publishing Company.

Warn, G. P. and Whittaker, A. S. (2004), "Performance Estimates in Seismically Isolated Bridge Structures", Engineering Structures, Vol. 26, pp. 1261-1278.

Wolff, E. D. and Constantinou, M. C. (2004), "Experimental Study of Seismic Isolation Systems with Emphasis on Secondary System Response and Verification of Accuracy of Dynamic Response History Analysis Methods", Technical Report MCEER-04-0001, Multidisciplinary Center for Earthquake Engineering Research, University at Buffalo, State University of New York.

APPENDIX

DERIVATIONS

A.1 Introduction

This appendix contains details on how some of the expressions in Section 3 were derived, namely the energy-based algorithm, the simplified solution (for insignificant conduction of heat) and the error estimation for the simplified solution.

A.2 Energy Approach

According to Section 3, the thermal energy stored inside each of the end plates, E_1, is

$$E_1 = \int_0^{t_{pf}(t)} \rho_S \cdot c_S \cdot A_p \cdot T_p(z,t) \cdot dz = \int_0^{t_{pf}(t)} \rho_S c_S A_p \frac{T_L}{2} \left(1 - \frac{z}{t_{pf}}\right) \cdot dz =$$

$$= \rho_S c_S A_p \frac{T_L}{2} \int_0^{t_{pf}(t)} \left(1 - \frac{z}{t_{pf}}\right) \cdot dz = \rho_S c_S A_p \frac{T_L}{2} \cdot \left[z - \frac{z^2}{2t_{pf}}\right]_0^{t_{pf}} =$$

$$= \rho_S c_S A_p \frac{T_L}{2} \frac{t_{pf}}{2} = \frac{\rho_S c_S A_p T_L t_{pf}}{4} \tag{A-1}$$

and the energy stored in the shim plates, E_2, is

$$E_2 = \int_a^{R_f(t)} \rho_S \cdot c_S \cdot t_s \cdot T_s(r,t) \cdot 2\pi r dr = \int_a^{R_f(t)} \rho_S c_S t_s \frac{T_L}{2} \frac{\ln(r/R_f)}{\ln(a/R_f)} 2\pi r dr =$$

235

$$= \int_{a}^{R_f(t)} \frac{\rho_S c_S t_s T_L \pi}{\ln(a/R_f)} r \ln(r/R_f) dr = \frac{\rho_S c_S t_s T_L \pi}{\ln(a/R_f)} \int_{a}^{R_f(t)} r \ln(r/R_f) dr =$$

$$= \frac{\rho_S c_S t_s T_L \pi}{\ln(a/R_f)} \int_{\frac{a}{R_f}}^{1} R_f \cdot x \ln x \cdot R_f dx = \frac{\rho_S c_S t_s T_L \pi (R_f)^2}{\ln(a/R_f)} \int_{\frac{a}{R_f}}^{1} x \ln x dx =$$

$$= \frac{\rho_S c_S t_s T_L \pi (R_f)^2}{\ln(a/R_f)} \int_{\frac{a}{R_f}}^{1} \left(\frac{x^2}{2}\right)' \ln x dx = \frac{\rho_S c_S t_s T_L \pi (R_f)^2}{\ln(a/R_f)} \left(\left[\frac{x^2}{2} \ln x\right]_{a/R_f}^{1} - \int_{\frac{a}{R_f}}^{1} \frac{x^2}{2} \frac{1}{x} dx \right) =$$

$$= \frac{\rho_S c_S t_s T_L \pi (R_f)^2}{2\ln(a/R_f)} \left(\left[x^2 \ln x\right]_{a/R_f}^{1} - \left[\frac{x^2}{2}\right]_{a/R_f}^{1} \right) =$$

$$= \frac{\rho_S c_S t_s T_L \pi (R_f)^2}{2\ln(a/R_f)} \left\{ \left[0 - \left(\frac{a}{R_f}\right)^2 \cdot \ln\left(\frac{a}{R_f}\right) \right] - \left[\frac{1}{2} - \frac{1}{2}\left(\frac{a}{R_f}\right)^2 \right] \right\} =$$

$$= \frac{\rho_S c_S t_s T_L \pi (R_f)^2}{2\ln(a/R_f)} \left[0.5\left(\frac{a}{R_f}\right)^2 - 0.5 - \left(\frac{a}{R_f}\right)^2 \cdot \ln\left(\frac{a}{R_f}\right) \right] =$$

$$= \frac{\rho_S c_S t_s T_L \pi (R_f)^2}{4\ln(a/R_f)} \left[\left(\frac{a}{R_f}\right)^2 - 1 - 2\left(\frac{a}{R_f}\right)^2 \ln\left(\frac{a}{R_f}\right) \right] \qquad \text{(A-2)}$$

Heat flux q_1 is given by

$$q_1(t) = -k_S \cdot A_p \cdot \left. \frac{\partial T_P}{\partial z} \right|_{z=0} = -k_S A_p \frac{T_L}{2} \left. \frac{\partial}{\partial z} \left(1 - \frac{z}{t_{pf}} \right) \right|_{z=0} = \frac{k_S A_p T_L}{2 t_{pf}} \tag{A-3}$$

Heat flux q_2 is given by

$$q_2(t) = -k_S \cdot A_s \cdot \left. \frac{\partial T_S}{\partial r} \right|_{r=a} = -k_S A_s \frac{T_L}{2} \left. \frac{\partial}{\partial r} \left(\frac{\ln(r/R_f)}{\ln(a/R_f)} \right) \right|_{r=a} =$$

$$= -k_S A_s \frac{T_L}{2} \frac{\dfrac{1}{R_f} \cdot \dfrac{1}{a/R_f}}{\ln(a/R_f)} = \frac{k_S A_s T_L}{2a \ln(R_f/a)} \tag{A-4}$$

The assumption is made that the ratio of the heat fluxes is equal to the ratio of the stored energies:

$$\frac{q_1}{q_2} = \frac{E_1}{E_2} \Rightarrow \frac{\dfrac{k_S A_p T_L}{2 t_{pf}}}{\dfrac{k_S A_s T_L}{2a \ln(R_f/a)}} = \frac{\dfrac{\rho_S c_S A_p T_L t_{pf}}{4}}{\dfrac{\rho_S c_S t_s T_L \pi (R_f)^2}{4 \ln(a/R_f)} \left[\left(\dfrac{a}{R_f} \right)^2 - 1 - 2 \left(\dfrac{a}{R_f} \right)^2 \ln\left(\dfrac{a}{R_f} \right) \right]} \Rightarrow$$

$$\frac{\dfrac{1}{t_{pf}}}{\dfrac{2\pi a t_s}{a \ln(R_f/a)}} = \frac{t_{pf}}{\dfrac{t_s \pi (R_f)^2}{\ln(a/R_f)} \left[\left(\dfrac{a}{R_f} \right)^2 - 1 - 2 \left(\dfrac{a}{R_f} \right)^2 \ln\left(\dfrac{a}{R_f} \right) \right]} \Rightarrow$$

$$\frac{\ln(R_f/a)}{2} = \frac{\left(t_{pf}\right)^2}{\frac{\left(R_f\right)^2}{\ln(a/R_f)}\left[\left(\frac{a}{R_f}\right)^2 - 1 - 2\left(\frac{a}{R_f}\right)^2 \ln\left(\frac{a}{R_f}\right)\right]} \Rightarrow$$

$$2\left(t_{pf}\right)^2 = -\left(R_f\right)^2\left[\left(\frac{a}{R_f}\right)^2 - 1 - 2\left(\frac{a}{R_f}\right)^2 \ln\left(\frac{a}{R_f}\right)\right] \Rightarrow$$

$$2\left(\frac{t_{pf}}{a}\right)^2 = -\left(\frac{R_f}{a}\right)^2\left[\left(\frac{a}{R_f}\right)^2 - 1 - 2\left(\frac{a}{R_f}\right)^2 \ln\left(\frac{a}{R_f}\right)\right] \Rightarrow$$

$$2\left(\frac{t_{pf}}{a}\right)^2 = \left[-1 + \left(\frac{R_f}{a}\right)^2 + 2\ln\left(\frac{a}{R_f}\right)\right] \Rightarrow 2\left(\frac{t_{pf}}{a}\right)^2 = \left(\frac{R_f}{a}\right)^2 - 1 - 2\ln\left(\frac{R_f}{a}\right) \quad \text{(A-5)}$$

Derivation of the right-hand side of (3-27) starts by observing that it is, because of (3-26), equal to

$$\frac{T_L \rho_L c_L V_L + 2 \cdot E_1 + E_2}{A_L} =$$

$$= \frac{T_L \rho_L c_L V_L + 2 \cdot \dfrac{\rho_S c_S A_p T_L t_{pf}}{4} + \dfrac{\rho_S c_S t_s T_L \pi \left(R_f\right)^2}{4\ln(a/R_f)}\left[\left(\dfrac{a}{R_f}\right)^2 - 1 - 2\left(\dfrac{a}{R_f}\right)^2 \ln\left(\dfrac{a}{R_f}\right)\right]}{\pi a^2} =$$

$$= T_L \rho_L c_L h_L + \frac{2 \cdot \dfrac{\rho_S c_S \pi a^2 T_L t_{pf}}{4} + \dfrac{\rho_S c_S t_s T_L \pi \left(R_f\right)^2}{4\ln(a/R_f)}\left[\left(\dfrac{a}{R_f}\right)^2 - 1 - 2\left(\dfrac{a}{R_f}\right)^2 \ln\left(\dfrac{a}{R_f}\right)\right]}{\pi a^2} =$$

238

$$= T_L \rho_L c_L h_L + \frac{\rho_S c_S T_L t_{pf}}{2} + \frac{\dfrac{\rho_S c_S t_s T_L \pi (R_f)^2}{4 \ln(a/R_f)} \left[\left(\dfrac{a}{R_f} \right)^2 - 1 - 2 \left(\dfrac{a}{R_f} \right)^2 \ln \left(\dfrac{a}{R_f} \right) \right]}{\pi a^2} =$$

$$= T_L \rho_L c_L h_L + \frac{\rho_S c_S T_L t_{pf}}{2} + \frac{\rho_S c_S t_s T_L (R_f/a)^2}{4 \ln(a/R_f)} \left[\left(\dfrac{a}{R_f} \right)^2 - 1 - 2 \left(\dfrac{a}{R_f} \right)^2 \ln \left(\dfrac{a}{R_f} \right) \right] =$$

$$= T_L \left\{ \rho_L c_L h_L + \frac{\rho_S c_S t_{pf}}{2} + \frac{\rho_S c_S t_s}{4 \ln(a/R_f)} \left[1 - \left(\dfrac{R_f}{a} \right)^2 - 2 \ln \left(\dfrac{a}{R_f} \right) \right] \right\} =$$

$$= T_L \left\{ \rho_L c_L h_L + \frac{\rho_S c_S t_{pf}}{2} + \frac{\rho_S c_S t_s}{- 4 \ln(R_f/a)} \left[1 - \left(\dfrac{R_f}{a} \right)^2 + 2 \ln \left(\dfrac{R_f}{a} \right) \right] \right\} =$$

$$= T_L \left\{ \rho_L c_L h_L + \frac{\rho_S c_S t_{pf}}{2} + \frac{\rho_S c_S t_s}{4 \ln(R_f/a)} \left[-1 + \left(\dfrac{R_f}{a} \right)^2 - 2 \ln \left(\dfrac{R_f}{a} \right) \right] \right\} =$$

$$= T_L \left\{ \rho_L c_L h_L + \frac{\rho_S c_S t_{pf}}{2} + \frac{\rho_S c_S t_s}{4 \ln(R_f/a)} 2 \left(\dfrac{t_{pf}}{a} \right)^2 \right\} =$$

$$= T_L \left\{ \rho_L c_L h_L + \frac{\rho_S c_S}{2} \left(t_{pf} + \frac{t_s}{\ln(R_f/a)} \left(\dfrac{t_{pf}}{a} \right)^2 \right) \right\} =$$

$$= T_L \left\{ \rho_L c_L h_L + \frac{\rho_S c_S}{2} \left(t_{pf} + t_s \frac{\left(\dfrac{t_{pf}}{a} \right)^2}{\ln \left(1 + 1.2 \dfrac{t_{pf}}{a} \right)} \right) \right\} \qquad (A\text{-}6)$$

239

where, in the last three lines, use of (3-24) and (3-25) was made.

Derivation of the negative term on the right-hand side of (3-28) starts by observing that it is, because of (3-8), equal to

$$\frac{2 \cdot q_1 + q_2}{A_L} = \frac{2 \cdot \dfrac{k_S A_p T_L}{2t_{pf}} + \dfrac{k_S A_s T_L}{2a \ln(R_f/a)}}{A_L} = \frac{k_S T_L}{t_{pf}} + \frac{\dfrac{k_S 2\pi a t_s T_L}{2a \ln(R_f/a)}}{\pi a^2} =$$

$$= \frac{k_S T_L}{t_{pf}} + \frac{\dfrac{k_S t_s T_L}{\ln(R_f/a)}}{a^2} = \frac{k_S T_L}{t_{pf}} + \frac{k_S t_s T_L t_{pf}}{a^2 \ln(R_f/a) t_{pf}} = \frac{k_S T_L}{t_{pf}} \left(1 + \left(\frac{t_s}{a}\right) \frac{\left(\dfrac{t_{pf}}{a}\right)}{\ln(R_f/a)} \right) =$$

$$= \frac{k_S T_L}{t_{pf}} \left(1 + \left(\frac{t_s}{a}\right) \frac{\left(\dfrac{t_{pf}}{a}\right)}{\ln\left(1 + 1.2\left(\dfrac{t_{pf}}{a}\right)\right)} \right) \tag{A-7}$$

where, in the last line, use of (3-25) was made.

A.3 Simplified Solution – The Case of Insignificant Conduction of Heat

Ignoring heat conduction through the steel plates, the heat equation for the lead core is

$$\frac{dT_L'}{dt} = \frac{\sigma_{YL}(T_L') \cdot |v(t)|}{\rho_L c_L h_L} \Rightarrow \frac{dT_L'}{dt} = \frac{\sigma_{YL0} \exp(-E_2 T_L') \cdot |v(t)|}{\rho_L c_L h_L} \Rightarrow \exp(E_2 T_L') dT_L' = \frac{\sigma_{YL0} \cdot |v(t)|}{\rho_L c_L h_L} dt \Rightarrow$$

$$\frac{1}{E_2}\int_0^t \exp(E_2 T_L')d(E_2 T_L') = \int_0^t \frac{\sigma_{YL0} \cdot |v(\tau)|}{\rho_L c_L h_L}d\tau \Rightarrow \frac{1}{E_2}[\exp(E_2 T_L')]_0^{T_L'} = \frac{\sigma_{YL0}}{\rho_L c_L h_L} \cdot \int_0^t |v(\tau)|d\tau \Rightarrow$$

$$\exp(E_2 T_L') - 1 = \frac{E_2 \sigma_{YL0}}{\rho_L c_L h_L} \cdot \int_0^t |v(\tau)|d\tau \Rightarrow \exp(E_2 T_L') = 1 + \frac{E_2 \sigma_{YL0}}{\rho_L c_L h_L} \cdot \int_0^t |v(\tau)|d\tau \Rightarrow$$

$$T_L' = \frac{1}{E_2} \cdot \ln\left(1 + \frac{E_2 \sigma_{YL0} \cdot \int_0^t |v(\tau)|d\tau}{\rho_L c_L h_L}\right) \tag{A-8}$$

A.4 Estimation of the Error of the Simplified Solution

We begin with the equation

$$\frac{dT_L}{dt} = \frac{\sigma_{YL0} \exp(-E_2 T_L) \cdot |v(t)|}{\rho_L c_L h_L} - \frac{k_S \cdot T_L}{a \cdot \rho_L c_L h_L} \cdot \left(\frac{\pi^{1/2}}{2}(t^+)^{-1/2} + 1.274 \cdot \left(\frac{t_s}{a}\right) \cdot (t^+)^{-1/3}\right) \tag{A-9}$$

which is derived from (3-50a) considering only the leading term in (3-37a) and assuming an exponential relation between effective yield stress and temperature. This equation may be integrated as follows

$$\int_0^t dT_L = \int_0^t \left[\frac{\sigma_{YL0} \exp(-E_2 T_L) \cdot |v(\tau)|}{\rho_L c_L h_L} - \frac{k_S \cdot T_L}{a \cdot \rho_L c_L h_L} \cdot \left(\frac{\pi^{1/2}}{2}(\tau^+)^{-1/2} + 1.274 \cdot \left(\frac{t_s}{a}\right) \cdot (\tau^+)^{-1/3}\right)\right]d\tau \Rightarrow$$

$$T_L = \int_0^t \left[\frac{\sigma_{YL0} \exp(-E_2 T_L) |v(\tau)|}{\rho_L c_L h_L} - \frac{k_S T_L}{a \rho_L c_L h_L}\left(\frac{\pi^{1/2}}{2}(\tau^+)^{-1/2} + 1.274\left(\frac{t_s}{a}\right)(\tau^+)^{-1/3}\right)\right]d\tau \tag{A-10}$$

The right-hand side in the above equation may be approximately evaluated by replacing T_L with the simplified expression T_L' in (A-8). Hence,

$$T_L = \int_0^t \left[\frac{\sigma_{YL0}\exp\left(-E_2 T_L'\right)|v(\tau)|}{\rho_L c_L h_L} - \frac{k_S T_L'}{a\rho_L c_L h_L}\left(\frac{\pi^{1/2}}{2}\left(\tau^+\right)^{-1/2} + 1.274\left(\frac{t_s}{a}\right)\left(\tau^+\right)^{-1/3}\right) \right] d\tau \Rightarrow$$

$$T_L = \int_0^t \left[\frac{\dfrac{\sigma_{YL0}\cdot|v(\tau)|}{1+\dfrac{E_2\sigma_{YL0}\cdot\displaystyle\int_0^\tau|v(x)|dx}{\rho_L c_L h_L}}}{\rho_L c_L h_L} - \frac{k_S T_L'}{a\rho_L c_L h_L}\left(\frac{\pi^{1/2}}{2}\left(\tau^+\right)^{-1/2} + 1.274\left(\frac{t_s}{a}\right)\left(\tau^+\right)^{-1/3}\right) \right] d\tau \Rightarrow$$

$$T_L = \int_0^t \left[\frac{\sigma_{YL0}\cdot|v(\tau)|}{\rho_L c_L h_L + E_2\sigma_{YL0}\cdot\displaystyle\int_0^\tau|v(x)|dx} - \frac{k_S T_L'}{a\rho_L c_L h_L}\left(\frac{\pi^{1/2}}{2}\left(\tau^+\right)^{-1/2} + 1.274\left(\frac{t_s}{a}\right)\left(\tau^+\right)^{-1/3}\right) \right] d\tau \Rightarrow$$

$$T_L = \int_0^t \frac{\sigma_{YL0}\cdot|v(\tau)|d\tau}{\rho_L c_L h_L + E_2\sigma_{YL0}\cdot\displaystyle\int_0^\tau|v(x)|dx} - \int_0^t \frac{k_S T_L'}{a\rho_L c_L h_L}\left(\frac{\pi^{1/2}}{2}\left(\tau^+\right)^{-1/2} + 1.274\left(\frac{t_s}{a}\right)\left(\tau^+\right)^{-1/3}\right) d\tau \Rightarrow$$

$$T_L = \frac{1}{E_2}\int_0^t \frac{E_2\sigma_{YL0}\cdot\dfrac{d}{d\tau}\left(\displaystyle\int_0^\tau|v(x)|dx\right)d\tau}{\rho_L c_L h_L + E_2\sigma_{YL0}\cdot\displaystyle\int_0^\tau|v(x)|dx} - \int_0^t \frac{k_S T_L'}{a\rho_L c_L h_L}\left(\frac{\pi^{1/2}}{2}\left(\tau^+\right)^{-1/2} + 1.274\left(\frac{t_s}{a}\right)\left(\tau^+\right)^{-1/3}\right) d\tau \Rightarrow$$

$$T_L = \frac{1}{E_2} \int_0^t \frac{\frac{d}{d\tau}\left(\rho_L c_L h_L + E_2 \sigma_{YL0} \int_0^\tau |v(x)| dx\right)}{\rho_L c_L h_L + E_2 \sigma_{YL0} \int_0^\tau |v(x)| dx} d\tau - \int_0^t \frac{k_S T_L'}{a\rho_L c_L h_L}\left(\frac{\pi^{1/2}}{2}\left(\tau^+\right)^{-1/2} + 1.274\left(\frac{t_s}{a}\right)\left(\tau^+\right)^{-1/3}\right) d\tau \Rightarrow$$

$$T_L = \frac{1}{E_2}\left[\ln\left(\rho_L c_L h_L + E_2 \sigma_{YL0} \int_0^\tau |v(x)| dx\right)\right]_0^t - \int_0^t \frac{k_S T_L'}{a\rho_L c_L h_L}\left(\frac{\pi^{1/2}}{2}\left(\tau^+\right)^{-1/2} + 1.274\left(\frac{t_s}{a}\right)\left(\tau^+\right)^{-1/3}\right) d\tau \Rightarrow$$

$$T_L = \frac{1}{E_2}\ln\frac{\rho_L c_L h_L + E_2 \sigma_{YL0} \int_0^t |v(\tau)| d\tau}{\rho_L c_L h_L} - \int_0^t \frac{k_S T_L'}{a\rho_L c_L h_L}\left(\frac{\pi^{1/2}}{2}\left(\tau^+\right)^{-1/2} + 1.274\left(\frac{t_s}{a}\right)\left(\tau^+\right)^{-1/3}\right) d\tau \Rightarrow$$

$$T_L = \frac{1}{E_2}\ln\left(1 + \frac{E_2 \sigma_{YL0} \int_0^t |v(\tau)| d\tau}{\rho_L c_L h_L}\right) - \int_0^t \frac{k_S T_L'}{a\rho_L c_L h_L}\left(\frac{\pi^{1/2}}{2}\left(\tau^+\right)^{-1/2} + 1.274\left(\frac{t_s}{a}\right)\left(\tau^+\right)^{-1/3}\right) d\tau \Rightarrow$$

$$T_L = T_L' - \int_0^t \frac{k_S T_L'}{a\rho_L c_L h_L}\left(\frac{\pi^{1/2}}{2}\left(\tau^+\right)^{-1/2} + 1.274\left(\frac{t_s}{a}\right)\left(\tau^+\right)^{-1/3}\right) d\tau \Rightarrow$$

$$\Delta T_L = T_L' - T_L = \int_0^t \frac{k_S T_L'}{a\rho_L c_L h_L}\left(\frac{\pi^{1/2}}{2}\left(\tau^+\right)^{-1/2} + 1.274\left(\frac{t_s}{a}\right)\left(\tau^+\right)^{-1/3}\right) d\tau =$$

$$= \int_0^{t^+} \frac{k_S T_L'}{a\rho_L c_L h_L}\left(\frac{\pi^{1/2}}{2}\left(\tau^+\right)^{-1/2} + 1.274\left(\frac{t_s}{a}\right)\left(\tau^+\right)^{-1/3}\right)\left(\frac{a^2}{\alpha_S}\right) d\tau^+ =$$

$$= \int_0^{t^+} \frac{a\rho_S c_S T_L'}{\rho_L c_L h_L} \left(\frac{\pi^{1/2}}{2} (\tau^+)^{-1/2} + 1.274 \left(\frac{t_s}{a} \right) (\tau^+)^{-1/3} \right) d\tau^+ =$$

$$= \frac{a\rho_S c_S}{\rho_L c_L h_L} \int_0^{t^+} T_L' \left(\frac{\pi^{1/2}}{2} (\tau^+)^{-1/2} + 1.274 \left(\frac{t_s}{a} \right) (\tau^+)^{-1/3} \right) d\tau^+ =$$

$$= \frac{a\rho_S c_S}{\rho_L c_L h_L} \left\{ \left[T_L' \left(1.772(\tau^+)^{1/2} + 1.911 \left(\frac{t_s}{a} \right) (\tau^+)^{2/3} \right) \right]_0^{t^+} - \int_0^{t^+} \left(\frac{dT_L'}{d\tau} \right) \cdot \left(1.772(\tau^+)^{1/2} + 1.911 \left(\frac{t_s}{a} \right) (\tau^+)^{2/3} \right) d\tau^+ \right\}$$

The (always positive) integral in the above equation may be neglected to provide a conservative estimate of the error as follows:

$$\Delta T_L = T_L' - T_L \le \frac{a\rho_S c_S T_L'}{\rho_L c_L h_L} \left(1.772(t^+)^{1/2} + 1.911 \left(\frac{t_s}{a} \right) (t^+)^{2/3} \right) \Rightarrow$$

$$\Delta T_L \le \left(\frac{\rho_S c_S}{\rho_L c_L} \right) \left(1.772 \frac{a}{h_L} (t^+)^{1/2} + 1.911 \left(\frac{t_s}{h_L} \right) (t^+)^{2/3} \right) \cdot T_L' \qquad \text{(A-11)}$$

MCEER Technical Reports

MCEER publishes technical reports on a variety of subjects written by authors funded through MCEER. These reports are available from both MCEER Publications and the National Technical Information Service (NTIS). Requests for reports should be directed to MCEER Publications, MCEER, University at Buffalo, State University of New York, Red Jacket Quadrangle, Buffalo, New York 14261. Reports can also be requested through NTIS, 5285 Port Royal Road, Springfield, Virginia 22161. NTIS accession numbers are shown in parenthesis, if available.

NCEER-87-0001   "First-Year Program in Research, Education and Technology Transfer," 3/5/87, (PB88-134275, A04, MF-A01).

NCEER-87-0002   "Experimental Evaluation of Instantaneous Optimal Algorithms for Structural Control," by R.C. Lin, T.T. Soong and A.M. Reinhorn, 4/20/87, (PB88-134341, A04, MF-A01).

NCEER-87-0003   "Experimentation Using the Earthquake Simulation Facilities at University at Buffalo," by A.M. Reinhorn and R.L. Ketter, to be published.

NCEER-87-0004   "The System Characteristics and Performance of a Shaking Table," by J.S. Hwang, K.C. Chang and G.C. Lee, 6/1/87, (PB88-134259, A03, MF-A01). This report is available only through NTIS (see address given above).

NCEER-87-0005   "A Finite Element Formulation for Nonlinear Viscoplastic Material Using a Q Model," by O. Gyebi and G. Dasgupta, 11/2/87, (PB88-213764, A08, MF-A01).

NCEER-87-0006   "Symbolic Manipulation Program (SMP) - Algebraic Codes for Two and Three Dimensional Finite Element Formulations," by X. Lee and G. Dasgupta, 11/9/87, (PB88-218522, A05, MF-A01).

NCEER-87-0007   "Instantaneous Optimal Control Laws for Tall Buildings Under Seismic Excitations," by J.N. Yang, A. Akbarpour and P. Ghaemmaghami, 6/10/87, (PB88-134333, A06, MF-A01). This report is only available through NTIS (see address given above).

NCEER-87-0008   "IDARC: Inelastic Damage Analysis of Reinforced Concrete Frame - Shear-Wall Structures," by Y.J. Park, A.M. Reinhorn and S.K. Kunnath, 7/20/87, (PB88-134325, A09, MF-A01). This report is only available through NTIS (see address given above).

NCEER-87-0009   "Liquefaction Potential for New York State: A Preliminary Report on Sites in Manhattan and Buffalo," by M. Budhu, V. Vijayakumar, R.F. Giese and L. Baumgras, 8/31/87, (PB88-163704, A03, MF-A01). This report is available only through NTIS (see address given above).

NCEER-87-0010   "Vertical and Torsional Vibration of Foundations in Inhomogeneous Media," by A.S. Veletsos and K.W. Dotson, 6/1/87, (PB88-134291, A03, MF-A01). This report is only available through NTIS (see address given above).

NCEER-87-0011   "Seismic Probabilistic Risk Assessment and Seismic Margins Studies for Nuclear Power Plants," by Howard H.M. Hwang, 6/15/87, (PB88-134267, A03, MF-A01). This report is only available through NTIS (see address given above).

NCEER-87-0012   "Parametric Studies of Frequency Response of Secondary Systems Under Ground-Acceleration Excitations," by Y. Yong and Y.K. Lin, 6/10/87, (PB88-134309, A03, MF-A01). This report is only available through NTIS (see address given above).

NCEER-87-0013   "Frequency Response of Secondary Systems Under Seismic Excitation," by J.A. HoLung, J. Cai and Y.K. Lin, 7/31/87, (PB88-134317, A05, MF-A01). This report is only available through NTIS (see address given above).

NCEER-87-0014   "Modelling Earthquake Ground Motions in Seismically Active Regions Using Parametric Time Series Methods," by G.W. Ellis and A.S. Cakmak, 8/25/87, (PB88-134283, A08, MF-A01). This report is only available through NTIS (see address given above).

NCEER-87-0015   "Detection and Assessment of Seismic Structural Damage," by E. DiPasquale and A.S. Cakmak, 8/25/87, (PB88-163712, A05, MF-A01). This report is only available through NTIS (see address given above).

NCEER-87-0016   "Pipeline Experiment at Parkfield, California," by J. Isenberg and E. Richardson, 9/15/87, (PB88-163720, A03, MF-A01). This report is available only through NTIS (see address given above).

NCEER-87-0017   "Digital Simulation of Seismic Ground Motion," by M. Shinozuka, G. Deodatis and T. Harada, 8/31/87, (PB88-155197, A04, MF-A01). This report is available only through NTIS (see address given above).

NCEER-87-0018   "Practical Considerations for Structural Control: System Uncertainty, System Time Delay and Truncation of Small Control Forces," J.N. Yang and A. Akbarpour, 8/10/87, (PB88-163738, A08, MF-A01). This report is only available through NTIS (see address given above).

NCEER-87-0019   "Modal Analysis of Nonclassically Damped Structural Systems Using Canonical Transformation," by J.N. Yang, S. Sarkani and F.X. Long, 9/27/87, (PB88-187851, A04, MF-A01).

NCEER-87-0020   "A Nonstationary Solution in Random Vibration Theory," by J.R. Red-Horse and P.D. Spanos, 11/3/87, (PB88-163746, A03, MF-A01).

NCEER-87-0021   "Horizontal Impedances for Radially Inhomogeneous Viscoelastic Soil Layers," by A.S. Veletsos and K.W. Dotson, 10/15/87, (PB88-150859, A04, MF-A01).

NCEER-87-0022   "Seismic Damage Assessment of Reinforced Concrete Members," by Y.S. Chung, C. Meyer and M. Shinozuka, 10/9/87, (PB88-150867, A05, MF-A01). This report is available only through NTIS (see address given above).

NCEER-87-0023   "Active Structural Control in Civil Engineering," by T.T. Soong, 11/11/87, (PB88-187778, A03, MF-A01).

NCEER-87-0024   "Vertical and Torsional Impedances for Radially Inhomogeneous Viscoelastic Soil Layers," by K.W. Dotson and A.S. Veletsos, 12/87, (PB88-187786, A03, MF-A01).

NCEER-87-0025   "Proceedings from the Symposium on Seismic Hazards, Ground Motions, Soil-Liquefaction and Engineering Practice in Eastern North America," October 20-22, 1987, edited by K.H. Jacob, 12/87, (PB88-188115, A23, MF-A01). This report is available only through NTIS (see address given above).

NCEER-87-0026   "Report on the Whittier-Narrows, California, Earthquake of October 1, 1987," by J. Pantelic and A. Reinhorn, 11/87, (PB88-187752, A03, MF-A01). This report is available only through NTIS (see address given above).

NCEER-87-0027   "Design of a Modular Program for Transient Nonlinear Analysis of Large 3-D Building Structures," by S. Srivastav and J.F. Abel, 12/30/87, (PB88-187950, A05, MF-A01). This report is only available through NTIS (see address given above).

NCEER-87-0028   "Second-Year Program in Research, Education and Technology Transfer," 3/8/88, (PB88-219480, A04, MF-A01).

NCEER-88-0001   "Workshop on Seismic Computer Analysis and Design of Buildings With Interactive Graphics," by W. McGuire, J.F. Abel and C.H. Conley, 1/18/88, (PB88-187760, A03, MF-A01). This report is only available through NTIS (see address given above).

NCEER-88-0002   "Optimal Control of Nonlinear Flexible Structures," by J.N. Yang, F.X. Long and D. Wong, 1/22/88, (PB88-213772, A06, MF-A01).

NCEER-88-0003   "Substructuring Techniques in the Time Domain for Primary-Secondary Structural Systems," by G.D. Manolis and G. Juhn, 2/10/88, (PB88-213780, A04, MF-A01).

NCEER-88-0004   "Iterative Seismic Analysis of Primary-Secondary Systems," by A. Singhal, L.D. Lutes and P.D. Spanos, 2/23/88, (PB88-213798, A04, MF-A01).

NCEER-88-0005   "Stochastic Finite Element Expansion for Random Media," by P.D. Spanos and R. Ghanem, 3/14/88, (PB88-213806, A03, MF-A01).

NCEER-88-0006   "Combining Structural Optimization and Structural Control," by F.Y. Cheng and C.P. Pantelides, 1/10/88, (PB88-213814, A05, MF-A01).

NCEER-88-0007   "Seismic Performance Assessment of Code-Designed Structures," by H.H-M. Hwang, J-W. Jaw and H-J. Shau, 3/20/88, (PB88-219423, A04, MF-A01). This report is only available through NTIS (see address given above).

NCEER-88-0008   "Reliability Analysis of Code-Designed Structures Under Natural Hazards," by H.H-M. Hwang, H. Ushiba and M. Shinozuka, 2/29/88, (PB88-229471, A07, MF-A01). This report is only available through NTIS (see address given above).

NCEER-88-0009   "Seismic Fragility Analysis of Shear Wall Structures," by J-W Jaw and H.H-M. Hwang, 4/30/88, (PB89-102867, A04, MF-A01).

NCEER-88-0010   "Base Isolation of a Multi-Story Building Under a Harmonic Ground Motion - A Comparison of Performances of Various Systems," by F-G Fan, G. Ahmadi and I.G. Tadjbakhsh, 5/18/88, (PB89-122238, A06, MF-A01). This report is only available through NTIS (see address given above).

NCEER-88-0011   "Seismic Floor Response Spectra for a Combined System by Green's Functions," by F.M. Lavelle, L.A. Bergman and P.D. Spanos, 5/1/88, (PB89-102875, A03, MF-A01).

NCEER-88-0012   "A New Solution Technique for Randomly Excited Hysteretic Structures," by G.Q. Cai and Y.K. Lin, 5/16/88, (PB89-102883, A03, MF-A01).

NCEER-88-0013   "A Study of Radiation Damping and Soil-Structure Interaction Effects in the Centrifuge," by K. Weissman, supervised by J.H. Prevost, 5/24/88, (PB89-144703, A06, MF-A01).

NCEER-88-0014   "Parameter Identification and Implementation of a Kinematic Plasticity Model for Frictional Soils," by J.H. Prevost and D.V. Griffiths, to be published.

NCEER-88-0015   "Two- and Three- Dimensional Dynamic Finite Element Analyses of the Long Valley Dam," by D.V. Griffiths and J.H. Prevost, 6/17/88, (PB89-144711, A04, MF-A01).

NCEER-88-0016   "Damage Assessment of Reinforced Concrete Structures in Eastern United States," by A.M. Reinhorn, M.J. Seidel, S.K. Kunnath and Y.J. Park, 6/15/88, (PB89-122220, A04, MF-A01). This report is only available through NTIS (see address given above).

NCEER-88-0017   "Dynamic Compliance of Vertically Loaded Strip Foundations in Multilayered Viscoelastic Soils," by S. Ahmad and A.S.M. Israil, 6/17/88, (PB89-102891, A04, MF-A01).

NCEER-88-0018   "An Experimental Study of Seismic Structural Response With Added Viscoelastic Dampers," by R.C. Lin, Z. Liang, T.T. Soong and R.H. Zhang, 6/30/88, (PB89-122212, A05, MF-A01). This report is available only through NTIS (see address given above).

NCEER-88-0019   "Experimental Investigation of Primary - Secondary System Interaction," by G.D. Manolis, G. Juhn and A.M. Reinhorn, 5/27/88, (PB89-122204, A04, MF-A01).

NCEER-88-0020   "A Response Spectrum Approach For Analysis of Nonclassically Damped Structures," by J.N. Yang, S. Sarkani and F.X. Long, 4/22/88, (PB89-102909, A04, MF-A01).

NCEER-88-0021   "Seismic Interaction of Structures and Soils: Stochastic Approach," by A.S. Veletsos and A.M. Prasad, 7/21/88, (PB89-122196, A04, MF-A01). This report is only available through NTIS (see address given above).

NCEER-88-0022   "Identification of the Serviceability Limit State and Detection of Seismic Structural Damage," by E. DiPasquale and A.S. Cakmak, 6/15/88, (PB89-122188, A05, MF-A01). This report is available only through NTIS (see address given above).

NCEER-88-0023   "Multi-Hazard Risk Analysis: Case of a Simple Offshore Structure," by B.K. Bhartia and E.H. Vanmarcke, 7/21/88, (PB89-145213, A05, MF-A01).

NCEER-88-0024   "Automated Seismic Design of Reinforced Concrete Buildings," by Y.S. Chung, C. Meyer and M. Shinozuka, 7/5/88, (PB89-122170, A06, MF-A01). This report is available only through NTIS (see address given above).

NCEER-88-0025   "Experimental Study of Active Control of MDOF Structures Under Seismic Excitations," by L.L. Chung, R.C. Lin, T.T. Soong and A.M. Reinhorn, 7/10/88, (PB89-122600, A04, MF-A01).

NCEER-88-0026   "Earthquake Simulation Tests of a Low-Rise Metal Structure," by J.S. Hwang, K.C. Chang, G.C. Lee and R.L. Ketter, 8/1/88, (PB89-102917, A04, MF-A01).

NCEER-88-0027   "Systems Study of Urban Response and Reconstruction Due to Catastrophic Earthquakes," by F. Kozin and H.K. Zhou, 9/22/88, (PB90-162348, A04, MF-A01).

NCEER-88-0028   "Seismic Fragility Analysis of Plane Frame Structures," by H.H-M. Hwang and Y.K. Low, 7/31/88, (PB89-131445, A06, MF-A01).

NCEER-88-0029   "Response Analysis of Stochastic Structures," by A. Kardara, C. Bucher and M. Shinozuka, 9/22/88, (PB89-174429, A04, MF-A01).

NCEER-88-0030   "Nonnormal Accelerations Due to Yielding in a Primary Structure," by D.C.K. Chen and L.D. Lutes, 9/19/88, (PB89-131437, A04, MF-A01).

NCEER-88-0031   "Design Approaches for Soil-Structure Interaction," by A.S. Veletsos, A.M. Prasad and Y. Tang, 12/30/88, (PB89-174437, A03, MF-A01). This report is available only through NTIS (see address given above).

NCEER-88-0032   "A Re-evaluation of Design Spectra for Seismic Damage Control," by C.J. Turkstra and A.G. Tallin, 11/7/88, (PB89-145221, A05, MF-A01).

NCEER-88-0033   "The Behavior and Design of Noncontact Lap Splices Subjected to Repeated Inelastic Tensile Loading," by V.E. Sagan, P. Gergely and R.N. White, 12/8/88, (PB89-163737, A08, MF-A01).

NCEER-88-0034   "Seismic Response of Pile Foundations," by S.M. Mamoon, P.K. Banerjee and S. Ahmad, 11/1/88, (PB89-145239, A04, MF-A01).

NCEER-88-0035   "Modeling of R/C Building Structures With Flexible Floor Diaphragms (IDARC2)," by A.M. Reinhorn, S.K. Kunnath and N. Panahshahi, 9/7/88, (PB89-207153, A07, MF-A01).

NCEER-88-0036   "Solution of the Dam-Reservoir Interaction Problem Using a Combination of FEM, BEM with Particular Integrals, Modal Analysis, and Substructuring," by C-S. Tsai, G.C. Lee and R.L. Ketter, 12/31/88, (PB89-207146, A04, MF-A01).

NCEER-88-0037   "Optimal Placement of Actuators for Structural Control," by F.Y. Cheng and C.P. Pantelides, 8/15/88, (PB89-162846, A05, MF-A01).

NCEER-88-0038   "Teflon Bearings in Aseismic Base Isolation: Experimental Studies and Mathematical Modeling," by A. Mokha, M.C. Constantinou and A.M. Reinhorn, 12/5/88, (PB89-218457, A10, MF-A01). This report is available only through NTIS (see address given above).

NCEER-88-0039   "Seismic Behavior of Flat Slab High-Rise Buildings in the New York City Area," by P. Weidlinger and M. Ettouney, 10/15/88, (PB90-145681, A04, MF-A01).

NCEER-88-0040   "Evaluation of the Earthquake Resistance of Existing Buildings in New York City," by P. Weidlinger and M. Ettouney, 10/15/88, to be published.

NCEER-88-0041   "Small-Scale Modeling Techniques for Reinforced Concrete Structures Subjected to Seismic Loads," by W. Kim, A. El-Attar and R.N. White, 11/22/88, (PB89-189625, A05, MF-A01).

NCEER-88-0042   "Modeling Strong Ground Motion from Multiple Event Earthquakes," by G.W. Ellis and A.S. Cakmak, 10/15/88, (PB89-174445, A03, MF-A01).

NCEER-88-0043   "Nonstationary Models of Seismic Ground Acceleration," by M. Grigoriu, S.E. Ruiz and E. Rosenblueth, 7/15/88, (PB89-189617, A04, MF-A01).

NCEER-88-0044   "SARCF User's Guide: Seismic Analysis of Reinforced Concrete Frames," by Y.S. Chung, C. Meyer and M. Shinozuka, 11/9/88, (PB89-174452, A08, MF-A01).

NCEER-88-0045   "First Expert Panel Meeting on Disaster Research and Planning," edited by J. Pantelic and J. Stoyle, 9/15/88, (PB89-174460, A05, MF-A01).

NCEER-88-0046   "Preliminary Studies of the Effect of Degrading Infill Walls on the Nonlinear Seismic Response of Steel Frames," by C.Z. Chrysostomou, P. Gergely and J.F. Abel, 12/19/88, (PB89-208383, A05, MF-A01).

NCEER-88-0047   "Reinforced Concrete Frame Component Testing Facility - Design, Construction, Instrumentation and Operation," by S.P. Pessiki, C. Conley, T. Bond, P. Gergely and R.N. White, 12/16/88, (PB89-174478, A04, MF-A01).

NCEER-89-0001   "Effects of Protective Cushion and Soil Compliancy on the Response of Equipment Within a Seismically Excited Building," by J.A. HoLung, 2/16/89, (PB89-207179, A04, MF-A01).

NCEER-89-0002   "Statistical Evaluation of Response Modification Factors for Reinforced Concrete Structures," by H.H-M. Hwang and J-W. Jaw, 2/17/89, (PB89-207187, A05, MF-A01).

NCEER-89-0003   "Hysteretic Columns Under Random Excitation," by G-Q. Cai and Y.K. Lin, 1/9/89, (PB89-196513, A03, MF-A01).

NCEER-89-0004   "Experimental Study of `Elephant Foot Bulge' Instability of Thin-Walled Metal Tanks," by Z-H. Jia and R.L. Ketter, 2/22/89, (PB89-207195, A03, MF-A01).

NCEER-89-0005   "Experiment on Performance of Buried Pipelines Across San Andreas Fault," by J. Isenberg, E. Richardson and T.D. O'Rourke, 3/10/89, (PB89-218440, A04, MF-A01). This report is available only through NTIS (see address given above).

NCEER-89-0006   "A Knowledge-Based Approach to Structural Design of Earthquake-Resistant Buildings," by M. Subramani, P. Gergely, C.H. Conley, J.F. Abel and A.H. Zaghw, 1/15/89, (PB89-218465, A06, MF-A01).

NCEER-89-0007   "Liquefaction Hazards and Their Effects on Buried Pipelines," by T.D. O'Rourke and P.A. Lane, 2/1/89, (PB89-218481, A09, MF-A01).

NCEER-89-0008   "Fundamentals of System Identification in Structural Dynamics," by H. Imai, C-B. Yun, O. Maruyama and M. Shinozuka, 1/26/89, (PB89-207211, A04, MF-A01).

NCEER-89-0009   "Effects of the 1985 Michoacan Earthquake on Water Systems and Other Buried Lifelines in Mexico," by A.G. Ayala and M.J. O'Rourke, 3/8/89, (PB89-207229, A06, MF-A01).

NCEER-89-R010   "NCEER Bibliography of Earthquake Education Materials," by K.E.K. Ross, Second Revision, 9/1/89, (PB90-125352, A05, MF-A01). This report is replaced by NCEER-92-0018.

NCEER-89-0011   "Inelastic Three-Dimensional Response Analysis of Reinforced Concrete Building Structures (IDARC-3D), Part I - Modeling," by S.K. Kunnath and A.M. Reinhorn, 4/17/89, (PB90-114612, A07, MF-A01). This report is available only through NTIS (see address given above).

NCEER-89-0012   "Recommended Modifications to ATC-14," by C.D. Poland and J.O. Malley, 4/12/89, (PB90-108648, A15, MF-A01).

NCEER-89-0013   "Repair and Strengthening of Beam-to-Column Connections Subjected to Earthquake Loading," by M. Corazao and A.J. Durrani, 2/28/89, (PB90-109885, A06, MF-A01).

NCEER-89-0014   "Program EXKAL2 for Identification of Structural Dynamic Systems," by O. Maruyama, C-B. Yun, M. Hoshiya and M. Shinozuka, 5/19/89, (PB90-109877, A09, MF-A01).

NCEER-89-0015   "Response of Frames With Bolted Semi-Rigid Connections, Part I - Experimental Study and Analytical Predictions," by P.J. DiCorso, A.M. Reinhorn, J.R. Dickerson, J.B. Radziminski and W.L. Harper, 6/1/89, to be published.

NCEER-89-0016   "ARMA Monte Carlo Simulation in Probabilistic Structural Analysis," by P.D. Spanos and M.P. Mignolet, 7/10/89, (PB90-109893, A03, MF-A01).

NCEER-89-P017   "Preliminary Proceedings from the Conference on Disaster Preparedness - The Place of Earthquake Education in Our Schools," Edited by K.E.K. Ross, 6/23/89, (PB90-108606, A03, MF-A01).

NCEER-89-0017   "Proceedings from the Conference on Disaster Preparedness - The Place of Earthquake Education in Our Schools," Edited by K.E.K. Ross, 12/31/89, (PB90-207895, A012, MF-A02). This report is available only through NTIS (see address given above).

NCEER-89-0018   "Multidimensional Models of Hysteretic Material Behavior for Vibration Analysis of Shape Memory Energy Absorbing Devices, by E.J. Graesser and F.A. Cozzarelli, 6/7/89, (PB90-164146, A04, MF-A01).

NCEER-89-0019   "Nonlinear Dynamic Analysis of Three-Dimensional Base Isolated Structures (3D-BASIS)," by S. Nagarajaiah, A.M. Reinhorn and M.C. Constantinou, 8/3/89, (PB90-161936, A06, MF-A01). This report has been replaced by NCEER-93-0011.

NCEER-89-0020   "Structural Control Considering Time-Rate of Control Forces and Control Rate Constraints," by F.Y. Cheng and C.P. Pantelides, 8/3/89, (PB90-120445, A04, MF-A01).

NCEER-89-0021   "Subsurface Conditions of Memphis and Shelby County," by K.W. Ng, T-S. Chang and H-H.M. Hwang, 7/26/89, (PB90-120437, A03, MF-A01).

NCEER-89-0022   "Seismic Wave Propagation Effects on Straight Jointed Buried Pipelines," by K. Elhmadi and M.J. O'Rourke, 8/24/89, (PB90-162322, A10, MF-A02).

NCEER-89-0023   "Workshop on Serviceability Analysis of Water Delivery Systems," edited by M. Grigoriu, 3/6/89, (PB90-127424, A03, MF-A01).

NCEER-89-0024   "Shaking Table Study of a 1/5 Scale Steel Frame Composed of Tapered Members," by K.C. Chang, J.S. Hwang and G.C. Lee, 9/18/89, (PB90-160169, A04, MF-A01).

NCEER-89-0025   "DYNA1D: A Computer Program for Nonlinear Seismic Site Response Analysis - Technical Documentation," by Jean H. Prevost, 9/14/89, (PB90-161944, A07, MF-A01). This report is available only through NTIS (see address given above).

NCEER-89-0026   "1:4 Scale Model Studies of Active Tendon Systems and Active Mass Dampers for Aseismic Protection," by A.M. Reinhorn, T.T. Soong, R.C. Lin, Y.P. Yang, Y. Fukao, H. Abe and M. Nakai, 9/15/89, (PB90-173246, A10, MF-A02). This report is available only through NTIS (see address given above).

NCEER-89-0027   "Scattering of Waves by Inclusions in a Nonhomogeneous Elastic Half Space Solved by Boundary Element Methods," by P.K. Hadley, A. Askar and A.S. Cakmak, 6/15/89, (PB90-145699, A07, MF-A01).

NCEER-89-0028   "Statistical Evaluation of Deflection Amplification Factors for Reinforced Concrete Structures," by H.H.M. Hwang, J-W. Jaw and A.L. Ch'ng, 8/31/89, (PB90-164633, A05, MF-A01).

NCEER-89-0029   "Bedrock Accelerations in Memphis Area Due to Large New Madrid Earthquakes," by H.H.M. Hwang, C.H.S. Chen and G. Yu, 11/7/89, (PB90-162330, A04, MF-A01).

NCEER-89-0030   "Seismic Behavior and Response Sensitivity of Secondary Structural Systems," by Y.Q. Chen and T.T. Soong, 10/23/89, (PB90-164658, A08, MF-A01).

NCEER-89-0031   "Random Vibration and Reliability Analysis of Primary-Secondary Structural Systems," by Y. Ibrahim, M. Grigoriu and T.T. Soong, 11/10/89, (PB90-161951, A04, MF-A01).

NCEER-89-0032   "Proceedings from the Second U.S. - Japan Workshop on Liquefaction, Large Ground Deformation and Their Effects on Lifelines, September 26-29, 1989," Edited by T.D. O'Rourke and M. Hamada, 12/1/89, (PB90-209388, A22, MF-A03).

NCEER-89-0033   "Deterministic Model for Seismic Damage Evaluation of Reinforced Concrete Structures," by J.M. Bracci, A.M. Reinhorn, J.B. Mander and S.K. Kunnath, 9/27/89, (PB91-108803, A06, MF-A01).

NCEER-89-0034   "On the Relation Between Local and Global Damage Indices," by E. DiPasquale and A.S. Cakmak, 8/15/89, (PB90-173865, A05, MF-A01).

NCEER-89-0035   "Cyclic Undrained Behavior of Nonplastic and Low Plasticity Silts," by A.J. Walker and H.E. Stewart, 7/26/89, (PB90-183518, A10, MF-A01).

NCEER-89-0036   "Liquefaction Potential of Surficial Deposits in the City of Buffalo, New York," by M. Budhu, R. Giese and L. Baumgrass, 1/17/89, (PB90-208455, A04, MF-A01).

NCEER-89-0037   "A Deterministic Assessment of Effects of Ground Motion Incoherence," by A.S. Veletsos and Y. Tang, 7/15/89, (PB90-164294, A03, MF-A01).

NCEER-89-0038   "Workshop on Ground Motion Parameters for Seismic Hazard Mapping," July 17-18, 1989, edited by R.V. Whitman, 12/1/89, (PB90-173923, A04, MF-A01).

NCEER-89-0039   "Seismic Effects on Elevated Transit Lines of the New York City Transit Authority," by C.J. Costantino, C.A. Miller and E. Heymsfield, 12/26/89, (PB90-207887, A06, MF-A01).

NCEER-89-0040   "Centrifugal Modeling of Dynamic Soil-Structure Interaction," by K. Weissman, Supervised by J.H. Prevost, 5/10/89, (PB90-207879, A07, MF-A01).

NCEER-89-0041   "Linearized Identification of Buildings With Cores for Seismic Vulnerability Assessment," by I-K. Ho and A.E. Aktan, 11/1/89, (PB90-251943, A07, MF-A01).

NCEER-90-0001   "Geotechnical and Lifeline Aspects of the October 17, 1989 Loma Prieta Earthquake in San Francisco," by T.D. O'Rourke, H.E. Stewart, F.T. Blackburn and T.S. Dickerman, 1/90, (PB90-208596, A05, MF-A01).

NCEER-90-0002   "Nonnormal Secondary Response Due to Yielding in a Primary Structure," by D.C.K. Chen and L.D. Lutes, 2/28/90, (PB90-251976, A07, MF-A01).

NCEER-90-0003   "Earthquake Education Materials for Grades K-12," by K.E.K. Ross, 4/16/90, (PB91-251984, A05, MF-A05). This report has been replaced by NCEER-92-0018.

NCEER-90-0004   "Catalog of Strong Motion Stations in Eastern North America," by R.W. Busby, 4/3/90, (PB90-251984, A05, MF-A01).

NCEER-90-0005   "NCEER Strong-Motion Data Base: A User Manual for the GeoBase Release (Version 1.0 for the Sun3)," by P. Friberg and K. Jacob, 3/31/90 (PB90-258062, A04, MF-A01).

NCEER-90-0006   "Seismic Hazard Along a Crude Oil Pipeline in the Event of an 1811-1812 Type New Madrid Earthquake," by H.H.M. Hwang and C-H.S. Chen, 4/16/90, (PB90-258054, A04, MF-A01).

NCEER-90-0007   "Site-Specific Response Spectra for Memphis Sheahan Pumping Station," by H.H.M. Hwang and C.S. Lee, 5/15/90, (PB91-108811, A05, MF-A01).

NCEER-90-0008   "Pilot Study on Seismic Vulnerability of Crude Oil Transmission Systems," by T. Ariman, R. Dobry, M. Grigoriu, F. Kozin, M. O'Rourke, T. O'Rourke and M. Shinozuka, 5/25/90, (PB91-108837, A06, MF-A01).

NCEER-90-0009   "A Program to Generate Site Dependent Time Histories: EQGEN," by G.W. Ellis, M. Srinivasan and A.S. Cakmak, 1/30/90, (PB91-108829, A04, MF-A01).

NCEER-90-0010   "Active Isolation for Seismic Protection of Operating Rooms," by M.E. Talbott, Supervised by M. Shinozuka, 6/8/9, (PB91-110205, A05, MF-A01).

NCEER-90-0011   "Program LINEARID for Identification of Linear Structural Dynamic Systems," by C-B. Yun and M. Shinozuka, 6/25/90, (PB91-110312, A08, MF-A01).

NCEER-90-0012   "Two-Dimensional Two-Phase Elasto-Plastic Seismic Response of Earth Dams," by A.N. Yiagos, Supervised by J.H. Prevost, 6/20/90, (PB91-110197, A13, MF-A02).

NCEER-90-0013   "Secondary Systems in Base-Isolated Structures: Experimental Investigation, Stochastic Response and Stochastic Sensitivity," by G.D. Manolis, G. Juhn, M.C. Constantinou and A.M. Reinhorn, 7/1/90, (PB91-110320, A08, MF-A01).

NCEER-90-0014   "Seismic Behavior of Lightly-Reinforced Concrete Column and Beam-Column Joint Details," by S.P. Pessiki, C.H. Conley, P. Gergely and R.N. White, 8/22/90, (PB91-108795, A11, MF-A02).

NCEER-90-0015   "Two Hybrid Control Systems for Building Structures Under Strong Earthquakes," by J.N. Yang and A. Danielians, 6/29/90, (PB91-125393, A04, MF-A01).

NCEER-90-0016   "Instantaneous Optimal Control with Acceleration and Velocity Feedback," by J.N. Yang and Z. Li, 6/29/90, (PB91-125401, A03, MF-A01).

NCEER-90-0017   "Reconnaissance Report on the Northern Iran Earthquake of June 21, 1990," by M. Mehrain, 10/4/90, (PB91-125377, A03, MF-A01).

NCEER-90-0018   "Evaluation of Liquefaction Potential in Memphis and Shelby County," by T.S. Chang, P.S. Tang, C.S. Lee and H. Hwang, 8/10/90, (PB91-125427, A09, MF-A01).

NCEER-90-0019   "Experimental and Analytical Study of a Combined Sliding Disc Bearing and Helical Steel Spring Isolation System," by M.C. Constantinou, A.S. Mokha and A.M. Reinhorn, 10/4/90, (PB91-125385, A06, MF-A01). This report is available only through NTIS (see address given above).

NCEER-90-0020   "Experimental Study and Analytical Prediction of Earthquake Response of a Sliding Isolation System with a Spherical Surface," by A.S. Mokha, M.C. Constantinou and A.M. Reinhorn, 10/11/90, (PB91-125419, A05, MF-A01).

NCEER-90-0021   "Dynamic Interaction Factors for Floating Pile Groups," by G. Gazetas, K. Fan, A. Kaynia and E. Kausel, 9/10/90, (PB91-170381, A05, MF-A01).

NCEER-90-0022   "Evaluation of Seismic Damage Indices for Reinforced Concrete Structures," by S. Rodriguez-Gomez and A.S. Cakmak, 9/30/90, PB91-171322, A06, MF-A01).

NCEER-90-0023   "Study of Site Response at a Selected Memphis Site," by H. Desai, S. Ahmad, E.S. Gazetas and M.R. Oh, 10/11/90, (PB91-196857, A03, MF-A01).

NCEER-90-0024   "A User's Guide to Strongmo: Version 1.0 of NCEER's Strong-Motion Data Access Tool for PCs and Terminals," by P.A. Friberg and C.A.T. Susch, 11/15/90, (PB91-171272, A03, MF-A01).

NCEER-90-0025   "A Three-Dimensional Analytical Study of Spatial Variability of Seismic Ground Motions," by L-L. Hong and A.H.-S. Ang, 10/30/90, (PB91-170399, A09, MF-A01).

NCEER-90-0026   "MUMOID User's Guide - A Program for the Identification of Modal Parameters," by S. Rodriguez-Gomez and E. DiPasquale, 9/30/90, (PB91-171298, A04, MF-A01).

NCEER-90-0027   "SARCF-II User's Guide - Seismic Analysis of Reinforced Concrete Frames," by S. Rodriguez-Gomez, Y.S. Chung and C. Meyer, 9/30/90, (PB91-171280, A05, MF-A01).

NCEER-90-0028   "Viscous Dampers: Testing, Modeling and Application in Vibration and Seismic Isolation," by N. Makris and M.C. Constantinou, 12/20/90 (PB91-190561, A06, MF-A01).

NCEER-90-0029   "Soil Effects on Earthquake Ground Motions in the Memphis Area," by H. Hwang, C.S. Lee, K.W. Ng and T.S. Chang, 8/2/90, (PB91-190751, A05, MF-A01).

NCEER-91-0001   "Proceedings from the Third Japan-U.S. Workshop on Earthquake Resistant Design of Lifeline Facilities and Countermeasures for Soil Liquefaction, December 17-19, 1990," edited by T.D. O'Rourke and M. Hamada, 2/1/91, (PB91-179259, A99, MF-A04).

NCEER-91-0002   "Physical Space Solutions of Non-Proportionally Damped Systems," by M. Tong, Z. Liang and G.C. Lee, 1/15/91, (PB91-179242, A04, MF-A01).

NCEER-91-0003   "Seismic Response of Single Piles and Pile Groups," by K. Fan and G. Gazetas, 1/10/91, (PB92-174994, A04, MF-A01).

NCEER-91-0004   "Damping of Structures: Part 1 - Theory of Complex Damping," by Z. Liang and G. Lee, 10/10/91, (PB92-197235, A12, MF-A03).

NCEER-91-0005   "3D-BASIS - Nonlinear Dynamic Analysis of Three Dimensional Base Isolated Structures: Part II," by S. Nagarajaiah, A.M. Reinhorn and M.C. Constantinou, 2/28/91, (PB91-190553, A07, MF-A01). This report has been replaced by NCEER-93-0011.

NCEER-91-0006   "A Multidimensional Hysteretic Model for Plasticity Deforming Metals in Energy Absorbing Devices," by E.J. Graesser and F.A. Cozzarelli, 4/9/91, (PB92-108364, A04, MF-A01).

NCEER-91-0007   "A Framework for Customizable Knowledge-Based Expert Systems with an Application to a KBES for Evaluating the Seismic Resistance of Existing Buildings," by E.G. Ibarra-Anaya and S.J. Fenves, 4/9/91, (PB91-210930, A08, MF-A01).

NCEER-91-0008   "Nonlinear Analysis of Steel Frames with Semi-Rigid Connections Using the Capacity Spectrum Method," by G.G. Deierlein, S-H. Hsieh, Y-J. Shen and J.F. Abel, 7/2/91, (PB92-113828, A05, MF-A01).

NCEER-91-0009   "Earthquake Education Materials for Grades K-12," by K.E.K. Ross, 4/30/91, (PB91-212142, A06, MF-A01). This report has been replaced by NCEER-92-0018.

NCEER-91-0010   "Phase Wave Velocities and Displacement Phase Differences in a Harmonically Oscillating Pile," by N. Makris and G. Gazetas, 7/8/91, (PB92-108356, A04, MF-A01).

NCEER-91-0011   "Dynamic Characteristics of a Full-Size Five-Story Steel Structure and a 2/5 Scale Model," by K.C. Chang, G.C. Yao, G.C. Lee, D.S. Hao and Y.C. Yeh," 7/2/91, (PB93-116648, A06, MF-A02).

NCEER-91-0012   "Seismic Response of a 2/5 Scale Steel Structure with Added Viscoelastic Dampers," by K.C. Chang, T.T. Soong, S-T. Oh and M.L. Lai, 5/17/91, (PB92-110816, A05, MF-A01).

NCEER-91-0013   "Earthquake Response of Retaining Walls; Full-Scale Testing and Computational Modeling," by S. Alampalli and A-W.M. Elgamal, 6/20/91, to be published.

NCEER-91-0014   "3D-BASIS-M: Nonlinear Dynamic Analysis of Multiple Building Base Isolated Structures," by P.C. Tsopelas, S. Nagarajaiah, M.C. Constantinou and A.M. Reinhorn, 5/28/91, (PB92-113885, A09, MF-A02).

NCEER-91-0015   "Evaluation of SEAOC Design Requirements for Sliding Isolated Structures," by D. Theodossiou and M.C. Constantinou, 6/10/91, (PB92-114602, A11, MF-A03).

NCEER-91-0016   "Closed-Loop Modal Testing of a 27-Story Reinforced Concrete Flat Plate-Core Building," by H.R. Somaprasad, T. Toksoy, H. Yoshiyuki and A.E. Aktan, 7/15/91, (PB92-129980, A07, MF-A02).

NCEER-91-0017   "Shake Table Test of a 1/6 Scale Two-Story Lightly Reinforced Concrete Building," by A.G. El-Attar, R.N. White and P. Gergely, 2/28/91, (PB92-222447, A06, MF-A02).

NCEER-91-0018   "Shake Table Test of a 1/8 Scale Three-Story Lightly Reinforced Concrete Building," by A.G. El-Attar, R.N. White and P. Gergely, 2/28/91, (PB93-116630, A08, MF-A02).

NCEER-91-0019   "Transfer Functions for Rigid Rectangular Foundations," by A.S. Veletsos, A.M. Prasad and W.H. Wu, 7/31/91, to be published.

NCEER-91-0020   "Hybrid Control of Seismic-Excited Nonlinear and Inelastic Structural Systems," by J.N. Yang, Z. Li and A. Danielians, 8/1/91, (PB92-143171, A06, MF-A02).

NCEER-91-0021   "The NCEER-91 Earthquake Catalog: Improved Intensity-Based Magnitudes and Recurrence Relations for U.S. Earthquakes East of New Madrid," by L. Seeber and J.G. Armbruster, 8/28/91, (PB92-176742, A06, MF-A02).

NCEER-91-0022   "Proceedings from the Implementation of Earthquake Planning and Education in Schools: The Need for Change - The Roles of the Changemakers," by K.E.K. Ross and F. Winslow, 7/23/91, (PB92-129998, A12, MF-A03).

NCEER-91-0023   "A Study of Reliability-Based Criteria for Seismic Design of Reinforced Concrete Frame Buildings," by H.H.M. Hwang and H-M. Hsu, 8/10/91, (PB92-140235, A09, MF-A02).

NCEER-91-0024   "Experimental Verification of a Number of Structural System Identification Algorithms," by R.G. Ghanem, H. Gavin and M. Shinozuka, 9/18/91, (PB92-176577, A18, MF-A04).

NCEER-91-0025   "Probabilistic Evaluation of Liquefaction Potential," by H.H.M. Hwang and C.S. Lee," 11/25/91, (PB92-143429, A05, MF-A01).

NCEER-91-0026   "Instantaneous Optimal Control for Linear, Nonlinear and Hysteretic Structures - Stable Controllers," by J.N. Yang and Z. Li, 11/15/91, (PB92-163807, A04, MF-A01).

NCEER-91-0027   "Experimental and Theoretical Study of a Sliding Isolation System for Bridges," by M.C. Constantinou, A. Kartoum, A.M. Reinhorn and P. Bradford, 11/15/91, (PB92-176973, A10, MF-A03).

NCEER-92-0001   "Case Studies of Liquefaction and Lifeline Performance During Past Earthquakes, Volume 1: Japanese Case Studies," Edited by M. Hamada and T. O'Rourke, 2/17/92, (PB92-197243, A18, MF-A04).

NCEER-92-0002   "Case Studies of Liquefaction and Lifeline Performance During Past Earthquakes, Volume 2: United States Case Studies," Edited by T. O'Rourke and M. Hamada, 2/17/92, (PB92-197250, A20, MF-A04).

NCEER-92-0003   "Issues in Earthquake Education," Edited by K. Ross, 2/3/92, (PB92-222389, A07, MF-A02).

NCEER-92-0004   "Proceedings from the First U.S. - Japan Workshop on Earthquake Protective Systems for Bridges," Edited by I.G. Buckle, 2/4/92, (PB94-142239, A99, MF-A06).

NCEER-92-0005   "Seismic Ground Motion from a Haskell-Type Source in a Multiple-Layered Half-Space," A.P. Theoharis, G. Deodatis and M. Shinozuka, 1/2/92, to be published.

NCEER-92-0006   "Proceedings from the Site Effects Workshop," Edited by R. Whitman, 2/29/92, (PB92-197201, A04, MF-A01).

NCEER-92-0007   "Engineering Evaluation of Permanent Ground Deformations Due to Seismically-Induced Liquefaction," by M.H. Baziar, R. Dobry and A-W.M. Elgamal, 3/24/92, (PB92-222421, A13, MF-A03).

NCEER-92-0008   "A Procedure for the Seismic Evaluation of Buildings in the Central and Eastern United States," by C.D. Poland and J.O. Malley, 4/2/92, (PB92-222439, A20, MF-A04).

NCEER-92-0009   "Experimental and Analytical Study of a Hybrid Isolation System Using Friction Controllable Sliding Bearings," by M.Q. Feng, S. Fujii and M. Shinozuka, 5/15/92, (PB93-150282, A06, MF-A02).

NCEER-92-0010   "Seismic Resistance of Slab-Column Connections in Existing Non-Ductile Flat-Plate Buildings," by A.J. Durrani and Y. Du, 5/18/92, (PB93-116812, A06, MF-A02).

NCEER-92-0011   "The Hysteretic and Dynamic Behavior of Brick Masonry Walls Upgraded by Ferrocement Coatings Under Cyclic Loading and Strong Simulated Ground Motion," by H. Lee and S.P. Prawel, 5/11/92, to be published.

NCEER-92-0012   "Study of Wire Rope Systems for Seismic Protection of Equipment in Buildings," by G.F. Demetriades, M.C. Constantinou and A.M. Reinhorn, 5/20/92, (PB93-116655, A08, MF-A02).

NCEER-92-0013 "Shape Memory Structural Dampers: Material Properties, Design and Seismic Testing," by P.R. Witting and F.A. Cozzarelli, 5/26/92, (PB93-116663, A05, MF-A01).

NCEER-92-0014 "Longitudinal Permanent Ground Deformation Effects on Buried Continuous Pipelines," by M.J. O'Rourke, and C. Nordberg, 6/15/92, (PB93-116671, A08, MF-A02).

NCEER-92-0015 "A Simulation Method for Stationary Gaussian Random Functions Based on the Sampling Theorem," by M. Grigoriu and S. Balopoulou, 6/11/92, (PB93-127496, A05, MF-A01).

NCEER-92-0016 "Gravity-Load-Designed Reinforced Concrete Buildings: Seismic Evaluation of Existing Construction and Detailing Strategies for Improved Seismic Resistance," by G.W. Hoffmann, S.K. Kunnath, A.M. Reinhorn and J.B. Mander, 7/15/92, (PB94-142007, A08, MF-A02).

NCEER-92-0017 "Observations on Water System and Pipeline Performance in the Limón Area of Costa Rica Due to the April 22, 1991 Earthquake," by M. O'Rourke and D. Ballantyne, 6/30/92, (PB93-126811, A06, MF-A02).

NCEER-92-0018 "Fourth Edition of Earthquake Education Materials for Grades K-12," Edited by K.E.K. Ross, 8/10/92, (PB93-114023, A07, MF-A02).

NCEER-92-0019 "Proceedings from the Fourth Japan-U.S. Workshop on Earthquake Resistant Design of Lifeline Facilities and Countermeasures for Soil Liquefaction," Edited by M. Hamada and T.D. O'Rourke, 8/12/92, (PB93-163939, A99, MF-E11).

NCEER-92-0020 "Active Bracing System: A Full Scale Implementation of Active Control," by A.M. Reinhorn, T.T. Soong, R.C. Lin, M.A. Riley, Y.P. Wang, S. Aizawa and M. Higashino, 8/14/92, (PB93-127512, A06, MF-A02).

NCEER-92-0021 "Empirical Analysis of Horizontal Ground Displacement Generated by Liquefaction-Induced Lateral Spreads," by S.F. Bartlett and T.L. Youd, 8/17/92, (PB93-188241, A06, MF-A02).

NCEER-92-0022 "IDARC Version 3.0: Inelastic Damage Analysis of Reinforced Concrete Structures," by S.K. Kunnath, A.M. Reinhorn and R.F. Lobo, 8/31/92, (PB93-227502, A07, MF-A02).

NCEER-92-0023 "A Semi-Empirical Analysis of Strong-Motion Peaks in Terms of Seismic Source, Propagation Path and Local Site Conditions, by M. Kamiyama, M.J. O'Rourke and R. Flores-Berrones, 9/9/92, (PB93-150266, A08, MF-A02).

NCEER-92-0024 "Seismic Behavior of Reinforced Concrete Frame Structures with Nonductile Details, Part I: Summary of Experimental Findings of Full Scale Beam-Column Joint Tests," by A. Beres, R.N. White and P. Gergely, 9/30/92, (PB93-227783, A05, MF-A01).

NCEER-92-0025 "Experimental Results of Repaired and Retrofitted Beam-Column Joint Tests in Lightly Reinforced Concrete Frame Buildings," by A. Beres, S. El-Borgi, R.N. White and P. Gergely, 10/29/92, (PB93-227791, A05, MF-A01).

NCEER-92-0026 "A Generalization of Optimal Control Theory: Linear and Nonlinear Structures," by J.N. Yang, Z. Li and S. Vongchavalitkul, 11/2/92, (PB93-188621, A05, MF-A01).

NCEER-92-0027 "Seismic Resistance of Reinforced Concrete Frame Structures Designed Only for Gravity Loads: Part I - Design and Properties of a One-Third Scale Model Structure," by J.M. Bracci, A.M. Reinhorn and J.B. Mander, 12/1/92, (PB94-104502, A08, MF-A02).

NCEER-92-0028 "Seismic Resistance of Reinforced Concrete Frame Structures Designed Only for Gravity Loads: Part II - Experimental Performance of Subassemblages," by L.E. Aycardi, J.B. Mander and A.M. Reinhorn, 12/1/92, (PB94-104510, A08, MF-A02).

NCEER-92-0029 "Seismic Resistance of Reinforced Concrete Frame Structures Designed Only for Gravity Loads: Part III - Experimental Performance and Analytical Study of a Structural Model," by J.M. Bracci, A.M. Reinhorn and J.B. Mander, 12/1/92, (PB93-227528, A09, MF-A01).

NCEER-92-0030   "Evaluation of Seismic Retrofit of Reinforced Concrete Frame Structures: Part I - Experimental Performance of Retrofitted Subassemblages," by D. Choudhuri, J.B. Mander and A.M. Reinhorn, 12/8/92, (PB93-198307, A07, MF-A02).

NCEER-92-0031   "Evaluation of Seismic Retrofit of Reinforced Concrete Frame Structures: Part II - Experimental Performance and Analytical Study of a Retrofitted Structural Model," by J.M. Bracci, A.M. Reinhorn and J.B. Mander, 12/8/92, (PB93-198315, A09, MF-A03).

NCEER-92-0032   "Experimental and Analytical Investigation of Seismic Response of Structures with Supplemental Fluid Viscous Dampers," by M.C. Constantinou and M.D. Symans, 12/21/92, (PB93-191435, A10, MF-A03). This report is available only through NTIS (see address given above).

NCEER-92-0033   "Reconnaissance Report on the Cairo, Egypt Earthquake of October 12, 1992," by M. Khater, 12/23/92, (PB93-188621, A03, MF-A01).

NCEER-92-0034   "Low-Level Dynamic Characteristics of Four Tall Flat-Plate Buildings in New York City," by H. Gavin, S. Yuan, J. Grossman, E. Pekelis and K. Jacob, 12/28/92, (PB93-188217, A07, MF-A02).

NCEER-93-0001   "An Experimental Study on the Seismic Performance of Brick-Infilled Steel Frames With and Without Retrofit," by J.B. Mander, B. Nair, K. Wojtkowski and J. Ma, 1/29/93, (PB93-227510, A07, MF-A02).

NCEER-93-0002   "Social Accounting for Disaster Preparedness and Recovery Planning," by S. Cole, E. Pantoja and V. Razak, 2/22/93, (PB94-142114, A12, MF-A03).

NCEER-93-0003   "Assessment of 1991 NEHRP Provisions for Nonstructural Components and Recommended Revisions," by T.T. Soong, G. Chen, Z. Wu, R-H. Zhang and M. Grigoriu, 3/1/93, (PB93-188639, A06, MF-A02).

NCEER-93-0004   "Evaluation of Static and Response Spectrum Analysis Procedures of SEAOC/UBC for Seismic Isolated Structures," by C.W. Winters and M.C. Constantinou, 3/23/93, (PB93-198299, A10, MF-A03).

NCEER-93-0005   "Earthquakes in the Northeast - Are We Ignoring the Hazard? A Workshop on Earthquake Science and Safety for Educators," edited by K.E.K. Ross, 4/2/93, (PB94-103066, A09, MF-A02).

NCEER-93-0006   "Inelastic Response of Reinforced Concrete Structures with Viscoelastic Braces," by R.F. Lobo, J.M. Bracci, K.L. Shen, A.M. Reinhorn and T.T. Soong, 4/5/93, (PB93-227486, A05, MF-A02).

NCEER-93-0007   "Seismic Testing of Installation Methods for Computers and Data Processing Equipment," by K. Kosar, T.T. Soong, K.L. Shen, J.A. HoLung and Y.K. Lin, 4/12/93, (PB93-198299, A07, MF-A02).

NCEER-93-0008   "Retrofit of Reinforced Concrete Frames Using Added Dampers," by A. Reinhorn, M. Constantinou and C. Li, to be published.

NCEER-93-0009   "Seismic Behavior and Design Guidelines for Steel Frame Structures with Added Viscoelastic Dampers," by K.C. Chang, M.L. Lai, T.T. Soong, D.S. Hao and Y.C. Yeh, 5/1/93, (PB94-141959, A07, MF-A02).

NCEER-93-0010   "Seismic Performance of Shear-Critical Reinforced Concrete Bridge Piers," by J.B. Mander, S.M. Waheed, M.T.A. Chaudhary and S.S. Chen, 5/12/93, (PB93-227494, A08, MF-A02).

NCEER-93-0011   "3D-BASIS-TABS: Computer Program for Nonlinear Dynamic Analysis of Three Dimensional Base Isolated Structures," by S. Nagarajaiah, C. Li, A.M. Reinhorn and M.C. Constantinou, 8/2/93, (PB94-141819, A09, MF-A02).

NCEER-93-0012   "Effects of Hydrocarbon Spills from an Oil Pipeline Break on Ground Water," by O.J. Helweg and H.H.M. Hwang, 8/3/93, (PB94-141942, A06, MF-A02).

NCEER-93-0013   "Simplified Procedures for Seismic Design of Nonstructural Components and Assessment of Current Code Provisions," by M.P. Singh, L.E. Suarez, E.E. Matheu and G.O. Maldonado, 8/4/93, (PB94-141827, A09, MF-A02).

NCEER-93-0014   "An Energy Approach to Seismic Analysis and Design of Secondary Systems," by G. Chen and T.T. Soong, 8/6/93, (PB94-142767, A11, MF-A03).

NCEER-93-0015   "Proceedings from School Sites: Becoming Prepared for Earthquakes - Commemorating the Third Anniversary of the Loma Prieta Earthquake," Edited by F.E. Winslow and K.E.K. Ross, 8/16/93, (PB94-154275, A16, MF-A02).

NCEER-93-0016   "Reconnaissance Report of Damage to Historic Monuments in Cairo, Egypt Following the October 12, 1992 Dahshur Earthquake," by D. Sykora, D. Look, G. Croci, E. Karaesmen and E. Karaesmen, 8/19/93, (PB94-142221, A08, MF-A02).

NCEER-93-0017   "The Island of Guam Earthquake of August 8, 1993," by S.W. Swan and S.K. Harris, 9/30/93, (PB94-141843, A04, MF-A01).

NCEER-93-0018   "Engineering Aspects of the October 12, 1992 Egyptian Earthquake," by A.W. Elgamal, M. Amer, K. Adalier and A. Abul-Fadl, 10/7/93, (PB94-141983, A05, MF-A01).

NCEER-93-0019   "Development of an Earthquake Motion Simulator and its Application in Dynamic Centrifuge Testing," by I. Krstelj, Supervised by J.H. Prevost, 10/23/93, (PB94-181773, A-10, MF-A03).

NCEER-93-0020   "NCEER-Taisei Corporation Research Program on Sliding Seismic Isolation Systems for Bridges: Experimental and Analytical Study of a Friction Pendulum System (FPS)," by M.C. Constantinou, P. Tsopelas, Y-S. Kim and S. Okamoto, 11/1/93, (PB94-142775, A08, MF-A02).

NCEER-93-0021   "Finite Element Modeling of Elastomeric Seismic Isolation Bearings," by L.J. Billings, Supervised by R. Shepherd, 11/8/93, to be published.

NCEER-93-0022   "Seismic Vulnerability of Equipment in Critical Facilities: Life-Safety and Operational Consequences," by K. Porter, G.S. Johnson, M.M. Zadeh, C. Scawthorn and S. Eder, 11/24/93, (PB94-181765, A16, MF-A03).

NCEER-93-0023   "Hokkaido Nansei-oki, Japan Earthquake of July 12, 1993, by P.I. Yanev and C.R. Scawthorn, 12/23/93, (PB94-181500, A07, MF-A01).

NCEER-94-0001   "An Evaluation of Seismic Serviceability of Water Supply Networks with Application to the San Francisco Auxiliary Water Supply System," by I. Markov, Supervised by M. Grigoriu and T. O'Rourke, 1/21/94, (PB94-204013, A07, MF-A02).

NCEER-94-0002   "NCEER-Taisei Corporation Research Program on Sliding Seismic Isolation Systems for Bridges: Experimental and Analytical Study of Systems Consisting of Sliding Bearings, Rubber Restoring Force Devices and Fluid Dampers," Volumes I and II, by P. Tsopelas, S. Okamoto, M.C. Constantinou, D. Ozaki and S. Fujii, 2/4/94, (PB94-181740, A09, MF-A02 and PB94-181757, A12, MF-A03).

NCEER-94-0003   "A Markov Model for Local and Global Damage Indices in Seismic Analysis," by S. Rahman and M. Grigoriu, 2/18/94, (PB94-206000, A12, MF-A03).

NCEER-94-0004   "Proceedings from the NCEER Workshop on Seismic Response of Masonry Infills," edited by D.P. Abrams, 3/1/94, (PB94-180783, A07, MF-A02).

NCEER-94-0005   "The Northridge, California Earthquake of January 17, 1994: General Reconnaissance Report," edited by J.D. Goltz, 3/11/94, (PB94-193943, A10, MF-A03).

NCEER-94-0006   "Seismic Energy Based Fatigue Damage Analysis of Bridge Columns: Part I - Evaluation of Seismic Capacity," by G.A. Chang and J.B. Mander, 3/14/94, (PB94-219185, A11, MF-A03).

NCEER-94-0007   "Seismic Isolation of Multi-Story Frame Structures Using Spherical Sliding Isolation Systems," by T.M. Al-Hussaini, V.A. Zayas and M.C. Constantinou, 3/17/94, (PB94-193745, A09, MF-A02).

NCEER-94-0008   "The Northridge, California Earthquake of January 17, 1994: Performance of Highway Bridges," edited by I.G. Buckle, 3/24/94, (PB94-193851, A06, MF-A02).

NCEER-94-0009   "Proceedings of the Third U.S.-Japan Workshop on Earthquake Protective Systems for Bridges," edited by I.G. Buckle and I. Friedland, 3/31/94, (PB94-195815, A99, MF-A06).

NCEER-94-0010   "3D-BASIS-ME: Computer Program for Nonlinear Dynamic Analysis of Seismically Isolated Single and Multiple Structures and Liquid Storage Tanks," by P.C. Tsopelas, M.C. Constantinou and A.M. Reinhorn, 4/12/94, (PB94-204922, A09, MF-A02).

NCEER-94-0011   "The Northridge, California Earthquake of January 17, 1994: Performance of Gas Transmission Pipelines," by T.D. O'Rourke and M.C. Palmer, 5/16/94, (PB94-204989, A05, MF-A01).

NCEER-94-0012   "Feasibility Study of Replacement Procedures and Earthquake Performance Related to Gas Transmission Pipelines," by T.D. O'Rourke and M.C. Palmer, 5/25/94, (PB94-206638, A09, MF-A02).

NCEER-94-0013   "Seismic Energy Based Fatigue Damage Analysis of Bridge Columns: Part II - Evaluation of Seismic Demand," by G.A. Chang and J.B. Mander, 6/1/94, (PB95-18106, A08, MF-A02).

NCEER-94-0014   "NCEER-Taisei Corporation Research Program on Sliding Seismic Isolation Systems for Bridges: Experimental and Analytical Study of a System Consisting of Sliding Bearings and Fluid Restoring Force/Damping Devices," by P. Tsopelas and M.C. Constantinou, 6/13/94, (PB94-219144, A10, MF-A03).

NCEER-94-0015   "Generation of Hazard-Consistent Fragility Curves for Seismic Loss Estimation Studies," by H. Hwang and J-R. Huo, 6/14/94, (PB95-181996, A09, MF-A02).

NCEER-94-0016   "Seismic Study of Building Frames with Added Energy-Absorbing Devices," by W.S. Pong, C.S. Tsai and G.C. Lee, 6/20/94, (PB94-219136, A10, A03).

NCEER-94-0017   "Sliding Mode Control for Seismic-Excited Linear and Nonlinear Civil Engineering Structures," by J. Yang, J. Wu, A. Agrawal and Z. Li, 6/21/94, (PB95-138483, A06, MF-A02).

NCEER-94-0018   "3D-BASIS-TABS Version 2.0: Computer Program for Nonlinear Dynamic Analysis of Three Dimensional Base Isolated Structures," by A.M. Reinhorn, S. Nagarajaiah, M.C. Constantinou, P. Tsopelas and R. Li, 6/22/94, (PB95-182176, A08, MF-A02).

NCEER-94-0019   "Proceedings of the International Workshop on Civil Infrastructure Systems: Application of Intelligent Systems and Advanced Materials on Bridge Systems," Edited by G.C. Lee and K.C. Chang, 7/18/94, (PB95-252474, A20, MF-A04).

NCEER-94-0020   "Study of Seismic Isolation Systems for Computer Floors," by V. Lambrou and M.C. Constantinou, 7/19/94, (PB95-138533, A10, MF-A03).

NCEER-94-0021   "Proceedings of the U.S.-Italian Workshop on Guidelines for Seismic Evaluation and Rehabilitation of Unreinforced Masonry Buildings," Edited by D.P. Abrams and G.M. Calvi, 7/20/94, (PB95-138749, A13, MF-A03).

NCEER-94-0022   "NCEER-Taisei Corporation Research Program on Sliding Seismic Isolation Systems for Bridges: Experimental and Analytical Study of a System Consisting of Lubricated PTFE Sliding Bearings and Mild Steel Dampers," by P. Tsopelas and M.C. Constantinou, 7/22/94, (PB95-182184, A08, MF-A02).

NCEER-94-0023   "Development of Reliability-Based Design Criteria for Buildings Under Seismic Load," by Y.K. Wen, H. Hwang and M. Shinozuka, 8/1/94, (PB95-211934, A08, MF-A02).

NCEER-94-0024   "Experimental Verification of Acceleration Feedback Control Strategies for an Active Tendon System," by S.J. Dyke, B.F. Spencer, Jr., P. Quast, M.K. Sain, D.C. Kaspari, Jr. and T.T. Soong, 8/29/94, (PB95-212320, A05, MF-A01).

NCEER-94-0025   "Seismic Retrofitting Manual for Highway Bridges," Edited by I.G. Buckle and I.F. Friedland, published by the Federal Highway Administration (PB95-212676, A15, MF-A03).

NCEER-94-0026   "Proceedings from the Fifth U.S.-Japan Workshop on Earthquake Resistant Design of Lifeline Facilities and Countermeasures Against Soil Liquefaction," Edited by T.D. O'Rourke and M. Hamada, 11/7/94, (PB95-220802, A99, MF-E08).

NCEER-95-0001 "Experimental and Analytical Investigation of Seismic Retrofit of Structures with Supplemental Damping: Part 1 - Fluid Viscous Damping Devices," by A.M. Reinhorn, C. Li and M.C. Constantinou, 1/3/95, (PB95-266599, A09, MF-A02).

NCEER-95-0002 "Experimental and Analytical Study of Low-Cycle Fatigue Behavior of Semi-Rigid Top-And-Seat Angle Connections," by G. Pekcan, J.B. Mander and S.S. Chen, 1/5/95, (PB95-220042, A07, MF-A02).

NCEER-95-0003 "NCEER-ATC Joint Study on Fragility of Buildings," by T. Anagnos, C. Rojahn and A.S. Kiremidjian, 1/20/95, (PB95-220026, A06, MF-A02).

NCEER-95-0004 "Nonlinear Control Algorithms for Peak Response Reduction," by Z. Wu, T.T. Soong, V. Gattulli and R.C. Lin, 2/16/95, (PB95-220349, A05, MF-A01).

NCEER-95-0005 "Pipeline Replacement Feasibility Study: A Methodology for Minimizing Seismic and Corrosion Risks to Underground Natural Gas Pipelines," by R.T. Eguchi, H.A. Seligson and D.G. Honegger, 3/2/95, (PB95-252326, A06, MF-A02).

NCEER-95-0006 "Evaluation of Seismic Performance of an 11-Story Frame Building During the 1994 Northridge Earthquake," by F. Naeim, R. DiSulio, K. Benuska, A. Reinhorn and C. Li, to be published.

NCEER-95-0007 "Prioritization of Bridges for Seismic Retrofitting," by N. Basöz and A.S. Kiremidjian, 4/24/95, (PB95-252300, A08, MF-A02).

NCEER-95-0008 "Method for Developing Motion Damage Relationships for Reinforced Concrete Frames," by A. Singhal and A.S. Kiremidjian, 5/11/95, (PB95-266607, A06, MF-A02).

NCEER-95-0009 "Experimental and Analytical Investigation of Seismic Retrofit of Structures with Supplemental Damping: Part II - Friction Devices," by C. Li and A.M. Reinhorn, 7/6/95, (PB96-128087, A11, MF-A03).

NCEER-95-0010 "Experimental Performance and Analytical Study of a Non-Ductile Reinforced Concrete Frame Structure Retrofitted with Elastomeric Spring Dampers," by G. Pekcan, J.B. Mander and S.S. Chen, 7/14/95, (PB96-137161, A08, MF-A02).

NCEER-95-0011 "Development and Experimental Study of Semi-Active Fluid Damping Devices for Seismic Protection of Structures," by M.D. Symans and M.C. Constantinou, 8/3/95, (PB96-136940, A23, MF-A04).

NCEER-95-0012 "Real-Time Structural Parameter Modification (RSPM): Development of Innervated Structures," by Z. Liang, M. Tong and G.C. Lee, 4/11/95, (PB96-137153, A06, MF-A01).

NCEER-95-0013 "Experimental and Analytical Investigation of Seismic Retrofit of Structures with Supplemental Damping: Part III - Viscous Damping Walls," by A.M. Reinhorn and C. Li, 10/1/95, (PB96-176409, A11, MF-A03).

NCEER-95-0014 "Seismic Fragility Analysis of Equipment and Structures in a Memphis Electric Substation," by J-R. Huo and H.H.M. Hwang, 8/10/95, (PB96-128087, A09, MF-A02).

NCEER-95-0015 "The Hanshin-Awaji Earthquake of January 17, 1995: Performance of Lifelines," Edited by M. Shinozuka, 11/3/95, (PB96-176383, A15, MF-A03).

NCEER-95-0016 "Highway Culvert Performance During Earthquakes," by T.L. Youd and C.J. Beckman, available as NCEER-96-0015.

NCEER-95-0017 "The Hanshin-Awaji Earthquake of January 17, 1995: Performance of Highway Bridges," Edited by I.G. Buckle, 12/1/95, to be published.

NCEER-95-0018 "Modeling of Masonry Infill Panels for Structural Analysis," by A.M. Reinhorn, A. Madan, R.E. Valles, Y. Reichmann and J.B. Mander, 12/8/95, (PB97-110886, MF-A01, A06).

NCEER-95-0019 "Optimal Polynomial Control for Linear and Nonlinear Structures," by A.K. Agrawal and J.N. Yang, 12/11/95, (PB96-168737, A07, MF-A02).

NCEER-95-0020 "Retrofit of Non-Ductile Reinforced Concrete Frames Using Friction Dampers," by R.S. Rao, P. Gergely and R.N. White, 12/22/95, (PB97-133508, A10, MF-A02).

NCEER-95-0021 "Parametric Results for Seismic Response of Pile-Supported Bridge Bents," by G. Mylonakis, A. Nikolaou and G. Gazetas, 12/22/95, (PB97-100242, A12, MF-A03).

NCEER-95-0022 "Kinematic Bending Moments in Seismically Stressed Piles," by A. Nikolaou, G. Mylonakis and G. Gazetas, 12/23/95, (PB97-113914, MF-A03, A13).

NCEER-96-0001 "Dynamic Response of Unreinforced Masonry Buildings with Flexible Diaphragms," by A.C. Costley and D.P. Abrams," 10/10/96, (PB97-133573, MF-A03, A15).

NCEER-96-0002 "State of the Art Review: Foundations and Retaining Structures," by I. Po Lam, to be published.

NCEER-96-0003 "Ductility of Rectangular Reinforced Concrete Bridge Columns with Moderate Confinement," by N. Wehbe, M. Saiidi, D. Sanders and B. Douglas, 11/7/96, (PB97-133557, A06, MF-A02).

NCEER-96-0004 "Proceedings of the Long-Span Bridge Seismic Research Workshop," edited by I.G. Buckle and I.M. Friedland, to be published.

NCEER-96-0005 "Establish Representative Pier Types for Comprehensive Study: Eastern United States," by J. Kulicki and Z. Prucz, 5/28/96, (PB98-119217, A07, MF-A02).

NCEER-96-0006 "Establish Representative Pier Types for Comprehensive Study: Western United States," by R. Imbsen, R.A. Schamber and T.A. Osterkamp, 5/28/96, (PB98-118607, A07, MF-A02).

NCEER-96-0007 "Nonlinear Control Techniques for Dynamical Systems with Uncertain Parameters," by R.G. Ghanem and M.I. Bujakov, 5/27/96, (PB97-100259, A17, MF-A03).

NCEER-96-0008 "Seismic Evaluation of a 30-Year Old Non-Ductile Highway Bridge Pier and Its Retrofit," by J.B. Mander, B. Mahmoodzadegan, S. Bhadra and S.S. Chen, 5/31/96, (PB97-110902, MF-A03, A10).

NCEER-96-0009 "Seismic Performance of a Model Reinforced Concrete Bridge Pier Before and After Retrofit," by J.B. Mander, J.H. Kim and C.A. Ligozio, 5/31/96, (PB97-110910, MF-A02, A10).

NCEER-96-0010 "IDARC2D Version 4.0: A Computer Program for the Inelastic Damage Analysis of Buildings," by R.E. Valles, A.M. Reinhorn, S.K. Kunnath, C. Li and A. Madan, 6/3/96, (PB97-100234, A17, MF-A03).

NCEER-96-0011 "Estimation of the Economic Impact of Multiple Lifeline Disruption: Memphis Light, Gas and Water Division Case Study," by S.E. Chang, H.A. Seligson and R.T. Eguchi, 8/16/96, (PB97-133490, A11, MF-A03).

NCEER-96-0012 "Proceedings from the Sixth Japan-U.S. Workshop on Earthquake Resistant Design of Lifeline Facilities and Countermeasures Against Soil Liquefaction, Edited by M. Hamada and T. O'Rourke, 9/11/96, (PB97-133581, A99, MF-A06).

NCEER-96-0013 "Chemical Hazards, Mitigation and Preparedness in Areas of High Seismic Risk: A Methodology for Estimating the Risk of Post-Earthquake Hazardous Materials Release," by H.A. Seligson, R.T. Eguchi, K.J. Tierney and K. Richmond, 11/7/96, (PB97-133565, MF-A02, A08).

NCEER-96-0014 "Response of Steel Bridge Bearings to Reversed Cyclic Loading," by J.B. Mander, D-K. Kim, S.S. Chen and G.J. Premus, 11/13/96, (PB97-140735, A12, MF-A03).

NCEER-96-0015 "Highway Culvert Performance During Past Earthquakes," by T.L. Youd and C.J. Beckman, 11/25/96, (PB97-133532, A06, MF-A01).

NCEER-97-0001 "Evaluation, Prevention and Mitigation of Pounding Effects in Building Structures," by R.E. Valles and A.M. Reinhorn, 2/20/97, (PB97-159552, A14, MF-A03).

NCEER-97-0002 "Seismic Design Criteria for Bridges and Other Highway Structures," by C. Rojahn, R. Mayes, D.G. Anderson, J. Clark, J.H. Hom, R.V. Nutt and M.J. O'Rourke, 4/30/97, (PB97-194658, A06, MF-A03).

NCEER-97-0003   "Proceedings of the U.S.-Italian Workshop on Seismic Evaluation and Retrofit," Edited by D.P. Abrams and G.M. Calvi, 3/19/97, (PB97-194666, A13, MF-A03).

NCEER-97-0004   "Investigation of Seismic Response of Buildings with Linear and Nonlinear Fluid Viscous Dampers," by A.A. Seleemah and M.C. Constantinou, 5/21/97, (PB98-109002, A15, MF-A03).

NCEER-97-0005   "Proceedings of the Workshop on Earthquake Engineering Frontiers in Transportation Facilities," edited by G.C. Lee and I.M. Friedland, 8/29/97, (PB98-128911, A25, MR-A04).

NCEER-97-0006   "Cumulative Seismic Damage of Reinforced Concrete Bridge Piers," by S.K. Kunnath, A. El-Bahy, A. Taylor and W. Stone, 9/2/97, (PB98-108814, A11, MF-A03).

NCEER-97-0007   "Structural Details to Accommodate Seismic Movements of Highway Bridges and Retaining Walls," by R.A. Imbsen, R.A. Schamber, E. Thorkildsen, A. Kartoum, B.T. Martin, T.N. Rosser and J.M. Kulicki, 9/3/97, (PB98-108996, A09, MF-A02).

NCEER-97-0008   "A Method for Earthquake Motion-Damage Relationships with Application to Reinforced Concrete Frames," by A. Singhal and A.S. Kiremidjian, 9/10/97, (PB98-108988, A13, MF-A03).

NCEER-97-0009   "Seismic Analysis and Design of Bridge Abutments Considering Sliding and Rotation," by K. Fishman and R. Richards, Jr., 9/15/97, (PB98-108897, A06, MF-A02).

NCEER-97-0010   "Proceedings of the FHWA/NCEER Workshop on the National Representation of Seismic Ground Motion for New and Existing Highway Facilities," edited by I.M. Friedland, M.S. Power and R.L. Mayes, 9/22/97, (PB98-128903, A21, MF-A04).

NCEER-97-0011   "Seismic Analysis for Design or Retrofit of Gravity Bridge Abutments," by K.L. Fishman, R. Richards, Jr. and R.C. Divito, 10/2/97, (PB98-128937, A08, MF-A02).

NCEER-97-0012   "Evaluation of Simplified Methods of Analysis for Yielding Structures," by P. Tsopelas, M.C. Constantinou, C.A. Kircher and A.S. Whittaker, 10/31/97, (PB98-128929, A10, MF-A03).

NCEER-97-0013   "Seismic Design of Bridge Columns Based on Control and Repairability of Damage," by C-T. Cheng and J.B. Mander, 12/8/97, (PB98-144249, A11, MF-A03).

NCEER-97-0014   "Seismic Resistance of Bridge Piers Based on Damage Avoidance Design," by J.B. Mander and C-T. Cheng, 12/10/97, (PB98-144223, A09, MF-A02).

NCEER-97-0015   "Seismic Response of Nominally Symmetric Systems with Strength Uncertainty," by S. Balopoulou and M. Grigoriu, 12/23/97, (PB98-153422, A11, MF-A03).

NCEER-97-0016   "Evaluation of Seismic Retrofit Methods for Reinforced Concrete Bridge Columns," by T.J. Wipf, F.W. Klaiber and F.M. Russo, 12/28/97, (PB98-144215, A12, MF-A03).

NCEER-97-0017   "Seismic Fragility of Existing Conventional Reinforced Concrete Highway Bridges," by C.L. Mullen and A.S. Cakmak, 12/30/97, (PB98-153406, A08, MF-A02).

NCEER-97-0018   "Loss Asssessment of Memphis Buildings," edited by D.P. Abrams and M. Shinozuka, 12/31/97, (PB98-144231, A13, MF-A03).

NCEER-97-0019   "Seismic Evaluation of Frames with Infill Walls Using Quasi-static Experiments," by K.M. Mosalam, R.N. White and P. Gergely, 12/31/97, (PB98-153455, A07, MF-A02).

NCEER-97-0020   "Seismic Evaluation of Frames with Infill Walls Using Pseudo-dynamic Experiments," by K.M. Mosalam, R.N. White and P. Gergely, 12/31/97, (PB98-153430, A07, MF-A02).

NCEER-97-0021   "Computational Strategies for Frames with Infill Walls: Discrete and Smeared Crack Analyses and Seismic Fragility," by K.M. Mosalam, R.N. White and P. Gergely, 12/31/97, (PB98-153414, A10, MF-A02).

NCEER-97-0022   "Proceedings of the NCEER Workshop on Evaluation of Liquefaction Resistance of Soils," edited by T.L. Youd and I.M. Idriss, 12/31/97, (PB98-155617, A15, MF-A03).

MCEER-98-0001   "Extraction of Nonlinear Hysteretic Properties of Seismically Isolated Bridges from Quick-Release Field Tests," by Q. Chen, B.M. Douglas, E.M. Maragakis and I.G. Buckle, 5/26/98, (PB99-118838, A06, MF-A01).

MCEER-98-0002   "Methodologies for Evaluating the Importance of Highway Bridges," by A. Thomas, S. Eshenaur and J. Kulicki, 5/29/98, (PB99-118846, A10, MF-A02).

MCEER-98-0003   "Capacity Design of Bridge Piers and the Analysis of Overstrength," by J.B. Mander, A. Dutta and P. Goel, 6/1/98, (PB99-118853, A09, MF-A02).

MCEER-98-0004   "Evaluation of Bridge Damage Data from the Loma Prieta and Northridge, California Earthquakes," by N. Basoz and A. Kiremidjian, 6/2/98, (PB99-118861, A15, MF-A03).

MCEER-98-0005   "Screening Guide for Rapid Assessment of Liquefaction Hazard at Highway Bridge Sites," by T. L. Youd, 6/16/98, (PB99-118879, A06, not available on microfiche).

MCEER-98-0006   "Structural Steel and Steel/Concrete Interface Details for Bridges," by P. Ritchie, N. Kauhl and J. Kulicki, 7/13/98, (PB99-118945, A06, MF-A01).

MCEER-98-0007   "Capacity Design and Fatigue Analysis of Confined Concrete Columns," by A. Dutta and J.B. Mander, 7/14/98, (PB99-118960, A14, MF-A03).

MCEER-98-0008   "Proceedings of the Workshop on Performance Criteria for Telecommunication Services Under Earthquake Conditions," edited by A.J. Schiff, 7/15/98, (PB99-118952, A08, MF-A02).

MCEER-98-0009   "Fatigue Analysis of Unconfined Concrete Columns," by J.B. Mander, A. Dutta and J.H. Kim, 9/12/98, (PB99-123655, A10, MF-A02).

MCEER-98-0010   "Centrifuge Modeling of Cyclic Lateral Response of Pile-Cap Systems and Seat-Type Abutments in Dry Sands," by A.D. Gadre and R. Dobry, 10/2/98, (PB99-123606, A13, MF-A03).

MCEER-98-0011   "IDARC-BRIDGE: A Computational Platform for Seismic Damage Assessment of Bridge Structures," by A.M. Reinhorn, V. Simeonov, G. Mylonakis and Y. Reichman, 10/2/98, (PB99-162919, A15, MF-A03).

MCEER-98-0012   "Experimental Investigation of the Dynamic Response of Two Bridges Before and After Retrofitting with Elastomeric Bearings," by D.A. Wendichansky, S.S. Chen and J.B. Mander, 10/2/98, (PB99-162927, A15, MF-A03).

MCEER-98-0013   "Design Procedures for Hinge Restrainers and Hinge Sear Width for Multiple-Frame Bridges," by R. Des Roches and G.L. Fenves, 11/3/98, (PB99-140477, A13, MF-A03).

MCEER-98-0014   "Response Modification Factors for Seismically Isolated Bridges," by M.C. Constantinou and J.K. Quarshie, 11/3/98, (PB99-140485, A14, MF-A03).

MCEER-98-0015   "Proceedings of the U.S.-Italy Workshop on Seismic Protective Systems for Bridges," edited by I.M. Friedland and M.C. Constantinou, 11/3/98, (PB2000-101711, A22, MF-A04).

MCEER-98-0016   "Appropriate Seismic Reliability for Critical Equipment Systems: Recommendations Based on Regional Analysis of Financial and Life Loss," by K. Porter, C. Scawthorn, C. Taylor and N. Blais, 11/10/98, (PB99-157265, A08, MF-A02).

MCEER-98-0017   "Proceedings of the U.S. Japan Joint Seminar on Civil Infrastructure Systems Research," edited by M. Shinozuka and A. Rose, 11/12/98, (PB99-156713, A16, MF-A03).

MCEER-98-0018   "Modeling of Pile Footings and Drilled Shafts for Seismic Design," by I. PoLam, M. Kapuskar and D. Chaudhuri, 12/21/98, (PB99-157257, A09, MF-A02).

MCEER-99-0001   "Seismic Evaluation of a Masonry Infilled Reinforced Concrete Frame by Pseudodynamic Testing," by S.G. Buonopane and R.N. White, 2/16/99, (PB99-162851, A09, MF-A02).

MCEER-99-0002   "Response History Analysis of Structures with Seismic Isolation and Energy Dissipation Systems: Verification Examples for Program SAP2000," by J. Scheller and M.C. Constantinou, 2/22/99, (PB99-162869, A08, MF-A02).

MCEER-99-0003   "Experimental Study on the Seismic Design and Retrofit of Bridge Columns Including Axial Load Effects," by A. Dutta, T. Kokorina and J.B. Mander, 2/22/99, (PB99-162877, A09, MF-A02).

MCEER-99-0004   "Experimental Study of Bridge Elastomeric and Other Isolation and Energy Dissipation Systems with Emphasis on Uplift Prevention and High Velocity Near-source Seismic Excitation," by A. Kasalanati and M. C. Constantinou, 2/26/99, (PB99-162885, A12, MF-A03).

MCEER-99-0005   "Truss Modeling of Reinforced Concrete Shear-flexure Behavior," by J.H. Kim and J.B. Mander, 3/8/99, (PB99-163693, A12, MF-A03).

MCEER-99-0006   "Experimental Investigation and Computational Modeling of Seismic Response of a 1:4 Scale Model Steel Structure with a Load Balancing Supplemental Damping System," by G. Pekcan, J.B. Mander and S.S. Chen, 4/2/99, (PB99-162893, A11, MF-A03).

MCEER-99-0007   "Effect of Vertical Ground Motions on the Structural Response of Highway Bridges," by M.R. Button, C.J. Cronin and R.L. Mayes, 4/10/99, (PB2000-101411, A10, MF-A03).

MCEER-99-0008   "Seismic Reliability Assessment of Critical Facilities: A Handbook, Supporting Documentation, and Model Code Provisions," by G.S. Johnson, R.E. Sheppard, M.D. Quilici, S.J. Eder and C.R. Scawthorn, 4/12/99, (PB2000-101701, A18, MF-A04).

MCEER-99-0009   "Impact Assessment of Selected MCEER Highway Project Research on the Seismic Design of Highway Structures," by C. Rojahn, R. Mayes, D.G. Anderson, J.H. Clark, D'Appolonia Engineering, S. Gloyd and R.V. Nutt, 4/14/99, (PB99-162901, A10, MF-A02).

MCEER-99-0010   "Site Factors and Site Categories in Seismic Codes," by R. Dobry, R. Ramos and M.S. Power, 7/19/99, (PB2000-101705, A08, MF-A02).

MCEER-99-0011   "Restrainer Design Procedures for Multi-Span Simply-Supported Bridges," by M.J. Randall, M. Saiidi, E. Maragakis and T. Isakovic, 7/20/99, (PB2000-101702, A10, MF-A02).

MCEER-99-0012   "Property Modification Factors for Seismic Isolation Bearings," by M.C. Constantinou, P. Tsopelas, A. Kasalanati and E. Wolff, 7/20/99, (PB2000-103387, A11, MF-A03).

MCEER-99-0013   "Critical Seismic Issues for Existing Steel Bridges," by P. Ritchie, N. Kauhl and J. Kulicki, 7/20/99, (PB2000-101697, A09, MF-A02).

MCEER-99-0014   "Nonstructural Damage Database," by A. Kao, T.T. Soong and A. Vender, 7/24/99, (PB2000-101407, A06, MF-A01).

MCEER-99-0015   "Guide to Remedial Measures for Liquefaction Mitigation at Existing Highway Bridge Sites," by H.G. Cooke and J. K. Mitchell, 7/26/99, (PB2000-101703, A11, MF-A03).

MCEER-99-0016   "Proceedings of the MCEER Workshop on Ground Motion Methodologies for the Eastern United States," edited by N. Abrahamson and A. Becker, 8/11/99, (PB2000-103385, A07, MF-A02).

MCEER-99-0017   "Quindío, Colombia Earthquake of January 25, 1999: Reconnaissance Report," by A.P. Asfura and P.J. Flores, 10/4/99, (PB2000-106893, A06, MF-A01).

MCEER-99-0018   "Hysteretic Models for Cyclic Behavior of Deteriorating Inelastic Structures," by M.V. Sivaselvan and A.M. Reinhorn, 11/5/99, (PB2000-103386, A08, MF-A02).

MCEER-99-0019 "Proceedings of the 7th U.S.- Japan Workshop on Earthquake Resistant Design of Lifeline Facilities and Countermeasures Against Soil Liquefaction," edited by T.D. O'Rourke, J.P. Bardet and M. Hamada, 11/19/99, (PB2000-103354, A99, MF-A06).

MCEER-99-0020 "Development of Measurement Capability for Micro-Vibration Evaluations with Application to Chip Fabrication Facilities," by G.C. Lee, Z. Liang, J.W. Song, J.D. Shen and W.C. Liu, 12/1/99, (PB2000-105993, A08, MF-A02).

MCEER-99-0021 "Design and Retrofit Methodology for Building Structures with Supplemental Energy Dissipating Systems," by G. Pekcan, J.B. Mander and S.S. Chen, 12/31/99, (PB2000-105994, A11, MF-A03).

MCEER-00-0001 "The Marmara, Turkey Earthquake of August 17, 1999: Reconnaissance Report," edited by C. Scawthorn; with major contributions by M. Bruneau, R. Eguchi, T. Holzer, G. Johnson, J. Mander, J. Mitchell, W. Mitchell, A. Papageorgiou, C. Scaethorn, and G. Webb, 3/23/00, (PB2000-106200, A11, MF-A03).

MCEER-00-0002 "Proceedings of the MCEER Workshop for Seismic Hazard Mitigation of Health Care Facilities," edited by G.C. Lee, M. Ettouney, M. Grigoriu, J. Hauer and J. Nigg, 3/29/00, (PB2000-106892, A08, MF-A02).

MCEER-00-0003 "The Chi-Chi, Taiwan Earthquake of September 21, 1999: Reconnaissance Report," edited by G.C. Lee and C.H. Loh, with major contributions by G.C. Lee, M. Bruneau, I.G. Buckle, S.E. Chang, P.J. Flores, T.D. O'Rourke, M. Shinozuka, T.T. Soong, C-H. Loh, K-C. Chang, Z-J. Chen, J-S. Hwang, M-L. Lin, G-Y. Liu, K-C. Tsai, G.C. Yao and C-L. Yen, 4/30/00, (PB2001-100980, A10, MF-A02).

MCEER-00-0004 "Seismic Retrofit of End-Sway Frames of Steel Deck-Truss Bridges with a Supplemental Tendon System: Experimental and Analytical Investigation," by G. Pekcan, J.B. Mander and S.S. Chen, 7/1/00, (PB2001-100982, A10, MF-A02).

MCEER-00-0005 "Sliding Fragility of Unrestrained Equipment in Critical Facilities," by W.H. Chong and T.T. Soong, 7/5/00, (PB2001-100983, A08, MF-A02).

MCEER-00-0006 "Seismic Response of Reinforced Concrete Bridge Pier Walls in the Weak Direction," by N. Abo-Shadi, M. Saiidi and D. Sanders, 7/17/00, (PB2001-100981, A17, MF-A03).

MCEER-00-0007 "Low-Cycle Fatigue Behavior of Longitudinal Reinforcement in Reinforced Concrete Bridge Columns," by J. Brown and S.K. Kunnath, 7/23/00, (PB2001-104392, A08, MF-A02).

MCEER-00-0008 "Soil Structure Interaction of Bridges for Seismic Analysis," I. PoLam and H. Law, 9/25/00, (PB2001-105397, A08, MF-A02).

MCEER-00-0009 "Proceedings of the First MCEER Workshop on Mitigation of Earthquake Disaster by Advanced Technologies (MEDAT-1), edited by M. Shinozuka, D.J. Inman and T.D. O'Rourke, 11/10/00, (PB2001-105399, A14, MF-A03).

MCEER-00-0010 "Development and Evaluation of Simplified Procedures for Analysis and Design of Buildings with Passive Energy Dissipation Systems, Revision 01," by O.M. Ramirez, M.C. Constantinou, C.A. Kircher, A.S. Whittaker, M.W. Johnson, J.D. Gomez and C. Chrysostomou, 11/16/01, (PB2001-105523, A23, MF-A04).

MCEER-00-0011 "Dynamic Soil-Foundation-Structure Interaction Analyses of Large Caissons," by C-Y. Chang, C-M. Mok, Z-L. Wang, R. Settgast, F. Waggoner, M.A. Ketchum, H.M. Gonnermann and C-C. Chin, 12/30/00, (PB2001-104373, A07, MF-A02).

MCEER-00-0012 "Experimental Evaluation of Seismic Performance of Bridge Restrainers," by A.G. Vlassis, E.M. Maragakis and M. Saiid Saiidi, 12/30/00, (PB2001-104354, A09, MF-A02).

MCEER-00-0013 "Effect of Spatial Variation of Ground Motion on Highway Structures," by M. Shinozuka, V. Saxena and G. Deodatis, 12/31/00, (PB2001-108755, A13, MF-A03).

MCEER-00-0014 "A Risk-Based Methodology for Assessing the Seismic Performance of Highway Systems," by S.D. Werner, C.E. Taylor, J.E. Moore, II, J.S. Walton and S. Cho, 12/31/00, (PB2001-108756, A14, MF-A03).

MCEER-01-0001 "Experimental Investigation of P-Delta Effects to Collapse During Earthquakes," by D. Vian and M. Bruneau, 6/25/01, (PB2002-100534, A17, MF-A03).

MCEER-01-0002 "Proceedings of the Second MCEER Workshop on Mitigation of Earthquake Disaster by Advanced Technologies (MEDAT-2)," edited by M. Bruneau and D.J. Inman, 7/23/01, (PB2002-100434, A16, MF-A03).

MCEER-01-0003 "Sensitivity Analysis of Dynamic Systems Subjected to Seismic Loads," by C. Roth and M. Grigoriu, 9/18/01, (PB2003-100884, A12, MF-A03).

MCEER-01-0004 "Overcoming Obstacles to Implementing Earthquake Hazard Mitigation Policies: Stage 1 Report," by D.J. Alesch and W.J. Petak, 12/17/01, (PB2002-107949, A07, MF-A02).

MCEER-01-0005 "Updating Real-Time Earthquake Loss Estimates: Methods, Problems and Insights," by C.E. Taylor, S.E. Chang and R.T. Eguchi, 12/17/01, (PB2002-107948, A05, MF-A01).

MCEER-01-0006 "Experimental Investigation and Retrofit of Steel Pile Foundations and Pile Bents Under Cyclic Lateral Loadings," by A. Shama, J. Mander, B. Blabac and S. Chen, 12/31/01, (PB2002-107950, A13, MF-A03).

MCEER-02-0001 "Assessment of Performance of Bolu Viaduct in the 1999 Duzce Earthquake in Turkey" by P.C. Roussis, M.C. Constantinou, M. Erdik, E. Durukal and M. Dicleli, 5/8/02, (PB2003-100883, A08, MF-A02).

MCEER-02-0002 "Seismic Behavior of Rail Counterweight Systems of Elevators in Buildings," by M.P. Singh, Rildova and L.E. Suarez, 5/27/02. (PB2003-100882, A11, MF-A03).

MCEER-02-0003 "Development of Analysis and Design Procedures for Spread Footings," by G. Mylonakis, G. Gazetas, S. Nikolaou and A. Chauncey, 10/02/02, (PB2004-101636, A13, MF-A03, CD-A13).

MCEER-02-0004 "Bare-Earth Algorithms for Use with SAR and LIDAR Digital Elevation Models," by C.K. Huyck, R.T. Eguchi and B. Houshmand, 10/16/02, (PB2004-101637, A07, CD-A07).

MCEER-02-0005 "Review of Energy Dissipation of Compression Members in Concentrically Braced Frames," by K.Lee and M. Bruneau, 10/18/02, (PB2004-101638, A10, CD-A10).

MCEER-03-0001 "Experimental Investigation of Light-Gauge Steel Plate Shear Walls for the Seismic Retrofit of Buildings" by J. Berman and M. Bruneau, 5/2/03, (PB2004-101622, A10, MF-A03, CD-A10).

MCEER-03-0002 "Statistical Analysis of Fragility Curves," by M. Shinozuka, M.Q. Feng, H. Kim, T. Uzawa and T. Ueda, 6/16/03, (PB2004-101849, A09, CD-A09).

MCEER-03-0003 "Proceedings of the Eighth U.S.-Japan Workshop on Earthquake Resistant Design f Lifeline Facilities and Countermeasures Against Liquefaction," edited by M. Hamada, J.P. Bardet and T.D. O'Rourke, 6/30/03, (PB2004-104386, A99, CD-A99).

MCEER-03-0004 "Proceedings of the PRC-US Workshop on Seismic Analysis and Design of Special Bridges," edited by L.C. Fan and G.C. Lee, 7/15/03, (PB2004-104387, A14, CD-A14).

MCEER-03-0005 "Urban Disaster Recovery: A Framework and Simulation Model," by S.B. Miles and S.E. Chang, 7/25/03, (PB2004-104388, A07, CD-A07).

MCEER-03-0006 "Behavior of Underground Piping Joints Due to Static and Dynamic Loading," by R.D. Meis, M. Maragakis and R. Siddharthan, 11/17/03, (PB2005-102194, A13, MF-A03, CD-A00).

MCEER-04-0001 "Experimental Study of Seismic Isolation Systems with Emphasis on Secondary System Response and Verification of Accuracy of Dynamic Response History Analysis Methods," by E. Wolff and M. Constantinou, 1/16/04 (PB2005-102195, A99, MF-E08, CD-A00).

MCEER-04-0002 "Tension, Compression and Cyclic Testing of Engineered Cementitious Composite Materials," by K. Kesner and S.L. Billington, 3/1/04, (PB2005-102196, A08, CD-A08).

MCEER-04-0003   "Cyclic Testing of Braces Laterally Restrained by Steel Studs to Enhance Performance During Earthquakes," by O.C. Celik, J.W. Berman and M. Bruneau, 3/16/04, (PB2005-102197, A13, MF-A03, CD-A00).

MCEER-04-0004   "Methodologies for Post Earthquake Building Damage Detection Using SAR and Optical Remote Sensing: Application to the August 17, 1999 Marmara, Turkey Earthquake," by C.K. Huyck, B.J. Adams, S. Cho, R.T. Eguchi, B. Mansouri and B. Houshmand, 6/15/04, (PB2005-104888, A10, CD-A00).

MCEER-04-0005   "Nonlinear Structural Analysis Towards Collapse Simulation: A Dynamical Systems Approach," by M.V. Sivaselvan and A.M. Reinhorn, 6/16/04, (PB2005-104889, A11, MF-A03, CD-A00).

MCEER-04-0006   "Proceedings of the Second PRC-US Workshop on Seismic Analysis and Design of Special Bridges," edited by G.C. Lee and L.C. Fan, 6/25/04, (PB2005-104890, A16, CD-A00).

MCEER-04-0007   "Seismic Vulnerability Evaluation of Axially Loaded Steel Built-up Laced Members," by K. Lee and M. Bruneau, 6/30/04, (PB2005-104891, A16, CD-A00).

MCEER-04-0008   "Evaluation of Accuracy of Simplified Methods of Analysis and Design of Buildings with Damping Systems for Near-Fault and for Soft-Soil Seismic Motions," by E.A. Pavlou and M.C. Constantinou, 8/16/04, (PB2005-104892, A08, MF-A02, CD-A00).

MCEER-04-0009   "Assessment of Geotechnical Issues in Acute Care Facilities in California," by M. Lew, T.D. O'Rourke, R. Dobry and M. Koch, 9/15/04, (PB2005-104893, A08, CD-A00).

MCEER-04-0010   "Scissor-Jack-Damper Energy Dissipation System," by A.N. Sigaher-Boyle and M.C. Constantinou, 12/1/04 (PB2005-108221).

MCEER-04-0011   "Seismic Retrofit of Bridge Steel Truss Piers Using a Controlled Rocking Approach," by M. Pollino and M. Bruneau, 12/20/04 (PB2006-105795).

MCEER-05-0001   "Experimental and Analytical Studies of Structures Seismically Isolated with an Uplift-Restraint Isolation System," by P.C. Roussis and M.C. Constantinou, 1/10/05 (PB2005-108222).

MCEER-05-0002   "A Versatile Experimentation Model for Study of Structures Near Collapse Applied to Seismic Evaluation of Irregular Structures," by D. Kusumastuti, A.M. Reinhorn and A. Rutenberg, 3/31/05 (PB2006-101523).

MCEER-05-0003   "Proceedings of the Third PRC-US Workshop on Seismic Analysis and Design of Special Bridges," edited by L.C. Fan and G.C. Lee, 4/20/05, (PB2006-105796).

MCEER-05-0004   "Approaches for the Seismic Retrofit of Braced Steel Bridge Piers and Proof-of-Concept Testing of an Eccentrically Braced Frame with Tubular Link," by J.W. Berman and M. Bruneau, 4/21/05 (PB2006-101524).

MCEER-05-0005   "Simulation of Strong Ground Motions for Seismic Fragility Evaluation of Nonstructural Components in Hospitals," by A. Wanitkorkul and A. Filiatrault, 5/26/05 (PB2006-500027).

MCEER-05-0006   "Seismic Safety in California Hospitals: Assessing an Attempt to Accelerate the Replacement or Seismic Retrofit of Older Hospital Facilities," by D.J. Alesch, L.A. Arendt and W.J. Petak, 6/6/05 (PB2006-105794).

MCEER-05-0007   "Development of Seismic Strengthening and Retrofit Strategies for Critical Facilities Using Engineered Cementitious Composite Materials," by K. Kesner and S.L. Billington, 8/29/05 (PB2006-111701).

MCEER-05-0008   "Experimental and Analytical Studies of Base Isolation Systems for Seismic Protection of Power Transformers," by N. Murota, M.Q. Feng and G-Y. Liu, 9/30/05 (PB2006-111702).

MCEER-05-0009   "3D-BASIS-ME-MB: Computer Program for Nonlinear Dynamic Analysis of Seismically Isolated Structures," by P.C. Tsopelas, P.C. Roussis, M.C. Constantinou, R. Buchanan and A.M. Reinhorn, 10/3/05 (PB2006-111703).

MCEER-05-0010   "Steel Plate Shear Walls for Seismic Design and Retrofit of Building Structures," by D. Vian and M. Bruneau, 12/15/05 (PB2006-111704).

MCEER-05-0011 "The Performance-Based Design Paradigm," by M.J. Astrella and A. Whittaker, 12/15/05 (PB2006-111705).

MCEER-06-0001 "Seismic Fragility of Suspended Ceiling Systems," H. Badillo-Almaraz, A.S. Whittaker, A.M. Reinhorn and G.P. Cimellaro, 2/4/06 (PB2006-111706).

MCEER-06-0002 "Multi-Dimensional Fragility of Structures," by G.P. Cimellaro, A.M. Reinhorn and M. Bruneau, 3/1/06 (PB2007-106974, A09, MF-A02, CD A00).

MCEER-06-0003 "Built-Up Shear Links as Energy Dissipators for Seismic Protection of Bridges," by P. Dusicka, A.M. Itani and I.G. Buckle, 3/15/06 (PB2006-111708).

MCEER-06-0004 "Analytical Investigation of the Structural Fuse Concept," by R.E. Vargas and M. Bruneau, 3/16/06 (PB2006-111709).

MCEER-06-0005 "Experimental Investigation of the Structural Fuse Concept," by R.E. Vargas and M. Bruneau, 3/17/06 (PB2006-111710).

MCEER-06-0006 "Further Development of Tubular Eccentrically Braced Frame Links for the Seismic Retrofit of Braced Steel Truss Bridge Piers," by J.W. Berman and M. Bruneau, 3/27/06 (PB2007-105147).

MCEER-06-0007 "REDARS Validation Report," by S. Cho, C.K. Huyck, S. Ghosh and R.T. Eguchi, 8/8/06 (PB2007-106983).

MCEER-06-0008 "Review of Current NDE Technologies for Post-Earthquake Assessment of Retrofitted Bridge Columns," by J.W. Song, Z. Liang and G.C. Lee, 8/21/06 (PB2007-106984).

MCEER-06-0009 "Liquefaction Remediation in Silty Soils Using Dynamic Compaction and Stone Columns," by S. Thevanayagam, G.R. Martin, R. Nashed, T. Shenthan, T. Kanagalingam and N. Ecemis, 8/28/06 (PB2007-106985).

MCEER-06-0010 "Conceptual Design and Experimental Investigation of Polymer Matrix Composite Infill Panels for Seismic Retrofitting," by W. Jung, M. Chiewanichakorn and A.J. Aref, 9/21/06 (PB2007-106986).

MCEER-06-0011 "A Study of the Coupled Horizontal-Vertical Behavior of Elastomeric and Lead-Rubber Seismic Isolation Bearings," by G.P. Warn and A.S. Whittaker, 9/22/06 (PB2007-108679).

MCEER-06-0012 "Proceedings of the Fourth PRC-US Workshop on Seismic Analysis and Design of Special Bridges: Advancing Bridge Technologies in Research, Design, Construction and Preservation," Edited by L.C. Fan, G.C. Lee and L. Ziang, 10/12/06 (PB2007-109042).

MCEER-06-0013 "Cyclic Response and Low Cycle Fatigue Characteristics of Plate Steels," by P. Dusicka, A.M. Itani and I.G. Buckle, 11/1/06 06 (PB2007-106987).

MCEER-06-0014 "Proceedings of the Second US-Taiwan Bridge Engineering Workshop," edited by W.P. Yen, J. Shen, J-Y. Chen and M. Wang, 11/15/06 (PB2008-500041).

MCEER-06-0015 "User Manual and Technical Documentation for the REDARS^{TM} Import Wizard," by S. Cho, S. Ghosh, C.K. Huyck and S.D. Werner, 11/30/06 (PB2007-114766).

MCEER-06-0016 "Hazard Mitigation Strategy and Monitoring Technologies for Urban and Infrastructure Public Buildings: Proceedings of the China-US Workshops," edited by X.Y. Zhou, A.L. Zhang, G.C. Lee and M. Tong, 12/12/06 (PB2008-500018).

MCEER-07-0001 "Static and Kinetic Coefficients of Friction for Rigid Blocks," by C. Kafali, S. Fathali, M. Grigoriu and A.S. Whittaker, 3/20/07 (PB2007-114767).

MCEER-07-0002 "Hazard Mitigation Investment Decision Making: Organizational Response to Legislative Mandate," by L.A. Arendt, D.J. Alesch and W.J. Petak, 4/9/07 (PB2007-114768).

MCEER-07-0003 "Seismic Behavior of Bidirectional-Resistant Ductile End Diaphragms with Unbonded Braces in Straight or Skewed Steel Bridges," by O. Celik and M. Bruneau, 4/11/07 (PB2008-105141).

MCEER-07-0004   "Modeling Pile Behavior in Large Pile Groups Under Lateral Loading," by A.M. Dodds and G.R. Martin, 4/16/07(PB2008-105142).

MCEER-07-0005   "Experimental Investigation of Blast Performance of Seismically Resistant Concrete-Filled Steel Tube Bridge Piers," by S. Fujikura, M. Bruneau and D. Lopez-Garcia, 4/20/07 (PB2008-105143).

MCEER-07-0006   "Seismic Analysis of Conventional and Isolated Liquefied Natural Gas Tanks Using Mechanical Analogs," by I.P. Christovasilis and A.S. Whittaker, 5/1/07.

MCEER-07-0007   "Experimental Seismic Performance Evaluation of Isolation/Restraint Systems for Mechanical Equipment – Part 1: Heavy Equipment Study," by S. Fathali and A. Filiatrault, 6/6/07 (PB2008-105144).

MCEER-07-0008   "Seismic Vulnerability of Timber Bridges and Timber Substructures," by A.A. Sharma, J.B. Mander, I.M. Friedland and D.R. Allicock, 6/7/07 (PB2008-105145).

MCEER-07-0009   "Experimental and Analytical Study of the XY-Friction Pendulum (XY-FP) Bearing for Bridge Applications," by C.C. Marin-Artieda, A.S. Whittaker and M.C. Constantinou, 6/7/07 (PB2008-105191).

MCEER-07-0010   "Proceedings of the PRC-US Earthquake Engineering Forum for Young Researchers," Edited by G.C. Lee and X.Z. Qi, 6/8/07.

MCEER-07-0011   "Design Recommendations for Perforated Steel Plate Shear Walls," by R. Purba and M. Bruneau, 6/18/07, (PB2008-105192).

MCEER-07-0012   "Performance of Seismic Isolation Hardware Under Service and Seismic Loading," by M.C. Constantinou, A.S. Whittaker, Y. Kalpakidis, D.M. Fenz and G.P. Warn, 8/27/07, (PB2008-105193).

MCEER-07-0013   "Experimental Evaluation of the Seismic Performance of Hospital Piping Subassemblies," by E.R. Goodwin, E. Maragakis and A.M. Itani, 9/4/07, (PB2008-105194).

MCEER-07-0014   "A Simulation Model of Urban Disaster Recovery and Resilience: Implementation for the 1994 Northridge Earthquake," by S. Miles and S.E. Chang, 9/7/07, (PB2008-106426).

MCEER-07-0015   "Statistical and Mechanistic Fragility Analysis of Concrete Bridges," by M. Shinozuka, S. Banerjee and S-H. Kim, 9/10/07, (PB2008-106427).

MCEER-07-0016   "Three-Dimensional Modeling of Inelastic Buckling in Frame Structures," by M. Schachter and AM. Reinhorn, 9/13/07, (PB2008-108125).

MCEER-07-0017   "Modeling of Seismic Wave Scattering on Pile Groups and Caissons," by I. Po Lam, H. Law and C.T. Yang, 9/17/07 (PB2008-108150).

MCEER-07-0018   "Bridge Foundations: Modeling Large Pile Groups and Caissons for Seismic Design," by I. Po Lam, H. Law and G.R. Martin (Coordinating Author), 12/1/07 (PB2008-111190).

MCEER-07-0019   "Principles and Performance of Roller Seismic Isolation Bearings for Highway Bridges," by G.C. Lee, Y.C. Ou, Z. Liang, T.C. Niu and J. Song, 12/10/07.

MCEER-07-0020   "Centrifuge Modeling of Permeability and Pinning Reinforcement Effects on Pile Response to Lateral Spreading," by L.L Gonzalez-Lagos, T. Abdoun and R. Dobry, 12/10/07 (PB2008-111191).

MCEER-07-0021   "Damage to the Highway System from the Pisco, Perú Earthquake of August 15, 2007," by J.S. O'Connor, L. Mesa and M. Nykamp, 12/10/07, (PB2008-108126).

MCEER-07-0022   "Experimental Seismic Performance Evaluation of Isolation/Restraint Systems for Mechanical Equipment – Part 2: Light Equipment Study," by S. Fathali and A. Filiatrault, 12/13/07 (PB2008-111192).

MCEER-07-0023   "Fragility Considerations in Highway Bridge Design," by M. Shinozuka, S. Banerjee and S.H. Kim, 12/14/07 (PB2008-111193).

MCEER-07-0024   "Performance Estimates for Seismically Isolated Bridges," by G.P. Warn and A.S. Whittaker, 12/30/07 (PB2008-112230).

MCEER-08-0001   "Seismic Performance of Steel Girder Bridge Superstructures with Conventional Cross Frames," by L.P. Carden, A.M. Itani and I.G. Buckle, 1/7/08, (PB2008-112231).

MCEER-08-0002   "Seismic Performance of Steel Girder Bridge Superstructures with Ductile End Cross Frames with Seismic Isolators," by L.P. Carden, A.M. Itani and I.G. Buckle, 1/7/08 (PB2008-112232).

MCEER-08-0003   "Analytical and Experimental Investigation of a Controlled Rocking Approach for Seismic Protection of Bridge Steel Truss Piers," by M. Pollino and M. Bruneau, 1/21/08 (PB2008-112233).

MCEER-08-0004   "Linking Lifeline Infrastructure Performance and Community Disaster Resilience: Models and Multi-Stakeholder Processes," by S.E. Chang, C. Pasion, K. Tatebe and R. Ahmad, 3/3/08 (PB2008-112234).

MCEER-08-0005   "Modal Analysis of Generally Damped Linear Structures Subjected to Seismic Excitations," by J. Song, Y-L. Chu, Z. Liang and G.C. Lee, 3/4/08 (PB2009-102311).

MCEER-08-0006   "System Performance Under Multi-Hazard Environments," by C. Kafali and M. Grigoriu, 3/4/08 (PB2008-112235).

MCEER-08-0007   "Mechanical Behavior of Multi-Spherical Sliding Bearings," by D.M. Fenz and M.C. Constantinou, 3/6/08 (PB2008-112236).

MCEER-08-0008   "Post-Earthquake Restoration of the Los Angeles Water Supply System," by T.H.P. Tabucchi and R.A. Davidson, 3/7/08 (PB2008-112237).

MCEER-08-0009   "Fragility Analysis of Water Supply Systems," by A. Jacobson and M. Grigoriu, 3/10/08 (PB2009-105545).

MCEER-08-0010   "Experimental Investigation of Full-Scale Two-Story Steel Plate Shear Walls with Reduced Beam Section Connections," by B. Qu, M. Bruneau, C-H. Lin and K-C. Tsai, 3/17/08.

MCEER-08-0011   "Seismic Evaluation and Rehabilitation of Critical Components of Electrical Power Systems," S. Ersoy, B. Feizi, A. Ashrafi and M. Ala Saadeghvaziri, 3/17/08 (PB2009-105546).

MCEER-08-0012   "Seismic Behavior and Design of Boundary Frame Members of Steel Plate Shear Walls," by B. Qu and M. Bruneau, 4/26/08.

MCEER-08-0013   "Development and Appraisal of a Numerical Cyclic Loading Protocol for Quantifying Building System Performance," by A. Filiatrault, A. Wanitkorkul and M. Constantinou, 4/27/08.

MCEER-08-0014   "Structural and Nonstructural Earthquake Design: The Challenge of Integrating Specialty Areas in Designing Complex, Critical Facilities," by W.J. Petak and D.J. Alesch, 4/30/08.

MCEER-08-0015   "Seismic Performance Evaluation of Water Systems," by Y. Wang and T.D. O'Rourke, 5/5/08.

MCEER-08-0016   "Seismic Response Modeling of Water Supply Systems," by P. Shi and T.D. O'Rourke, 5/5/08.

MCEER-08-0017   "Numerical and Experimental Studies of Self-Centering Post-Tensioned Steel Frames," by D. Wang and A. Filiatrault, 5/12/08.

MCEER-08-0018   "Development, Implementation and Verification of Dynamic Analysis Models for Multi-Spherical Sliding Bearings," by D.M. Fenz and M.C. Constantinou, 8/15/08.

MCEER-08-0019   "Performance Assessment of Conventional and Base Isolated Nuclear Power Plants for Earthquake Blast Loadings," by Y.N. Huang, A.S. Whittaker and N. Luco, 10/28/08.

MCEER-08-0020   "Remote Sensing for Resilient Multi-Hazard Disaster Response – Volume I: Introduction to Damage Assessment Methodologies," by B.J. Adams and R.T. Eguchi, 11/17/08.

MCEER-08-0021   "Remote Sensing for Resilient Multi-Hazard Disaster Response – Volume II: Counting the Number of Collapsed Buildings Using an Object-Oriented Analysis: Case Study of the 2003 Bam Earthquake," by L. Gusella, C.K. Huyck and B.J. Adams, 11/17/08.

MCEER-08-0022   "Remote Sensing for Resilient Multi-Hazard Disaster Response – Volume III: Multi-Sensor Image Fusion Techniques for Robust Neighborhood-Scale Urban Damage Assessment," by B.J. Adams and A. McMillan, 11/17/08.

MCEER-08-0023   "Remote Sensing for Resilient Multi-Hazard Disaster Response – Volume IV: A Study of Multi-Temporal and Multi-Resolution SAR Imagery for Post-Katrina Flood Monitoring in New Orleans," by A. McMillan, J.G. Morley, B.J. Adams and S. Chesworth, 11/17/08.

MCEER-08-0024   "Remote Sensing for Resilient Multi-Hazard Disaster Response – Volume V: Integration of Remote Sensing Imagery and VIEWS[TM] Field Data for Post-Hurricane Charley Building Damage Assessment," by J.A. Womble, K. Mehta and B.J. Adams, 11/17/08.

MCEER-08-0025   "Building Inventory Compilation for Disaster Management: Application of Remote Sensing and Statistical Modeling," by P. Sarabandi, A.S. Kiremidjian, R.T. Eguchi and B. J. Adams, 11/20/08.

MCEER-08-0026   "New Experimental Capabilities and Loading Protocols for Seismic Qualification and Fragility Assessment of Nonstructural Systems," by R. Retamales, G. Mosqueda, A. Filiatrault and A. Reinhorn, 11/24/08.

MCEER-08-0027   "Effects of Heating and Load History on the Behavior of Lead-Rubber Bearings," by I.V. Kalpakidis and M.C. Constantinou, 12/1/08.